

IRIDIUM CORROLES: SYNTHESIS,  
PROPERTIES, AND ELECTRONIC  
STRUCTURE

Thesis by

Joshua Palmer

In Partial Fulfillment of the Requirements for the

degree of

Ph. D., Chemistry

CALIFORNIA INSTITUTE OF TECHNOLOGY

Pasadena, California

2011

(Defended February 11, 2011)

© 2011

Joshua Palmer

All Rights Reserved

## ACKNOWLEDGEMENTS

My graduate school experience was something of a festival of collaboration, so there are a great many people to thank for the existence of this thesis. First of all, I have to thank my advisor, Harry Gray, who rolled the dice on me when he barely had space and then let me do almost anything I wanted with my time in his lab. Harry has been a boon and an inspiration to generations of chemists young and old, and I'm proud to count myself among them. I also have to thank my thesis committee: John Bercaw, Brian Stoltz, and Jonas Peters. We didn't meet very often, but I always got valuable scientific advice from them when we did. Additionally, I would like to acknowledge the aid of Zeev Gross, a professor at the Technion in Haifa, who initially got me interested in corroles and who always has time to discuss an idea, even if it's just by e-mail. I also have to thank Jay Winkler, director of the Beckman Institute Laser Resource Center, who allowed me to utilize a broad array of extremely expensive laser instruments during my time at Caltech and even purchased one custom-made item for a set of experiments I wanted to perform. I'd like to acknowledge the ongoing influence of my wonderful undergraduate advisor, David I. Schuster, as well. He set me on the path that landed me at Caltech, and he taught me most of what I know about organic reactions and photochemistry.

In terms of other students and postdoctoral fellows in the Gray lab, a few have been particularly important to me in the realm of scientific research. Lionel Cheruzel, a postdoc in the Gray lab, set me up with a fume hood when I first arrived and showed me how to use a Schlenk line. Kyle Lancaster, a fellow graduate student one year ahead of me, taught me how to acquire and interpret EPR, XAS, and EXAFS data, introduced me to computational

chemistry, and has generally acted as a guiding star and a good friend to me throughout my graduate research career. Jillian Dempsey, also a year ahead of me, was instrumental in the repair of the Gray group glove box, taught me her Peters-inspired methods of using it, and introduced me to the BILRC laser apparatus. Alec Durrell, a graduate student in my year, was a helpful collaborator on all things photophysical and a most agreeable companion.

I also have to thank my various other scientific collaborators: Mike Day and Larry Henling at the Beckman Institute, whose crystallographic expertise allowed me to turn barely-visible microcrystalline flakes into publishable diffraction structures; Aaron Wilson, a postdoc in the Bercaw lab, who introduced me to practical molecular electrochemistry; Atif Mahammed, a scientist in Zeev Gross' lab with whom I collaborated extensively; Bill Goddard, Robert Nielsen (never did find out why they call him "Smith"), Sijia Dong, and Siddharth Dasgupta, with whom I co-wrote my first piece of computational work; Theis Brock-Nannestad, a graduate student from the Bendix lab at the University of Copenhagen who was a tremendous collaborator and friend both during his brief summer stay at Caltech and afterward; Stephen Sproules at the Max Planck Institute for Bioinorganic Chemistry in Mülheim an der Ruhr, with whom I collaborated on a number of side projects; Serena DeBeer, a professor at Cornell who walked me through my first X-ray spectroscopic experiments; and David Vandervelde of the Caltech NMR facility, who introduced me to a multitude of 2D NMR experiments with unpronounceable names and clever acronyms.

Additionally, I have to thank my family and friends for supporting me throughout the sundry ups and downs that grad school brings. My mom and dad are both researchers

themselves, and they instilled me with a lust for knowledge at an early age. My brother has always helped keep me afloat as well with his ample curiosity and encouragement. My friends on the East Coast supported my decision to move West for school from the beginning and have always understood when I couldn't make it home for long weekends or even some holidays; my new friends on the West Coast, especially my bandmates in Lost City Radio, have kept me sane and happy throughout my graduate school years.

I got married in graduate school, and it was the best decision I've made while at Caltech or otherwise. My wife, Eleanore Olszewski, followed me out here while we were still dating, and has stuck with me despite the long hours, trips to other schools, and occasional odor of putrefaction that come along with the job of research in chemistry. In addition, her family has always made life easy for me, supporting me in my career choice, cheering me on from the sidelines, and providing companionship for Eleanore during my various stints of academically necessary travel.

In no particular order, I would also like to acknowledge the friendship and support of the following people not already named above: Len Gutkin, Elon Plotkin, and Mark Schwager, my old friends from back home; Matthew Smith, Avi Glijansky, and Chintan Pandya, my close friends and bandmates in Lost City Radio (saving the L.A. rock scene from itself); Jesper Bendix and Michael Pittelkow at the University of Copenhagen; and Gretchen Keller, Morgan Cable, Jeff Warren, Bryan Stubbett, Maraia Ener, James McKone, Judith Lattimer, Astrid Mueller, Ian Tonks, David Weinberg, Oliver Shafaat, Peter Agbo, Paul

Oblad, Alex Miller, Ted Weintrob and Adina Cappell, Greg Kimball, Pia Ghosh, Nicole Bouley, Matt Hartings, and my other friends at Caltech.

My last acknowledgment goes out to the people who keep things running for graduate students at Caltech, and who rarely get the credit they deserve: Tom Dunn in the electronics shop, who spent hours helping me fix the Gray group glove box so I could perform air- and water-sensitive reactions in a convenient fashion; Angelo di Bilio, who was willing to set up and break down the cryostat for the EPR any time of the night or day; Scott Virgil, who allowed me to use his fancy HPLC for a decidedly high-risk experiment that turned out very well; Agnes Tong, who made sure I actually got this thesis to the right people at the right time; Joe, Barry, Cora, and Reginald, who in their various ways make sure that we get the chemicals and supplies that we need to do our research; and all the other staff members who quietly make life easy for us.

## ABSTRACT

The synthesis, properties, and electronic structures of a family of iridium corrole complexes are discussed in detail. These compounds represent the first well-characterized examples of third-row metals being inserted successfully into the small corrole binding pocket; they possess a planar macrocycle, which neither saddles nor ruffles upon bromination, and are bound at the axial positions by either two amine ligands or one phosphine. Unlike their well-studied cobalt and rhodium analogues, whose redox activity is restricted primarily to the corrole ring, iridium corroles can be oxidized to produce an electron paramagnetic resonance spectrum that has extremely anisotropic  $g$  tensor components, implying mixing of the 5d orbitals into the oxidized ground state and opening the door to possible higher-valent iridium complexes. Detailed experimental and computational studies are presented showing that this oxidized ground state is actually mostly corrole-based, as has been found in the past for numerous other supposedly high-valent corrole compounds, but the percentage of iridium character varies from 10 to 18% and tracks with the electron-donating ability of the ligand. Additionally, the unique (among corrole complexes) near-IR phosphorescence of Ir(III) corroles is presented and discussed. Iridium(III) corroles phosphoresce with lifetimes ranging from hundreds of nanoseconds to a few microseconds at room temperature, with slightly longer lifetimes at low temperature. Unfortunately, the quantum yields of phosphorescence are low, 1% or less, and this appears to be due to an exceptionally slow set of radiative rates for the corroles. An examination of the reactivity of ammine-ligated Ir(III) corroles is also described. These compounds can be oxidized in the presence of an ammonia source to form novel six-coordinate iridium(III) azaporphyrins

in an unprecedented chemical transformation. The characterization and properties of these iridium azaporphyrin complexes are detailed as well, with a focus on nuclear magnetic resonance characterization techniques and a discussion of the red phosphorescence of the azaporphyrins.



## TABLE OF CONTENTS

Acknowledgments .....	iii
Abstract .....	vii
Table of Contents .....	ix
List of Figures and Tables .....	x
Nomenclature and Abbreviations .....	xiv
Opening Remarks .....	1
Chapter 1 .....	3
Chapter 2 .....	13
Chapter 3 .....	47
Chapter 4 .....	56
Chapter 5 .....	78
Epilogue .....	92
Appendix A: Methodology and Instrumentation .....	96
Appendix B: Synthesis and Characterization .....	101
Corroles .....	101
Azaporphyrins .....	123
Appendix C: X-Ray Diffraction Reports .....	127
<b>1-Ir(tma)<sub>2</sub></b> .....	128
<b>1b-Ir(tma)<sub>2</sub></b> .....	139
<b>1-Ir(py)<sub>2</sub></b> .....	151
<b>1-Ir(dmap)<sub>2</sub></b> .....	162
<b>1-Ir(NH<sub>3</sub>)<sub>2</sub></b> .....	186

## LIST OF FIGURES AND TABLES

<i>Number</i>	<i>Page</i>
1. Figure 1-1: NMR and UV-vis of <b>1-Ir(tma)<sub>2</sub></b> and <b>1b-Ir(tma)<sub>2</sub></b> .....	7
2. Figure 1-2: CV traces of <b>1-Ir(tma)<sub>2</sub></b> and <b>1b-Ir(tma)<sub>2</sub></b> .....	9
3. Figure 1-3: XRD of <b>1-Ir(tma)<sub>2</sub></b> and <b>1b-Ir(tma)<sub>2</sub></b> .....	10
4. Figure 2-1: Various Ir(III) complexes .....	16
5. Figure 2-2: Group 9 metallocorroles .....	20
6. Figure 2-3: <sup>1</sup> H and <sup>19</sup> F NMR of <b>1-Ir(py)<sub>2</sub></b> .....	27
7. Figure 2-4: UV-vis of <b>1-M(py)<sub>2</sub></b> and <b>1-M(PPh<sub>3</sub>)</b> .....	29
8. Figure 2-5: XRD of <b>1-Ir(py)<sub>2</sub></b> .....	30
9. Figure 2-6: UV-vis titrations of <b>1-M(PPh<sub>3</sub>)</b> with PPh <sub>3</sub> .....	32
10. Figure 2-7: CV traces of <b>1-M(py)<sub>2</sub></b> and <b>1-M(PPh<sub>3</sub>)</b> .....	35
11. Figure 2-8: UV-vis titrations of <b>1-Co(PPh<sub>3</sub>)</b> and <b>1-Rh(PPh<sub>3</sub>)</b> .....	37
12. Figure 2-9: UV-vis titrations of <b>1-Co(py)<sub>2</sub></b> and <b>1-Rh(py)<sub>2</sub></b> .....	39
13. Figure 2-10: UV-vis titrations of <b>1-Ir(L)<sub>2</sub></b> .....	40
14. Figure 2-11: EPR of oxidized M(III) corroles.....	43
15. Figure 3-1: Iridium corrole complexes .....	50
16. Figure 3-2: Emission of <b>1-Ir(tma)<sub>2</sub></b> , <b>1b-Ir(tma)<sub>2</sub></b> , and <b>1-Ir(py)<sub>2</sub></b> .....	51
17. Figure 3-3: UV-vis of <b>1-Ir(tma)<sub>2</sub></b> , <b>1b-Ir(tma)<sub>2</sub></b> , and <b>1-Ir(py)<sub>2</sub></b> .....	52
18. Figure 3-4: Solvatochromic effects on Ir(III) corroles.....	53
19. Figure 4-1: XRD structure of <b>1-Ir(tma)<sub>2</sub></b> .....	63
20. Figure 4-2: MO surfaces of <b>1-M(NH<sub>3</sub>)<sub>2</sub></b> .....	65
21. Figure 4-1: XRD structure of <b>1-Ir(tma)<sub>2</sub></b> .....	63
22. Figure 4-2: MO surfaces of <b>1-M(NH<sub>3</sub>)<sub>2</sub></b> .....	65
23. Figure 4-3: MO surfaces of <b>[1-M(NH<sub>3</sub>)<sub>2</sub>]<sup>+</sup></b> .....	68
24. Figure 4-4: MO surfaces of <b>1f-M(NH<sub>3</sub>)<sub>2</sub></b> .....	70
25. Figure 5-1: Synthesis of <b>1-Ir(NH<sub>3</sub>)<sub>2</sub></b> .....	80
26. Figure 5-2: XRD structure of <b>1-Ir(NH<sub>3</sub>)<sub>2</sub></b> .....	65
27. Figure 5-3: <sup>1</sup> H NMR of <b>1-Ir(NH<sub>3</sub>)<sub>2</sub></b> .....	63

28. Figure 5-4: $^{15}\text{N}$ - $^1\text{H}$ HSQC NMR of <b>1-Ir(NH<sub>3</sub>)<sub>2</sub></b> .....	65
29. Figure 5-1: Synthesis of <b>1-Ir(NH<sub>3</sub>)<sub>2</sub></b> .....	80
30. Figure 5-2: XRD structure of <b>1-Ir(NH<sub>3</sub>)<sub>2</sub></b> .....	81
31. Figure 5-3: $^1\text{H}$ NMR of <b>1-Ir(NH<sub>3</sub>)<sub>2</sub></b> .....	82
32. Figure 5-4: $^{15}\text{N}$ - $^1\text{H}$ HSQC NMR of <b>1-Ir(NH<sub>3</sub>)<sub>2</sub></b> .....	82
33. Figure 5-5: CV traces (differing scan speeds) of <b>1-Ir(NH<sub>3</sub>)<sub>2</sub></b> .....	83
34. Figure 5-6: $^1\text{H}$ NMR of <b>2-Ir(NH<sub>3</sub>)<sub>2</sub></b> .....	81
35. Figure 5-7: UV-vis spectra of <b>2-Ir(NH<sub>3</sub>)<sub>2</sub></b> and <b>2b<sub>2</sub>-Ir(NH<sub>3</sub>)<sub>2</sub></b> .....	86
36. Figure 5-8: Synthesis of <b>2-Ir(NH<sub>3</sub>)<sub>2</sub></b> and <b>2b<sub>2</sub>-Ir(NH<sub>3</sub>)<sub>2</sub></b> .....	87
37. Figure 5-9: $^1\text{H}$ NMR of <b>2b<sub>2</sub>-Ir(NH<sub>3</sub>)<sub>2</sub></b> .....	88
38. Figure 5-10: $^{15}\text{N}$ - $^1\text{H}$ HMBC NMR of <b>2b<sub>2</sub>-Ir(NH<sub>3</sub>)<sub>2</sub></b> .....	88
39. Figure 5-11: Emission of <b>2-Ir(NH<sub>3</sub>)<sub>2</sub></b> and <b>2b<sub>2</sub>-Ir(NH<sub>3</sub>)<sub>2</sub></b> .....	90
40. Figure B-1: $^1\text{H}$ NMR of <b>1-Ir(tma)<sub>2</sub></b> .....	102
41. Figure B-2: UV-vis of <b>1-Ir(tma)<sub>2</sub></b> .....	102
42. Figure B-3: ESI-MS of <b>1-Ir(tma)<sub>2</sub></b> .....	103
43. Figure B-4: $^{19}\text{F}$ NMR of <b>1b-Ir(tma)<sub>2</sub></b> .....	104
44. Figure B-5: ESI-MS of <b>1b-Ir(tma)<sub>2</sub></b> .....	104
45. Figure B-6: UV-vis of <b>1b-Ir(tma)<sub>2</sub></b> .....	105
46. Figure B-7: $^1\text{H}$ NMR of <b>1-Ir(py)<sub>2</sub></b> .....	106
47. Figure B-8: $^{19}\text{F}$ NMR of <b>1-Ir(py)<sub>2</sub></b> .....	106
48. Figure B-9: ESI-MS of <b>1-Ir(py)<sub>2</sub></b> .....	107
49. Figure B-10: UV-vis of <b>1-Ir(py)<sub>2</sub></b> .....	107
50. Figure B-11: $^1\text{H}$ NMR of <b>1-Ir(PPh<sub>3</sub>)</b> .....	108
51. Figure B-12: $^{19}\text{F}$ NMR of <b>1-Ir(PPh<sub>3</sub>)</b> .....	109
52. Figure B-13: ESI-MS of <b>1-Ir(PPh<sub>3</sub>)</b> .....	109
53. Figure B-14: ESI-MS of <b>1-Ir(PPh<sub>3</sub>)</b> .....	110
54. Figure B-15: $^1\text{H}$ NMR of <b>1-Ir(cnpy)<sub>2</sub></b> .....	111
55. Figure B-16: $^{19}\text{F}$ NMR of <b>1-Ir(cnpy)<sub>2</sub></b> .....	111
56. Figure B-17: ESI-MS of <b>1-Ir(cnpy)<sub>2</sub></b> .....	112
57. Figure B-18: UV-vis of <b>1-Ir(cnpy)<sub>2</sub></b> .....	112
58. Figure B-19: $^1\text{H}$ NMR of <b>1-Ir(meopy)<sub>2</sub></b> .....	113

59. Figure B-20: UV-vis of <b>1-Ir(meopy)<sub>2</sub></b> .....	114
60. Figure B-21: <sup>1</sup> H NMR of <b>1-Ir(cfpy)<sub>2</sub></b> .....	115
61. Figure B-22: <sup>19</sup> F NMR of <b>1-Ir(cfpy)<sub>2</sub></b> .....	115
62. Figure B-23: UV-vis of <b>1-Ir(cfpy)<sub>2</sub></b> .....	116
63. Figure B-24: <sup>1</sup> H NMR of <b>1-Ir(clpy)<sub>2</sub></b> .....	117
64. Figure B-25: <sup>19</sup> F NMR of <b>1-Ir(clpy)<sub>2</sub></b> .....	117
65. Figure B-26: UV-vis of <b>1-Ir(clpy)<sub>2</sub></b> .....	118
66. Figure B-27: <sup>1</sup> H NMR of <b>1-Ir(dmap)<sub>2</sub></b> .....	119
67. Figure B-28: UV-vis of <b>1-Ir(dmap)<sub>2</sub></b> .....	119
68. Figure B-29: <sup>1</sup> H NMR of <b>1-Ir(NH<sub>3</sub>)<sub>2</sub></b> .....	120
69. Figure B-30: ESI-MS of <b>1-Ir(NH<sub>3</sub>)<sub>2</sub></b> .....	121
70. Figure B-31: UV-vis of <b>1-Ir(NH<sub>3</sub>)<sub>2</sub></b> .....	121
71. Figure B-32: <sup>1</sup> H NMR of <b>1b-Ir(NH<sub>3</sub>)<sub>2</sub></b> .....	122
72. Figure B-33: UV-vis of <b>1b-Ir(NH<sub>3</sub>)<sub>2</sub></b> .....	122
73. Figure B-34: <sup>1</sup> H NMR of <b>2-Ir(NH<sub>3</sub>)<sub>2</sub></b> .....	124
74. Figure B-35: <sup>19</sup> F NMR of <b>2-Ir(NH<sub>3</sub>)<sub>2</sub></b> .....	124
75. Figure B-36: UV-vis of <b>2-Ir(NH<sub>3</sub>)<sub>2</sub></b> .....	125
76. Figure B-37: <sup>1</sup> H NMR of <b>2b-Ir(NH<sub>3</sub>)<sub>2</sub></b> .....	125
77. Figure B-38: <sup>1</sup> H NMR of <b>2b<sub>2</sub>-Ir(NH<sub>3</sub>)<sub>2</sub></b> .....	126
78. Figure B-39: UV-vis of <b>2 b<sub>2</sub>-Ir(NH<sub>3</sub>)<sub>2</sub></b> .....	126
79. Table 2-1: Corrole nitrogen-metal bond lengths .....	30
80. Table 2-2: Reduction potentials for group 9 corroles .....	34
81. Table 3-1: Emission data for Ir(III) corroles .....	52
82. Table 4-1: Computed bond lengths for [ <b>1-M(NH<sub>3</sub>)<sub>2</sub></b> ] <sup>0/+</sup> .....	64
83. Table 4-2: Spin densities/energies for [ <b>1-M(NH<sub>3</sub>)<sub>2</sub></b> ] <sup>+</sup> .....	67
84. Table 4-3: Spin densities/energies for [ <b>1f-M(NH<sub>3</sub>)<sub>2</sub></b> ] <sup>+</sup> .....	69
85. Table C-1-1. Crystal data and structure refinement for <b>1-Ir(tma)<sub>2</sub></b> ...	130
86. Table C-1-2. Atomic coordinates and equivalent isotropic displacement parameters for <b>1-Ir(tma)<sub>2</sub></b> .....	133
87. Table C-1-3. Selected bond lengths and angles for <b>1-Ir(tma)<sub>2</sub></b> .....	134
88. Table C-1-4. Bond lengths and angles for <b>1-Ir(tma)<sub>2</sub></b> .....	135

89. Table C-1-5. Anisotropic displacement parameters for <b>1-Ir(tma)<sub>2</sub></b> ..	137
90. Table C-2-1. Crystal data and structure refinement for <b>1b-Ir(tma)<sub>2</sub></b>	140
91. Table C-2-2. Atomic coordinates and equivalent isotropic displacement parameters for <b>1b-Ir(tma)<sub>2</sub></b> .....	143
92. Table C-2-3. Selected bond lengths and angles for <b>1b-Ir(tma)<sub>2</sub></b> .....	145
93. Table C-2-4. Bond lengths and angles for <b>1b-Ir(tma)<sub>2</sub></b> .....	146
94. Table C-2-5. Anisotropic displacement parameters for <b>1b-Ir(tma)<sub>2</sub></b> .	149
95. Table C-3-1. Crystal data and structure refinement for <b>1-Ir(py)<sub>2</sub></b> .....	152
96. Table C-3-2. Atomic coordinates and equivalent isotropic displacement parameters for <b>1-Ir(py)<sub>2</sub></b> .....	155
97. Table C-3-3. Selected bond lengths and angles for <b>1-Ir(py)<sub>2</sub></b> .....	156
98. Table C-3-4. Bond lengths and angles for <b>1-Ir(py)<sub>2</sub></b> .....	157
99. Table C-3-5. Anisotropic displacement parameters for <b>1-Ir(py)<sub>2</sub></b> .....	160
100. Table C-3-6. Hydrogen bonding for <b>1-Ir(py)<sub>2</sub></b> .....	161
101. Table C-4-1. Crystal data and structure refinement for <b>1-Ir(dmap)<sub>2</sub></b> .	164
102. Table C-4-2. Atomic coordinates and equivalent isotropic displacement parameters for <b>1-Ir(dmap)<sub>2</sub></b> .....	172
103. Table C-4-3. Selected bond lengths and angles for <b>1-Ir(dmap)<sub>2</sub></b> .....	176
104. Table C-4-4. Bond lengths and angles for <b>1-Ir(dmap)<sub>2</sub></b> .....	177
105. Table C-4-5. Anisotropic displacement parameters for <b>1-Ir(dmap)<sub>2</sub></b> .	182
106. Table C-5-1. Crystal data and structure refinement for <b>1-Ir(NH<sub>3</sub>)<sub>2</sub></b> .	188
107. Table C-5-2. Atomic coordinates and equivalent isotropic displacement parameters for <b>1-Ir(NH<sub>3</sub>)<sub>2</sub></b> .....	195
108. Table C-5-3. Selected bond lengths and angles for <b>1-Ir(NH<sub>3</sub>)<sub>2</sub></b> .....	198
109. Table C-5-4. Bond lengths and angles for <b>1-Ir(NH<sub>3</sub>)<sub>2</sub></b> .....	199
110. Table C-5-5. Anisotropic displacement parameters for <b>1-Ir(NH<sub>3</sub>)<sub>2</sub></b> .	203

## NOMENCLATURE AND ABBREVIATIONS

**BILRC** Beckman Institute Laser Resource Center

**bpy** 2,2'-bipyridine

**btmfp** (bis)-3,5-trifluoromethylpyridine

**dcpy** 3,5-dichloropyridine

**cnp** 4-cyanopyridine

**cod** 1,5-cyclooctadiene

**COSY** correlation spectroscopy

**CV** cyclic voltammetry, cyclic voltammogram

**dcm** dichloromethane

**DFT** density functional theory

**dmap** 4-(N,N-dimethylamino)pyridine

**edta** ethylenediaminetetraacetic acid

**ESI** electrospray ionization

**HMBC** heteronuclear multiple-bond correlation

**HSQC** heteronuclear single-quantum correlation

**HOMO** highest occupied molecular orbital

**HPLC** high-performance liquid chromatography

**H<sub>3</sub>tpfc** 5,10,15-(tris)pentafluorophenylcorrole (tpfc is the trianionic form)

**H<sub>3</sub>tfc** 5,10,15-trifluorocorrole (tfc is the trianionic form)

**IC** Inorganic Chemistry (journal)

**ISC** inter-system crossing

**JACS** Journal of the American Chemical Society

**meopy** 4-methoxypyridine

**MS** mass spectrometry

**NBS** N-bromosuccinimide

**NMR** nuclear magnetic resonance

**ppm** parts per million

**py** pyridine

**SCE** saturated calomel electrode

**SOMO** singly occupied molecular orbital

**SSRL** Stanford Synchrotron Lightsource

***t*-4bpa** (tris)(4-bromophenyl)ammoniumyl hexachloroantimonate

**tma** trimethylamine

**TLC** thin-layer chromatography

**XAS** X-ray absorption spectroscopy

*Opening Remarks*

## A BRIEF INTRODUCTION

I'm an inveterate experimentalist, and for better or for worse, this thesis has come to reflect that. It is split into a large number of bite-sized chapters, much like my research here at Caltech, and I hope that the end result proves refreshing rather than disorienting. Harry Gray, my graduate supervisor, advised me to reformat rather than rewrite my published work, and the first four chapters of the thesis are published work presented here in essentially the same form as they have been presented to the larger scientific community (with some additional notes, changes to figures, formatting, and nomenclature for consistency between chapters, and introductory statements added in for flavor, background, and feel). The papers discussed herein include: my first JACS communication, "Iridium Corroles" (DOI: 10.1021/ja801049t); a detailed electronic structural study from IC entitled "Structures and Reactivity Patterns of Group 9 Metallocorroles" (DOI: 10.1021/ic901164r); another JACS communication focusing on corrole photophysics, "Near-IR Phosphorescence of Iridium(III) Corroles at Ambient Temperature" (DOI: 10.1021/ja101647t); and a computational study from IC, very recently published and performed in collaboration with members of Bill Goddard's group, entitled "Electronic Structures of Group 9 Metallocorroles with Axial Ammines" (DOI: 10.1021/ic1005902).

Additionally, two pieces of unpublished work will be presented. These include a description of some unique reactivity of an easily oxidized Ir(III) corrole complex, which will be presented as if it were a journal article, and a combined DFT, EPR, and XAS study of the electronic structures of a host of iridium corroles, which is less close to completion



and will be discussed only briefly. I have attempted to present these unpublished studies in a similar fashion to the published ones, but these latter chapters may have a slightly more informal tone in keeping with my own stylistic tendencies. I hope they will provide an interesting and informative read nonetheless.

## *Chapter 1*

### IRIDIUM CORROLES

A few months after showing up in the lab, I had a meeting with Harry Gray and Zeev Gross (of the Technion, in Haifa, Israel) where I apparently suggested that we might be able to use iridium(III) corroles to achieve the type of oxygen atom transfer reactions that had been demonstrated by Seth Brown and co-workers for George Wilkinson's trimesityliridium(III)/oxotimesityliridium(V) system. Synthetically, it took a lot of barking up a lot of trees before I located one that actually contained something interesting. In the beginning, I naively believed that iridium(III) or iridium(IV) chlorides could somehow be induced to give up their halide atoms and enter a deprotonated corrole coordination sphere as if waltzing into an octahedral chelate complex of bpy or edta. Not only that, but I thought that I would obtain a square-planar Ir(III) complex as well, one that could activate dioxygen bonds to form a square-planar oxoiridium(V) corrole. After all, it works for chromium, right?

As it turns out, both of these expectations were wildly inaccurate on a variety of counts. For one thing, octahedral Ir(III) complexes are notoriously kinetically inert, while Ir(IV) hexachloride and hexabromide compounds are highly oxidizing and liable to halogenate or otherwise degrade any electron-rich aromatics they stumble across in solution. In addition, the  $d^6$  Ir(III) ion is just not stable in a square-planar coordination environment, much preferring to form octahedral or pseudo-octahedral complexes (like every other low-spin  $d^6$  metal ion). In fact, even the three-coordinate Ir(III) complex that inspired my work is

horribly unstable; thus, it activates the strong O<sub>2</sub> double bond immediately upon exposure to air.

All of my initial attempts to incorporate iridium into a corrole having failed, I sought a new starting material that would be neither as inert as hexachloroiridium(III) nor as oxidizing (and therefore chlorinating) as hexachloroiridium(IV). I had some old [Ir(cod)Cl]<sub>2</sub> sitting around in a glove box from my prior attempts at producing iridium complexes of the Kläui ligand, and so, borrowing a J. Young NMR tube from Dave Weinberg in the Bercaw group, I resolved to attempt the synthesis of an Ir(III) corrole complex starting from an iridium(I) material which is neither inert nor capable of oxidizing much of anything. I was certain it would work, and I would have an oxoiridium(V) corrole complex by the next afternoon.

This time, unlike the last, I was 50% correct. The initial reaction run in d<sup>8</sup>-thf (thanks, BP!) at 90°C in a J. Young tube, produced a new set of sharply resolved proton NMR doublets in the corrole β-proton chemical shift region along with what appeared to be shifted cod peaks. These signals have been assigned to a four-coordinate iridium(I)(cod)(tpfc) in chemical analogy to products observed upon reaction of corroles with low-valent rhodium complexes, but this compound is very reactive and has not been isolated (full *in situ* characterization presents other difficulties, mostly owing to large quantities of [Ir(cod)Cl]<sub>2</sub> and K<sub>2</sub>CO<sub>3</sub> in the reaction mixture making both proton NMR and ESI-MS unpalatable). When tma N-oxide was added in excess to the warm reaction mixture, the color of the solution changed from brown to red, and a new deep red compound could be observed by TLC. What was this new compound? That, dear reader, is the subject of the JACS Communication presented in this section, Iridium Corroles.

### Iridium Corroles

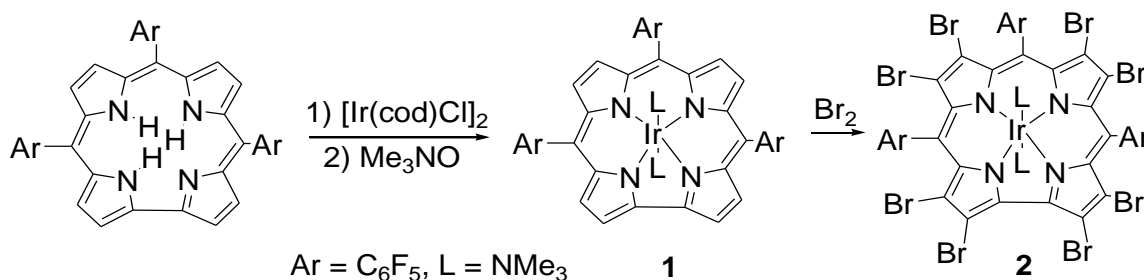
Reproduced with permission from: Joshua H. Palmer, Michael W. Day, Aaron D. Wilson, Lawrence M. Henling, Zeev Gross, and Harry B. Gray. *J. Am. Chem. Soc.*, **2008**, *130* (25), pp 7786–7787. Copyright 2008 American Chemical Society

Interest in the chemistry of iridium has accelerated greatly in recent years,<sup>1</sup> owing in part to reports of high-valent oxo and nitrido species as well as other complexes possessing wide ranging catalytic activities.<sup>2</sup> Concurrent with this increased interest, much effort has been directed toward the goal of developing new metallocorrole systems for applications including, but not limited to, medical diagnostics and therapeutics, as well as catalysis.<sup>3</sup> This recent surge in corrole research is due in large part to the development of facile methods for the synthesis of the stable 5,10,15-*tris*-pentafluorophenylcorrole [ $\text{H}_3\text{tpfc}$ ;  $\text{tpfc}$  (**1**) is the trianionic form] synthon and of other *tris*-aryl-substituted corroles.<sup>4,5</sup>

First-row transition metal corroles exhibit striking reactivity, including the activation of  $\text{O}_2$  by trivalent chromium,<sup>6</sup> manganese,<sup>7</sup> and iron;<sup>8</sup> catalytic reduction of  $\text{CO}_2$  by iron(I) and cobalt(I);<sup>9</sup> and iron(IV)-mediated aziridination of olefins.<sup>10</sup> Metals in high oxidation states enjoy the strong  $\sigma$ -donor environment of corroles; this property is typified by stable nitrido chromium(VI) and manganese(VI) species.<sup>11</sup> Several second-row transition metals also form stable corrole complexes: (oxo)molybdenum(V);<sup>12</sup> ruthenium(III), as triply bonded Ru-Ru dimers and nitric oxide bound monomers;<sup>13</sup> rhodium(III), which catalyzes carbene-transfer reactions;<sup>14</sup> and silver(III).<sup>15</sup> It is noteworthy that hitherto there has been only one report of a third-row metallocorrole, an (oxo)rhenium(V) species.<sup>16</sup>

Trianionic ligands should stabilize high oxidation states of iridium, so an Ir(III) corrole might be as reactive as porphyrinic Ir(II) toward substrates.<sup>17</sup> Herein we report the first fully characterized corrolato Ir(III) complex,  $(\text{tpfc})\text{Ir(III)}(\text{tma})_2$  [**1-Ir(tma)**]<sub>2</sub>, and an

octabromo- $\beta$ -pyrrole derivative,  $(\text{Br}_8\text{-tpfc})\text{Ir(III)}(\text{tma})_2$  [**1b-Ir(tma)**<sub>2</sub>], where tma = trimethylamine (Scheme 1:1).



Scheme 1-1: Synthesis of iridium(III) corroles

Compound **1-Ir(tma)**<sub>2</sub> was obtained in 27% yield *via* reaction of H<sub>3</sub>tpfc with excess [Ir(cod)Cl]<sub>2</sub> (cod = cyclooctadiene) and K<sub>2</sub>CO<sub>3</sub> in hot THF under Ar to form (tpfc)Ir(I)(cod), which was converted to an axially tma-ligated Ir(III) complex upon addition of tma *N*-oxide and exposure to the atmosphere.<sup>18</sup> Full bromination of **1-Ir(tma)**<sub>2</sub> was achieved via reaction with excess Br<sub>2</sub> in methanol, providing green crystals of **1b-Ir(tma)**<sub>2</sub> in about 65% yield.<sup>19</sup> Both complexes were fully characterized by spectroscopy, electrochemistry, and X-ray diffraction as six-coordinate Ir(III) corroles. The <sup>19</sup>F and <sup>1</sup>H NMR spectra (Figure 1-1, and Supporting Information) demonstrate that they are diamagnetic (sharp resonances), possess high symmetry (only one type of *ortho*-F for any C<sub>6</sub>F<sub>5</sub> ring), and contain two axial tma groups (18 H atoms at −2.96 ppm for **1-Ir(tma)**<sub>2</sub> and −2.59 ppm for **1b-Ir(tma)**<sub>2</sub>).

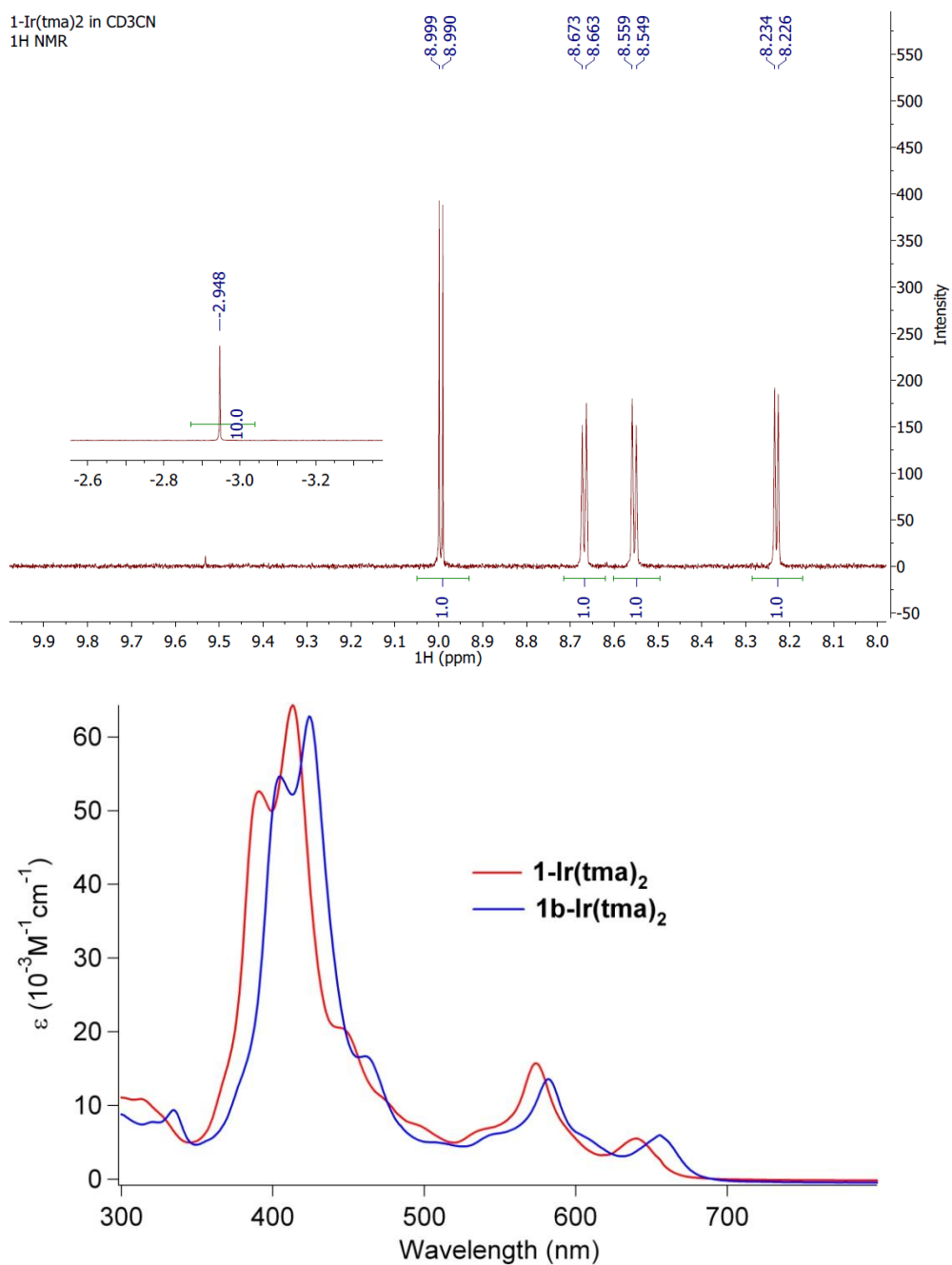


Figure 1-1: <sup>1</sup>H NMR spectrum of **1** in CD<sub>3</sub>CN (top, inset is the tma methyl proton resonances) and UV-vis spectra of **1-Ir(tma)<sub>2</sub>** (red, higher energy) and **1b-Ir(tma)<sub>2</sub>** (blue, lower energy) in toluene (bottom)

The red shifts of the principal features in the electronic spectrum of **1b-Ir(tma)<sub>2</sub>** relative to **1-Ir(tma)<sub>2</sub>** (8–16 nm, Figure 1-1) are similar to those observed upon bromination of

other metallocorroles,<sup>6,20</sup> but the intense Soret band system is uniquely split, as are the Q-bands (roughly 70 nm). We suggest that the shoulders at 448 and 458 nm for **1-Ir(tma)<sub>2</sub>** and **1b-Ir(tma)<sub>2</sub>**, respectively, are attributable to MLCT transitions, and that couplings to these excited states give rise to large splittings of the corrole-based  $\pi$ - $\pi^*$  states. Based on HOMO and LUMO energies extracted from the redox potentials of **1b-Ir(tma)<sub>2</sub>**, the MLCT transitions should indeed fall in the 400–500 nm region of the visible spectrum.

Cyclic voltammetry (CV, Figure 1-2)<sup>21</sup> reveals that Ir(III) corroles are very electron-rich: Ir(II) is not electrochemically accessible and Ir(IV) is obtained at relatively low potentials. Only **1b-Ir(tma)<sub>2</sub>** could be reduced within the electrochemical window of the solvent and the reversibility of that process ( $E_{1/2} = -1.21$  V vs. SCE) is consistent with the formation of a corrole radical anion rather than Ir(II), as the latter would rapidly release its axial ligand(s) and most likely also dimerize.<sup>17</sup> All other reversible electron transfer processes are also obtained at quite positive potentials. Guided by the electrochemistry of other metallocorroles,<sup>8</sup> the first and second redox processes of **1-Ir(tma)<sub>2</sub>** ( $E_{1/2} = +0.66$  and  $+1.28$  V vs. SCE, respectively) may tentatively be assigned as metal-centered ( $\text{Ir}^{\text{III}}/\text{Ir}^{\text{IV}}$ ) and corrole-centered ( $\text{tpfc}/\text{tpfc}^+$ ), respectively. As full bromination at the  $\beta$ -pyrrole positions is known to upshift the potentials of metallocorroles by a few hundred mV,<sup>6,20</sup> the feature at  $+1.19$  V can be assigned to the  $\text{Ir}^{\text{III}}/\text{Ir}^{\text{IV}}$  couple in **1b-Ir(tma)<sub>2</sub>**. Our data show clearly that Ir(III) is more electron-rich in corroles than in other coordination environments. The  $E_{1/2}$  value for the  $[(\text{tpp})\text{Ir}]^+ / [(\text{tpp})\text{Ir}]^{2+}$  ( $\text{tpp} = \text{tetraphenylporphyrinato}$ ) redox couple is about  $+1.4$  V vs. SCE,<sup>22</sup> and  $\text{Ir}^{\text{III}}/\text{Ir}^{\text{IV}}$  processes in cyclometalated bpy complexes also occur at much more positive potentials than in **1-Ir(tma)<sub>2</sub>**.<sup>23</sup>

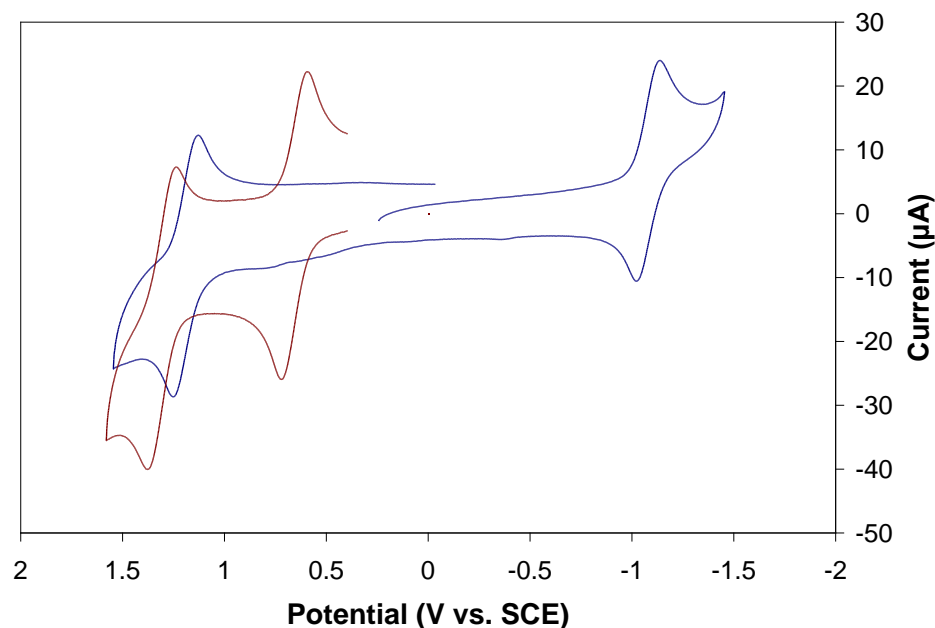


Figure 1-2: CV traces of **1-Ir(tma)<sub>2</sub>** (red) and **1b-Ir(tma)<sub>2</sub>** (blue) in CH<sub>2</sub>Cl<sub>2</sub> solution at 23 °C

The molecular structures of **1-Ir(tma)<sub>2</sub>** and **1b-Ir(tma)<sub>2</sub>** (Figure 1-3) reveal that their macrocyclic frameworks are isostructural, with the iridium atom located in the plane of an essentially flat corrole.<sup>24</sup> The Ir-N axial bonds are about 0.2 Å longer than the in-plane Ir-N equatorial bonds, as might be expected. The one clear difference between **1-Ir(tma)<sub>2</sub>** and **1b-Ir(tma)<sub>2</sub>** is that the aryl rings are nearly perpendicular with respect to the corrole in the latter to avoid steric clash with the bromine atoms. The structure of **1b-Ir(tma)<sub>2</sub>** is distinctly different from those of analogous tetraarylporphyrins, where  $\beta$ -pyrrole bromination induces large distortions of the macrocycle that produce dramatic red shifts in UV-vis absorptions and higher reduction potentials.<sup>25</sup> For iridium corroles, the 530 mV upshift in the potential of **1b-Ir(tma)<sub>2</sub>** vs. **1-Ir(tma)<sub>2</sub>** implies major Br-induced electronic effects.



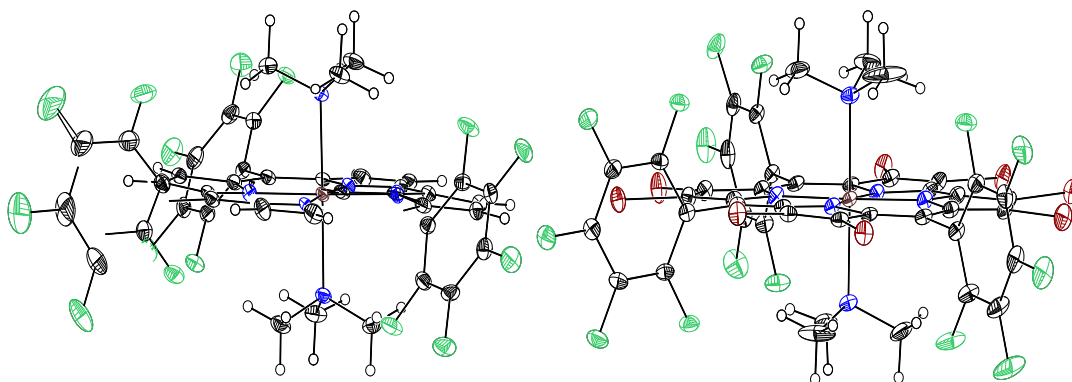


Figure 1-3: X-ray structures of **1-Ir(tma)<sub>2</sub>** (left) and **1b-Ir(tma)<sub>2</sub>** (right): 50% probability displacement ellipsoids. Average distances (Å), for **1-Ir(tma)<sub>2</sub>**, **1b-Ir(tma)<sub>2</sub>**: Ir-N(equatorial), 1.965(9), 1.974(3); Ir-N(axial), 2.185(9), 2.189(3)

We have demonstrated that a corrole can readily accommodate a 5d transition metal in our work on the first nonorganometallic Ir(III) porphyrinoid. We also report an X-ray diffraction structure of a fully brominated derivative. The electron transfer processes demonstrated for **1-Ir(tma)<sub>2</sub>** and **1b-Ir(tma)<sub>2</sub>** suggest that they may prove useful as redox catalysts. Studies are in progress to develop methodologies for opening an axial coordination site on the metal, a requirement for testing the catalytic potential of these complexes.

**Acknowledgment:** This work was supported by the US-Israel BSF (Z.G. and H.B.G.), BP, NSF, CCSER (Gordon and Betty Moore Foundation), and the Arnold and Mabel Beckman Foundation (H.B.G.).

## References

- (1) (a) Jacobi, B. G.; Laitar, D. S.; Pu, L.; Wargocki, M. F.; DiPasquale, A. G.; Fortner, K. C.; Schuck, S. M.; Brown, S. N. *Inorg. Chem.* **2002**, *41*, 4815–4823. (b) Crowhurst, J.C.; Goncharov, A.F.; Sadigh, B.; Evans, C.L.; Morrall, P. G.; Ferreira, J. L.; Nelson, A. J. *Science*. **2006**, *311*, 1275–1278.
- (2) McDaniel, N. D.; Coughlin, F. L.; Tinker, L. L.; Bernhard, S. *J. Am. Chem. Soc.* **2008**, *130*, 210–217. Lai, R-Y.; Surekha, K.; Hayashi, A.; Ozawa, F.; Liu, Y-H.; Peng, S-M.; Liu, S-T. *Organomet.* **2007**, *26*, 1062–1068.
- (3) Aviv, I.; Gross, Z. *Chem. Commun.* **2007**, *20*, 1987–1999. Gershman, Z.; Goldberg, I.; Gross, Z. *Angew. Chem Int. Ed.* **2007**, *46*, 4320–4324. Gross, Z.; Gray, H.B. *Adv. Synth. Catal.* **2004**, *346*, 165–170. Gryko, D. T.; Fox, J. P.; Goldberg, D. P. *J. Porphyrins Phthalocyanines* **2004**, *8*, 1091–1105.
- (4) Gross, Z.; Galili, N.; Saltsman, I. *Angew. Chem. Int. Ed. Eng.* **1999**, *38*, 1427–9. Gross, Z.; Galili, N.; Simkhovich, L.; Saltsman, I.; Botoshansky, M.; Blaser, D.; Boese, R.; Goldberg, I. *Org. Lett.* **1999**, *1*, 599–602.
- (5) Koszarna, B.; Gryko, D.T. *J. Org. Chem.* **2006**, *71*, 3707–3717. Nardis, S.; Monti, D.; Paolesse, R. *Mini-Rev. Org. Chem.* **2005**, *2*, 355–372.
- (6) Mahammed, A.; Gray, H. B.; Meier-Callahan, A. E.; Gross, Z. *J. Am. Chem. Soc.* **2003**, *125*, 1162–1163.
- (7) Ou, Z.; Erben, C.; Autret, M.; Will, S.; Rosen, D.; Lex, J.; Vogel, E.; Kadish, K. M. *J. Porphyrins Phthalocyanines*. **2005**, *9*, 398–412.
- (8) Simkhovich, L.; Mahammed, A.; Goldberg, I.; Gross, Z. *Chem. Eur. J.* **2001**, *7*, 1041–1055.
- (9) Grodkowski, J.; Neta, P.; Fujita, E.; Mahammed, A.; Simkhovich, L.; Gross, Z. *J. Phys. Chem. A*. **2002**, *106*, 4772–4778.
- (10) Simkhovich, L.; Gross, Z. *Tet. Lett.* **2001**, *42*, 8089–8092.
- (11) (a) Golubkov, G.; Gross, Z. *Angew. Chem. Int. Ed.* **2003**, *42*, 4507–4510. (b) Golubkov, G.; Gross, Z. *J. Am. Chem. Soc.* **2005**, *127*, 3258–3259.
- (12) Luobeznova, I.; Raizman, M.; Goldberg, I.; Gross, Z. *Inorg. Chem.* **2006**, *45*, 386–394.
- (13) Simkhovich, L.; Luobeznova, I.; Goldberg, I.; Gross, Z. *Chem. Eur. J.* **2003**, *9*, 201–208.
- (14) Saltsman, I.; Simkhovich, L.; Balazs, Y.; Goldberg, I.; Gross, Z. *Inorg. Chim. Acta.* **2004**, *357*, 3038–3046.
- (15) Bruckner, C.; Barta, C. A.; Brinas, R. P.; Krause Bauer, J. A. *Inorg. Chem.* **2003**, *42*, 1673–1680.
- (16) Tse, M. K.; Zhang, Z.; Mak, T. C. W.; Chan, K. S. *Chem. Commun.* **1998**, 1199–1200.
- (17) Iridium(II) porphyrins react readily with olefins; they also form Ir–Ir bonded dimers (de Bruin, B.; Hetterscheid, D.G.H. *Eur. J. Inorg. Chem.* **2007**, 211–230. Song, X.; Chan, K.S. *Organomet.* **2007**, *26*, 965–970). Nearly all reported iridium(III) porphyrins are organometallic in nature (Zhai, H.; Bunn, A.; Wayland, B. *Chem. Commun.* **2001**, 1294–1295).
- (18) H<sub>3</sub>tpfc (80 mg), [Ir(cod)Cl]<sub>2</sub> (335 mg), and K<sub>2</sub>CO<sub>3</sub> (140 mg) were dissolved/suspended in 150 mL of degassed THF, and the mixture was refluxed under argon for 90 min (until the corrole fluorescence was negligible to the eye upon long-wave irradiation with a hand-held lamp). Tma N-oxide (110 mg) was added, and the solution was allowed to slowly cool to room temperature while open to the laboratory atmosphere. Column chromatography of the black solution (silica, 4:1 hexanes:CH<sub>2</sub>Cl<sub>2</sub>) provided purple crystals of (tpfc)Ir(III)(tma)<sub>2</sub> (30 mg, 27% yield). <sup>1</sup>H NMR (CD<sub>2</sub>Cl<sub>2</sub>): δ 8.93 (d, 2H), 8.54 (d, 2H), 8.42 (d, 2H), 8.12 (d, 2H), –2.96 (s, 18H). <sup>19</sup>F NMR (CD<sub>2</sub>Cl<sub>2</sub>): δ –139.1 (m, 6H), –156.2 (m, 3H), –164.3 (m, 6H). MS (ESI): 1105.1 ([M<sup>+</sup>]), 1046.0 ([M<sup>+</sup>–tma]), 986.5 ([M<sup>+</sup>–2tma]). UV–vis (nm): 390, 412, 448 (sh), 572, 638.
- (19) Complex **1** (15 mg) and Br<sub>2</sub> (70 μL) were dissolved in 20 mL MeOH and stirred overnight. Column chromatography (silica, 4:1 hexanes:CH<sub>2</sub>Cl<sub>2</sub>) of the red solution provided green crystals of (Br<sub>8</sub>–tpfc)Ir(III)(tma)<sub>2</sub> (15 mg, 63% yield). <sup>1</sup>H NMR (CD<sub>2</sub>Cl<sub>2</sub>): δ –2.59 (s, 18H). <sup>19</sup>F NMR (CD<sub>2</sub>Cl<sub>2</sub>): δ –138.4 (q, 2H), –139.0 (q, 4H), –153.9 (t, 3H), –164.4 (m, 4H), –164.7 (m, 2H). UV–vis (nm): 406, 422, 458 (sh), 580, 646.
- (20) Golubkov, G.; Bendix, J.; Gray, H. B.; Mahammed, A.; Goldberg, I.; DiBilio, A. J.; Gross, Z. *Angew. Chem. Int. Ed. Eng.* **2001**, *40*, 2132–2134.
- (21) In degassed CH<sub>2</sub>Cl<sub>2</sub> solutions under Ar containing 0.3 M NEt<sub>4</sub>BF<sub>4</sub>, using a glassy carbon disk working electrode, a Pt wire auxiliary electrode, and a Ag/AgCl quasi-reference electrode.
- (22) Kadish, K. M.; Deng, Y. J.; Yao, C-L.; Anderson, J. E. *Organomet.* **1988**, *7*, 1979–1983.

- 
- (23) King, K. A.; Watts, R. J. *J. Am. Chem. Soc.* **1987**, *109*, 1589–1590.
- (24) The macrocyclic framework of a fully brominated cobalt corrole also is flat (Paolesse, R.; Nardis, S.; Sagone, F.; Khoury, R.G. *J. Org. Chem.* **2001**, *66*, 550–556)
- (25) Ou, Z.; Shao, J.; D'Souza, F.; Tagliatesta, P.; Kadish, K.M. *J. Porphyrins Pthalocyanines*. **2004**, *8*, 201–214, and references therein.

*Chapter 2*STRUCTURES AND REACTIVITY PATTERNS OF GROUP 9  
METALLOCORROLES

In “Iridium Corroles,” I detailed the synthesis, characterization, and electrochemical properties of the corroles **1-Ir(tma)<sub>2</sub>** and **1b-Ir(tma)<sub>2</sub>**. I also assigned the lower-potential redox process in these systems to a metal-based oxidation, claiming that corroles, because of their powerful sigma-donating properties, have a unique ability to stabilize higher-valent transition metal ions. Having the first fully characterized set of third-row metallocorroles in hand, I wanted to compare their properties with those of more well-studied first and second row metallocorrole derivatives. The first order of business was to develop syntheses for Ir(III) corroles analogous to known Co(III) and Rh(III) derivatives. Since the pyridine- and triphenylphosphine-ligated tpfc compounds of both cobalt and rhodium had been published previously by my Israeli collaborator Zeev, I decided to go after Ir(III) corroles with axial py and PPh<sub>3</sub> ligands.

The synthesis of **1-Ir(py)<sub>2</sub>** was achieved in a fashion similar to that which produced the original tma-ligated corrole complexes; however, instead of using the N-oxide as both oxidant and ligand source, I found I could simply add pyridine and allow oxygen to enter the reaction mixture at the same time. This simple procedure would form the basis of most of my future synthetic endeavors in the Ir(III) corrole arena, and in fact I have used it (with greater or lesser success depending on the ligand) to produce analogous compounds with dimethylaminopyridine (dmap), 4-cyanopyridine (cnpy), 4-methoxypyridine (meopy), 3,5-(bis)trifluoromethylpyridine (cfpy), 3,5-dichloropyridine (dcpy), and ammine axial ligands.

The triphenylphosphine-ligated Ir(III) complex **1-Ir(PPh<sub>3</sub>)** could also be synthesized in this fashion, but unlike the corroles with N-donor axial ligands, the phosphine-ligated complex is only five coordinate unless large excesses of an additional axial ligand are introduced.

After I had completed the syntheses of the two iridium complexes, it was time to compare their properties with the analogous cobalt and rhodium corroles. A postdoctoral fellow in Zeev Gross' lab, Atif Mahammed, graciously provided me with the Co and Rh derivatives **1-Co(PPh<sub>3</sub>)**, **1-Rh(PPh<sub>3</sub>)**, **1-Co(py)<sub>2</sub>**, and **1-Rh(py)<sub>2</sub>**. I set out to compare: the structural parameters of the complexes; their UV-vis absorption spectra; their electrochemical properties; their affinities for a sixth ligand (in the case of the PPh<sub>3</sub>-ligated compounds); and, finally, the nature of their one-electron oxidized forms.

The XRD structures of the rhodium and iridium py-ligated corroles are quite similar, whereas the cobalt complex possesses significantly foreshortened bonds between the central metal and the surrounding nitrogen atoms. Additionally, the Co(III) corrole complexes are quite labile; unlike their 4d and 5d analogues, the complexes **1-Co(PPh<sub>3</sub>)** and **1-Co(py)<sub>2</sub>** can be rapidly interconverted by the introduction of excess ligand. Furthermore, the preference of **1-Co(PPh<sub>3</sub>)** for a five-coordinate geometry is staggeringly larger than that of the Rh(III) and Ir(III) derivatives (presumably owing to the increased van der Waals radii and electropositivity of the second and third row metals); addition of a 100,000-fold excess of triphenylphosphine to a solution of **1-Co(PPh<sub>3</sub>)** causes almost no change in the observed absorption spectrum, whereas **1-Rh(PPh<sub>3</sub>)** and **1-Ir(PPh<sub>3</sub>)** can be converted to their six-coordinate forms by the addition of thousands and hundreds of equivalents of PPh<sub>3</sub>, respectively.

In terms of molecular structure and bonding, the Co(III) complexes differ significantly from the Rh(III) and Ir(III) compounds, but in terms of electronic structure, it is the iridium that stands apart from the pack. The **1-M(py)<sub>2</sub>** complexes possess similar formal M<sup>IV/III</sup> reduction potentials of approximately 0.7 V vs. Ag/AgCl in dcm solution, and they can all be oxidized by either the persistent organic radical oxidant (tris)(4-bromophenyl)ammoniumyl hexachloroantimonate (**t-4bpa**) or by large excesses of iodine. By UV-vis spectroscopy, the one-electron oxidized compounds look quite similar, displaying weak transitions in the red that have been associated in the literature with corrole radical cations. However, the EPR spectrum of the iridium complex could hardly be more different from the spectra of its 3d and 4d analogues. Both the formal “Co(IV)” and “Rh(IV)” corroles (with either py or PPh<sub>3</sub> axial ligands) display isotropic g tensors close to the free-electron value of 2.0023. The implication in this case is that the radical is essentially organic and carbon-centered (i.e., the oxidation is ligand-centered), consistent with the UV-vis results. On the other hand, the one-electron oxidized iridium complexes **[1-Ir(py)<sub>2</sub>]<sup>+</sup>** and **[1-Ir(tma)<sub>2</sub>]<sup>+</sup>** possess extremely anisotropic g tensor components and rhombic EPR spectra; these parameters are inconsistent with a carbon-based organic radical but similar to the expected spectra for a low-spin, d<sup>5</sup> metal ion (for example, the low-spin Fe(III) complex **1-Fe(py)<sub>2</sub>** displays this type of spectrum). Thus, I concluded that the oxidation of the Ir(III) complexes occurs on the metal instead of the ligand, and that corrole complexes of third-row metals might be able to open up new types of reactivity owing to the ability of the electron-donating macrocycles to stabilize high-valent transition metal ions. The view of the one-electron oxidized product as a pure Ir(IV) complex has been challenged by recently published theoretical work as well as unpublished XAS and DFT

studies, and these contributions will be discussed at length later in the thesis. However, the bulk of the experimental evidence, particularly the EPR spectroscopy, still suggests that the description of the one-electron oxidized products as Ir(IV) complexes is an acceptable designation.

The work summarized above was collated, edited, and interpreted over a long period of time, and finally resulted in the paper below. Many thanks are due to Kyle Lancaster, a fellow graduate student in the Gray lab, for introducing me to practical EPR spectroscopy and sparking my interest in the somewhat arcane subject of electronic structural studies. Without the early introduction of EPR spectroscopy to my arsenal (an obligatory tool in hindsight), I do not think this paper could have been written. In any case, the Inorganic Chemistry article “Structures and Reactivity Patterns of Group 9 Metallocorroles” is presented below.

### Structures and Reactivity Patterns of Group 9 Metallocorroles

Reproduced with permission from: Joshua H. Palmer, Atif Mahammed, Kyle M. Lancaster, Zeev Gross, and Harry B. Gray. *Inorg. Chem.*, **2009**, 48 (19), pp 9308–9315. Copyright 2009 American Chemical Society

**Abstract:** Group 9 metallocorroles **1-M(PPh<sub>3</sub>)** and **1-M(py)<sub>2</sub>** [**M** = Co(III), Rh(III), Ir(III); **1** denotes the trianion of 5,10,15-*tris*-pentafluorophenylcorrole] have been fully characterized by structural, spectroscopic, and electrochemical methods. Crystal structure analyses reveal that average metal-N(pyrrole) bond lengths of the bis-pyridine metal(III) complexes increase from Co (1.886 Å) to Rh (1.957 Å)/Ir (1.963 Å); and the average metal-N(pyridine) bond lengths also increase from Co (1.995 Å) to Rh (2.065 Å)/Ir (2.059 Å). Ligand affinities for **1-M(PPh<sub>3</sub>)** axial coordination sites increase dramatically in the order **1-Co(PPh<sub>3</sub>)** < **1-Rh(PPh<sub>3</sub>)** < **1-Ir(PPh<sub>3</sub>)**. There is a surprising invariance in the **M(+/0)** reduction potentials within the five- and six-coordinate corrole series, and even between them; the average **M(+/0)** potential of **1-M(PPh<sub>3</sub>)** is 0.78 V vs. Ag/AgCl in CH<sub>2</sub>Cl<sub>2</sub> solution, whereas that of **1-M(py)<sub>2</sub>** is 0.70 V under the same conditions. Electronic structures of one-electron-oxidized **1-M(py)<sub>2</sub>** complexes have been assigned by analysis of EPR spectroscopic measurements: oxidation is corrole-centered for **1-Co(py)<sub>2</sub>** (*g* = 2.008) and **1-Rh(py)<sub>2</sub>** (*g* = 2.003), and metal-centered for **1-Ir(tma)<sub>2</sub>** (*g<sub>zz</sub>* = 2.489, *g<sub>yy</sub>* = 2.010, *g<sub>xx</sub>* = 1.884, *g<sub>av</sub>* = 2.128) and **1-Ir(py)<sub>2</sub>** (*g<sub>zz</sub>* = 2.401, *g<sub>yy</sub>* = 2.000, *g<sub>xx</sub>* = 1.937, *g<sub>av</sub>* = 2.113).

### Introduction

Systematic investigations of transition metal corrole complexes have accelerated recently due to major advances in synthetic methods.<sup>1,2,3</sup> Many of these complexes, especially of



first-row transition metals, exhibit striking reactivity: iron(IV) derivatives remain the only non-copper catalysts for the aziridination of olefins by chloramine-T;<sup>4</sup> manganese(III) forms (oxo)manganese(V) during oxygenation catalysis;<sup>5</sup> chromium(III) mediates the aerobic oxidation of thiophenol to diphenyl disulfide;<sup>6</sup> and iron(I) and cobalt(I) corroles catalyze the reduction of carbon dioxide.<sup>7</sup> These reactivity patterns highlight the role of strong corrole  $\sigma$ -donation in the activation of low-valent metal centers.<sup>8</sup> This same electronic property, which accounts for the unusual stability of nitrido chromium(VI) and manganese(VI) complexes,<sup>9</sup> clearly is an important factor in metallocorrole-catalyzed processes.<sup>10</sup> Complexes of triarylcorroles with group 13–15 elements have been characterized as well, often with a focus on photophysical properties;<sup>11</sup> importantly, a gallium(III) corrole has been shown to be both an *in vivo* imaging agent and an anticancer drug candidate.<sup>12</sup> Second-row metallocorroles have not been investigated extensively, although there are reports of silver(III),<sup>13</sup> ruthenium(III),<sup>14</sup> and rhodium(III) derivatives, with the latter functioning as a catalyst in carbene-transfer reactions.<sup>15</sup> An (oxo)molybdenum(V) corrole also has been characterized.<sup>16</sup>

Third-row transition metal corroles are extremely rare, with fully characterized (oxo)Re(V) and Ir(III) compounds representing the only known oxidation states.<sup>17,18</sup> We predicted that trianionic corroles, based on their ability to stabilize numerous metals in high oxidation states,<sup>19</sup> would greatly stabilize iridium(III) and that these derivatives would exhibit strikingly different redox properties than iridium(III) porphyrins or organoiridium(III) complexes such as [Ir(ppy)<sub>3</sub>] (ppy = 2-phenylpyridine, Figure 2-1). Indeed, Ir(III) corroles can be stabilized even by weakly donating axial ligands, whereas Ir(III) porphyrins are only stable when the metal is further coordinated by organometallic

ligands [such as in (por)Ir(CO)Cl and (por)Ir-R, where por stands for the porphyrin dianion and R = alkyl or hydride)].<sup>20</sup>

A stable six-coordinate (tpfc)Ir(tma)<sub>2</sub> complex (**1-Ir(tma)<sub>2</sub>**, Figure 2-2) was obtained via the reaction of [Ir(cod)Cl]<sub>2</sub> with 5,10,15-*tris*-pentafluorophenylcorrole (H<sub>3</sub>tpfc), followed by treatment with tma-N-oxide.<sup>21</sup> Treatment of **1-Ir(tma)<sub>2</sub>** with elemental bromine in methanol yielded an octabromo complex (Br<sub>8</sub>-tpfc)Ir(tma)<sub>2</sub> (**1b-Ir(tma)<sub>2</sub>**, Figure 2-2); both iridium(III) derivatives were characterized by nuclear magnetic resonance (NMR) spectroscopy, mass spectrometry (MS), X-ray crystallography, UV-vis spectroscopy, and cyclic voltammetry (CV). The planar macrocyclic framework in both **1-Ir(tma)<sub>2</sub>** and **1b-Ir(tma)<sub>2</sub>** is quite unlike that of porphyrins, which tend to saddle or ruffle when brominated.<sup>22</sup> In addition, the electrochemical data suggested that the metal, rather than the macrocycle, is oxidized to Ir(IV) in both complexes, in contrast with recent findings for analogous cobalt(III) corroles.<sup>23</sup>

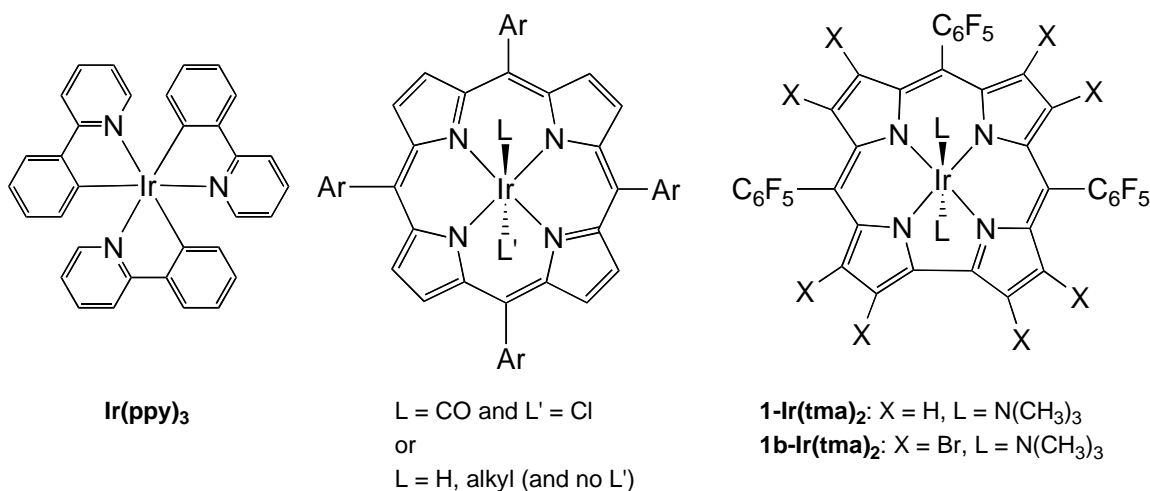


Figure 2-1: Complexes of 2-phenylpyridine, porphyrins, and corroles with iridium(III)

Here we report the synthesis and characterization of corroles **1-Ir(py)<sub>2</sub>** and **1-Ir(PPh<sub>3</sub>)**, whose properties are compared with those of isostructural cobalt(III) and rhodium(III) analogues **1-Co(py)<sub>2</sub>**, **1-Rh(py)<sub>2</sub>**, **1-Co(PPh<sub>3</sub>)**, and **1-Rh(PPh<sub>3</sub>)** (Figure 2-2). Each set, **1-M(py)<sub>2</sub>** or **1-M(PPh<sub>3</sub>)**, represents a rare example of an entire transition metal group with the same oxidation state and coordination number, another being the Group 8 (por)M-CO series.<sup>24</sup> Our research has focused on the substitutional lability of Group 9 metallocorroles and the sites of oxidation reactions, as both change markedly within the group. We have found that: Co(III) corroles are far more substitutionally labile than analogous Rh(III) or Ir(III) derivatives; the affinity of five-coordinate **1-M(PPh<sub>3</sub>)** for a sixth ligand increases dramatically down the row; and oxidation of **1-M(py)<sub>2</sub>** occurs primarily on the metal rather than on the macrocyclic ligand only in the case of iridium (Ir<sup>III/IV</sup>). We report extensive electronic absorption, electrochemical, and EPR data that support these conclusions.

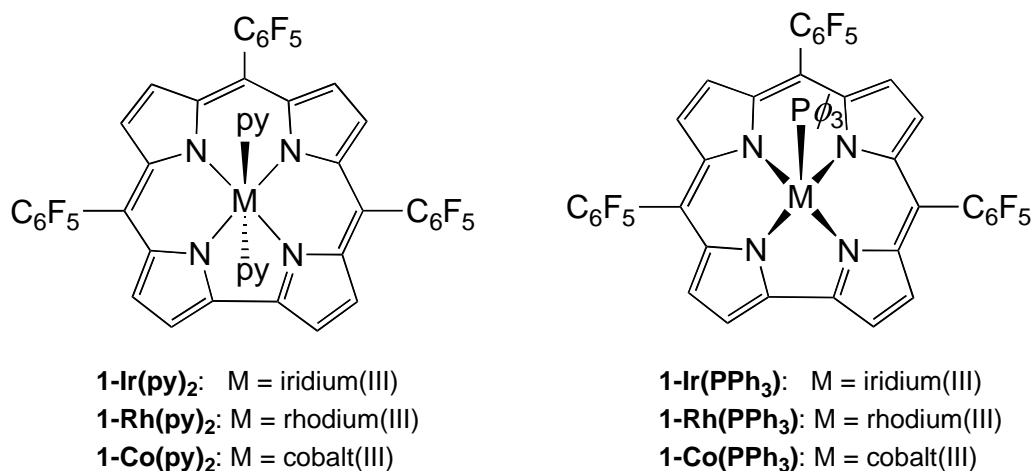


Figure 2-2: Axially ligated metal(III) corroles (py = pyridine)

## Experimental Section

**Materials.** Silica gel for column chromatography (Silica Gel 60, 63-200 micron mesh) was obtained from EMD Chemicals, as were all solvents (THF, toluene,  $\text{CH}_2\text{Cl}_2$ , hexanes, and methanol). Most starting materials for syntheses were from Sigma-Aldrich and used without further purification. Exceptions are pyrrole and pentafluorobenzaldehyde, which were both purified by vacuum distillation before use. Tetrabutylammonium hexafluorophosphate, which was used as a supporting electrolyte in the CV experiments, was also from Sigma-Aldrich and used without further purification. Electrodes for CV were obtained from CH Instruments.

**Syntheses.** The synthesis of 5,10,15-*tris*-pentafluorophenylcorrole (the  $\text{H}_3\text{tpfc}$  ligand) was accomplished by a simplified version of the standard procedure outlined in reference 1c.<sup>25</sup> The cobalt(III) and rhodium(III) corroles were available from previous studies.<sup>15,26</sup> Compounds **1-Ir(tma)<sub>2</sub>** and **1b-Ir(tma)<sub>2</sub>** have only been reported in a previous communication,<sup>18</sup> hence their syntheses are summarized below along with those of the new corroles.

**5,10,15-*tris*-pentafluorophenylcorrolato-iridium(III) *bis*-trimethylamine, 1-Ir(tma)<sub>2</sub>.**  $\text{H}_3\text{tpfc}$  (80 mg),  $[\text{Ir}(\text{cod})\text{Cl}]_2$  (335 mg), and  $\text{K}_2\text{CO}_3$  (140 mg) were dissolved/suspended in 150 mL of degassed THF, and the mixture was heated at reflux under argon for 90 min (until corrole fluorescence was negligible to the eye upon long-wavelength irradiation with a hand-held lamp). Tma N-oxide (110 mg) was added, and the solution was allowed to slowly cool to room temperature while open to the laboratory atmosphere. Column chromatography of the black mixture (silica, 4:1 hexanes: $\text{CH}_2\text{Cl}_2$ ) provided an auburn

solution, from which purple crystals of (tpfc)Ir(III)(tma)<sub>2</sub> (30 mg, 27% yield) could be grown by slow evaporation. <sup>1</sup>H NMR (CDCl<sub>3</sub>): δ 8.90 (d, 2H, J = 4.2), 8.50 (d, 2H, J = 5.1), 8.38 (d, 2H, J = 4.5), 8.09 (d, 2H, J = 4.2), -2.95 (s, 18H). <sup>19</sup>F NMR (CDCl<sub>3</sub>): δ -138.38 (m, 6F), -154.89 (m, 3F), -163.27 (m, 6F). MS (ESI): 1105.1 ([M<sup>+</sup>]), 1046.0 ([M<sup>+</sup>-tma]), 986.5 ([M<sup>+</sup>-2tma]). UV-vis (CH<sub>2</sub>Cl<sub>2</sub>, nm, ε x 10<sup>-3</sup> M<sup>-1</sup>cm<sup>-1</sup>): 388 (47), 412 (56), 572 (14), 640 (5.3)

**2,3,7,8,12,13,17,18-octabromo-5,10,15-tris-pentafluorophenylcorrolato-iridium(III)**

**bis-trimethylamine, 1b-Ir(tma)<sub>2</sub>.** Compound 1-Ir(tma)<sub>2</sub> (15 mg) and Br<sub>2</sub> (70 μL) were dissolved in 20 mL MeOH and stirred overnight. Column chromatography (silica, 4:1 hexanes:CH<sub>2</sub>Cl<sub>2</sub>) of the red mixture provided a ruddy solution from which purple crystals of (Br<sub>8</sub>-tpfc)Ir(III)(tma)<sub>2</sub> (15 mg, 63% yield) could be grown by addition of methanol followed by slow evaporation. <sup>1</sup>H NMR (CDCl<sub>3</sub>): δ -2.60 (s, 18H). <sup>19</sup>F NMR (CDCl<sub>3</sub>): δ -137.78 (d/d, 2F, <sup>3</sup>J = 35.1, <sup>4</sup>J = 18.3), -138.54 (d/d, 4F, <sup>3</sup>J = 33.9, <sup>4</sup>J = 17.1), -152.89 (m, 3F), -163.38 (m, 4F), -163.70 (m, 2F). MS (ESI): 1616.4 ([M<sup>+</sup>-2tma]). UV-vis (CH<sub>2</sub>Cl<sub>2</sub>, nm, ε x 10<sup>-3</sup> M<sup>-1</sup>cm<sup>-1</sup>): 404 (61), 424 (70), 580 (16), 654 (7.3)

**5,10,15-tris-pentafluorophenylcorrolato-iridium(III) bis-pyridine, 1-Ir(py)<sub>2</sub>.**

H<sub>3</sub>tpfc (40 mg), [Ir(cod)Cl]<sub>2</sub> (170 mg), and K<sub>2</sub>CO<sub>3</sub> (70 mg) were dissolved/suspended in 75 mL of degassed THF, and the mixture was heated at reflux under argon for 90 min. Pyridine (1 mL) was added, and the solution was allowed to slowly cool to room temperature while open to the laboratory atmosphere. Column chromatography of the forest green mixture (silica, 4:1 hexanes:CH<sub>2</sub>Cl<sub>2</sub> followed by 3:2 hexanes:CH<sub>2</sub>Cl<sub>2</sub>) afforded a bright green solution, from which thin, green crystals of (tpfc)Ir(III)(py)<sub>2</sub> (26 mg, 50% yield)

could be grown by addition of methanol followed by slow evaporation.  $^1\text{H}$  NMR ( $\text{CDCl}_3$ ):  $\delta$  8.84 (d, 2H,  $J = 4.5$ ), 8.53 (d, 2H,  $J = 4.8$ ), 8.32 (d, 2H,  $J = 4.8$ ), 8.17 (d, 2H,  $J = 4.5$ ), 6.21 (t, 2H,  $J = 7.8$ ), 5.19 (t, 4H,  $J = 7.0$ ), 1.72 (d, 4H,  $J = 5.1$ ).  $^{19}\text{F}$  NMR ( $\text{CDCl}_3$ ):  $\delta$  -138.68 (m, 6F), -154.84 (t, 2F,  $J = 22.2$ ), -155.20 (t, 1F,  $J = 22.2$ ), -163.28 (m, 4F), -163.65 (m, 2F). MS (ESI): 1144.1 ( $[\text{M}^+]$ ). UV-vis ( $\text{CH}_2\text{Cl}_2$ , nm,  $\epsilon \times 10^{-3} \text{ M}^{-1}\text{cm}^{-1}$ ): 390 (28), 412 (43), 582 (12), 619 (6.5)

**5,10,15-*tris*-pentafluorophenylcorrolato-iridium(III) triphenylphosphine, 1-Ir(PPh<sub>3</sub>).**  $\text{H}_3\text{tpfc}$  (40 mg),  $[\text{Ir}(\text{cod})\text{Cl}]_2$  (170 mg), and  $\text{K}_2\text{CO}_3$  (70 mg) were dissolved/suspended in 75 mL of degassed THF, and the mixture was heated at reflux under argon for 90 min. Triphenylphosphine (260 mg dissolved in 5 mL THF) was added, and the solution was heated at reflux for another half hour under laboratory atmosphere before being allowed to cool to room temperature. Column chromatography of the deep green mixture (silica, 3:1 hexanes: $\text{CH}_2\text{Cl}_2$ ) afforded a bright red-orange solution, which could be evaporated to give  $(\text{tpfc})\text{Ir}(\text{III})(\text{PPh}_3)$  (30 mg, 64% yield) as a ruby-colored solid.  $^1\text{H}$  NMR ( $\text{CDCl}_3$ ):  $\delta$  8.67 (d, 2H,  $J = 4.5$ ), 8.36 (d, 2H,  $J = 5.1$ ), 8.18 (d, 2H,  $J = 5.1$ ), 8.00 (d, 2H,  $J = 4.5$ ), 6.98 (t, 3H,  $J = 7.2$ ), 6.69 (t, 6H,  $J = 6.9$ ), 4.52 (d/d, 6H,  $^3J = 19.5$ ,  $^4J = 3.6$ ).  $^{19}\text{F}$  NMR ( $\text{CDCl}_3$ ):  $\delta$  -137.44 (m, 6F), -154.05 (m, 3F), -162.54 (m, 3F). MS (ESI): 1248.1 ( $[\text{M}^+]$ ). UV-vis ( $\text{CH}_2\text{Cl}_2$ , nm,  $\epsilon \times 10^{-3} \text{ M}^{-1}\text{cm}^{-1}$ ): 398 (66), 554 (8.8), 588 (6.7)

**Nuclear Magnetic Resonance Spectroscopy.**  $^1\text{H}$  and  $^{19}\text{F}$  NMR data were obtained on  $\text{CDCl}_3$  solutions of each compound at room temperature using a Varian Mercury 300

MHz NMR spectrometer.  $^1\text{H}$  chemical shifts are reported relative to solvent peaks and  $^{19}\text{F}$  chemical shifts are reported relative to a saved, external  $\text{CFCl}_3$  standard.

**Mass Spectrometry.** Measurements were made on  $\text{CH}_3\text{OH}$  solutions of each compound by electrospray ionization into a Thermofinnigan LCQ ion trap mass spectrometer.

**X-ray Crystallography.** Concentrated  $\text{CH}_2\text{Cl}_2/\text{CH}_3\text{OH}$  solutions of corroles 1-Ir(tma) $_2$ , 1b-Ir(tma) $_2$ , and 1- Ir(py) $_2$  were allowed to undergo slow evaporation from scintillation vials. The resultant crystals were mounted on a glass fiber using Paratone oil and then placed on a Bruker Kappa Apex II diffractometer under a nitrogen stream at 100 K. The SHELXS-97 program was used to solve the structures.

**Cyclic Voltammetry.** CV measurements were made with a WaveNow USB Potentiostat/Galvanostat (Pine Research Instrumentation) using Pine AfterMath Data Organizer software. A three electrode system consisting of a platinum wire working electrode, a platinum wire counter electrode, and an Ag/AgCl reference electrode, was employed. The CV measurements were made using dichloromethane solutions, 0.1 M in tetrabutylammonium perchlorate (TBAP, Fluka, recrystallized twice from absolute ethanol) and  $10^{-3}$  M substrate under an argon atmosphere at ambient temperature. The scan rate was 0.1 V/s and the  $E_{1/2}$  value for oxidation of ferrocene under these conditions was 0.55 V.

UV-visible spectroelectrochemical measurements were made on dichloromethane solutions, 0.5 M in TBAP and 0.1–0.3 mM in substrate with an optically transparent platinum thin-layer electrode working electrode, a platinum wire counter electrode, and

an Ag/AgCl reference electrode under an argon atmosphere at ambient temperature. Potentials were applied with a WaveNow USB Potentiostat/Galvanostat. Time-resolved UV-visible spectra were recorded with a Hewlett-Packard Model 8453 diode array rapid-scanning spectrophotometer.

**Electron Paramagnetic Resonance Spectroscopy.** Solutions for EPR were prepared by adding 50  $\mu\text{L}$  of a 10 mM  $\text{CH}_2\text{Cl}_2$  solution of iodine to 100  $\mu\text{L}$  of a 1 mM  $\text{CH}_2\text{Cl}_2$  solution of the corrole being examined, ensuring complete one-electron oxidation of the substrate. In order to rule out side reactions with iodine, sub-stoichiometric amounts of the radical cation *tris*(4-bromophenyl)aminium hexachloroantimonate (***t*-4bpa**) also were employed for oxidations. Spectra taken of the products obtained from reactions with both oxidants were virtually identical. EPR spectroscopy was performed using a Bruker EMX Biospin instrument, with a Gunn diode microwave source. Solutions were pre-cooled by rapid freezing in liquid nitrogen; spectra of samples at 20 K were obtained using liquid helium as a coolant. The SPINCOUNT package was used to simulate EPR parameters.

**UV-vis Absorption Spectroscopy.** Absorption spectral measurements were made on solutions of each compound in  $\text{CH}_2\text{Cl}_2$ , using a Hewlett-Packard 8452A Diode Array Spectrophotometer. Extinction coefficients were calculated from measurements on corroles at variable concentrations in  $\text{CH}_2\text{Cl}_2$  solutions. UV-vis spectroscopic titrations were performed by stepwise addition of small aliquots of  $\text{CH}_2\text{Cl}_2$  solutions of ***t*-4bpa** to  $\text{CH}_2\text{Cl}_2$  solutions of each corrole. The ***t*-4bpa** oxidant was employed rather than iodine owing to overlapping absorptions due to excess reagent in the latter case.



## Results and Discussion

**Iridium(III) corroles.** The insertion of the metal ion into the free base corrole  $H_3(tpfc)$  was achieved via heating with  $[Ir(cod)Cl]_2$  and  $K_2CO_3$  in THF under an inert atmosphere. This procedure was followed by addition of pyridine or triphenylphosphine and opening the reaction mixture to the laboratory atmosphere to effect aerobic oxidation.<sup>27</sup> Owing to their low-spin  $d^6$  electronic configurations, iridium(III) corroles display highly resolved NMR spectra that are characteristic of diamagnetic complexes,<sup>28</sup> as shown in Figure 2-3 (upper) for **1-Ir(py)<sub>2</sub>**. The  $^1H$  NMR spectra reveal four  $\beta$ -pyrrole CH proton resonances as doublets with  $J$  coupling constants of about 4.5 Hz at 8–9 ppm and axial ligand resonances at high field attributable to the diamagnetic ring current of the aromatic corrole. The **1-Ir(py)<sub>2</sub>** pyridine proton resonances are more shifted than those of  $PPh_3$  in **1-Ir(PPh<sub>3</sub>)** (both relative to their positions in the absence of a metal center) due to the proximity of py protons to the corrole ring. The coordination number [six for the bis-pyridine complex **1-Ir(py)<sub>2</sub>** and five for the triphenylphosphine complex **1-Ir(PPh<sub>3</sub>)**] can be deduced from  $^1H$  NMR spectra via integration of the relevant proton resonances. The same information can also be extracted from the  $^{19}F$  NMR spectra (Figure 2-3, lower), since the  $C_{2v}$  symmetry of **1-Ir(py)<sub>2</sub>** requires equivalence of above- and below-plane *ortho*- and *meta*-fluorine atoms on each  $C_6F_5$  ring.

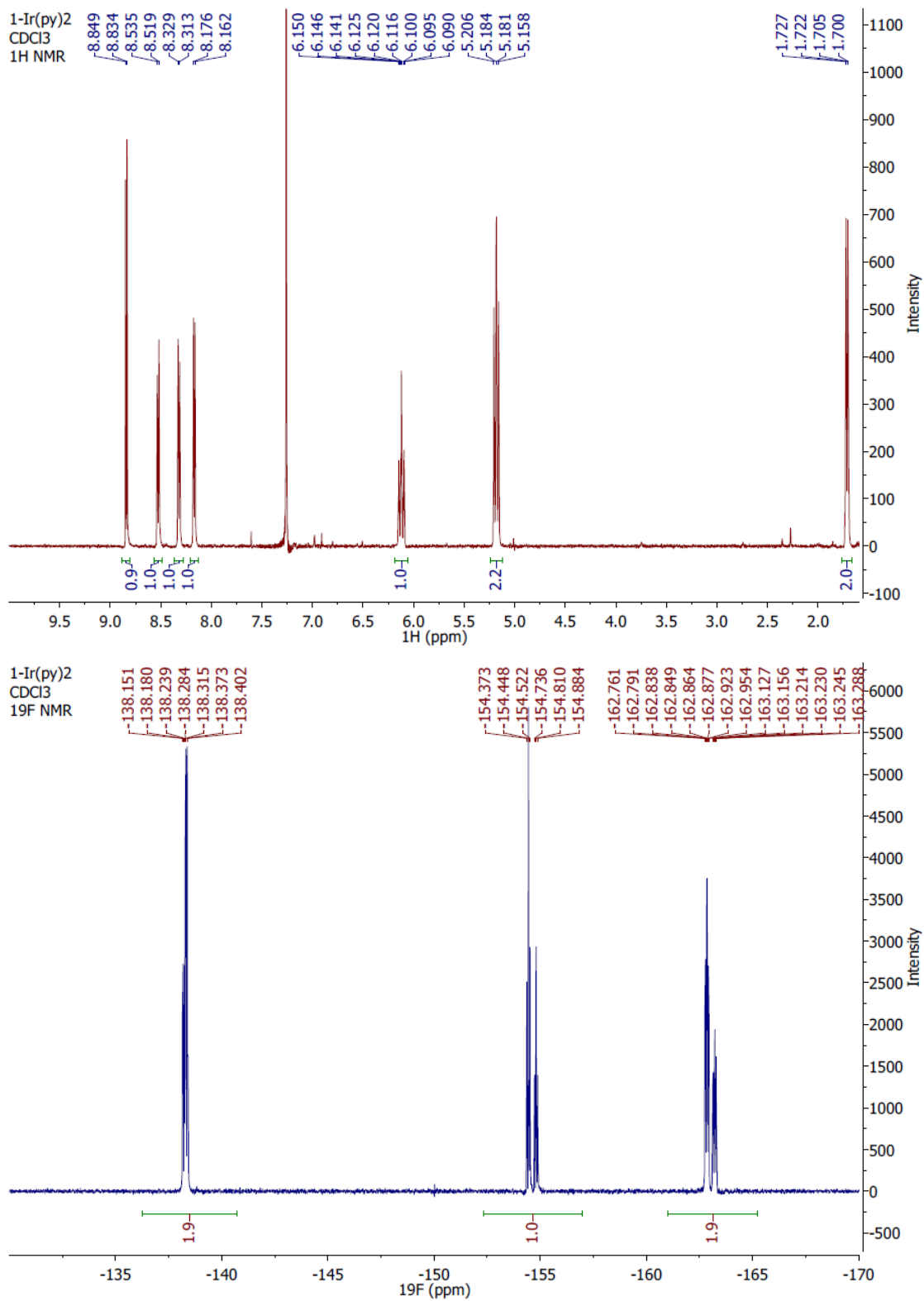


Figure 2-3: <sup>1</sup>H (top) and <sup>19</sup>F (bottom) NMR spectra of **1-Ir(py)<sub>2</sub>**

The electronic absorption spectra of six-coordinate metal(III) corroles are shown in Figure 2-4. The spectra of **1-Co(py)<sub>2</sub>** and **1-Rh(py)<sub>2</sub>** are similar, each with one major Soret band and Q bands near 580 and 600 nm, whereas the spectrum of **1-Ir(py)<sub>2</sub>** exhibits highly structured Soret absorption with Q bands that are red-shifted by about 20 nm compared to those of the 3d and 4d analogues. We emphasize that **1-Co(py)<sub>2</sub>** is in equilibrium with the (mono)pyridine complex **1-Co(py)** in CH<sub>2</sub>Cl<sub>2</sub> solution [which is not the case for **1-Rh(py)<sub>2</sub>** or **1-Ir(py)<sub>2</sub>**].<sup>26b</sup> The spectrum of **1-Co(py)<sub>2</sub>** in 5% pyridine (where only the (bis)ligated form exists in solution) is in Supporting Information. As the main components of the electronic spectra are attributable to corrole-based  $\pi$ - $\pi^*$  transitions, the differences likely reflect increased mixing with MLCT in the order Co < Rh < Ir. Red-shifted Q bands also are exhibited by five-coordinate **1-Ir(PPh<sub>3</sub>)**, while the Soret bands differ markedly, as follows: **1-Co(PPh<sub>3</sub>)** has a highly split system, **1-Rh(PPh<sub>3</sub>)** displays less splitting but is red-shifted, and **1-Ir(PPh<sub>3</sub>)** exhibits a single, relatively sharp Soret band.

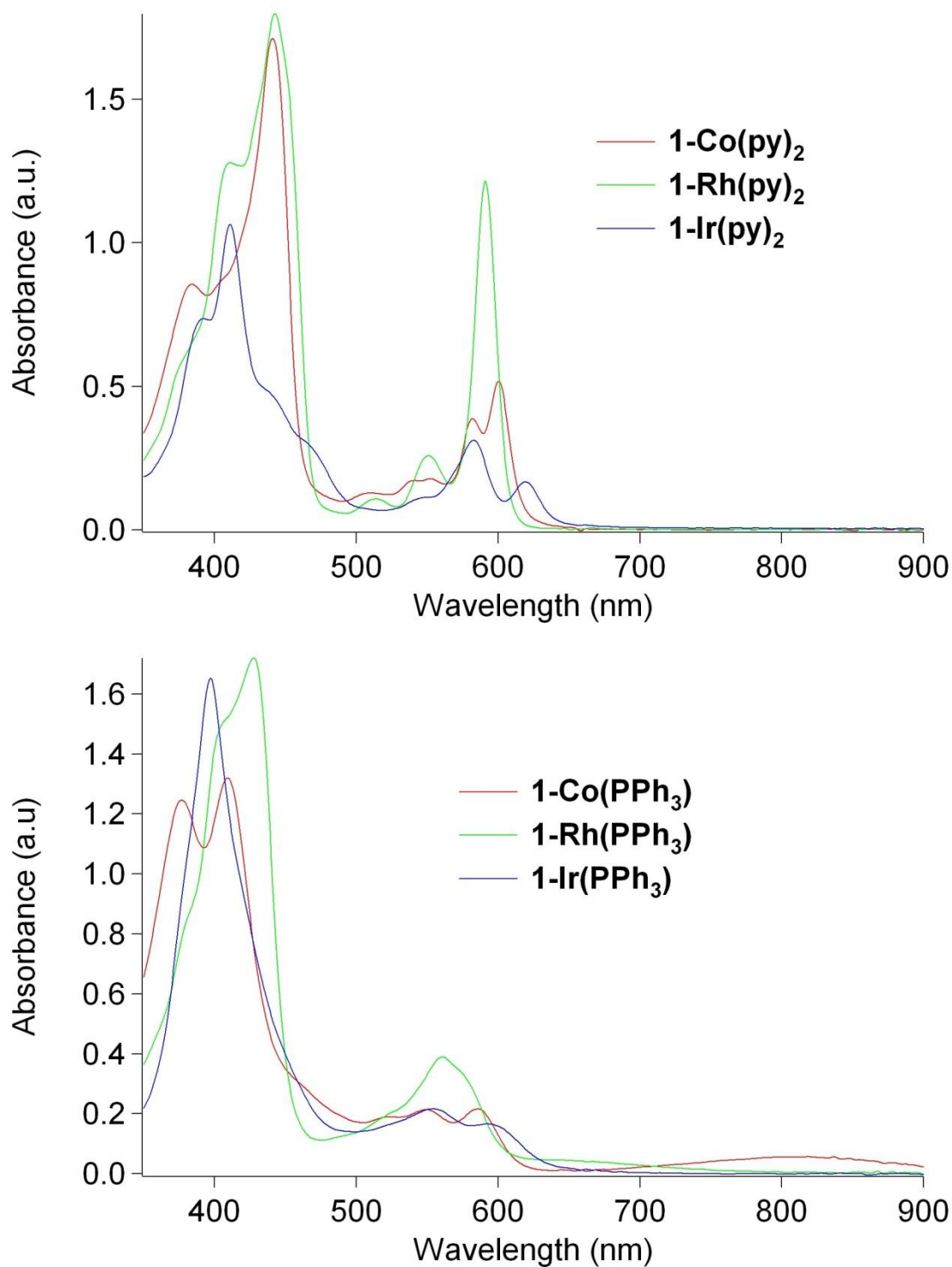


Figure 2-4: Electronic absorption spectra of six-coordinate (bis)pyridine metal(III) corroles (top) and five-coordinate PPh<sub>3</sub>-ligated metal(III) corroles (bottom); 2.5  $\mu$ M in CH<sub>2</sub>Cl<sub>2</sub> solution

	M-N(corrole)	M-N(axial)	Reference
<b>1-Co(py)<sub>2</sub></b>	1.873(4)–1.900(4)	1.994(4)–1.995(4)	26b
<b>1-Rh(py)<sub>2</sub></b>	1.938(5)–1.976(5)	2.060(5)–2.071(5)	15
<b>1-Ir(py)<sub>2</sub></b>	1.947(2)–1.979(2)	2.052(2)–2.066(2)	This work
<b>1-Ir(tma)<sub>2</sub></b>	1.940(3)–1.981(3)	2.184(3)–2.186(3)	18
<b>1b-Ir(tma)<sub>2</sub></b>	1.959(2)–1.989(2)	2.186(2)–2.192(2)	18

Table 2-1: Metal-nitrogen bond lengths (Å) in **1-Co(py)<sub>2</sub>**, **1-Rh(py)<sub>2</sub>**, **1-Ir(py)<sub>2</sub>**, **1-Ir(tma)<sub>2</sub>**, and **1b-Ir(tma)<sub>2</sub>**

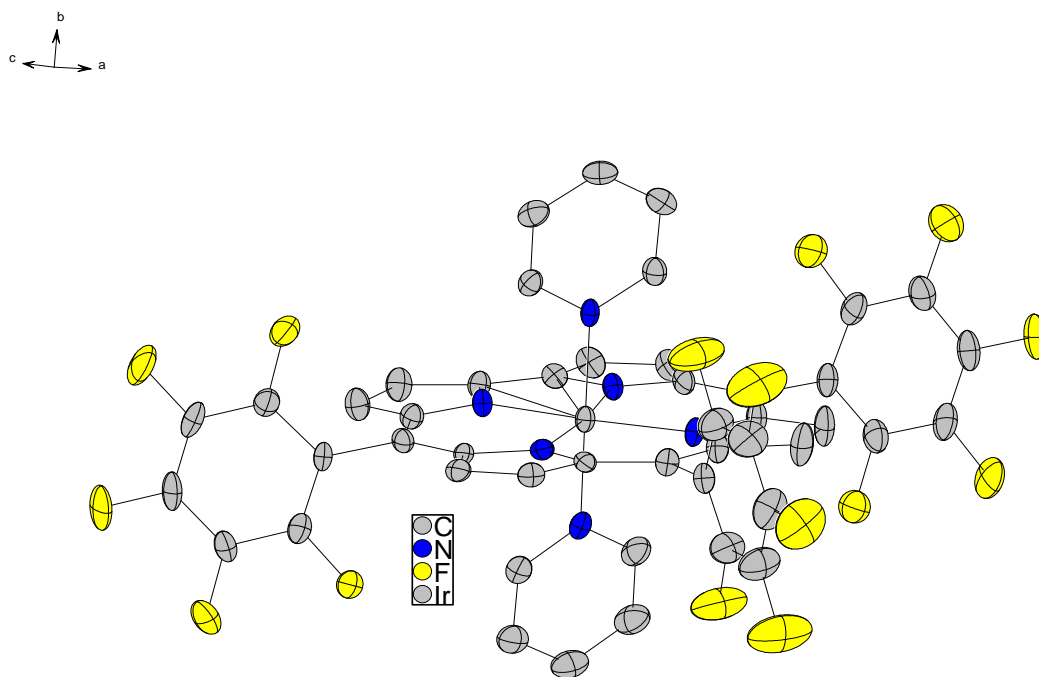
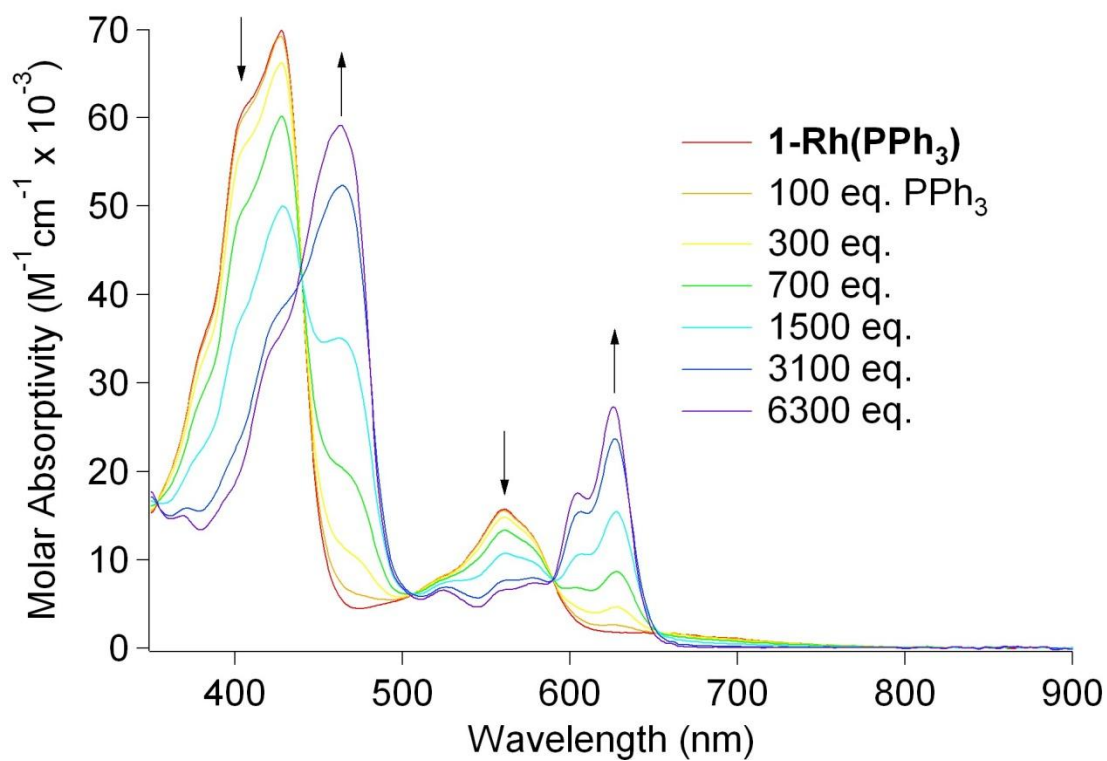
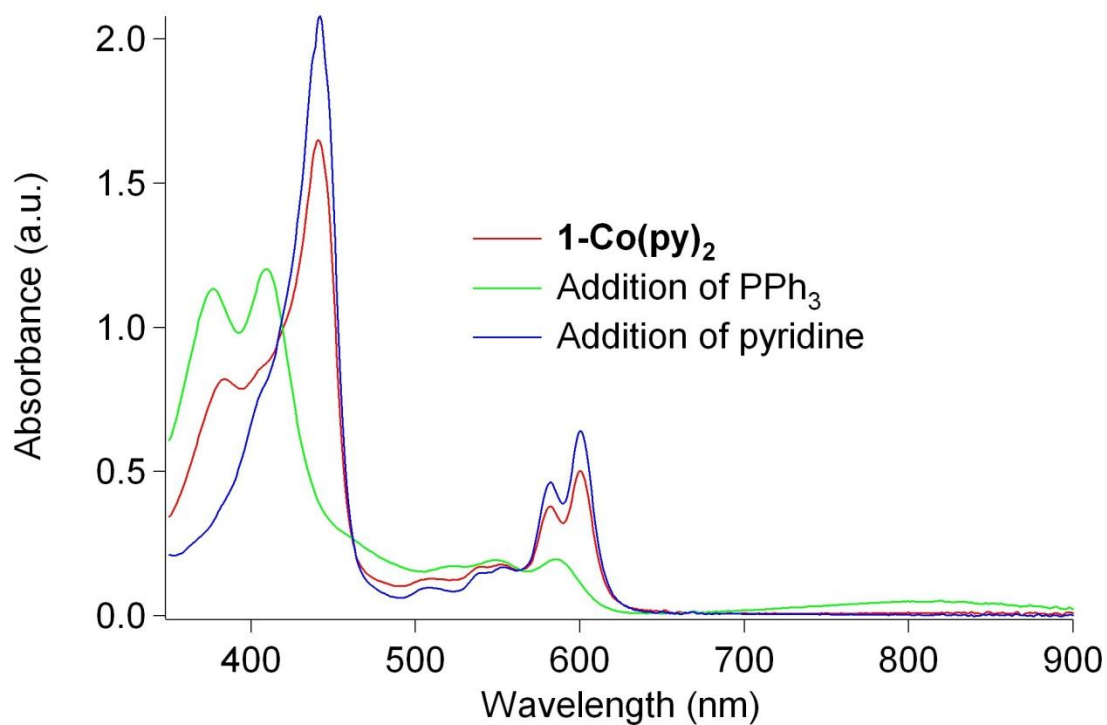


Figure 2-5: Structure of **1-Ir(py)<sub>2</sub>** (H atoms omitted)

**Substitution and addition reactions.** Previous investigations have revealed that **1-Co(PPh<sub>3</sub>)** and **1-Rh(PPh<sub>3</sub>)** react differently with pyridine: both ligand substitution and addition to Co(III) yield **1-Co(py)<sub>2</sub>**, but Rh(III) undergoes only addition to give **1-Rh(PPh<sub>3</sub>)(py)**.<sup>26b,29</sup> The reactivity of **1-Ir(PPh<sub>3</sub>)** is similar to that of Rh(III), i.e., addition of pyridine produces a mixed-ligand complex (see Supporting Information). Additional confirmation of the substitutional lability of the Co(III) corrole is the observation (Figure 2-6a) that addition of PPh<sub>3</sub> to **1-Co(py)<sub>2</sub>** rapidly yields **1-Co(PPh<sub>3</sub>)** [addition of excess pyridine regenerates the bis-pyridine complex; the spectrum changes slightly due to the absence of 5-coordinate **1-Co(py)** under these conditions]. Complementary information was obtained by examination of spectral changes upon the addition of PPh<sub>3</sub> to five-coordinate metallocorroles. While addition of a 100,000-fold excess of triphenylphosphine produced only minor changes in the spectrum of **1-Co(PPh<sub>3</sub>)** (see Supporting Information), the spectra of **1-Rh(PPh<sub>3</sub>)** (Figure 2-6b) and **1-Ir(PPh<sub>3</sub>)** (Figure 2-6c) changed completely after the addition of 6300 and 350 equivalents, respectively. The similarity of the visible spectra obtained upon addition of triphenylphosphine to **1-Rh(PPh<sub>3</sub>)** and **1-Ir(PPh<sub>3</sub>)** to those of **1-Rh(py)<sub>2</sub>** and **1-Ir(py)<sub>2</sub>** suggests that the products are six-coordinate (bis)triphenylphosphine species, **1-Rh(PPh<sub>3</sub>)<sub>2</sub>** and **1-Ir(PPh<sub>3</sub>)<sub>2</sub>**. While many corrole-chelated metal(III) ions possess surprisingly low affinities for a sixth ligand,<sup>26b,30,31</sup> our work demonstrates that this property is not as pronounced for 4d and especially for 5d metals.



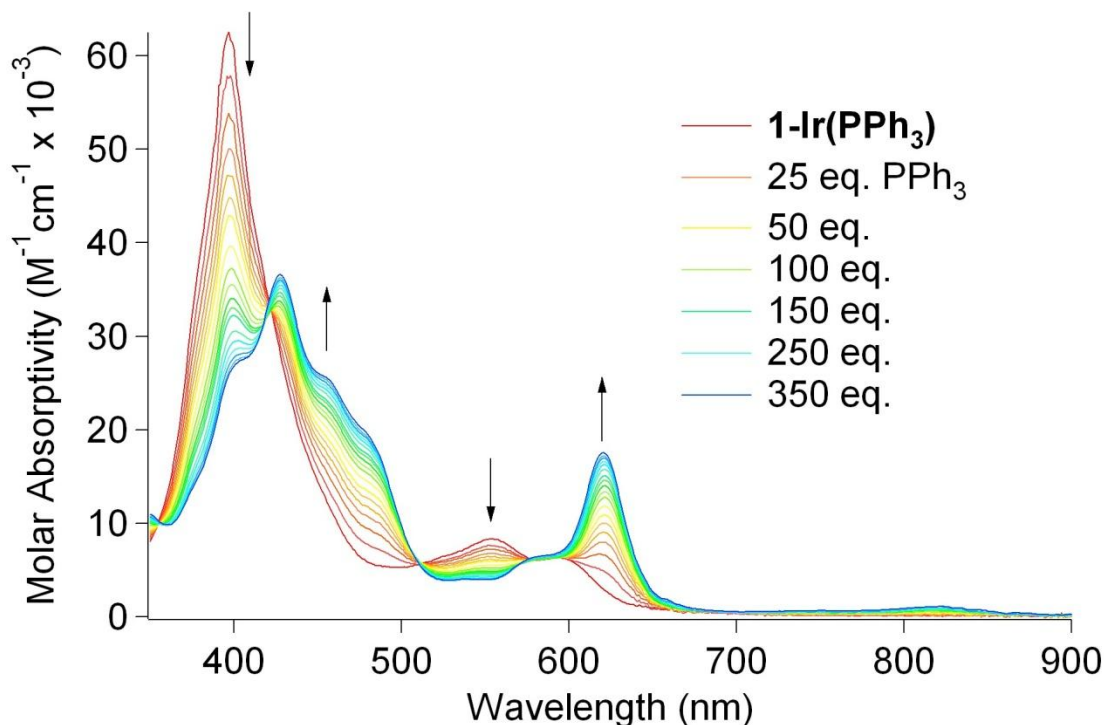


Figure 2-6: Electronic absorption spectra of metal(III) corroles in  $\text{CH}_2\text{Cl}_2$  solution demonstrate: (a, top), reversible transformations between **1-Co(py)<sub>2</sub>** and **1-Co(PPh<sub>3</sub>)** upon addition of PPh<sub>3</sub> and pyridine; (b, middle), formation of **1-Rh(PPh<sub>3</sub>)<sub>2</sub>**; (c, bottom), formation of **1-Ir(PPh<sub>3</sub>)<sub>2</sub>**. Only a representative selection of the many individual traces (25 to 350 eq. ligand) that are shown in the bottom panel are specifically identified

**Electrochemistry.** Our earlier work focused on the differences between the  $\beta$ -pyrrole-unsubstituted complex **1-Ir(tma)<sub>2</sub>** and its fully brominated analogue, **1b-Ir(tma)<sub>2</sub>**. The latter displays one oxidation (at 1.19 V vs. SCE) and one reduction (at -1.21 V vs. SCE) within the solvent potential window of  $\text{CH}_2\text{Cl}_2$ , while two reversible oxidations (at 0.66 and 1.28 V vs. SCE) were observed for the former.<sup>18</sup> The current emphasis is on the **M(+0)** reduction potential of each of the complexes, because it should correspond to either a metal-centered ( $\text{M}^{\text{III}}/\text{M}^{\text{IV}}$ , where M = Co, Rh, or Ir) or ligand-centered (tpfc/tpfc<sup>+</sup>) process. The CVs of all complexes are shown in Figure 2-7; and Table 2-2 lists the corresponding reduction potentials. The results reveal that six-coordinate **1-M(py)<sub>2</sub>** complexes are oxidized at lower potentials than five-coordinate **1-M(PPh<sub>3</sub>)** and



that the differences become larger in the order  $\text{Ir} < \text{Rh} < \text{Co}$ . It is surprising that there are only very small differences in reduction potentials for the two series:  $0.70 \pm 0.03$  for **1-M(py)<sub>2</sub>** and  $0.78 \pm 0.06$  for **1-M(PPh<sub>3</sub>)<sub>2</sub>**. Very large potential shifts would be expected for metal-based processes ( $\text{M}^{\text{III/IV}}$ ), as documented by the finding that  $\text{Rh}^{\text{III/IV}}$  reduction potentials are 0.2 to 0.3 V more positive than  $\text{Ir}^{\text{III/IV}}$  potentials in cyclometalated complexes.<sup>32</sup> A caveat is that the central metal ion should have some effect on the potential even in the case of macrocycle-centered oxidation, as observed previously for both corroles and porphyrins.<sup>33,34</sup>

<b>1-M(PPh<sub>3</sub>)<sub>2</sub></b>	$E_{1/2}$	<b>1-M(py)<sub>2</sub></b>	$E_{1/2}$
M= Co	0.83	M= Co	0.67
M = Rh	0.79	M = Rh	0.72
M = Ir	0.72	M = Ir	0.71

Table 2-2: Reduction potentials ( $\text{CH}_2\text{Cl}_2$ , TBAP, V vs. Ag/AgCl) for Group 9 metal(III) corroles. Under virtually identical conditions,  $E_{1/2}$  for ferrocene is 0.55 V; and iodine has  $E_{\text{pa}}$  of 0.89 V and  $E_{\text{pc}}$  of 0.39 V.

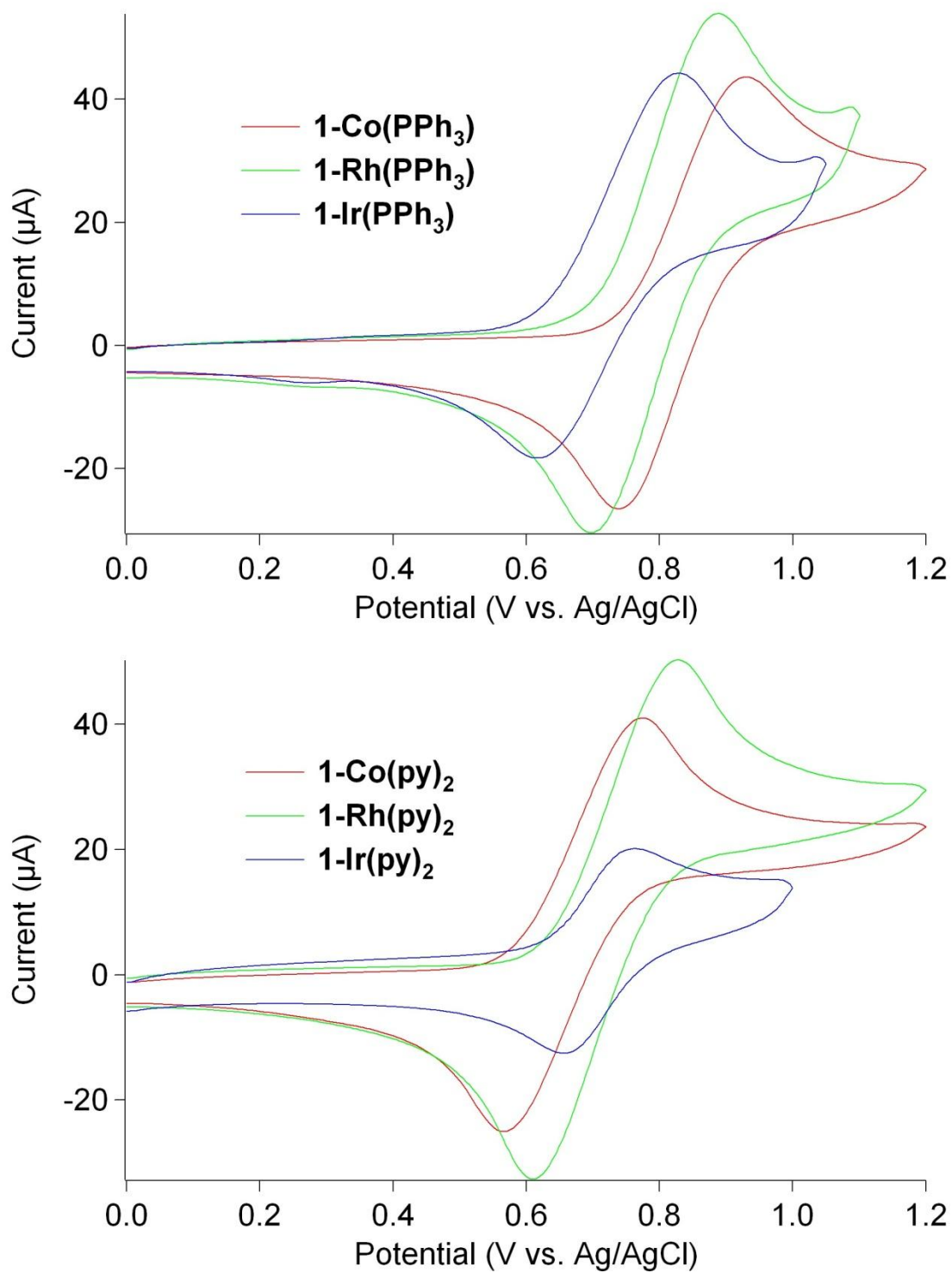


Figure 2-7: CV traces of **1-M(PPh<sub>3</sub>)** (top) and **1-M(py)<sub>2</sub>** (bottom), in CH<sub>2</sub>Cl<sub>2</sub> solution

**Electronic structures of one-electron-oxidized metallo(III)corroles.** Changes in electronic spectra upon M(III) corrole oxidation can be used as a tool for analyzing whether an electron is removed primarily from a metal or ligand orbital. One-electron oxidation of 1-Co(PPh<sub>3</sub>) or 1-Rh(PPh<sub>3</sub>) by ***t*-4bpa** (Figure 2-8) was marked by substantial intensity reductions of the M(III) Soret and Q bands and formation of a broad absorption system at 690 ( $\epsilon = 4000 \text{ M}^{-1}\text{cm}^{-1}$ ) for cobalt and 710 nm ( $\epsilon = 2300 \text{ M}^{-1}\text{cm}^{-1}$ ) for rhodium. These long-wavelength absorption features, which appear at 673 nm ( $\epsilon = 3000 \text{ M}^{-1}\text{cm}^{-1}$  for Co and  $4100 \text{ M}^{-1}\text{cm}^{-1}$  for Rh) in the spectra of chemically oxidized 1-Co(py)<sub>2</sub> and 1-Rh(py)<sub>2</sub> complexes (Figure 2-9), represent signature spectroscopic features for corrole-centered oxidations.

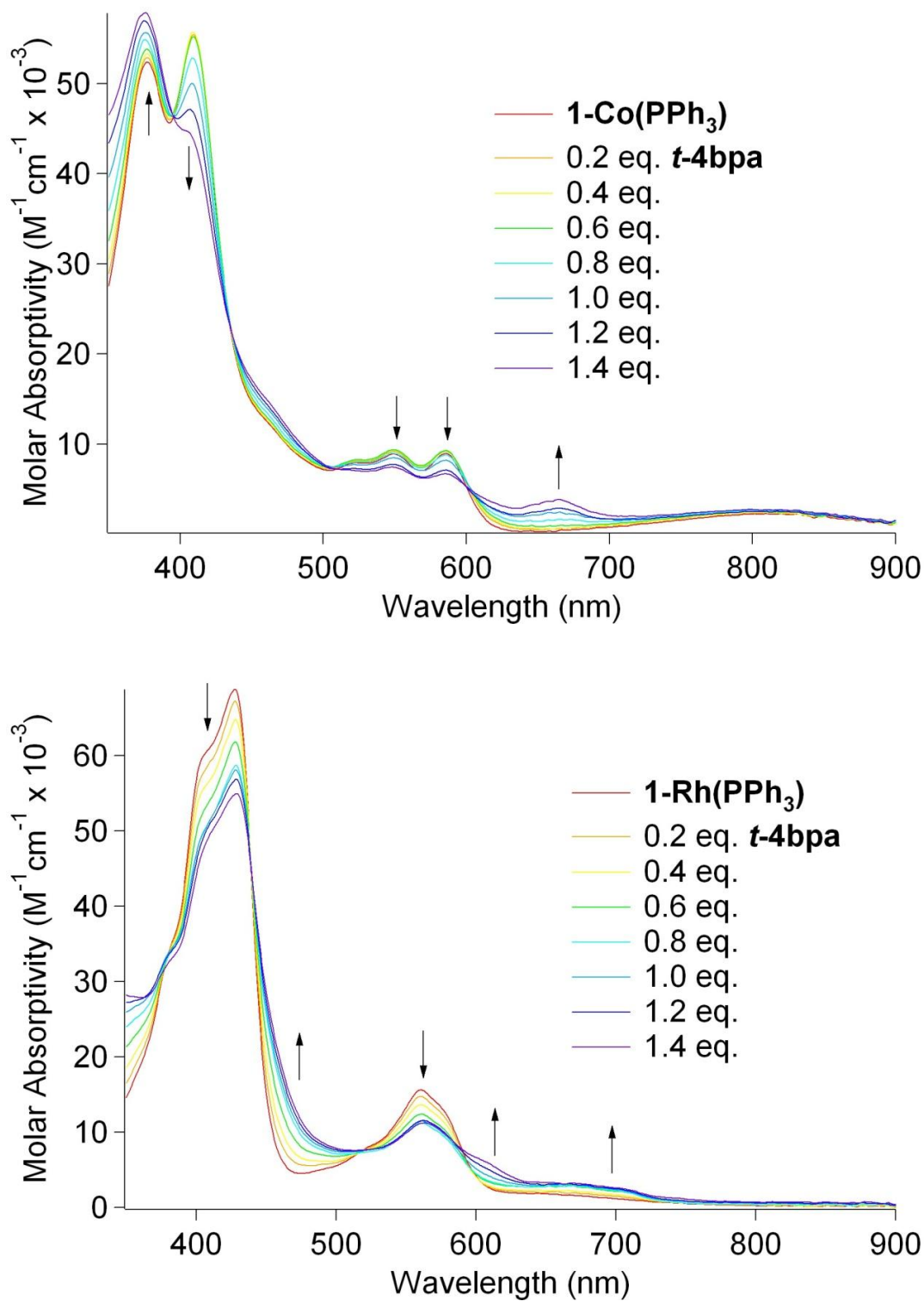


Figure 2-8: Absorption spectral changes accompanying oxidation of **1-Co(PPh)<sub>3</sub>** (top) and **1-Rh(PPh)<sub>3</sub>** (bottom) by *t*-4bpa in CH<sub>2</sub>Cl<sub>2</sub> solution

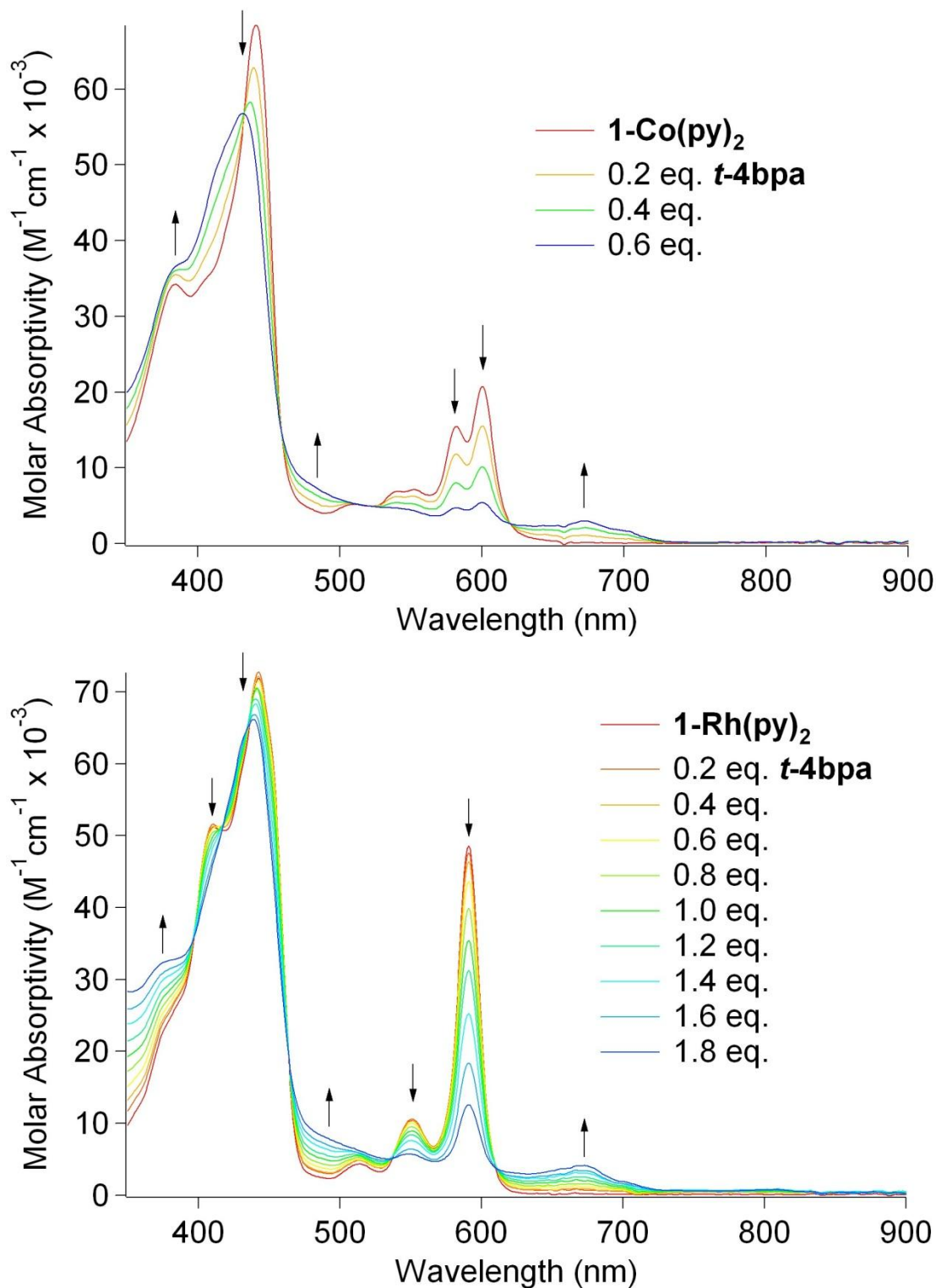
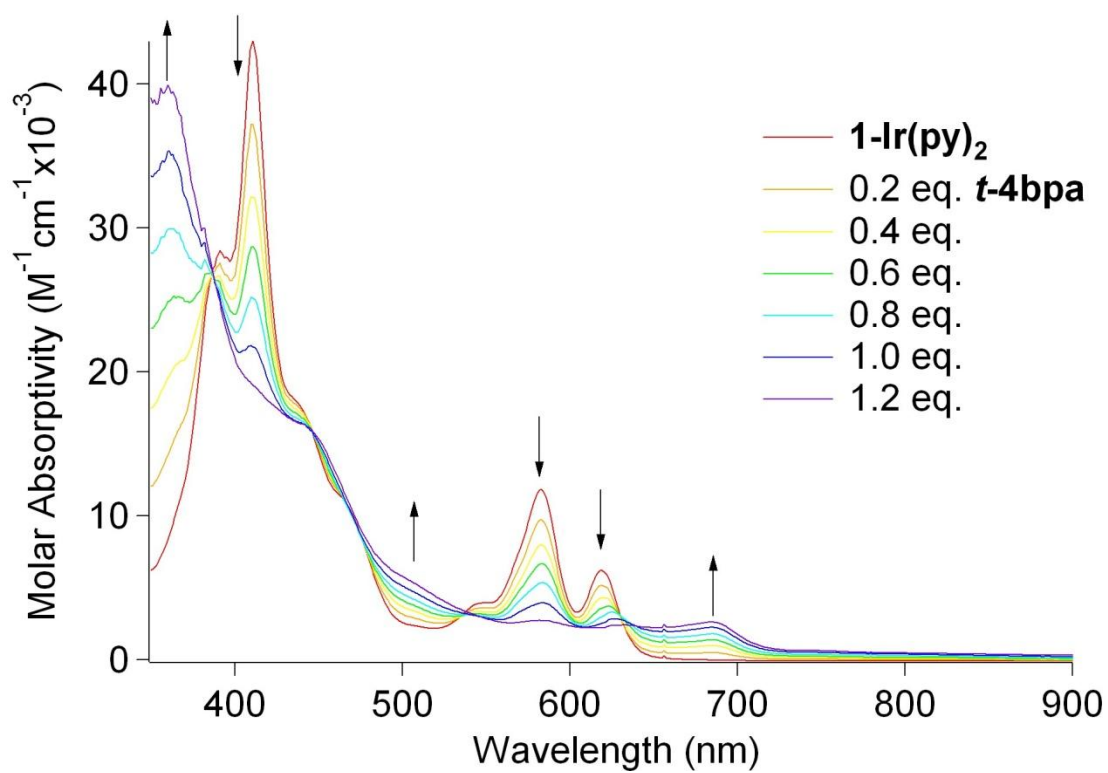
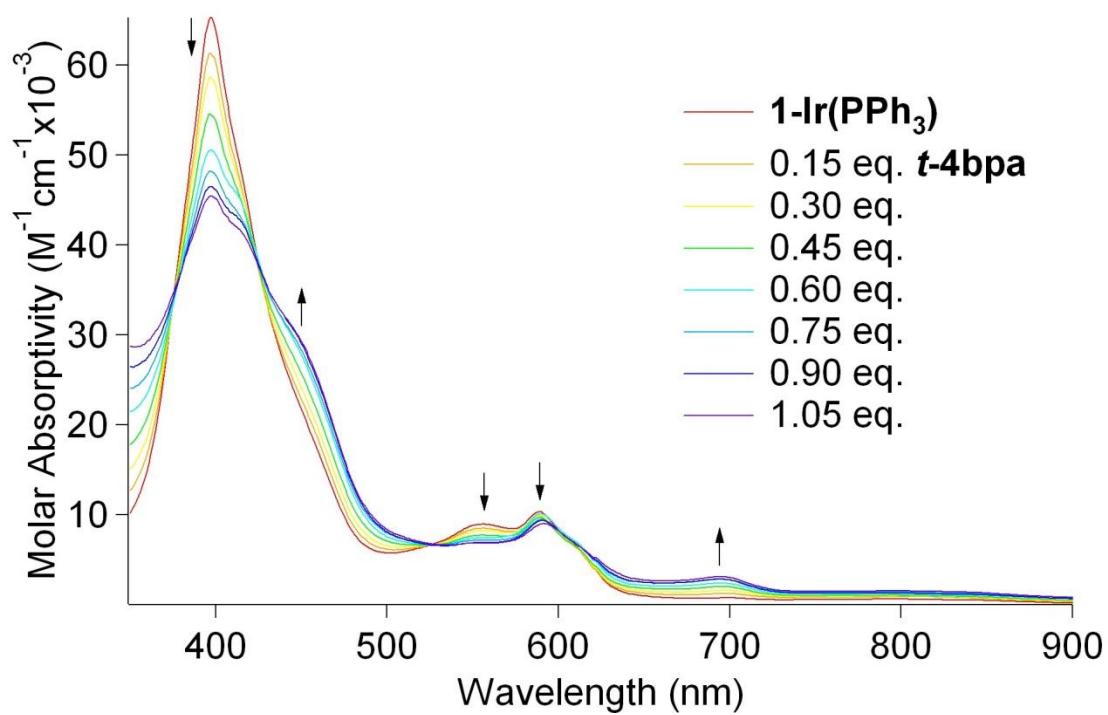


Figure 2-9: Absorption spectral changes accompanying oxidation of  $\mathbf{1-Co(py)_2}$  (top) and  $\mathbf{1-Rh(py)_2}$  (bottom) by  $\mathbf{t-4bpa}$  in  $\text{CH}_2\text{Cl}_2$  solutions. Reaction with the Co(III) complex was terminated after addition of 0.6 equivalents, owing to product instability.<sup>26b</sup>

Absorption spectral changes upon oxidation of iridium(III) corroles are substantially different from those of 3d and 4d analogues. Oxidations of **1-Ir(PPh<sub>3</sub>)**, **1-Ir(py)<sub>2</sub>**, and **1-Ir(tma)<sub>2</sub>** by ***t*-4bpa** in CH<sub>2</sub>Cl<sub>2</sub> were performed, and their progress was tracked by UV-visible spectroscopy (Figure 2-10). In the case of the five-coordinate complex **1-Ir(PPh<sub>3</sub>)**, oxidation causes a significant reduction in the intensity of the Soret system, accompanied by broadening, and the Q-bands are slightly red-shifted. For each of the six-coordinate complexes **1-Ir(py)<sub>2</sub>** and **1-Ir(tma)<sub>2</sub>**, the Soret band blue shifts over 30 nm to 366 nm and the Q-bands all but vanish. A weak absorption appears at 695 nm ( $\epsilon = 3000 \text{ M}^{-1}\text{cm}^{-1}$ ) in the spectrum of **1-Ir(PPh<sub>3</sub>)**; and a similar system is centered at 685 nm ( $\epsilon = 2600 \text{ M}^{-1}\text{cm}^{-1}$ ) in the spectra of the six-coordinate complexes; these features are red-shifted from the 673 nm band observed upon oxidation of either **1-Co(py)<sub>2</sub>** or **1-Rh(py)<sub>2</sub>**, suggesting that the site of oxidation is different for Ir(III). As it is well established that substantial blue shifts of Soret bands accompany metal-centered oxidations<sup>1</sup> of metallocorroles,<sup>5b,35</sup> an Ir(IV) oxidation state is indicated for each of the one-electron-oxidized Ir(III) complexes.

---

<sup>1</sup> Note that a 32 nm blue shift in the Soret peak occurs upon oxidation of **[1-Cr<sup>IV</sup>(O)]<sup>+</sup>** to **[1-Cr<sup>V</sup>(O)]** (see reference 35).



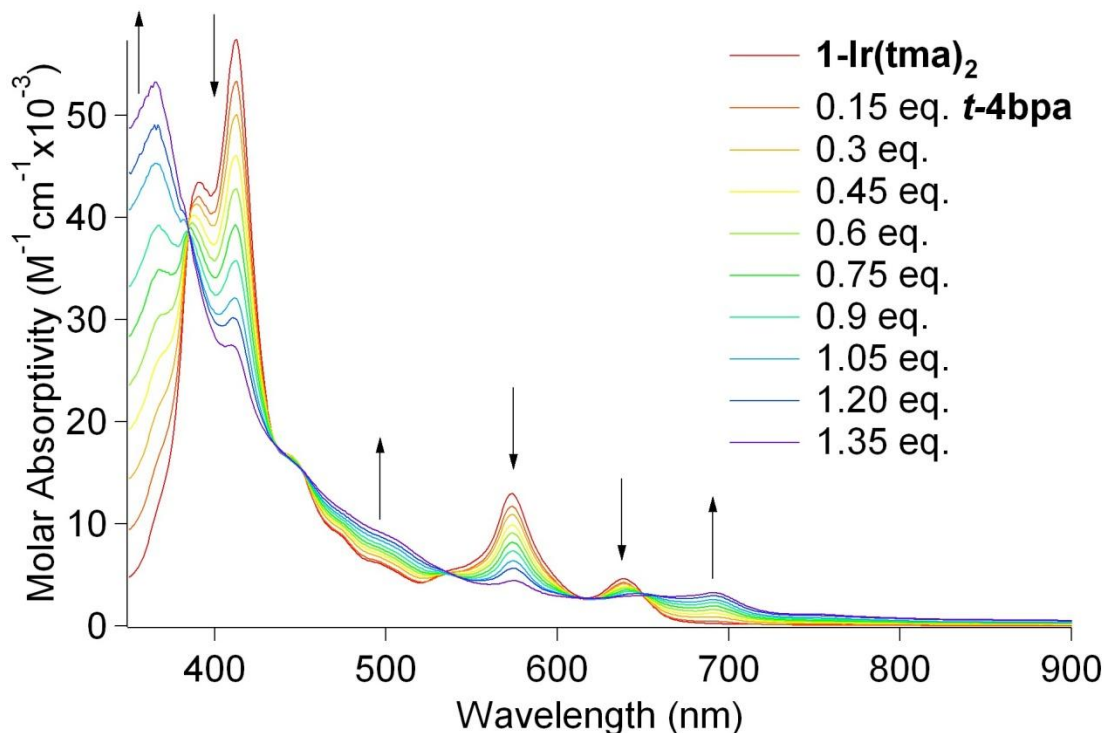


Figure 2-10: Absorption spectral changes accompanying oxidation of **1-Ir(PPh<sub>3</sub>)<sub>3</sub>** (top), **1-Ir(py)<sub>2</sub>** (middle), and **1-Ir(tma)<sub>2</sub>** by ***t*-4bpa**

**EPR spectra.** Carbon-based organic radicals, such as those obtained from oxidation of corrole complexes with non-redox-active metals like gallium(III), exhibit EPR spectra with isotropic  $g$  values near 2.0023.<sup>30</sup> In stark contrast, low-spin  $d^5$  metal complexes with organic ligands display highly anisotropic EPR signals, often with hyperfine splittings attributable to electron-nucleus interactions.<sup>36</sup>

Complexes **1-Co(py)<sub>2</sub>**, **1-Rh(py)<sub>2</sub>**, **1-Ir(py)<sub>2</sub>**, and **1-Ir(tma)<sub>2</sub>** were oxidized chemically with 5 equivalents of elemental iodine in CH<sub>2</sub>Cl<sub>2</sub>, and EPR spectra of the resultant solutions were recorded at 20 K. Each of the spectra of the oxidized cobalt and rhodium complexes displays a single, narrow band [centered at  $g = 2.008$  (Co, Figure 2-11a) or  $g = 2.003$  (Rh, Figure 2-11b), respectively] clearly attributable to a corrole-based radical.



Such a radical signature is not found in the EPR spectrum of either of the oxidized **1-Ir(py)<sub>2</sub>** and **1-Ir(tma)<sub>2</sub>** complexes. The oxidation product of **1-Ir(tma)<sub>2</sub>** (Figure 2-11c) exhibits a highly rhombic spectrum, with g tensor components ( $g_{zz} = 2.489$ ,  $g_{yy} = 2.010$ ,  $g_{xx} = 1.884$ ) that are very similar to those of low-spin d<sup>5</sup> metalloporphyrinoids such as bis-amine-iron(III) porphyrins<sup>37</sup> and **1-Fe(py)<sub>2</sub>**,<sup>38</sup> thereby demonstrating the presence of a *bona fide* iridium(IV) corrole. The spectrum of the product of oxidation of **1-Ir(py)<sub>2</sub>** under the same conditions also is highly anisotropic, albeit with less rhombicity, with  $g_{zz} = 2.401$ ,  $g_{yy} = 2.000$ ,  $g_{xx} = 1.937$  (Figure 2-11d).

Interpretation of the EPR spectra of oxidized five-coordinate complexes **1-Co(PPh<sub>3</sub>)**, **1-Rh(PPh<sub>3</sub>)**, and **1-Ir(PPh<sub>3</sub>)** is problematic. Oxidized **1-Co(PPh<sub>3</sub>)** and **1-Rh(PPh<sub>3</sub>)** appear to be corrole radicals (with isotropic g tensors centered near the free-electron value), but the electronic structure of oxidized **1-Ir(PPh<sub>3</sub>)** cannot be assigned, as its EPR spectrum is obscured by signals likely generated from side reactions with iodine.

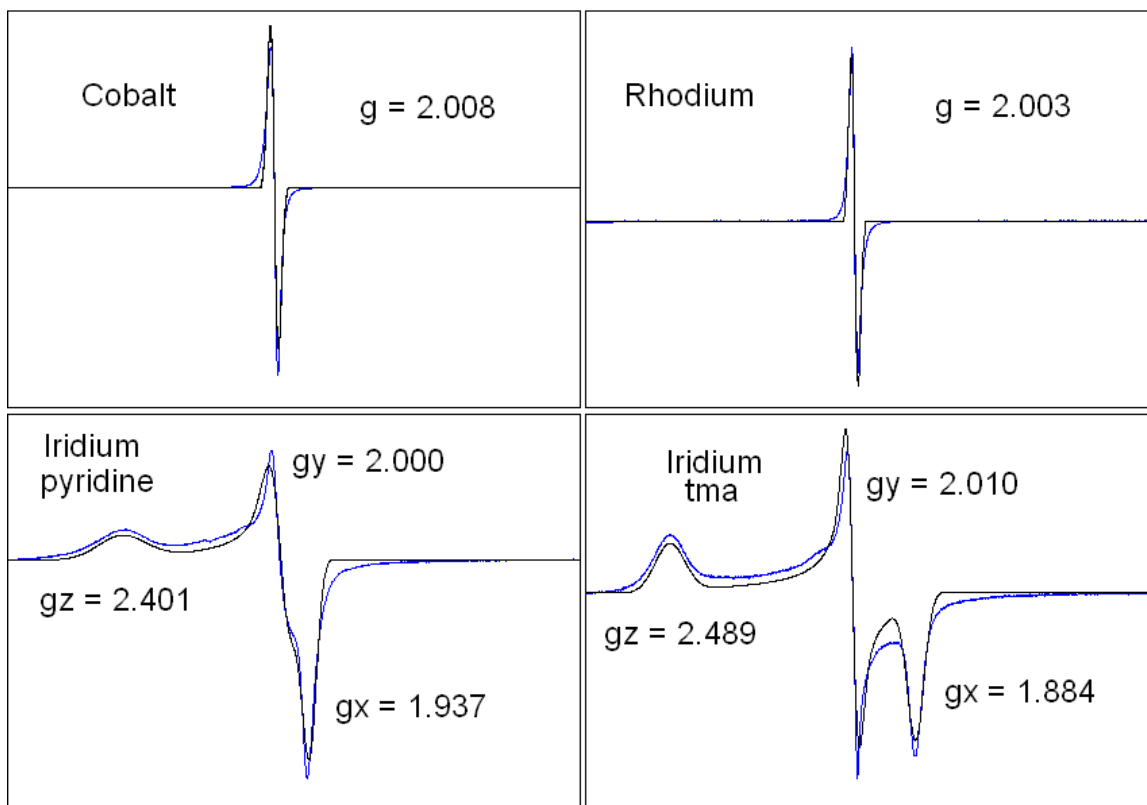


Figure 2-11: EPR spectra taken at 20 K in frozen toluene solutions ( $\text{CH}_2\text{Cl}_2$  was added to Co and Rh toluene solutions with ***t*-4bpa**) of the chemically oxidized forms of (clockwise from top left): (a) **1-Co(py)<sub>2</sub>**; (b) **1-Rh(py)<sub>2</sub>**; (c) **1-Ir(tma)<sub>2</sub>**; (d) **1-Ir(py)<sub>2</sub>**. The blue traces are experimental spectra; the black traces are simulations performed using the SPINCOUNT package.

## Concluding Remarks

Our investigation is the first to focus on the reactivity patterns of an isostructural series of corrole-chelated transition metals. The results shed new light on the chemical reactivity and stability of high oxidation states of metallocorroles. There is a clear trend within each series in terms of ligand substitution (only cobalt(III) corroles appear labile at room temperature) and ligand addition to the five-coordinate **1-M(PPh<sub>3</sub>)** ( $\text{Co} < \text{Rh} < \text{Ir}$ ), whereas all complexes display similar reduction potentials. The unexpected insensitivity of reduction potentials to metal identity has been interpreted in terms of different centers of oxidation for each complex. Absorption and EPR spectral data demonstrate that the

first oxidation is corrole-centered for cobalt and rhodium, but metal-centered for iridium. Our demonstration that the reactivity patterns of Ir(III) corroles are so different from those of 3d and 4d analogues suggests that increased efforts should be made to obtain complexes of other 5d metals, as it is likely that such materials will exhibit rich and in some cases unexpected physical and chemical properties that will further expand the range of useful applications for these electronically unique macrocycles.

### Acknowledgment

This work was supported by the Center for Chemical Innovation Grant NSF CHE-0802907, US-Israel BSF (ZG and HBG), BP, CCSER (Gordon and Betty Moore Foundation), and the Arnold and Mabel Beckman Foundation. We thank Dr. Angelo Di Bilio for help with measurements of low-temperature EPR spectra; and Drs. Lawrence M. Henling and Michael W. Day for assistance with the acquisition and analysis of crystallographic data.

---

### References

- (1) a) Gross, Z.; Galili, N.; Saltsman, I. *Angew. Chem. Int. Ed.* **1999**, *38*, 1427–1429. b) Paolesse, R.; Jaquinod, L.; Nurco, D. J.; Mini, S.; Sagone, F.; Boschi, T.; Smith, K. M. *Chem. Commun.* **1999**, 1307–1308. c) Gross, Z.; Galili, N.; Simkhovich, L.; Saltsman, I.; Botoshansky, M.; Blaser, D.; Boese, R.; Goldberg, I. *Org. Lett.* **1999**, *1*, 599–602. d) Koszarna, B.; Gryko, D.T. *J. Org. Chem.* **2006**, *71*, 3707–3717.
- (2) a) Gryko, D. T. *J. Porphyrins Phthalocyanines*, **2008**, *12*, 906. b) Nardis, S.; Monti, D.; Paolesse, R. *Mini-Rev. Org. Chem.* **2005**, *2*, 355–372.
- (3) a) Aviv, I.; Gross, Z. *Chem. Commun.* **2007**, 1987–1999. b) Goldberg, D. P. *Acc. Chem. Res.* **2007**, *40*, 626–634. c) Gryko, D. T.; Fox, J. P.; Goldberg, D. P. *J. Porphyrins and Phthalocyanines* **2004**, *8*, 1091–1105.
- (4) Simkhovich, L.; Gross, Z. *Tet. Lett.* **2001**, *42*, 8089–8092.
- (5) a) Gross, Z.; Golubkov, G.; Simkhovich, L. *Angew. Chem. Int. Ed. Eng.* **2000**, *39*, 4045–4047. b) Golubkov, G.; Bendix, J.; Gray, H. B.; Mahammed, A.; Goldberg, I.; DiBilio, A. J.; Gross, Z. *Angew. Chem. Int. Ed. Eng.* **2001**, *40*, 2132–2134. c) Mandimutsira, B. S.; Ramdhanie, B.; Todd, R. C.; Wang, H. L.; Zareba, A. A.; Czernuszewicz, R. S.; Goldberg, D. P. *J. Am. Chem. Soc.* **2002**, *124*, 15170–15171.
- (6) Mahammed, A.; Gray, H. B.; Meier-Callahan, A. E.; Gross, Z. *J. Am. Chem. Soc.* **2003**, *125*, 1162–1163.

- (7) Grodkowski, J.; Neta, P.; Fujita, E.; Mohammed, A.; Simkhovich, L.; Gross, Z. *J. Phys. Chem. A* **2002**, *106*, 4772–4778.
- (8) a) Gross, Z.; Gray, H. B. *Comm. Inorg. Chem.* **2006**, *27*, 61. b) Hocking, R. K.; DeBeer George, S.; Gross, Z.; Walker, F. A.; Hodgson, K. O.; Hedman, B.; Solomon, E. I. *Inorg. Chem.* **2009**, *48*, 1678–1688.
- (9) a) Golubkov, G.; Gross, Z. *Angew. Chem. Int. Ed.* **2003**, *42*, 4507–4510. b) Golubkov, G.; Gross, Z. *J. Am. Chem. Soc.* **2005**, *127*, 3258–3259.
- (10) a) Gross, Z.; Gray, H. B. *Adv. Synth. Catal.* **2004**, *346*, 165–170. b) Mohammed, A.; Gross, Z. *Angew. Chem. Int. Ed.* **2006**, *45*, 6544–6547. c) Agadjanian, H.; Weaver, J. J.; Mohammed, A.; Rentsendorj, A.; Bass, S.; Kim, J.; Dmochowski, I. J.; Margalit, R.; Gray, H. B.; Gross, Z.; Medina-Kauwe, L. K. *Pharm. Res.* **2006**, *23*, 367–377. d) Haber, A.; Mohammed, A.; Fuhrman, B.; Volkova, N.; Coleman, R.; Hayek, T.; Aviram, M.; Gross, Z. *Angew. Chem. Int. Ed.* **2008**, *47*, 7896–7900.
- (11) Flamigni, L.; Gryko, D. T. *Chem. Soc. Rev.* **2009**, *in press*.
- (12) Agadjanian, H.; Ma, J.; Rensendorj, A.; Valluripalli, V.; Hwang, J. Y.; Mohammed, A.; Farkas, D. L.; Gray, H. B. *Proc. Natl. Acad. Sci. USA* **2009**, *106*, 6105–6110.
- (13) Bruckner, C.; Barta, C. A.; Brinas, R. P.; Krause Bauer, J. A. *Inorg. Chem.* **2003**, *42*, 1673–1680.
- (14) Simkhovich, L.; Luobeznova, I.; Goldberg, I.; Gross, Z. *Chem. Eur. J.* **2003**, *9*, 201–208.
- (15) Saltzman, I.; Simkhovich, L.; Balazs, Y.; Goldberg, I.; Gross, Z. *Inorg. Chim. Acta* **2004**, *357*, 3038–3046.
- (16) Luobeznova, I.; Raizman, M.; Goldberg, I.; Gross, Z. *Inorg. Chem.* **2006**, *45*, 386–394.
- (17) Tse, M. K.; Zhang, Z.; Mak, T. C. W.; Chan, K. S. *Chem. Commun.* **1998**, 1199–1200.
- (18) Palmer, J. H.; Day, M. W.; Wilson, A. D.; Henling, L. M.; Gross, Z.; Gray, H. B. *J. Am. Chem. Soc.* **2008**, *130*, 7786–7787.
- (19) a) Gryko, D. T.; Fox, J. P.; Goldberg, D. P. *Journal of Porphyrins and Phthalocyanines* **2004**, *8*, 1091–1105. b) Goldberg, D. P. *Acc. Chem. Res.* **2007**, *40*, 626–634. c) Kerber, W. D.; Goldberg, D. P. *J. Inorg. Biochem.* **2006**, *100*, 838–857. d) Aviv, I.; Gross, Z. *Chem. Commun.* **2007**, 1987–1999. e) Ghosh, A.; Steene, E. J. *Inorg. Biochem.* **2002**, *91*, 423–436. f) Kadish, K. M.; Shen, J.; Fremond, L.; Chen, P.; El Ojaimi, M.; Chkounda, M.; Gros, C. P.; Barbe, J. M.; Ohkubo, K.; Fukuzumi, S.; Guillard, R. *Inorg. Chem.* **2008**, *47*, 6726–6737.
- (20) a) Cheung, C. W.; Chan, K. S. *Organometallics* **2008**, *27*, 3043–3055. b) Li, B.; Chan, K. S. *Organometallics* **2008**, *27*, 4034–4042. c) Cui, W.; Li, S.; Wayland, B. B. *J. Organomet. Chem.* **2007**, *692*, 3198–3206. d) Yanagisawa, M.; Tashiro, K.; Yamasaki, M.; Aida, T. *J. Am. Chem. Soc.* **2007**, *129*, 11912–11913. e) Song, X.; Chan, K. S. *Organometallics* **2007**, *26*, 965–970. f) Deng, Y.; Huang, M.-J. *Chem. Phys.* **2006**, *321*, 133–139. g) Toganoh, M.; Konagawa, J.; Furuta, H. *Inorg. Chem.* **2006**, *45*, 3852–3854. h) Flamigni, L.; Marconi, G.; Dixon, I. M.; Collin, J.-P.; Sauvage, J.-P. *J. Phys. Chem. B* **2002**, *106*, 6663–6671. i) Zhai, H.; Bunn, A.; Wayland B. *Chem. Commun.* **2001**, 1294–1295. j) Shi, C.; Mak, K. W.; Chan, K. S.; Anson, F. C. *J. Electroanal. Chem.* **1995**, *397*, 321–324. k) Collman, J. P.; Chng, L. L.; Tyvoll, D. A. *Inorg. Chem.* **1995**, *34*, 1311–1324. l) Kadish, K. M.; Deng, Y. J.; Yao, C.-L.; Anderson, J. E. *Organometallics* **1988**, *7*, 1979–1983.
- (21) Abbreviations: [Ir(cod)Cl]<sub>2</sub>, H<sub>3</sub>(tpfc), tpfc, Br<sub>8</sub>-tpfc, *t-4bpa*, tma-N-oxide, tma, and py stand for iridium(I) cyclooctadiene chloride dimer, 5,10,15-*tris*-pentafluorophenylcorrole, 5,10,15-*tris*-pentafluorophenylcorrolato trianion, 2,3,7,8,12,13,17,18-octabromo-5,10,15-*tris*-pentafluorophenylcorrolato trianion, *tris*(4-bromophenyl)aminium hexachloroantimonate, trimethylamine N-oxide, trimethylamine, and pyridine, respectively.
- (22) Ou, Z.; Shao, J.; D'Souza, F.; Tagliatesta, P.; Kadish, K. M. *J. Porphyrins Phthalocyanines* **2004**, *8*, 201–214, and references therein.
- (23) Kadish, K. M.; Shen, J.; Fremond, L.; Chen, P.; El Ojaimi, M.; Chkounda, M.; Gros, C. P.; Barbe, J. M.; Ohkubo, K.; Fukuzumi, S.; Guillard, R. *Inorg. Chem.* **2008**, *47*, 6726–6737.
- (24) Brown, G. M.; Hopf, F. R.; Meyer, T. J.; Whitten, D. G.; *J. Am. Chem. Soc.* **1975**, *97*, 5385–5390.
- (25) 140  $\mu$ L of a solution of 0.5 mL of trifluoroacetic acid in 5 mL of CH<sub>2</sub>Cl<sub>2</sub> was added to 1.73 mL of warm (liquid) pentafluorobenzaldehyde, with rapid stirring. Addition of 1.46 mL of freshly distilled pyrrole resulted in the rapid formation of a viscous red solution. After 10 minutes, 20 mL of CH<sub>2</sub>Cl<sub>2</sub> was added and the mixture was allowed to stir briefly, followed by slow addition of 3.84 g of DDQ to oxidize the newly formed macrocycle. Purification was accomplished by successive chromatographic treatments

- 
- with 6.5:3.5 CH<sub>2</sub>Cl<sub>2</sub>:hexanes and 8.5:1.5 CH<sub>2</sub>Cl<sub>2</sub>:hexanes on silica, followed by recrystallization from hot pentane.
- (26) a) Simkhovich, L.; Galili, N.; Saltsman, I.; Goldberg, I.; Gross, Z. *Inorg. Chem.* **2000**, *39*, 2704–2705.  
b) Mahammed, A.; Giladi, I.; Goldberg, I.; Gross, Z. *Chem. Eur. J.* **2001**, *7*, 4259–4265.
- (27) Analogous procedures were employed for the synthesis of iridium(III) corroles with substituted pyridines; characterization data are reported in Supporting Information.
- (28) Balazs, Y. S.; Saltsman, I.; Mahammed, A.; Tkachenko, E.; Golubkov, G.; Levine, J.; Gross, Z. *Magn. Reson. Chem.* **2004**, *42*, 624–635.
- (29) Simkhovich, L.; Goldberg, I.; Gross, Z. *J. Porphyrins Phthalocyanines*. **2002**, *6*, 439–444.
- (30) Bendix, J.; Dmochowski, I. J.; Gray, H. B.; Mahammed, A.; Simkhovich, L.; Gross, Z. *Angew. Chem. Int. Ed.* **2000**, *39*, 4048–4051.
- (31) Kowalska, D.; Liu, X.; Tripathy, U.; Mahammed, A.; Gross, Z.; Hirayama, S.; Steer, R. P. *Inorg. Chem.* **2009**, *48*, 2670–2676.
- (32) Calogero, G.; Giuffrida, G.; Serroni, S.; Ricevuto, V.; Campagna, S. *Inorg. Chem.* **1995**, *34*(3), 541–545.
- (33) Gross, Z. *J. Biol. Inorg. Chem.* **2001**, *6*, 733–738.
- (34) Fuhrhop, J. H.; Kadish, K. M.; Davis, D. G. *J. Am. Chem. Soc.* **1973**, *95*, 5140–5147.
- (35) Meier–Callahan, A. E.; di Bilio, A. J.; Simkhovich, L.; Mahammed, A.; Goldberg, I.; Gray, H. B.; Gross, Z. *Inorg. Chem.* **2001**, *40*, 6788–6793.
- (36) a) Diversi, P.; Iaconi, S.; Ingrosso, G.; Laschi, F.; Lucherini, A.; Pinzino, C.; Ucello–Barretta, G.; Zanello, P. *Organometallics* **1995**, *14*, 3275–3287. b) Diversi, P.; de Biani, F. F.; Ingrosso, G.; Laschi, F.; Lucherini, A.; Pinzino, C.; Ucello–Barretta, G.; Zanello, P. *J. Organomet. Chem.* **1999**, *584*, 73–86.
- (37) Walker, F. A. *Coord. Chem. Rev.* **1999**, *185–186*, 471–534.
- (38) Simkhovich, L.; Goldberg, I.; Gross, Z. *Inorg. Chem.* **2002**, *41*, 5433–5439.

*Chapter 3*

## NEAR-IR PHOSPHORESCENCE OF IRIIDIUM(III) CORROLES AT AMBIENT TEMPERATURE

In my initial communication to JACS, I noted that the progress of iridium insertion into the corrole framework could be monitored by observing the disappearance of the strong red luminescence of free-base H<sub>3</sub>tpfc. The lack of any visible fluorescence from the iridium products hardly comes as a surprise, given that heavy metal atoms often promote ultra-fast ISC from a luminescent singlet state to a non-radiating triplet. However, cyclometalated and polyimine Ir(III) complexes often display bright phosphorescence from the triplet state, and heavy-metal porphyrins (particularly platinum complexes) are well-known for their triplet luminescence. With this in mind, I decided to measure the luminescence of a few of my compounds despite the fact that they are not visibly fluorescent, and the results turned out to be quite intriguing.

At first, I thought the large emission peaks I was seeing around 800 nm from degassed Ir corrole solutions might be artifacts of the correction file on my group's fluorimeter. R928P Hamamatsu PMTs are not particularly sensitive past 750 nm, and the multiplication of photon intensity that the software performs to make up for this lack of sensitivity can sometimes cause strange effects. However, the experiments were reproducible, and the intensity of the emission scaled well with the concentration of the luminophore, so Jay Winkler, director of BILRC at Caltech, purchased an instrument designed for detection of more red-shifted luminescence than the fluorimeter could comfortably handle, and I

quickly confirmed that the near-IR phosphorescence being observed was true emission and not an instrumental artifact.

Along with another Gray group student, Alec Durrell, I set about examining the luminescence lifetimes and quantum yields of the Ir(III) corroles. Our main findings were as follows: the lifetimes of the luminescence are in the range of hundreds of nanoseconds to a few microseconds, becoming a bit longer at low temperature; the quantum yields of luminescence are low, topping out around 1% for the py-ligated complex; and the UV-vis absorption peaks of the corroles display a strong dependence on the polarizability of the solvent, suggesting that the initial excited states of the complexes are quite a bit more polar than their ground states. Interestingly, the non-radiative decay rates of these near-IR emitters are fairly slow considering the low energy of the excited state; indeed, the low quantum yields (compared with, say, cyclometalated red Ir emitters) appear to stem from exceptionally slow radiative rates as opposed to the rapid non-radiative decay that usually foreshortens the luminescence lifetimes of near-IR emitters. Experiments to determine the reasons for this apparently slow radiative decay (which could perhaps be an artifactual result of incomplete  $S_1 \rightarrow T_0$  ISC) are underway. Additionally, a number of other Ir(III) corroles are being examined for their luminescence properties, and TD-DFT calculations, thus far unsuccessful at modeling the absorption spectra of the compounds, are also being run with an eye toward determining more exactly the nature of the initial excited states and the emitting triplet states. Our work up to mid-2010 is presented below in JACS communication format.

### Near-IR Phosphorescence of Iridium(III) Corroles at Ambient Temperature

Reproduced with permission from: Joshua H. Palmer, Alec C. Durrell, Zeev Gross, Jay R. Winkler, and Harry B. Gray. *J. Am. Chem. Soc.*, **2010**, 132 (27), pp 9230–9231. Copyright 2010 American Chemical Society

Porphyrin complexes displaying phosphorescence at ambient temperatures have been employed for photodynamic therapy,<sup>1</sup> oxygen detection,<sup>2</sup> and organic light-emitting diodes.<sup>3</sup> A great deal of research has been done on d<sup>8</sup> (mainly Pt<sup>II</sup>, Pd<sup>II</sup>, and Au<sup>III</sup>) complexes,<sup>4</sup> which emit at relatively long wavelengths (> 600 nm) with lifetimes in the microsecond range. In sharp contrast, d<sup>6</sup> metalloporphyrins have scarcely been investigated, although room temperature phosphorescence of ruthenium(II) porphyrins has been reported.<sup>5</sup>

Metallocorroles have shown promise as therapeutic agents,<sup>6</sup> with biodistribution and bioavailability profiles as well as cellular uptake and intracellular locations<sup>7</sup> determined for fluorescent gallium(III) derivatives.<sup>8</sup> Although progress has been made, much work remains before we can claim to have developed optimized compounds for optical examination of biological systems.<sup>9</sup> It would be beneficial to have agents that emit with microsecond lifetimes beyond 700 nm, as the most common obstacles to efficient biological imaging—tissue absorbance and intrinsic fluorescence—could thus be circumvented.

Here we report the photophysical properties of iridium(III) corroles,<sup>10</sup> which differ significantly from those of cyclometalated and polyimine Ir(III) compounds,<sup>11</sup> other luminescent metallocorroles,<sup>12</sup> and free-base corroles.<sup>13</sup> Iridium(III) corrole phosphorescence is observed at ambient temperature at wavelengths much longer (> 800



nm) than those of most other luminescent Ir(III) complexes.<sup>11</sup> Our investigations focused on the three corroles shown in Figure 3-1.

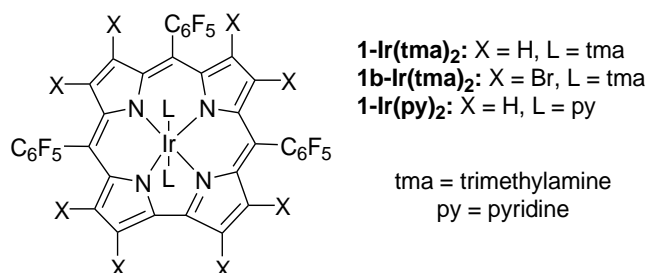


Figure 3-1: Details of synthesis and characterization (NMR, MS, XRD) of the three corroles are reported in Supporting Information

Emission spectra were recorded in toluene at 298 and 77 K (Figure 3-2). The spectra display two intense features separated by approximately  $1400\text{ cm}^{-1}$ . It is likely that a ring-based vibration is excited in the transition to the lower energy component.<sup>14</sup> At low temperature, the higher energy emission maximum of each Ir(III) corrole blue shifts by 10 nm (a rigidochromic effect indicating that the transition involves charge transfer)<sup>15</sup> (Figure 3-2b). The narrow linewidth and  $\sim 1400\text{ cm}^{-1}$  spacing suggest that the emission is from a  $\pi \rightarrow \pi^*$  excited state. Electronic structure calculations place an occupied orbital with metal character close to the HOMO in related Ir(III) corroles,<sup>16</sup> indicating that  $^3\text{MLCT}$  states will be near those of the lowest corrole-localized excited states. Other investigators have reported that  $^3\text{MLCT}$  is the emissive state in cyclometalated Ir(III) complexes.<sup>17</sup>

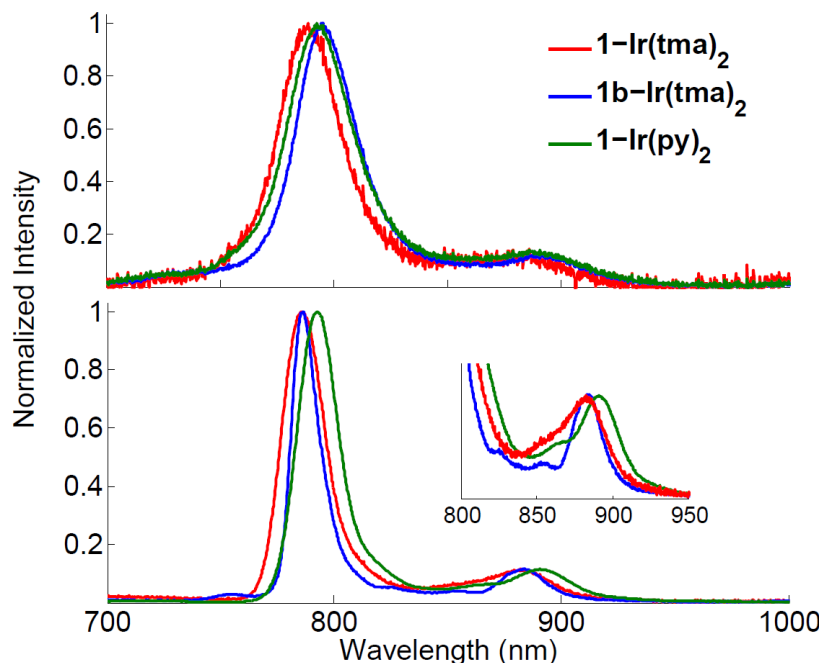


Figure 3-2: Emission spectra of Ir(III) corroles in degassed toluene solution at 298 K (top) and 77K (bottom)

Luminescence quantum yields and lifetimes in degassed and aerated toluene solutions at room temperature (and lifetimes at 77 K) are set out in Table 3-1. **1-Ir(tma)<sub>2</sub>** and **1b-Ir(tma)<sub>2</sub>** have relatively short lifetimes and low quantum yields. **1-Ir(py)<sub>2</sub>** exhibits a much higher luminescence quantum yield (1.2%) and a longer lifetime.<sup>18</sup> It is apparent even from these initial results that Ir(III)-corrole photophysical properties depend markedly on the nature of the axial ligand.

Table 3-1: Photophysical data for Ir(III) corroles in toluene solutions<sup>a</sup>

Compound	<i>1</i> -Ir( <i>tma</i> ) <sub>2</sub>	<i>1b</i> -Ir( <i>tma</i> ) <sub>2</sub>	<i>1</i> -Ir( <i>py</i> ) <sub>2</sub>
$\Phi_{\text{ph}}^{\text{b}}$	$3.3 \times 10^{-4}$	$3.9 \times 10^{-3}$	$1.2 \times 10^{-2}$
$\lambda_{\text{Ar}}$ (nm)/ $\tau_{\text{Ar}}$ ( $\mu\text{s}$ )	788 / 0.220	795 / 1.19	792 / 4.91
$\tau_{\text{air}}^{\text{c}}$ ( $\mu\text{s}$ )	0.170	0.760	0.380
$\lambda_{77\text{K}}$ (nm)/ $\tau_{77\text{K}}$ ( $\mu\text{s}$ )	786 / 2.77	786 / 4.72	793 / 7.69
$k_{\text{r}}$ ( $\text{s}^{-1}$ )	$1.5 \times 10^3$	$3.28 \times 10^3$	$2.44 \times 10^3$
$k_{\text{nr}}$ ( $\text{s}^{-1}$ )	$4.54 \times 10^6$	$8.4 \times 10^5$	$2.0 \times 10^5$

<sup>a</sup>At 298 K unless noted otherwise. <sup>b</sup>Luminescence quantum yields were standardized against free-base tetraphenylporphyrin ( $\Phi_{\text{f}} = 0.13$  in toluene solution at 298 K). <sup>c</sup>Measured under atmospheric conditions. UV-vis absorption spectra (Figure 3-3) of the three Ir(III) corroles exhibit split Soret ( $S_0 \rightarrow S_2$ ) and Q ( $S_0 \rightarrow S_1$ ) bands. The splitting of the Soret bands is 1400–1700  $\text{cm}^{-1}$  in all cases; the Q bands are split by roughly 1800  $\text{cm}^{-1}$  in the spectra of *1*-Ir(*tma*)<sub>2</sub> and *1b*-Ir(*tma*)<sub>2</sub> but only by 1000  $\text{cm}^{-1}$  in the spectrum of *1*-Ir(*py*)<sub>2</sub>.

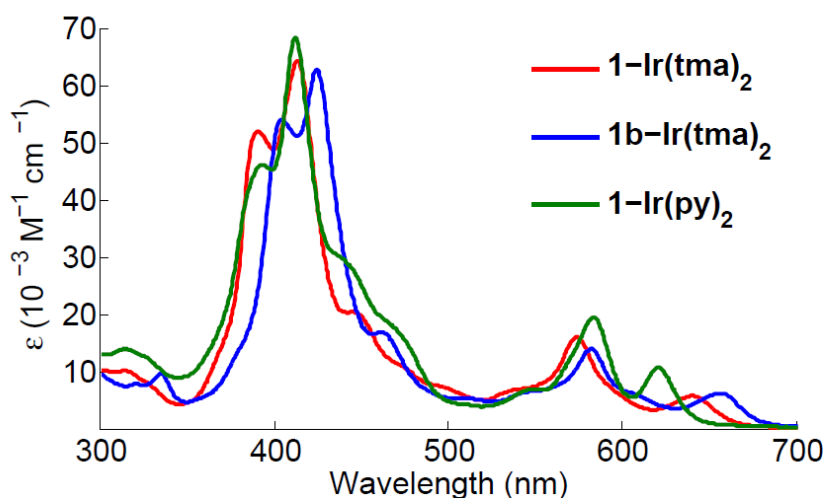


Figure 3-3: UV-vis spectra of Ir(III) corroles in toluene solution at 298 K. *1b*-Ir(*tma*)<sub>2</sub> is red-shifted and *1*-Ir(*py*)<sub>2</sub> has the tightened Q band system

The effect of solvent polarizability on Ir(III)–corrole spectra was investigated to probe the extent of charge transfer in initially formed electronic excited states. UV-vis spectra were obtained in a variety of solvents: Soret band maxima were plotted against polarizability  $f$  (Figure 3-4), defined as  $f(n) = (n^2 - 1)/(2n^2 + 1)$ ,<sup>19</sup> where  $n$  is the refractive index of the solvent. (The ground states are relatively nonpolar, so inclusion of a solvent dielectric term is not appropriate.) The strong negative correlation ( $R^2 > 0.9$ ) between the polarizability of the solvent and the energy of the Soret transition indicates that in each

case the excited state is substantially more polar than the ground state.<sup>20</sup> The Q band maxima display a similar trend. The striking solvatochromic behavior of Ir(III) corroles potentially could be exploited in optical sensors as well as other applications requiring solvent-based tuning of absorption and emission properties.

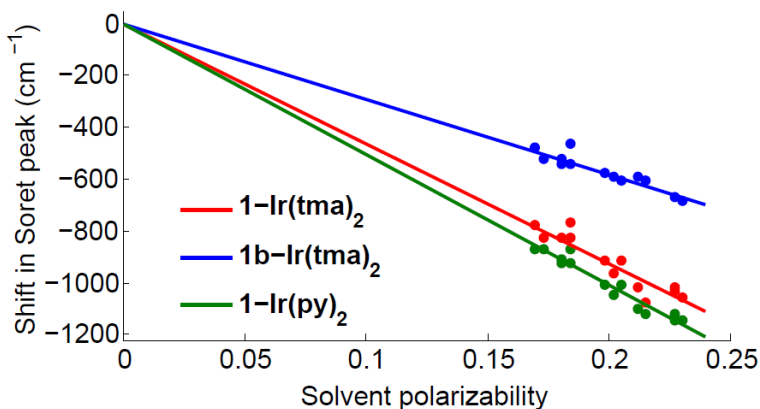


Figure 3-4: Shift in the lower energy Soret component as a function of solvent polarizability ( $n$  used is that of the sodium D line at 20 °C; **1b-Ir(tma)<sub>2</sub>** is at the top, then **1-Ir(tma)<sub>2</sub>** and **1-Ir(py)<sub>2</sub>**)

Although the Soret solvatochromic shifts of **1-Ir(tma)<sub>2</sub>** and **1-Ir(py)<sub>2</sub>** are similar, **1b-Ir(tma)<sub>2</sub>** exhibits a somewhat weaker trend, which we suggest is attributable to bromine atom “prepolarization” of the electron density on the corrole, thereby decreasing the change in dipole moment upon excitation. But we cannot rule out a simpler explanation, namely, that the initially formed **1b-Ir(tma)<sub>2</sub>** excited state is not as polar as those of the other corroles.

Our work has established that Ir(III) corroles phosphoresce in the near infrared region at ambient temperatures with lifetimes and quantum yields that depend strongly on the nature of the axial ligands. We conclude from emission band shapes and vibronic splittings taken together with results from electronic structure calculations that the phosphorescence in each

case is attributable to a transition from a corrole  $\pi \rightarrow \pi^*$  triplet state that likely has some  $^3\text{MLCT}$  character.

**Acknowledgment:** This work was supported by the NSF Center for Chemical Innovation (CCI Powering the Planet, Grants CHE-0802907 and CHE-0947829), the US-Israel BSF, CC SER (Gordon and Betty Moore Foundation), and the Arnold and Mabel Beckman Foundation.

## References

- (1) Zenkevich, E.; Sagun, E.; Knyukshto, V.; Shulga, A.; Mironov, A.; Efremova, O.; Bonnett, R.; Phinda Songca, S.; Kassem, M. *J. Photochem. Photobiol. B: Bio.* **1996**, *33*, 171–180.
- (2) Papkovsky, D. B.; Ponomarev, G. V.; Trettnak, W.; O'Leary, P. *Anal. Chem.* **1995**, *67*, 4112–4117.
- (3) a) Kwong, R. C.; Sibley, S.; Baldo, M. A.; Forrest, S. R.; Thompson, M. E. *Chem. Mater.* **1999**, *11*, 3709–3713. b) Antipas, A.; Dolphin, D.; Gouterman, M.; Johnson, E. C. *J. Am. Chem. Soc.* **1978**, *100*, 7705–7709.
- (4) a) Sun, Y.; Borek, C.; Hanson, K.; Djurovich, P. I.; Thompson, M. E.; Brooks, J.; Brown, J. J.; Forrest, S. R. *App. Phys. Lett.* **2007**, *90*, 213503/1–213503/3. b) Wiehe, A.; Stollberg, H.; Runge, S.; Paul, A.; Senge, M. O.; Roder, B. *J. Porph. Pthalo.* **2001**, *5*, 853–860.
- (5) Tait, C. D.; Holten, D.; Barley, M. H.; Dolphin, D.; James, B. R. *J. Am. Chem. Soc.* **1985**, *107*, 1930–1934, and references therein.
- (6) a) Okun, Z.; Kupersmidt, L.; Amit, T.; Mandel, S.; Bar-Am, O.; Youdim, M. B. H.; Gross, Z. *ACS Chem. Biol.* **2009**, *4*, 910–914. b) Agadjanian, H.; Ma, J.; Rentsendorj, A.; Valluripalli, V.; Hwang, J. Y.; Mahammed, A.; Farkas, D. L.; Gray, H. B.; Gross, Z.; Medina-Kauwe, L. K. *Proc. Nat. Acad. Sci.* **2009**, *106*, 6100–6105.
- (7) Agadjanian, H.; Weaver, J. J.; Mahammed, A.; Rentsendorj, A.; Bass, S.; Kim, J.; Domchowski, I. J.; Margalit, R.; Gray, H. B.; Gross, Z.; Medina-Kauwe, L. K. *Pharmaceutical Res.* **2006**, *23*, 367–377.
- (8) Weaver, J. J.; Sorasaene, K.; Sheikh, M.; Goldschmidt, R.; Tkachenko, E.; Gross, Z.; Gray, H. B. *J. Porph. Pthalo.* **2004**, *8*, 76–81.
- (9) Hwang, J. Y.; Agadjanian, H.; Medina-Kauwe, L. K.; Gross, Z.; Gray, H. B.; Sorasaene, K.; Farkas, D. L. *SPIE* **2008**, *6859*, 68590G.
- (10) a) Palmer, J. H.; Day, M. W.; Wilson, A. D.; Henling, L. M.; Gross, Z.; Gray, H. B. *J. Am. Chem. Soc.* **2008**, *130*, 7786–7787. b) Palmer, J. H.; Mahammed, A.; Lancaster, K. M.; Gross, Z.; Gray, H. B. *Inorg. Chem.* **2009**, *48*, 9308–9315.
- (11) a) Dixon, I. M.; Collin, J.-P.; Sauvage, J.-P.; Flamigni, L.; Encinas, S.; Barigelletti, F. *Chem. Soc. Rev.* **2000**, *29*, 385–391. b) Tsuboyama, A.; Iwawaki, H.; Furugori, M.; Mukaide, T.; Kamatani, J.; Igawa, S.; Moriyama, T.; Miura, S.; Takiguchi, T.; Okada, S.; Hoshino, M.; Ueno, K. *J. Am. Chem. Soc.* **2003**, *125*, 12971–12979. c) Hung, J.-Y.; Chi, Y.; Pai, I.-H.; Yu, Y.-C.; Lee, G.-H.; Chou, P.-T.; Wong, K.-T.; Chen, C.-C.; Wu, C.-C. *Dalton Trans.* **2009**, *33*, 6472–6475. d) Shin, C. H.; Huh, J. O.; Lee, M. H.; Do, Y. *Dalton Trans.* **2009**, *33*, 6476–6479.
- (12) a) Flamigni, L.; Gryko, D. T. *Chem. Soc. Rev.* **2009**, *38*, 1635–1646. b) Nardis, S.; Mandoj, F.; Paolesse, R.; Fronczek, F. R.; Smith, K. M.; Prodi, L.; Montalti, M.; Battistini, G. *Eur. J. Inorg. Chem.* **2007**, *16*, 2345–2352. c) Poulin, J.; Stern, C.; Guillard, R.; Harvey, P. D. *Photochem. Photobiol.* **2006**, *82*, 171–176. d) Liu, X.; Mahammed, A.; Tripathy, U.; Gross, Z.; Steer, R. P. *Chem. Phys. Lett.* **2008**, *459*, 113–118.
- (13) Ding, T.; Alemán, E. A.; Modarelli, D. A.; Ziegler, C. J. *J. Phys. Chem. A.* **2005**, *109*, 7411–7417.
- (14) Steene, E.; Wondimagegn, T.; Ghosh, A. *Inorg. Biochem.* **2002**, *88*, 113–118.
- (15) Chen, P.; Meyer, T. J. *Chem. Rev.* **1998**, *98*, 1439.
- (16) Dong, S. S.; Nielsen, R. J.; Palmer, J. H.; Gray, H. B.; Gross, Z.; Dasgupta, S.; Goddard, W. A. *submitted*.
- (17) Rausch, A. F.; Thompson, M. E.; Yersin, H. *J. Phys. Chem. A.* **2009**, *113*, 5927–5932.

- 
- (18) Ir(III) complexes with 3% quantum yields have been used successfully to stain living cells, see: Yu, M.; Zhao, Q.; Shi, L.; Li, F.; Zhou, Z.; Yang, H.; Yi, T.; Huang, C. *Chem. Commun.* **2008**, 2115–2117.
- (19) Lakowicz, J. R. *Principles of Fluorescence Spectroscopy*, 2nd. Ed.; Kluwer Academic/Plenum Publishers: New York, **1999**.
- (20) a) Marcus, R.A. *J. Chem Phys.* **1965**, *43*, 1261–1274. b) Mody, V. V.; Fitzpatrick, M. B.; Zabaneh, S. S.; Czernuszewicz, R. S.; Galezowski, M.; Gryko, D. T. *J. Porph. Pthalo.* **2009**, *13*, 1040–1052.

*Chapter 4*

## ELECTRONIC STRUCTURES OF GROUP 9 METALLOCORROLES WITH AXIAL AMMINES

During the summer of 2009, an undergraduate student named Scarlett, from Chi-Ming Che's group at the University of Hong Kong, came to work with me doing DFT calculations on some iridium corrole complexes. Along with a postdoctoral student from Bill Goddard's group named Smith, who has significantly more experience with computational chemistry than I do, Scarlett ran geometry optimizations and single-point energy calculations on a variety of hypothetical corrole complexes. I wanted to see what theory had to say about the results I detailed previously in Chapter 2 of this work, so we ran calculations on Co(III), Rh(III), and Ir(III) complexes of tpfc (as well as analogous complexes of the hypothetical, and less computationally intensive, macrocycle tfc) and their one-electron oxidized forms.

The calculations, which were performed in the absence of explicitly included spin-orbit coupling terms, produced ground states for all three cations in which the highest-lying SOMO is localized largely on the corrole, with negligible metal character. Later, more sophisticated computational results will be discussed later in the thesis, and suggest significant spin on the metal in the case of iridium. However, those calculations include (and examine) parameters with which we were not concerned at the time we did the work presented in this chapter, and the inspiration for performing them stemmed from the computational work discussed below.

### Electronic Structures of Group 9 Metallocorroles with Axial Ammines

Reproduced with permission from: Sijia S. Dong, Robert J. Nielsen, Joshua H. Palmer, Harry B. Gray, Zeev Gross, Siddharth Dasgupta, and William A. Goddard III. *Inorg. Chem.*, **2011**, 50 (3), pp 764–770. Copyright 2011 American Chemical Society

#### Abstract

The electronic structures of metallocorroles (tpfc)M(NH<sub>3</sub>)<sub>2</sub> [**1-M(NH<sub>3</sub>)<sub>2</sub>**] and (tfc)M(NH<sub>3</sub>)<sub>2</sub> [**1f-M(NH<sub>3</sub>)<sub>2</sub>**] (tpfc is the trianion of 5,10,15-(tris)pentafluorophenylcorrole, tfc is the trianion of 5,10,15-trifluorocorrole, and M = Co, Rh, Ir) have been computed using first principles quantum mechanics [B3LYP flavor of Density Functional Theory (DFT) with Poisson-Boltzmann continuum solvation]. The geometry was optimized for both the neutral systems (formal M<sup>III</sup> oxidation state) and the one-electron oxidized systems (formally M<sup>IV</sup>). As expected, the M<sup>III</sup> systems have a closed shell d<sup>6</sup> configuration; for all three metals, the one-electron oxidation was calculated to occur from a ligand-based orbital (HOMO of B<sub>1</sub> symmetry). The ground state of the formal M<sup>IV</sup> system has M<sup>III</sup>-C $\pi$  character, indicating that the metal remains d<sup>6</sup>, with the hole in the corrole  $\pi$  system. As a result the calculated M<sup>IV/III</sup> reduction potentials are quite similar (0.64, 0.67, and 0.56 V vs. SCE for M = Ir, Rh and Co, respectively), whereas the differences would have been large for purely metal-based oxidations. Vertically excited states with substantial metal character are well separated from the ground state in one-electron-oxidized cobalt (0.27 eV) and rhodium (0.24 eV) corroles, but become closer in energy in the iridium (0.15 eV) analogues. The exact splittings depend on the chosen functional and vary by ~ 0.1 eV.



## Introduction

Understanding the factors that determine the stability and reactivity of metal complexes in high oxidation states could greatly facilitate the design of catalysts for substrate oxidation reactions.<sup>1</sup> A major problem that must be addressed is that the ligands themselves often undergo redox changes during catalysis.<sup>2,3,4</sup> Such non-innocent ligand behavior is a hallmark of oxidative catalytic cycles of heme enzymes, where a highly reactive intermediate (Compound I) formed by two-electron oxidation of an iron(III) precursor is better described as an oxoiron(IV) ligand radical than as an iron(V) complex.<sup>5</sup> Depending on the particular enzyme, one unpaired electron is located on either an orbital of the chelating porphyrin or on a nearby amino acid residue.<sup>6</sup> Importantly, advances in synthesis, together with high level spectroscopy and theory, have shed new light on these and related issues, with surprising findings in certain cases: for example, the likelihood of a role for electronic excited-state coupling in promoting catalytic hydroxylations by heme and nonheme-iron enzymes.<sup>7</sup>

The recent explosive growth in corrole chemistry has provided many new examples that challenge current views of the electronic structures of complexes containing non-innocent ligands.<sup>8</sup> Although corroles (both metal-free and in complexes with non-redox-active elements) are prone to oxidation,<sup>9</sup> it is well established that they stabilize transition metals in unusually high oxidation states.<sup>10</sup> In some cases, non-innocent behavior has made it particularly difficult to assign metal and ligand oxidation states, as in five-coordinate (chloro)iron corroles, where a combination of spectroscopy and DFT calculations has established that metal- and corrole-based orbitals are strongly coupled.<sup>11</sup>

Our recent experimental work has highlighted the need to develop electronic structural descriptions of analogous 3d-4d-5d Group 9 metallocorroles, as the successful syntheses of five- and six-coordinate iridium(III) corroles completed a very rare isostructural 3d ( $\text{Co}^{\text{III}}$ ), 4d ( $\text{Rh}^{\text{III}}$ ), and 5d ( $\text{Ir}^{\text{III}}$ ) series.<sup>12</sup> Surprisingly, the reduction potentials show very little variation among the three corroles, while EPR results suggest a shift from corrole- to metal-centered oxidation in moving from 3d and 4d to 5d complexes. These findings have led us to attempt full electronic structural elucidation of Group 9 metallocorroles by computational methods.

Third-row transition metal corroles are rare<sup>13</sup> (in addition to Ir, one Re complex has been reported).<sup>14</sup> Among elements in the periodic table, only those in Group 9 feature corrole complexes for all three metals. The structures and reactivity patterns of the Group 9 metallocorroles have been characterized previously using a battery of experimental techniques, and we believe that computational analyses of their electronic structures will allow us to refine our interpretations of the properties of these interesting molecules. In particular, we do not have a satisfactory explanation for the small differences in  $\text{Co}^{\text{IV/III}}$ ,  $\text{Rh}^{\text{IV/III}}$ , and  $\text{Ir}^{\text{IV/III}}$  reduction potentials. And another puzzle is the greatly enhanced metal character indicated by EPR spectra in going from “ $\text{Co}^{\text{IV}}$ ” and “ $\text{Rh}^{\text{IV}}$ ” to “ $\text{Ir}^{\text{IV}}$ ”.

We have employed density functional theory (DFT)<sup>15</sup> as the method of choice for determination of metallocorrole electronic structures. The structural parameters of **1-Ir(NH<sub>3</sub>)<sub>2</sub>** from the calculations are consistent with those obtained from X-ray diffraction crystallographic measurements on **1-Ir(tma)<sub>2</sub>** and **1-Ir(py)<sub>2</sub>** (tma = trimethylamine and py = pyridine).<sup>12,13</sup> Calculations were made of the reduction potentials as well as the

electronic structures of  $[\mathbf{1-M(NH_3)_2}]^{0/+}$ . Additionally, less computationally taxing  $[\mathbf{1f-M(NH_3)_2}]^{0/+}$  models were examined. Our computational results show that the very small  $n$  ( $n = 3,4,5$ ) dependence of the reduction potentials of Group 9 metallocorroles is accompanied by a marked decrease in metal orbital energies (compared with those of the corrole) in the order 3d-4d-5d.

### Computational Details

All computations were conducted with the Jaguar 7.0 package (release 207),<sup>16</sup> applying the hybrid density functional B3LYP.<sup>17</sup> B3LYP has proved useful in the calculation of oxidation potentials<sup>18</sup> and yielded spin density distributions and excited state orderings similar to CASPT2 results for an iron-heme model.<sup>19</sup>

Free energies used in the calculation of oxidation potentials are equal to:

$$G = E_{\text{el,gas}} + G_{\text{solv}} + \text{ZPE} + H_{\text{vib}} - S_{\text{vib}}T$$

where  $E_{\text{el,gas}}$  is the gas phase electronic energy,  $G_{\text{solv}}$  is the solvation energy of the compound in dichloromethane, ZPE is the zero-point energy of the complex,  $H_{\text{vib}}$  is the vibrational enthalpy, and  $S_{\text{vib}}$  is the vibrational entropy. The temperature was set to 298 K for all calculations.

Angular-momentum-projected nonlocal effective core potentials<sup>20</sup> (pseudopotentials) optimized by Hay and Wadt<sup>21</sup> were used to replace the core electrons. Thus, the Co, Rh, and Ir atoms were each described with 17 explicit electrons (two 5s, six 5p, plus nine (6s,5d) for neutral Ir). Geometries of the neutral and cationic complexes were optimized

and Hessians for vibrational spectra were calculated in vacuum using the 2- $\zeta$  valence functions for the metals and 6-31G\*\*<sup>22</sup> for all other atoms. Single point energies were then calculated using a 3- $\zeta$  contraction of the Los Alamos valence functions augmented with two f-functions<sup>23</sup> for metals and 6-311G\*\*<sup>++</sup> for other atoms. These single point energies were used to calculate the oxidation potentials. Solvation energies were obtained at the vacuum-optimized geometries with the PBF Poisson-Boltzmann continuum solvation model<sup>24</sup> using default atomic radii, a dielectric constant of  $\epsilon = 8.93$  and probe radius of 2.33 Å to represent dichloromethane. The accuracy of this methodology has been validated in several recent reports.<sup>18,25</sup>

The oxidation potentials (in V) relative to the standard hydrogen electrode (SHE) were calculated using the Nernst equation

$$E_{\text{SHE}} = (G_{\text{ox}} - G_{\text{red}}) / (N_{\text{el}})(23.06 \text{ kcal/mol}\cdot\text{eV}) - 4.3\text{V},$$

where  $N_{\text{el}}$  is 1  $e^-$ , the number of electrons removed. The absolute potential of the standard hydrogen electrode (4.3V) is derived from Tissandier et al.'s determination of the absolute solvation energy of a proton.<sup>26</sup>  $G_{\text{ox}}$  is the Gibbs free energy (in kcal/mol) of the oxidized form of the complex and  $G_{\text{red}}$  is that of the reduced form. The corresponding potentials relative to the saturated calomel electrode (SCE) are

$$E_{\text{SCE}} = E_{\text{SHE}} - 0.24\text{V}^{27}.$$

To simplify orbital analysis of excited states, geometries of the neutral **1-M(NH<sub>3</sub>)<sub>2</sub>** and **1f-M(NH<sub>3</sub>)<sub>2</sub>** complexes were re-optimized with  $C_{2v}$  symmetry enforced. Then, single point energy calculations using the 2- $\zeta$  basis were performed on the corresponding

“M(IV)” complexes to obtain the energies of various states with the electron taken from different orbitals of the M(III) complexes. Level-shifting was applied to aid convergence of the excited states, and the obtained states were resubmitted to the SCF procedure without level-shifting for verification. Orthogonality of excited states in our SCF approach is only guaranteed for the lowest-lying states. This is sufficient because our primary concern involves distinguishing metal-based from ligand-based oxidation in the ground states.

All doublet states used unrestricted orbitals. The spin densities and charges on the metals were also obtained through Mulliken analysis. Unless otherwise stated in the text, upper-case symmetry labels (e.g.,  $1^2A_2$ ) denote excited states with the electron ionized from an orbital of the corresponding symmetry. The orbitals themselves are denoted by lower-case symmetry labels (e.g.,  $1a_2$ ). The numbering of both orbitals and states proceeds from lower to higher energy in both cases.

## Results

*Geometry of the Ground State.* The crystal structures of known iridium corroles show that there is a quasi-twofold axis that passes through Ir and C10 (Figure 4-1). Both Ir-N(tma) bond lengths in **1-Ir(tma)<sub>2</sub>** are 2.185 Å; Ir-N(pyridine) bond lengths in **1-M(py)<sub>2</sub>** are 2.052 and 2.066 Å; and Ir-N(pyrrole) bond lengths range from 1.940 to 1.981 Å. The computed Ir-N(amine) and Ir-N(pyrrole) bond lengths are, respectively, 2.112 and 1.976 to 1.996 Å, in good agreement with the crystallographic data of the aforementioned Ir(III) corroles. Dihedral angles of the pentafluorophenyl groups in vacuum-optimized structures are 66–76 degrees. The energy change caused by rotation of the

pentafluorophenyl groups away from perpendicular averages 0.03 eV, which we consider as less than the energy accuracy in computations.

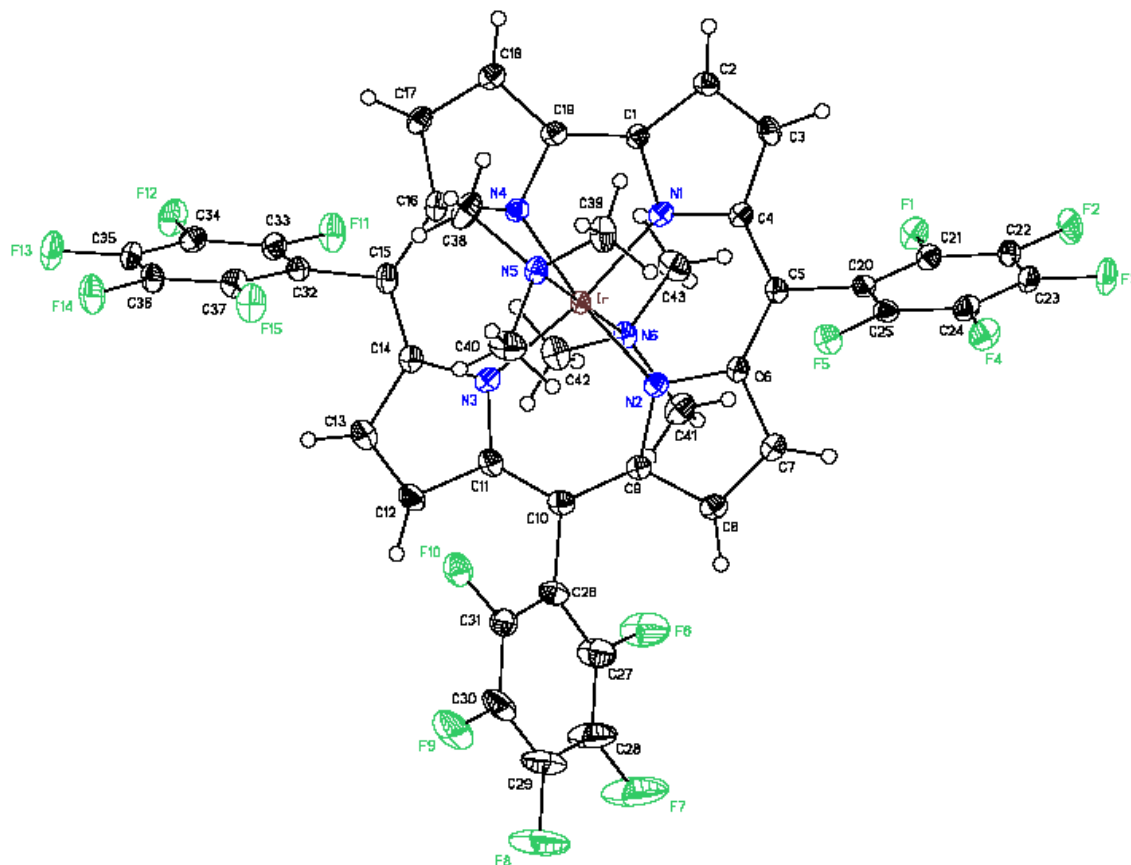


Figure 4-1: X-ray structure of **1-Ir(tma)<sub>2</sub>** (structure previously published in ref. 13). Hydrogen atoms are in white, carbon atoms are in black, nitrogen atoms are in blue, fluorine atoms are in green, and iridium is in red

The computed increases in the lengths of bonds C5-C6 and C1-C19 (Table 4-1) upon removal of an electron from the neutral complexes, along with the concomitant decrease in the length of the bond C4-C5, are consistent with Ghosh's description of alternating bond length changes upon formation of a corrole-based cation radical of B<sub>1</sub> symmetry.<sup>28</sup>

Table 4-1: Key bond lengths of  $[\mathbf{1-M(NH_3)_2}]^{0/+}$  in angstrom, for M = Co, Rh, and Ir. All structures relaxed without symmetry with their ground state wavefunction. The row  $r(\text{M-NH}_3)$  corresponds to the average distance from the metal to the axial amine nitrogen atoms. The geometries were calculated in vacuum by DFT using the 2- $\zeta$  valence functions with Hay and Wadt pseudopotentials for the metals and a 6-31G\*\* basis set for all the other atoms. The B3LYP functional was employed. <sup>a</sup>Indicates the change of the given bond length upon oxidation of the complex

Distance (Å)	[(tpfc)Co (NH <sub>3</sub> ) <sub>2</sub> ] <sup>0</sup>	[(tpfc)Co (NH <sub>3</sub> ) <sub>2</sub> ] <sup>+</sup>	Change <sup>a</sup>	[(tpfc)Rh (NH <sub>3</sub> ) <sub>2</sub> ] <sup>0</sup>	[(tpfc)Rh (NH <sub>3</sub> ) <sub>2</sub> ] <sup>+</sup>	Change <sup>a</sup>	[(tpfc)Ir (NH <sub>3</sub> ) <sub>2</sub> ] <sup>0</sup>	[(tpfc)Ir (NH <sub>3</sub> ) <sub>2</sub> ] <sup>+</sup>	Change <sup>a</sup>
r(M-N5)	1.988	1.995	0.007	2.107	2.114	0.007	2.112	2.119	0.007
r(M-N6)	1.987	1.992	0.005	2.108	2.116	0.008	2.112	2.120	0.008
r(M-NH <sub>3</sub> )	1.988	1.994	0.006	2.108	2.115	0.007	2.112	2.120	0.008
r(M-N1)	1.887	1.888	0.001	1.967	1.968	0.001	1.976	1.976	0.000
r(M-N2)	1.916	1.913	-0.003	1.993	1.991	-0.002	1.997	1.996	-0.001
r(N1-C1)	1.370	1.356	-0.014	1.369	1.355	-0.014	1.371	1.356	-0.015
r(N1-C4)	1.360	1.371	0.011	1.356	1.365	0.009	1.360	1.367	0.007
r(N2-C6)	1.386	1.373	-0.013	1.380	1.368	-0.012	1.383	1.370	-0.013
r(N2-C9)	1.371	1.375	0.004	1.365	1.369	0.004	1.368	1.371	0.003
r(C1-C19)	1.425	1.442	0.017	1.446	1.466	0.020	1.450	1.471	0.021
r(C4-C5)	1.414	1.401	-0.013	1.428	1.414	-0.014	1.429	1.415	-0.014
r(C5-C6)	1.408	1.431	0.023	1.422	1.447	0.025	1.425	1.449	0.024
r(C9-C10)	1.410	1.414	-0.004	1.424	1.428	-0.004	1.426	1.429	-0.003

*Wavefunction Character of the Ground State.* As expected, the ground state of (tpfc)Ir(NH<sub>3</sub>)<sub>2</sub> has six electrons in the t<sub>2g</sub>-derived d orbitals (d<sub>xy</sub>, d<sub>xz</sub>, d<sub>yz</sub>) with a closed-shell corrole  $\pi$ -system (Figure 4-2). However for the ground state of [(tpfc)Ir(NH<sub>3</sub>)<sub>2</sub>]<sup>+</sup>, we find that the d<sup>6</sup> configuration on Ir remains intact while the 2b<sub>1</sub> orbital of the corrole is singly occupied. There is effectively no spin density on the metal, and the atomic charge of Ir from Mulliken population analysis remains essentially constant (0.87 to 0.89). Thus this system, which is formally Ir(IV), is better described as Ir(III)-C $\pi$  where C $\pi$  denotes a hole in the highest HOMO of the corrole. However, experimental EPR data from other iridium corroles,<sup>12</sup> showing significant anisotropy in the g tensor for the oxidized species [(tpfc)Ir(tma)<sub>2</sub>]<sup>+</sup> and [(tpfc)Ir(py)<sub>2</sub>]<sup>+</sup>, demonstrate that there is some degree of iridium d

orbital character mixed into the ground state of the oxidized iridium corroles. Co and Rh are similar as shown in the supporting information.

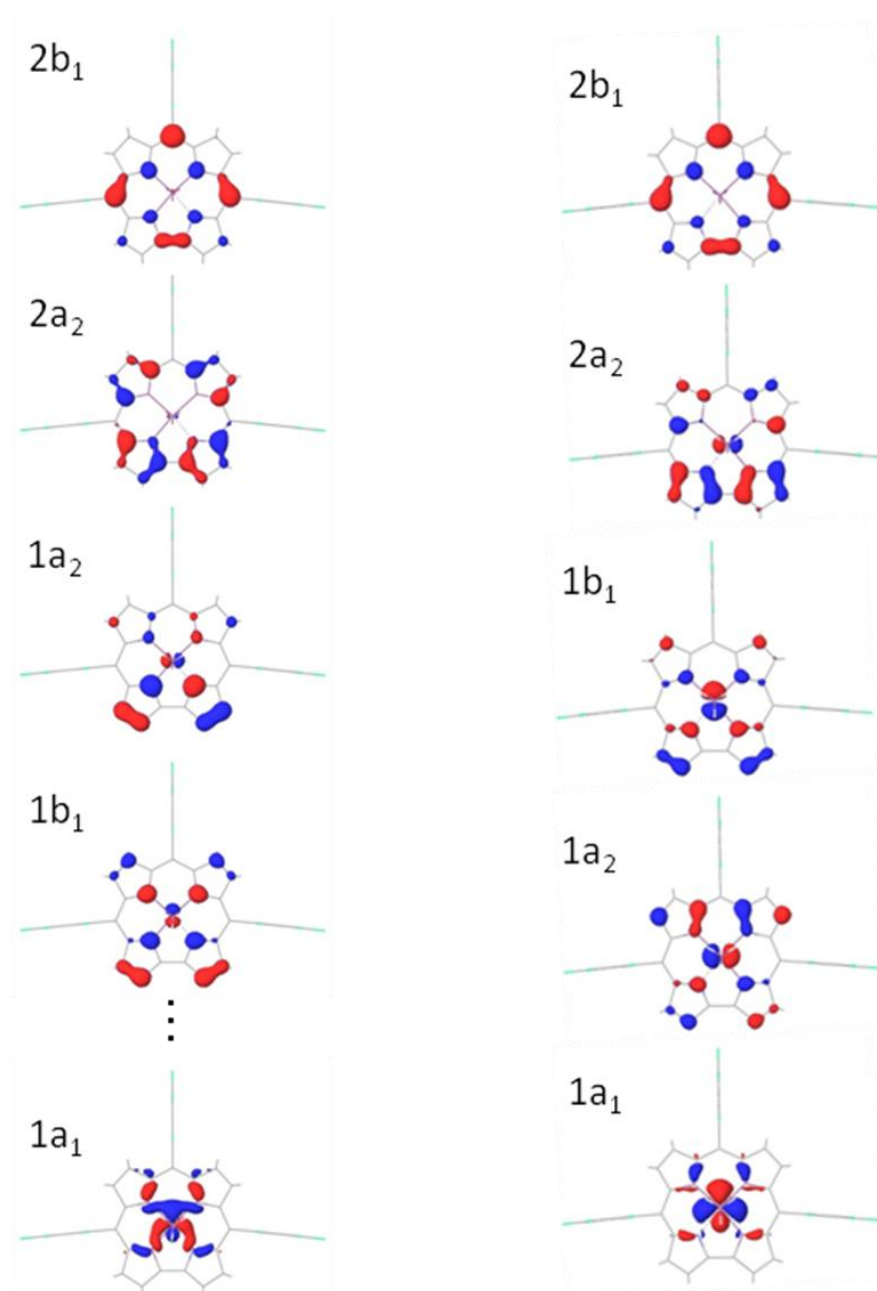


Figure 4-2: Molecular orbital (MO) surfaces (isovalue = 0.05 a. u.) of **1-M(NH<sub>3</sub>)<sub>2</sub>**, where M = Rh (left, Co is similar) or Ir (right). The topmost MO is the HOMO, which is followed by HOMO-1, and so on. 1a<sub>1</sub> is HOMO-13 when M = Rh, HOMO-14 when M = Co, and HOMO-4 when M = Ir. The omitted orbitals on the left side are corrole-based. The geometries were calculated in vacuum by DFT using the 2- $\zeta$  valence functions with Hay and Wadt pseudopotentials for the metals and a 6-31G\*\* basis set for all the other atoms. The B3LYP functional was employed.



The relative energies as well as the metal spin densities of  $[\mathbf{1-M(NH_3)_2}]^+$  excited states are compared in Table 4-2. The spin density plots in Figure 4-3 show that the higher-energy excited states for each metal, particularly for iridium, contain significant metal character. Typically, two imaginary frequencies with magnitude less than  $10\text{ cm}^{-1}$  were obtained when no symmetry was applied to the tpfc complexes. These frequencies generally involve motions of the  $\text{C}_6\text{F}_5$  groups on the corrole rings and are not important in defining metal-based transitions. For the purposes of calculating thermodynamic contributions, imaginary frequencies were excluded. Symmetry constraints changed the combination modes that have imaginary frequencies, and increased the number of the imaginary frequencies to three with each lying a bit over  $20\text{ cm}^{-1}$ . Upon oxidation, the imaginary frequencies tend to be of smaller magnitude or even become non-imaginary, but the changes show no universal trend.

Although the pentafluorophenyl group ( $\text{C}_6\text{F}_5$ ) is the meso substituent in experimentally characterized compounds, the model  $[\mathbf{1f-M(NH_3)_2}]^+$  complexes also were examined in order to reduce computation times and control for computational artifacts arising from the presence of imaginary frequencies in the tpfc complexes. Parameters for the tfc complexes are set out in Table 4-3; and spin density surfaces and energy levels of these complexes are shown in Figure 4-4.

Table 4-2: Spin densities and energies of the excited states of the tpfc complexes. The symmetry label of the state is the symmetry of the orbital from which the electron has been ionized. For Rh and Co, other states lying between  $2^2B_1$  and  $1^2A_1$  but having the unpaired electron in corrole-based orbitals were omitted in order to include the metal-dominated  $1^2A_1$ . The calculations were conducted in vacuum by DFT using the 2- $\zeta$  valence functions with Hay and Wadt pseudopotentials for the metals and 6-31G\*\* basis set for all the other atoms. The B3LYP functional was employed. <sup>a</sup>Energy of the state in question minus that of the lowest energy ionized state of the same compound. <sup>b</sup>Spin given in total unpaired electrons

$[(\text{tpfc})\text{M}(\text{NH}_3)_2]^+$	M = Co		M = Rh		M = Ir	
State	Relative		Relative		Relative	
	energy	<i>Metal spin</i>	energy (eV)	<i>Metal spin</i>	energy (eV)	<i>Metal spin</i>
	(eV) <sup>a</sup>	<i>density</i> <sup>b</sup>	<sup>a</sup>	<i>density</i> <sup>b</sup>	<sup>a</sup>	<i>density</i> <sup>b</sup>
$1^2B_1$	0.00	-0.02	0.00	-0.01	0.00	-0.01
$1^2A_2$	0.27	0.00	0.24	0.02	0.15	0.07
$2^2A_2$	1.63	0.10	1.23	0.21	0.59	0.08
$2^2B_1$	1.71	0.12	1.27	0.24	0.86	0.38
$1^2A_1$	2.74	1.13	2.71	0.75	2.06	0.89

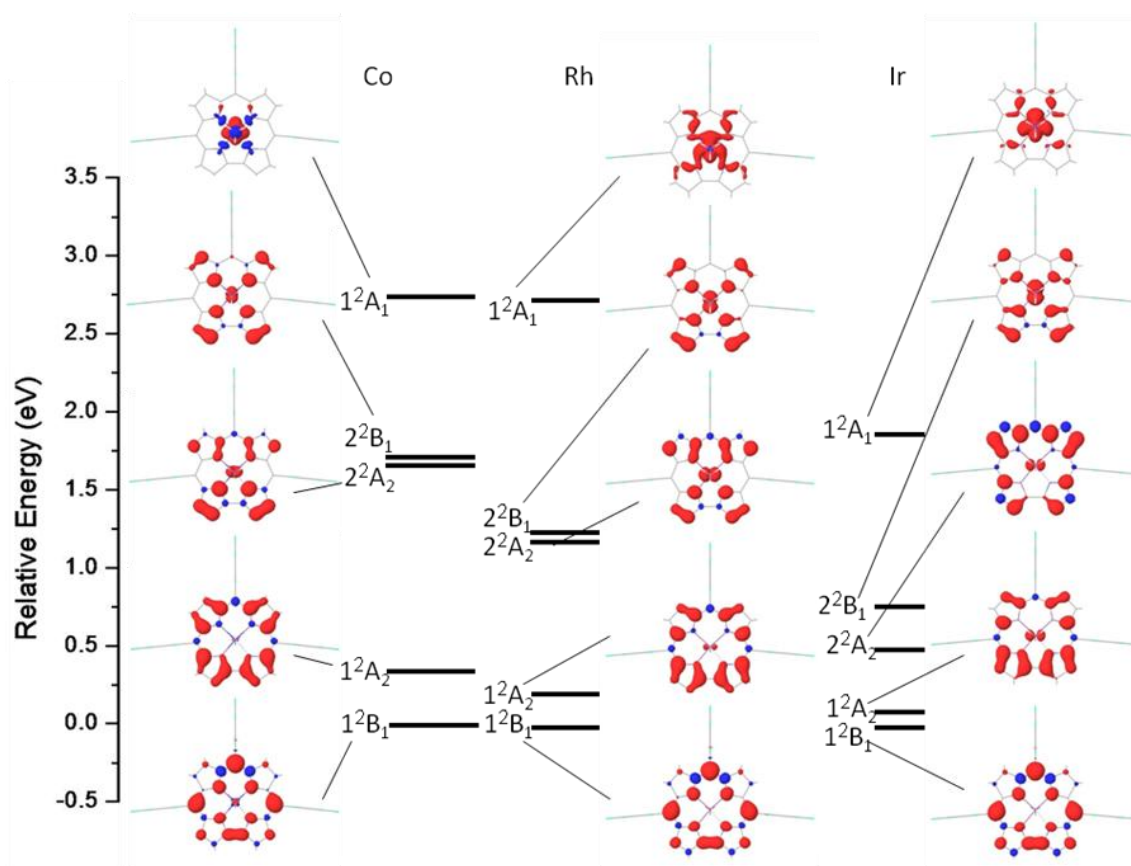


Figure 4-3: Relative energies and spin density surfaces (isovalue = 0.002 a.u.) of  $[1-M(NH_3)_2]^+$  ( $M = Co, Rh, Ir$ ). The calculations were conducted in vacuum by DFT using the 2- $\zeta$  valence functions with Hay and Wadt pseudopotentials for the metals and 6-31G\*\* basis set for all the other atoms. The B3LYP functional was employed.

Table 4-3: Spin densities and energies of the excited states of the tfc complexes. The symmetry label of the state is the symmetry of the orbital from which the electron has been ionized. For Rh and Co, other states lying between  $3^2B_1$  and  $1^2A_1$  but having the unpaired electron in corrole-based orbitals were omitted in order to include the metal-dominated  $1^2A_1$ . The calculations were conducted in vacuum by DFT using the 2- $\zeta$  valence functions with Hay and Wadt pseudopotentials for the metals and 6-31G\*\* basis set for all the other atoms. The B3LYP functional was employed. <sup>a</sup>Energy of the state in question minus that of the lowest energy ionized state of the same compound. <sup>b</sup>Spin given in total unpaired electrons.

$[(tfc)M(NH_3)_2]^+$	M = Co		M = Rh		M = Ir	
State	Relative energy (eV) <sup>a</sup>	Metal spin density <sup>b</sup>	Relative energy (eV) <sup>a</sup>	Metal spin density <sup>b</sup>	Relative energy (eV) <sup>a</sup>	Metal spin density <sup>b</sup>
$1^2B_1$	0.00	-0.02	0.00	-0.01	0.00	-0.01
$1^2A_2$	0.67	0.00	0.63	0.02	0.54	0.07
$2^2A_2$	1.94	0.08	1.58	0.19	1.21	0.24
$2^2B_1$	2.02	0.10	1.62	0.22	1.21	0.35
$3^2B_1$	2.33	-0.01	2.28	0.00	2.27	0.00
$1^2A_1$	3.19	1.16	3.19	0.77	2.53	0.91

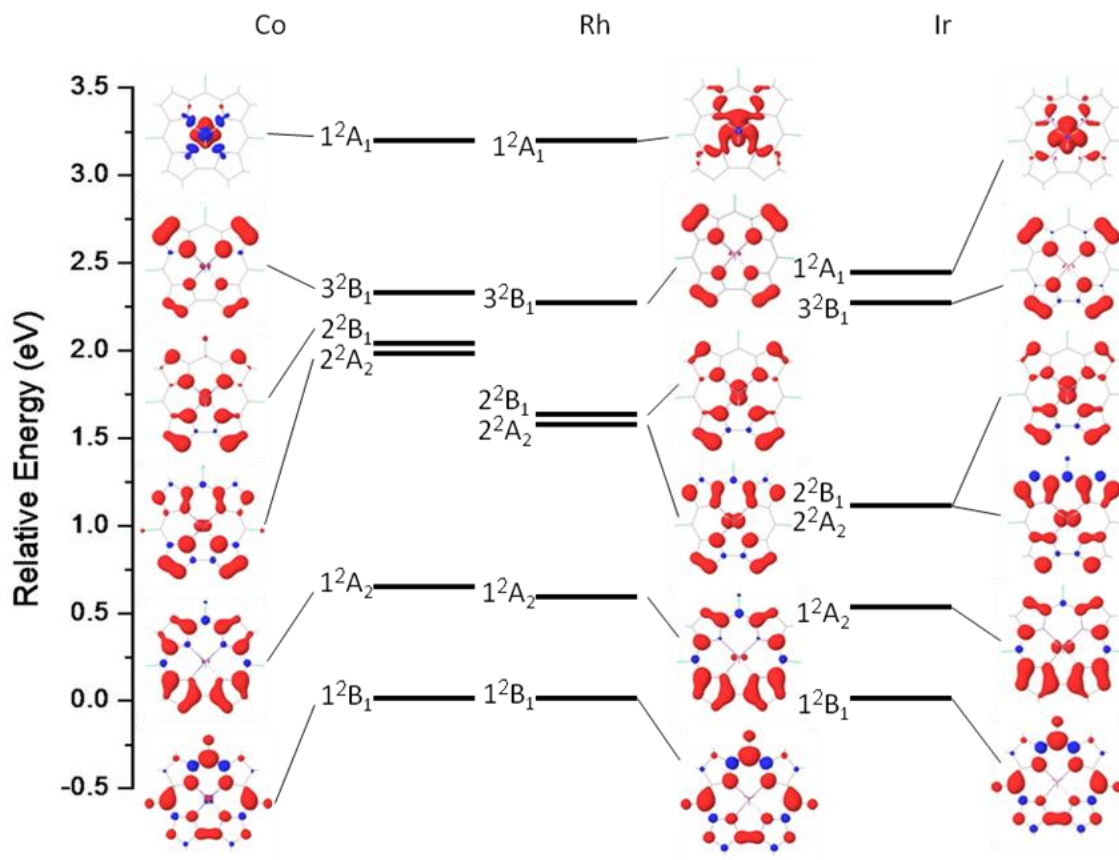


Figure 4-4: Relative energies and spin density surfaces (isovalue = 0.002 a.u.) of  $[1f-M(NH_3)_2]^+$  ( $M = Co, Rh, Ir$ ). The calculations were conducted in vacuum by DFT using the 2- $\zeta$  valence functions with Hay and Wadt pseudopotentials for the metals and 6-31G\*\* basis set for all the other atoms. The B3LYP functional was employed.

From the energy levels in both the tpfc and the tfc systems, it is apparent that the separation between states decreases in the order  $Co > Rh > Ir$  for each corrole system. Also, it is noteworthy that the spin density localized on the metal generally increases in the order  $Co < Rh < Ir$  for a given orbital level, except for the high-lying  $1^2A_1$  state, which occurs in the order  $Rh < Ir < Co$ . States classified as  $3^2B_1$  only appear in the tfc complexes because they are pushed upward in energy when the ligand is tpfc. Figure 4-4 shows that the energy of the  $3^2B_1$  state relative to the  $1^2B_1$  state in the three tfc complexes is roughly the same for all three metals.

For a given metal center, the tpfc complex has smaller energy gaps between different states than the tfc complex. An exception is the gap between the nearly degenerate  $2^2B_1/2^2A_2$  states and the adjacent  $1^2A_2$  state, which is actually greater by around 0.04 eV in the tpfc case due to stabilization of the  $1^2A_2$  state by the pentafluorophenyl substituents on tpfc. The contraction observed between the lowest two energy states for the different corroles is of a greater order than the difference brought about by changing the metal center for each corrole, presumably because the ground  $1^2B_1$  state is more effectively stabilized by fluorine than by pentafluorophenyl meso-substituents.  $[1\text{-Ir}(\text{NH}_3)_2]^+$  has the smallest state separations of all compounds under study, such that the energy gap between  $1^2B_1$  and  $1^2A_2$  states is only approximately 0.15 eV in vacuum, dropping to 0.10 eV if dichloromethane solvation is added to the model. Solvation with dichloromethane generally decreases the energy gaps between states in the systems examined.

Focusing on the two lowest energy states of  $[1\text{-Ir}(\text{NH}_3)_2]^+$ , we separately relaxed the geometry (with  $C_2$  symmetry to allow aryl group rotation) of both the  $1^2B_1$  and  $1^2A_2$  states within the continuum solvent employing three functionals: GGA (BP86), hybrid (B3LYP), and meta hybrid (M06). Relaxing the  $1^2A_2$  state further reduces the splitting, as does solvation as mentioned above. The final  $1^2B_1/1^2A_2$  splittings, including solvation and relaxation of the states, are 0.00 eV (BP86), 0.07 eV (B3LYP), and 0.03 eV (M06). Thus all three functionals agree that the  $[1\text{-Ir}(\text{NH}_3)_2]^+$  state has two nearly degenerate states: a slightly lower energy corrole-based radical state and a slightly higher energy state (by 0.03–0.10 eV) with mixed metal-corrole character.

The calculated reduction potential of  $[\mathbf{1-Ir(NH_3)_2}]^{0/+}$  (0.64 V vs. SCE) is in excellent agreement with experimental values for  $\mathbf{1-Ir(tma)_2}$  and  $\mathbf{1-Ir(py)_2}$  (0.66 and 0.63 V vs. SCE, respectively) obtained *via* cyclic voltammetry.<sup>12,13</sup> The computed reduction potentials of  $[\mathbf{1-M(NH_3)_2}]^{0/+}$  are 0.64, 0.67, and 0.56 V vs. SCE for M = Ir, Rh, and Co, respectively.

## Discussion

Our DFT calculations point toward a common description of the positively charged (singly oxidized) cobalt, rhodium, and iridium corroles as metal(III) complexes chelated by an oxidized, open-shell macrocycle, with an unpaired electron that resides in a corrole-based  $B_1$  symmetry orbital. For a given metal center, substitution of  $C_6F_5$  for F at the meso positions decreases the energetic difference between the vertical excited states of the cations. This energy gap also is strongly affected by the metal, in the order  $Co > Rh > Ir$ . The effect of the metal center and that of the meso-substituents on the state energies of the system are largely decoupled for the rhodium and cobalt complexes. However, in the case of iridium, the electronically excited tfc complex exhibits degenerate states ( $2^2B_1/2^2A_2$ ) that are nondegenerate in the corresponding tpfc complex.

The remarkable effects of meso substituents on the energy levels of the corrole complexes may be rationalized by the following arguments: While pentafluorophenyl is a poorer electron-withdrawing group (EWG) than fluorine by inductive effects,<sup>29</sup> the electron-withdrawing effect of the latter substituent is mitigated by its ability to donate electron density from filled fluorine 2p orbitals into the  $\pi$ -system of the corrole, resulting in an overall greater electron-withdrawing effect of the  $C_6F_5$  substituent on the electronic

structure of the complex. This proposal is supported by the finding that the bonds immediately adjacent to the fluorine atoms in the tfc complexes are shorter than the corresponding bonds in tpfc, but the bonds farther away from the meso substituents are similar in the two corrole scaffolds. Additionally, in vacuum, the sum of atomic charges obtained by Mulliken population analysis on the three meso -CF fragments in [**1f-Ir(NH<sub>3</sub>)<sub>2</sub>]<sup>+</sup> is +0.41, while in [**1-Ir(NH<sub>3</sub>)<sub>2</sub>]<sup>+</sup>, the sum over three meso -CC<sub>6</sub>F<sub>5</sub> fragments is -0.32. These values are basis set dependent, and are also affected by solvation, but the charges on the -CF fragments are always more positive than those on the -CC<sub>6</sub>F<sub>5</sub> fragments.****

The expansion of the energy gaps for the tfc complexes implies that the antibonding interaction between the occupied corrole- $\pi$  and fluorine- $\pi$  orbitals destabilizes the 2b<sub>1</sub> orbital. This in turn stabilizes the 1<sup>2</sup>B<sub>1</sub> state relative to excited states that have more metal character. There also is a computed contraction of energy gaps upon moving from Co to Rh to Ir, and the combined effects of having a C<sub>6</sub>F<sub>5</sub> meso-substituent and the 5d metal in [**1-M(NH<sub>3</sub>)<sub>2</sub>]<sup>+</sup> lead to a situation where the 1<sup>2</sup>A<sub>2</sub> state (which has substantial unpaired spin density on the metal atom) is essentially degenerate with the lowest energy <sup>2</sup>B<sub>1</sub> state when solvation effects are included.**

These observations help explain the experimental finding of increased metal character in singly oxidized **1-M(tma)<sub>2</sub>** and **1-M(py)<sub>2</sub>** complexes going from Co to Rh to Ir,<sup>12</sup> especially when the effect of spin-orbit coupling, which should stabilize metal-based radicals more in the 5d case than in the lighter metal complexes, is taken into account. Addition of spin-orbit effects into our DFT models is beyond the scope of our current



report, but given that spin-orbit coupling in 5d metals is known to be on the order of 0.5 eV, the  $1^2A_2$  state of  $[1\text{-Ir}(\text{NH}_3)_2]^+$ , which is of mixed metal-corrole character, could easily drop lower in energy than the  $1^2B_1$  corrole  $\pi$ -cation state. It should be emphasized that the experimental EPR spectra of  $[1\text{-Ir}(\text{tma})_2]^+$  and  $[1\text{-Ir}(\text{py})_2]^+$  display highly rhombic g-tensors attributable to largely Ir-based SOMOs.<sup>12</sup> A study on the  $\text{Fe}^{\text{II}}$ ,  $\text{Ru}^{\text{II}}$ , and  $\text{Os}^{\text{II}}$  complexes of octaethylporphyrin (OEP) by Brown and co-workers similarly found that  $\text{Ru}(\text{OEP})(\text{CO})(\text{thf})$  is oxidized at the macrocycle while  $\text{Os}(\text{OEP})(\text{CO})(\text{py})$  is oxidized on the metal.<sup>30</sup> For cobalt and rhodium, on the other hand, the energy difference between the  $1^2A_2$  and  $1^2B_1$  states is larger than for iridium and, moreover, spin-orbit effects on their  $1^2A_2$  states will be much smaller.

The calculated reduction potentials are very similar among the series of  $[1\text{-M}(\text{NH}_3)_2]^{0/+}$  redox pairs. The metal centers have very minor effects on the energy of the corrole-based HOMO of each complex, leading to the computed result that their energies (and therefore their reduction potentials) are the same regardless of the metal center. We had expected that the metal center would perturb the energy levels of the corrole orbitals by providing an altered electric field, and that these differences in the effective electronic shielding by each metal would lead to large changes in the reduction potentials of the complexes. However, we observe fairly minor differences among the computed reduction potentials of the three Group 9 corrole complexes, consistent with experimental data. The computed reduction potential for the Ir case (0.64 V vs. SCE) agrees quite well with experiment (0.63 to 0.66 V vs. SCE). The calculated values for Rh (0.67 V vs. SCE) and Co (0.56 V vs. SCE) are similar to Ir, compared to experimental  $1\text{-Rh}(\text{py})_2$  and  $1\text{-Co}(\text{py})_2$  potentials of 0.71 and 0.67 V vs. SCE, respectively. These results suggest that corrole-based

orbitals offset any changes to the redox potentials that would be introduced by changing the metal, leading to the conclusion that the ground state wavefunction cannot be metal-centered in the complex cations.

## Conclusion

DFT calculations (B3LYP with Poisson-Boltzmann continuum solvation) applied to the series of Group 9 metallocorrole complexes **1-M(NH<sub>3</sub>)<sub>2</sub>** (M = Co, Rh, Ir) and the corresponding cations predict a common, ligand-based one-electron oxidation from the corrole HOMO in each case. Wavefunctions for the neutral M<sup>III</sup> molecules share a HOMO of B<sub>1</sub> symmetry with very small contributions from the metal. The ground state wavefunctions for the cations yield spin densities with little contribution (~ 0.01 electron) from the metals. Calculated reduction potentials (0.64 V, 0.67 V, and 0.56 V vs. SCE for M = Ir, Rh and Co, respectively) are insensitive to the metal within the accuracy of the calculation, and are consistent with the measured reduction potentials of similar Ir(III) corroles (0.63 to 0.66 V vs. SCE).

In the cations, vertical excitation energies to states with significant metal character decrease in the order Co > Rh > Ir, and are negligible in [**1-Ir(NH<sub>3</sub>)<sub>2</sub>**]<sup>+</sup>. Spin-orbit coupling, omitted in the calculations at this level of theory, must mix the low-lying states incorporating Ir d<sub>π</sub> character to yield a mixed metal-ligand radical ground state that accords with the experimental EPR spectra of the iridium corrole cations.

**Acknowledgements:** This work was supported by an NSF Center for Chemical Innovation (CCI Powering the Planet, Grants CHE-0802907 and CHE-0947829), the US-

Israel BSF (Z.G. and H.B.G.), CCSER (Gordon and Betty Moore Foundation), and the Arnold and Mabel Beckman Foundation. S.S.D. was supported from the Overseas Research Fellowship Scheme from the Faculty of Science, University of Hong Kong.

## References

- (1) Shilov, A. E.; Shul'pin, G. B. *Chem. Rev.* **1997**, *97*, 2879–2932.
- (2) Cape, J. L.; Siems, W. F.; Hurst, J. K. *Inorg. Chem.* **2009**, *48*, 8832–8846.
- (3) Ringenberg, M. R.; Kokatam, S. L.; Heiden, Z. M.; Rauchfuss, T. B. *J. Am. Chem. Soc.* **2008**, *130*, 788–789.
- (4) Han, A.-R.; Jeong, Y. J.; Kang, Y.; Lee, J. Y.; Seo, M. S.; Nam, W. *Chem. Comm.* **2008**, *9*, 1076–1078.
- (5) Loew, G. H.; Harris, D. *Chem. Rev.* **2000**, *100*, 407–420.
- (6) Green, M. T. *J. Am. Chem. Soc.* **1999**, *121*, 7939–7940.
- (7) Shaik, S.; Cohen, S.; Wang, Y.; Chen, H.; Kumar, D.; Thiel, W. *Chem. Rev.* **2010**, *110*, 949–1017.
- (8) Aviv-Harel, I.; Gross, Z. *Chem. Eur. J.* **2009**, *15*, 8382–8394.
- (9) a) Kadish, K. M.; Shen, J.; Fremont, L.; Chen, P.; El-Ojaimi, M.; Chkounda, M.; Gros, C. P.; Barbe, J.-M.; Ohkubo, K.; Fukuzumi S.; Guillard R. *Inorg. Chem.* **2008**, *47*, 6726–6737. b) Bendix, J.; Dmochowski, I. J.; Gray, H. B.; Mahammed, A.; Simkhovich, L.; Gross, Z. *Angew. Chem., Int. Ed.* **2000**, *39*, 4048–4051.
- (10) Gross, Z.; Gray, H. B. *Comm. Inorg. Chem.*, **2006**, *27*, 61–72.
- (11) a) Roos, B. O.; Veryazov, V.; Conradie, J.; Taylor, P. R.; Ghosh, A. *J. Phys. Chem. B.* **2008**, *112*, 14099–14102. b) Zakharieva, O.; Schunemann V.; Gerdan M.; Licoccia S.; Cai S.; Walker F. A.; Trautwein A. X. *J. Am. Chem. Soc.* **2002**, *124*, 6636–6648.
- (12) Palmer, J. H.; Mahammed, A.; Lancaster, K. M.; Gross, Z.; Gray, H. B. *Inorg. Chem.* **2009**, *48*, 9308–9315.
- (13) Palmer, J. H.; Day, M. W.; Wilson, A. D.; Henling, L. M.; Gross, Z.; Gray, H. B. *J. Am. Chem. Soc.* **2008**, *130*, 7786–7787.
- (14) Tse, M. K.; Zhang, Z.; Mak, T. C. W.; Chan, K. S. *Chem. Commun.* **1998**, 1199–1200.
- (15) Ghosh, A.; Steene, E. *J. Inorg. Biochem.* **2002**, *91*, 423–436.
- (16) Jaguar 7.0, release 207; Schrödinger, LLC: New York, **2006**. see Greeley, B. H.; Russo, T. V.; Mainz, D. T.; Friesner, R. A.; Langlois, J.-M.; Goddard, W. A., III; Donnelly, R. E. and Ringnalda, M. N. *J. Chem. Phys.* **1994**, *101*, 4028–4041.
- (17) a) Becke, A. D. *Phys. Rev. A.* **1998**, *38*, 3098–3100. b) Lee, C.; Yang, W.; Parr, R. G. *Phys. Rev. B.* **1988**, *37*, 785–789. c) Stephens, P. J.; Devlin, F. J.; Chabalowski, C. F.; Frisch, M. J. *J. Phys. Chem.* **1994**, *98*, 11623–11627.
- (18) a) Baik, M.-H.; Friesner, R. A.; *J. Phys. Chem. A.* **2002**, *106*, 7407–7412. b) Chiorescu, I.; Deubel, D. V.; Arion, V. B.; Keppler, B. K. *J. Chem. Theory Comput.* **2008**, *4*, 499–506. c) Roy, L. E.; Jakubikova, E.; Guthrie, M. G.; Batista, E. R. *J. Phys. Chem. A* **2009**, *113*, 6745–6750.
- (19) Radon, M.; Broclawik, E. *J. Chem. Theory Comput.*, **2007**, *3*, 728–734.
- (20) a) Goddard, W.A, III. *Phys. Rev.* **1968**, *174*, 659–662. b) Melius, C.F.; Goddard, W.A, III. *Phys. Rev. A* **1974**, *10*, 1528–1540. c) Melius, C. F.; Olafson, B. D.; Goddard, W. A., III. *Chem. Phys. Lett.* **1974**, *28*, 457–462.
- (21) Hay, P. J.; Wadt, W. R. *J. Chem. Phys.* **1985**, *82*, 299–310.
- (22) a) Hehre, W. J.; Ditchfield, R.; Pople, J. A. *J. Chem. Phys.* **1972**, *56*, 2257–2261. b) Hariharan, P. C.; Pople, J. A. *Theor. Chim. Acta* **1973**, *28*, 213–222.
- (23) Martin, J. M. L.; Sundermann, A. *J. Chem. Phys.* **2001**, *114*, 3408–3420.
- (24) a) Tannor, D. J.; Marten, B.; Murphy, R.; Friesner, R. A.; Sitkoff, D.; Nicholls, A.; Ringnalda, M.; Goddard, W. A., III; Honig, B. *J. Am. Chem. Soc.* **1994**, *116*, 11875–11882. b) Marten, B.; Kim, K.; Cortis, C.; Friesner, R. A.; Murphy, R. B.; Ringnalda, M. N.; Sitkoff, D.; Honig, B. *J. Phys. Chem.* **1996**, *100*, 11775–11788. The Poisson–Boltzmann method is well suited to this application given the absence of extreme, localized electrostatic potentials and opportunities for solvent coordination.
- (25) a) Bryantsev, V. S.; Diallo, M. S.; Goddard, W. A., III. *J. Phys. Chem. A*, **2007**, *111*, 4422–4430. b) Nielsen, R. J.; Keith, J. M.; Stoltz, B. M.; Goddard, W. A., III. *J. Am. Chem. Soc.* **2004**, *126*, 7967–7974.
- (26)  $\Delta G(\text{H}^+(1\text{atm}) \rightarrow \text{H}^+(1\text{M})) = -264.0 \text{ kcal/mol}$ ; Tissandier, M. D.; Cowen, K. A.; Feng, W. Y.; Gundlach, E.; Cohen, M. H.; Earhart, A. D.; Coe, J.V.; Tuttle, T. R., Jr. *J. Phys. Chem. A* **1998**, *102*, 7787–7794.

- 
- (27) "Electrochemical Series" in *CRC Handbook of Chemistry and Physics, Internet Version 2007*, (87<sup>th</sup> Edition), David R. Lide, ed., Taylor and Francis, Boca Raton, FL.
- (28) Ghosh, A.; Wondimagegn, T.; Parusel, A. B. J. *J. Am. Chem. Soc.* **2000**, *122*, 5100–5104.
- (29) Hansch, C.; Leo, A.; Taft, R. W. *Chem. Rev.* **1991**, *91*, 165–195.
- (30) Brown, G. M.; Hopf, F. R.; Meyer, T. J.; Whitten, D. G. *J. Am. Chem. Soc.* **1975**, *97*, 5385–5390.

*Chapter 5*THE UNPRECEDENTED REACTIVITY OF AMMINE-LIGATED IRIIDIUM  
CORROLES

In April of 2009, Theis Brock-Nannestad, a graduate student from Jesper Bendix' group at the University of Copenhagen, showed up in the Gray group to fulfill a Danish Ph.D. requirement mandating a six-month period of study in a foreign lab. During that time, we worked extensively on two main projects: one, the briefer, involved the development of an optimized synthesis of  $H_3tpfc$ , and mostly acted as a facilitator of our inorganic research by allowing us to produce unprecedentedly large amounts of corrole at once; the other project, which will be discussed here, began with an idea for the development of high-valent nitrido-iridium corroles and ended with the synthesis of a novel porphyrinoid molecule. Throughout the course of this research project, I was introduced to a number of new techniques, including the safe use of corrosive gasses (ammonia in particular) and a battery of 2D NMR experiments. Atif Mahammed, a postdoctoral fellow in Zeev Gross' lab, was instrumental in developing some of the initial synthetic procedures which eventually led us to the formation of our new porphyrinoids. Additionally, David Vandervelde and Scott Virgil, two Caltech staff scientists, contributed important expertise to the project. David introduced me to a number of useful 2D NMR experiments, and Scott allowed Theis to use his HPLC for a very long and messy separation.

### **The Unprecedented Reactivity of Ammine-Ligated Iridium Corroles**

Joshua H. Palmer, Theis N. Brock-Nannestad, Atif Mahammed, David Vandervelde, Alec C. Durrell, Scott Virgil, Zeev Gross, and Harry B. Gray

Corroles, macrocycles similar to porphyrins but possessed of lower symmetry and greater electron density, have often been posited as scaffolds for the synthesis and stabilization of high-valent metal complexes.<sup>1</sup> This goal has been achieved in numerous cases, especially with the first-row transition metals chromium and manganese,<sup>2</sup> which can both be induced to form stable oxometallocorrole complexes under fairly gentle treatment. Other claimed high-valent metallocorrole complexes, notably those of iron(IV)<sup>3</sup> and cobalt(IV),<sup>4</sup> have been subjects of controversy when detailed studies suggested they could more accurately be described as oxidized corrole radicals complexed to lower-valent metal centers.<sup>5</sup>

We have added a new entry to the list of high-valent metal-corrole complexes with our report of two Ir(III) corrole complexes<sup>6</sup> best characterized as possessing iridium(IV) central metal ions and unionized corrole ligands when they are oxidized.<sup>7</sup> In this report, we showed that UV-vis absorption and electron paramagnetic resonance spectroscopy are both consistent with a paramagnetic metal center possessing a rhombic ligand field. Recent computational results from our group have cast some doubt on the original experimental findings,<sup>8</sup> but the overall picture is of an oxidation event that produces a state with partial Ir(IV) and partial corrole radical character.<sup>9</sup>

Our published results suggest that corroles can provide a welcoming environment for iridium(IV) complexes, but they do not provide significant insight into the potential for developing possible catalysts with Ir(V) or even higher-valent central metals. Our original targets for such compounds comprised both oxoiridium(V) and (bis)oxoiridium(VII) corrole complexes, but these species have proven elusive. In an attempt to create

alternative high-valent iridium compounds, namely nitrido-iridium(VI) corroles, we have synthesized and fully characterized the ammine-ligated iridium 5,10,15-*(tris)*pentafluorophenylcorrole complex **1-Ir(NH<sub>3</sub>)<sub>2</sub>** (Figure 5-1) and its fully brominated analogue **1b-Ir(NH<sub>3</sub>)<sub>2</sub>**. Their surprising reactivity is discussed below.

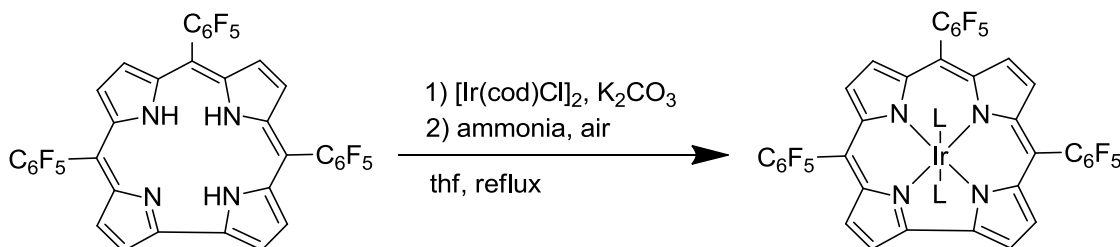


Figure 5-1: Synthesis of **1-Ir(NH<sub>3</sub>)<sub>2</sub>**. Conversion to **1b-Ir(NH<sub>3</sub>)<sub>2</sub>** could be achieved by stirring in C<sub>6</sub>H<sub>6</sub> with Br<sub>2</sub> for a period of hours.

The synthesis of the ammine-ligated complexes was achieved in analogy to the published procedures for synthesis of our previous corrole complexes.<sup>7</sup> In the case of **1-Ir(NH<sub>3</sub>)<sub>2</sub>**, gaseous ammonia is run through the solution after the initial iridium insertion step. **1b-Ir(NH<sub>3</sub>)<sub>2</sub>** can then be synthesized in essentially quantitative yield by stirring **1-Ir(NH<sub>3</sub>)<sub>2</sub>** with an excess of elemental bromine in benzene for 2 hours. The complexes are green in solution, and display UV-vis absorption spectra similar to the known complex **1-Ir(py)<sub>2</sub>** (py = pyridine).<sup>7</sup> The crystallographically determined axial Ir-N bond lengths (Figure 5-2) are quite a bit shorter for **1-Ir(NH<sub>3</sub>)<sub>2</sub>** as compared to **1-Ir(tma)<sub>2</sub>** (tma = trimethylamine; the equatorial Ir-N bond lengths are equivalent within error), in line with the computed geometries published previously by our group. This is in spite of the stronger sigma-donating capability of the methylated ligand, so we assume the greater steric encumbrance of the methyl groups on tma leads to the longer bond length.

The  $^1\text{H}$  NMR of **1-Ir(NH<sub>3</sub>)<sub>2</sub>** (Figure 5-3) shows a standard pattern of four doublets corresponding to the eight ring protons and a large upfield resonance ( $\delta = -4.057$  ppm) corresponding to the ammine protons. The  $^1\text{H}$  NMR of **1b-Ir(NH<sub>3</sub>)<sub>2</sub>** also contains this peak, whose identity can be confirmed by comparison of its  $^{15}\text{N}$ - $^1\text{H}$  coupling magnitude to a  $^{15}\text{N}$ - $^1\text{H}$  HSQC NMR spectrum of **1-Ir(NH<sub>3</sub>)<sub>2</sub>** (Figure 5-4).

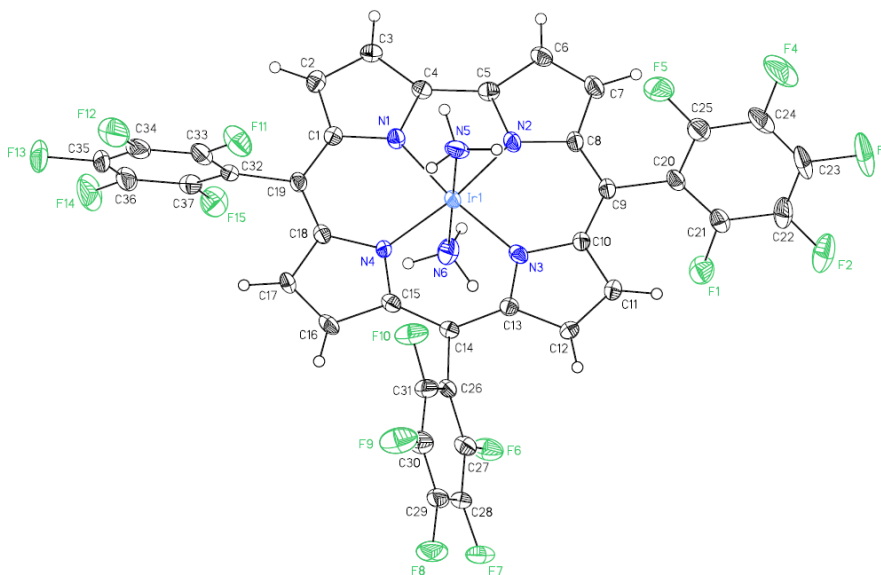


Figure 5-2: X-ray diffraction structure of **1-Ir(NH<sub>3</sub>)<sub>2</sub>**. Ir-N equatorial bond lengths average 1.964 Å and Ir-N axial bond lengths average 2.074 Å. In **1-Ir(tma)<sub>2</sub>**, these bond lengths average 1.965 and 2.185 Å, respectively.

In line with the shorter axial Ir-N bonds in the ammine-ligated system, **1-Ir(NH<sub>3</sub>)<sub>2</sub>** is also more easily oxidized ( $E_{1/2} = 0.53$  V vs. SCE) than either **1-Ir(tma)<sub>2</sub>** or **1-Ir(py)<sub>2</sub>** ( $E_{1/2} = 0.66$  and  $0.69$  V vs. SCE, respectively), implying greater electron density on both the central metal and the ring. Like the published corroles **1-Ir(tma)<sub>2</sub>**, **1b-Ir(tma)<sub>2</sub>**, and **1-Ir(py)<sub>2</sub>**, **1-Ir(NH<sub>3</sub>)<sub>2</sub>** and **1b-Ir(NH<sub>3</sub>)<sub>2</sub>** are luminescent in the near-IR, although their emission is slightly red-shifted compared to the previously reported complexes.



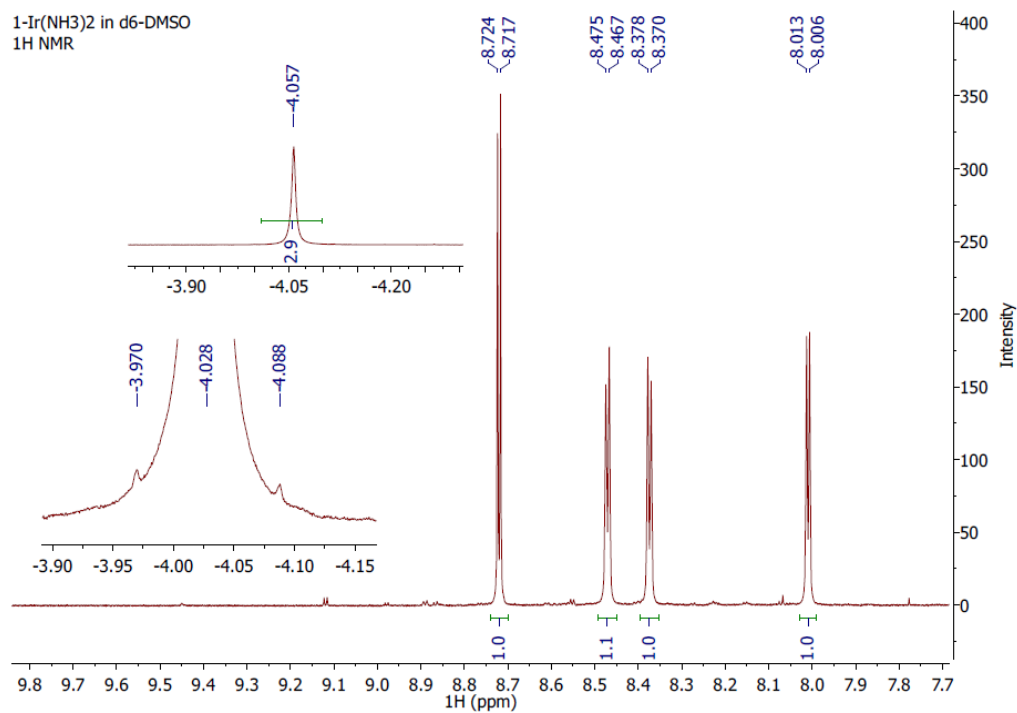


Figure 5-3:  $^1\text{H}$  NMR of **1-Ir(NH<sub>3</sub>)<sub>2</sub>** in d<sup>6</sup>-DMSO. The top inset shows the resonance peak corresponding to the ammine ligand protons, while the bottom inset shows the corresponding peak for **1b-Ir(NH<sub>3</sub>)<sub>2</sub>**, zoomed in so that the 71 Hz  $^{15}\text{N}$ - $^1\text{H}$  coupling to the ammine nitrogen is clearly visible.

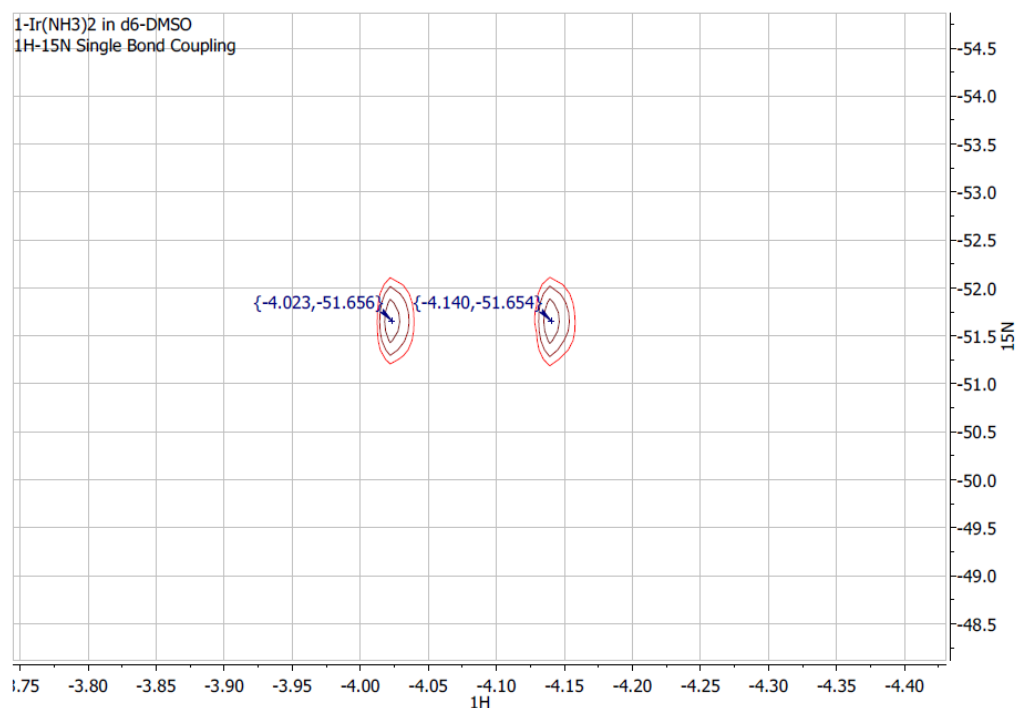


Figure 5-4: Natural abundance  $^{15}\text{N}$ - $^1\text{H}$  HSQC of **1-Ir(NH<sub>3</sub>)<sub>2</sub>** in d<sup>6</sup>-DMSO, showing the 71 Hz coupling between the ammine nitrogen and protons

The CV of **1-Ir(NH<sub>3</sub>)<sub>2</sub>** (Figure 5-5) shows two anodic waves in methylene chloride solution, one of which (0.53 V vs. SCE) is essentially reversible (though this wave becomes irreversible in CH<sub>3</sub>CN, presumably due to ligand substitution on the oxidized species) and the other of which (1.13 V vs. SCE) displays scan rate dependent reversibility. The first oxidation appears to produce a mixed Ir(IV)-corrole  $\pi$ -cation radical, with similar EPR and spectroelectrochemical signatures to the one-electron oxidized form of **1-Ir(tma)<sub>2</sub>**. We reasoned that the more anodic wave might represent the formation of an Ir(V) compound, with the irreversibility being caused by loss of either ammonia protons or an ammine ligand, and we attempted to chemically oxidize the corrole and isolate the resulting product. Reaction with traditional harsh oxidants such as ammonium ceric nitrate led to the appearance of multiple unstable products by UV-vis, and appeared to promote decomposition, but oxidation with either sodium hypochlorite and ammonia or NBS and ammonium hydroxide (both in CH<sub>3</sub>CN/H<sub>2</sub>O) led to a color change to red and the appearance of new, highly polar pink spots on a TLC plate.

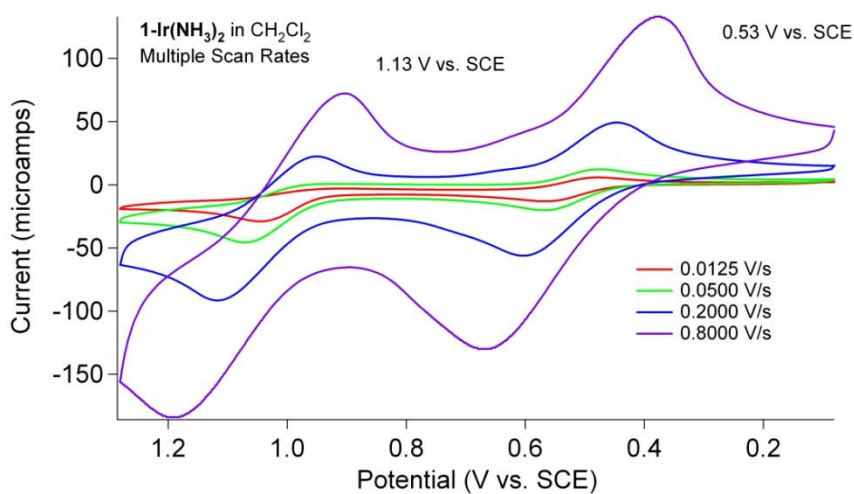


Figure 5-5: CV traces of **1-Ir(NH<sub>3</sub>)<sub>2</sub>** in dcm at a variety of scan rates, showing the dependence upon the scan rate of the reversibility of the more anodic process

The hypochlorite/ammonia reaction produced a mélange of reddish products; the only isolable product, eluted by HPLC in 1% yield in a 14 hour procedure, was a pink compound, insoluble in dcm or hexanes but quite soluble in acetonitrile or methanol, that showed four downfield-shifted doublets in its proton NMR spectrum, along with a three times as intense singlet at -3.6 ppm (in  $d^6$ -DMSO). Additionally, this compound, dubbed **2-Ir(NH<sub>3</sub>)<sub>2</sub>**, has an MS corresponding to **1-Ir(NH<sub>3</sub>)<sub>2</sub>** plus one additional nitrogen atom.

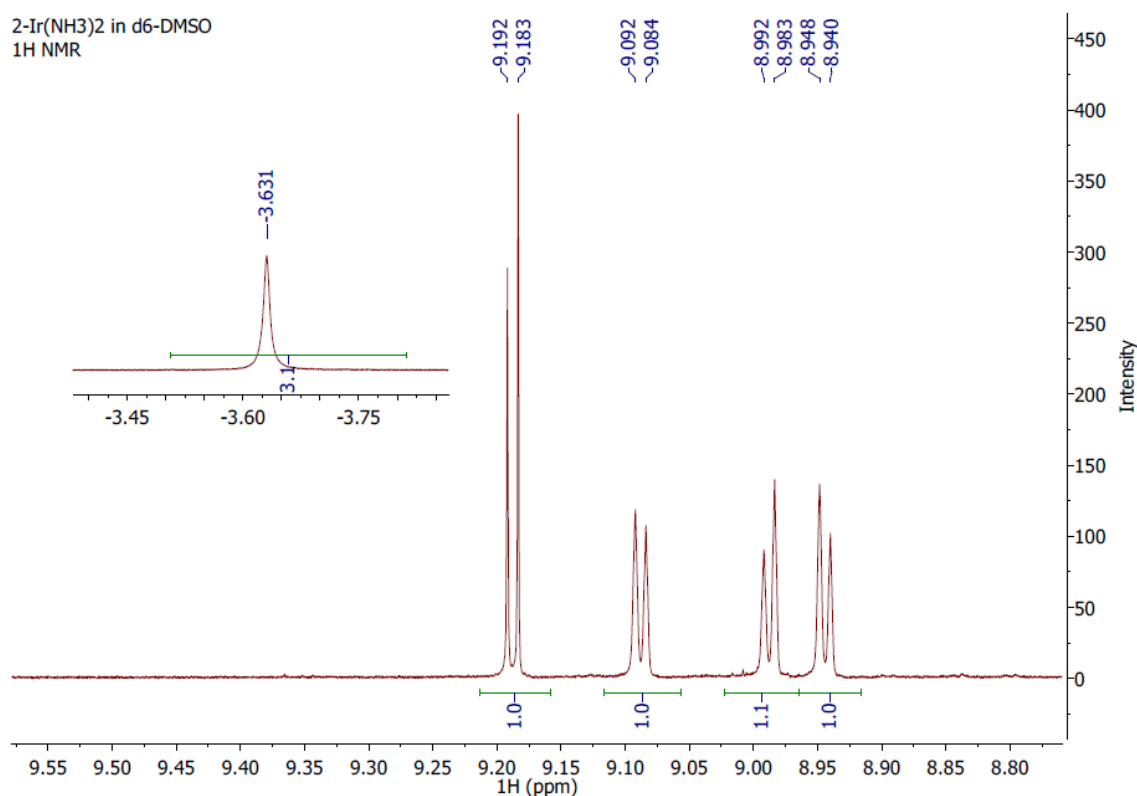


Figure 5-6:  $^1\text{H}$  NMR of **2-Ir(NH<sub>3</sub>)<sub>2</sub>** in  $d^6$ -DMSO. Note the similarity to the parent corrole, as well as the downfield shifting of the  $\beta$ -proton resonances.

In order to more fully characterize the new complex, we had to first develop a more reliable and convenient synthesis of it. To that end, we tried a number of oxidants in the presence of  $\text{NH}_4\text{OH}$  (which we assumed to be critical to the success of the reaction owing to the insertion of an extra nitrogen atom somewhere along the way), and we found that addition

of NBS to a mixture of **1-Ir(NH<sub>3</sub>)<sub>2</sub>** and NH<sub>4</sub>OH in acetonitrile causes the immediate evolution of gas (presumably ammonia) from the reaction vessel and a concomitant color change from green to a deep red-purple. Three different compounds, with an overall yield of about 50%, could be isolated from the reaction mixture by gradient column chromatography (the Danish “dry column” technique is recommended) in 1–5% CH<sub>3</sub>OH/CH<sub>2</sub>Cl<sub>2</sub>. The least polar of these complexes, and the major product, has two additional bromine atoms and two fewer protons than the original complex, and its UV-vis absorption spectrum displays significant bathochromic shifting. The second complex to elute from the column contains one additional bromine atom and is asymmetric by proton NMR, while the final complex to be removed from the column is the same compound produced by the hypochlorite reaction. All three compounds are fuchsia and display similar NMR and UV-vis spectral characteristics.

The UV-vis spectral signatures of the pink compounds, with their narrow, high-energy Soret bands and muted Q-band systems (Figure 5-7), look similar to those of the iron(III) azaporphyrin complexes explored as verdohemochrome analogues and spin-state curiosities by a number of groups in Japan and the United States.<sup>10</sup>

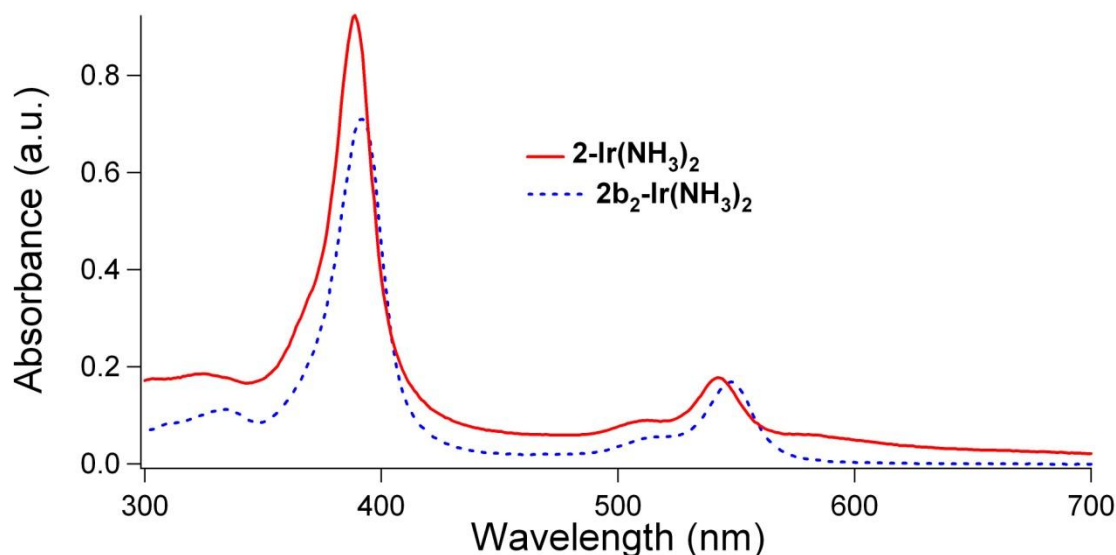


Figure 5-7: UV-vis absorption spectra of **2-Ir(NH<sub>3</sub>)<sub>2</sub>** (solid) and **2b<sub>2</sub>-Ir(NH<sub>3</sub>)<sub>2</sub>** (dashed) in CH<sub>3</sub>CN.

Based on this observation as well as our MS and NMR data, we have classified our new compounds as 3,17-dibromo-5,10,15-(tris)pentafluorophenylmonoazaporphyrinatoiridium(III) (bis)ammine [**2b<sub>2</sub>-Ir(NH<sub>3</sub>)<sub>2</sub>**], 3-bromo-5,10,15-(tris)pentafluorophenylmonoazaporphyrinatoiridium(III) (bis)ammine [**2b-Ir(NH<sub>3</sub>)<sub>2</sub>**], and 5,10,15-(tris)pentafluorophenylmonoazaporphyrinatoiridium(III) (bis)ammine [**2-Ir(NH<sub>3</sub>)<sub>2</sub>**] (Figure 5-8). To the best of our knowledge, these compounds represent the first examples of true iridium azaporphyrins in the scientific literature, although there is a report, from 2002, of an iridium(III) tetraazaporphine compound.<sup>11</sup> Additionally, our complexes are unique in that they have unsubstituted beta positions but are fully substituted at the meso positions, whereas the vast majority of azaporphyrins and azaporphines in the literature are derived from porphyrins or verdohemochrome-type macrocycles with complete  $\beta$ -substitution and no meso-substituents.

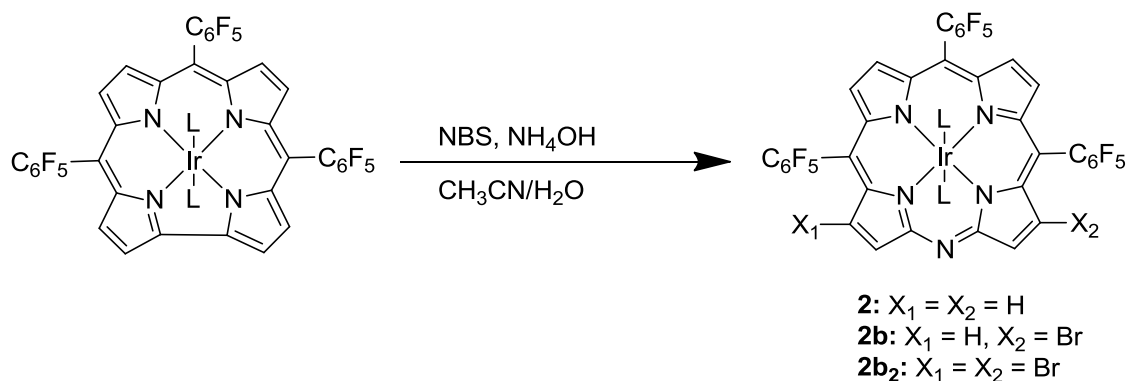


Figure 5-8: Synthesis of **2-Ir(NH<sub>3</sub>)<sub>2</sub>** and its brominated derivatives

In order to gain insight into the mechanism of formation of **2-Ir(NH<sub>3</sub>)<sub>2</sub>** and its brominated derivatives, we ran the NBS/NH<sub>4</sub>OH reaction using <sup>15</sup>N-substituted ammonium hydroxide; additionally, we attempted to drive the reaction to the hypothetical end product 2,3,7,8,12,13,17,18-octabromo-5,10,15-(tris)pentafluorophenylmonoazaporphyrinatoiridium(III) (bis)ammine using both massive excesses of NBS (in which case bromination is still halted at the **2b<sub>2</sub>-Ir(NH<sub>3</sub>)<sub>2</sub>** stage) and elemental bromine (resulting in a deep red but inseparable mixture of variously brominated analogues). The <sup>1</sup>H NMR spectra of the monoazaporphyrin products formed in the NBS/<sup>15</sup>NH<sub>4</sub>OH reaction (Figure 5-9) continues to display a singlet resonance far upfield corresponding to the ammine ligands; substitution by <sup>15</sup>N would be expected to produce a doublet due to <sup>15</sup>N-<sup>1</sup>H coupling. In addition, the <sup>15</sup>N-<sup>1</sup>H HMBC NMR spectrum of <sup>15</sup>N-**2b<sub>2</sub>-Ir(NH<sub>3</sub>)<sub>2</sub>**, which displays resonance between nitrogen and hydrogen atoms between two and three bonds distant (Figure 5-10), shows a strong signal corresponding to coupling between the new N atom on the azaporphyrin ring and the protons at the two and eighteen positions on the ring.

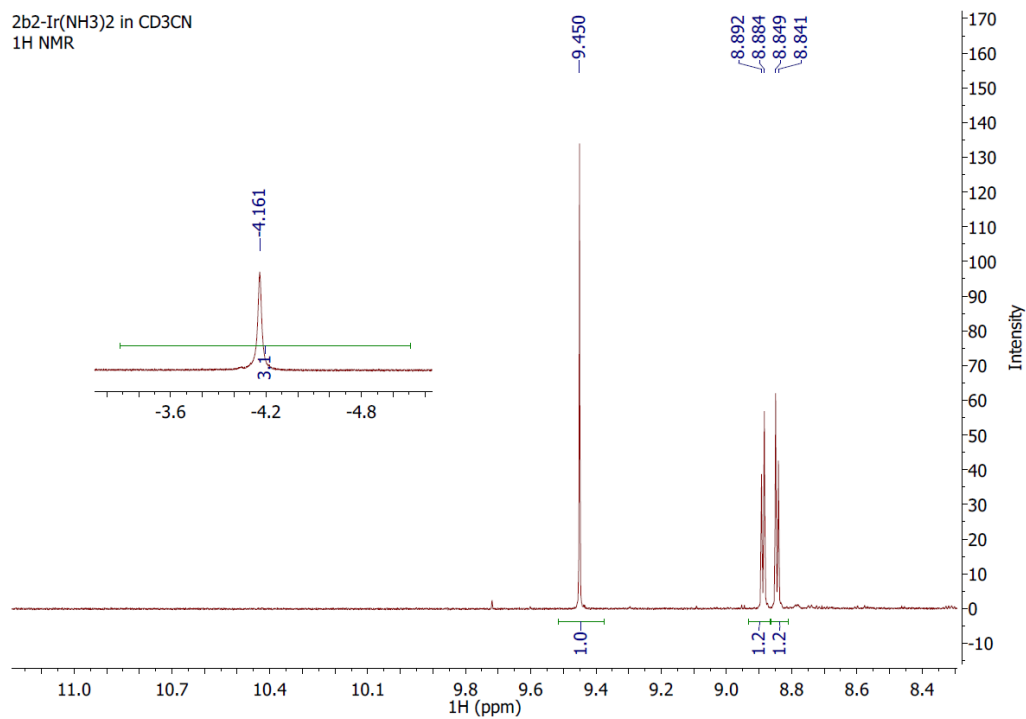


Figure 5-9: <sup>1</sup>H NMR of <sup>15</sup>N- labeled **2b<sub>2</sub>-Ir(NH<sub>3</sub>)<sub>2</sub>**. *Inset*: Upfield singlet resonance corresponding to the ammine ligand protons

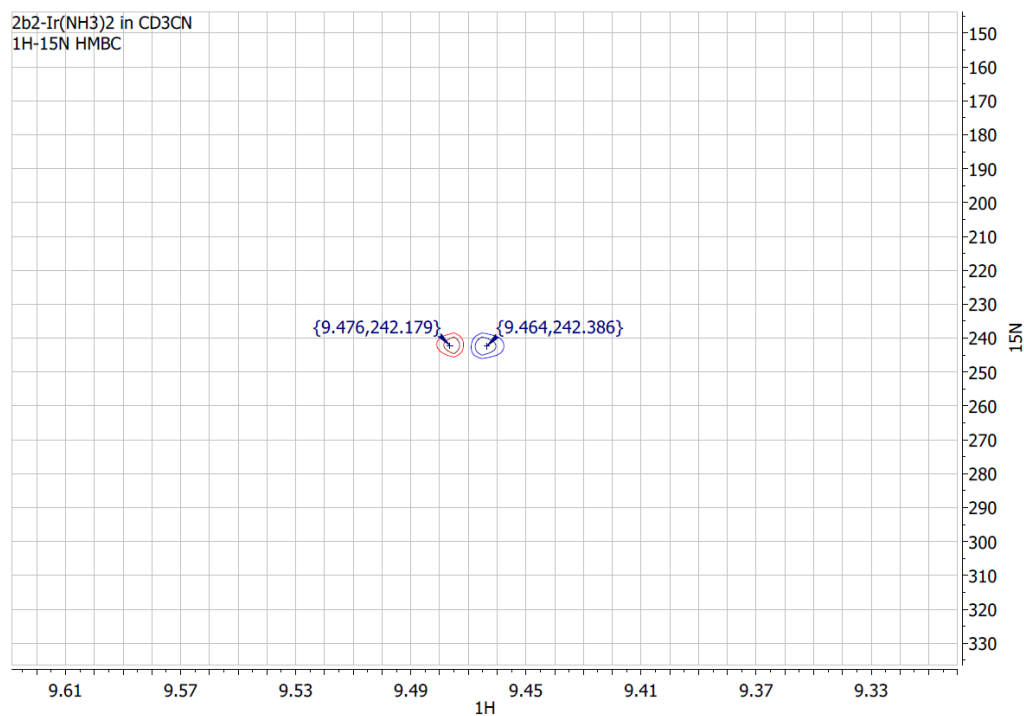


Figure 5-10: <sup>15</sup>N-<sup>1</sup>H HMBC spectrum of **2b<sub>2</sub>-Ir(NH<sub>3</sub>)<sub>2</sub>**, showing the correlation between the ring protons at positions two and eighteen and the inserted <sup>15</sup>N atom

The clear implication of the labeling studies is that the ammonium hydroxide is acting as the source of the nitrogen atom that becomes inserted into the corrole framework during the reaction, so it seems, at first glance, that this reaction should work on any of the iridium corroles in our possession. However, attempts at performing a similar reaction on either **1-Ir(tma)<sub>2</sub>** or **1-Ir(py)<sub>2</sub>** were completely unsuccessful. Given that our simple labeling studies imply strongly that the ammine ligands on the iridium play no active role in the formation of the monoazaporphyrin, we tentatively posit that the willingness of **1-Ir(NH<sub>3</sub>)<sub>2</sub>** to undergo nitrogen insertion stems from its low redox potential; the ammine-ligated corrole is more than 0.1 V easier to oxidize than either of the other corroles mentioned.

Based on the data we currently have, we can postulate a tentative mechanism of nitrogen insertion wherein the corrole is first oxidized by NBS to a mixed metal/ $\pi$ -cation radical state and then undergoes nucleophilic attack by the ammonia in solution. Then the protons on the newly inserted nitrogen atom must be removed by the hydroxide in solution resulting in rearomatization of the ring system. The resulting azaporphyrins are quite resistant to bromination (**2-Ir(NH<sub>3</sub>)<sub>2</sub>** and **2b-Ir(NH<sub>3</sub>)<sub>2</sub>** are not converted to **2b<sub>2</sub>-Ir(NH<sub>3</sub>)<sub>2</sub>** even upon standing for long periods with excess NBS in solution), so the halogenation step must take place prior to insertion of the nitrogen atom. We cannot say for certain whether the bromination takes place on the corrole before oxidation or during the intermediate steps, but the distribution of the products and the speed of the reaction (the solution turns purple immediately upon adding NBS to the corrole/NH<sub>4</sub>OH mixture) slightly favor the latter pathway.



In addition to their interesting molecular structures, **2-Ir(NH<sub>3</sub>)<sub>2</sub>** and **2b<sub>2</sub>-Ir(NH<sub>3</sub>)<sub>2</sub>**, like their parent corroles, display long-lived phosphorescence at room temperature [**2b-Ir(NH<sub>3</sub>)<sub>2</sub>** was extremely difficult to purify, and therefore not subjected to photophysical studies]. Unlike the iridium(III) corrole compounds we have studied, the monoazaporphyrin complexes luminesce in the red end of the visible region (as opposed to the near-IR), with maxima at 695 and 691 nm for **2b<sub>2</sub>-Ir(NH<sub>3</sub>)<sub>2</sub>** and **2-Ir(NH<sub>3</sub>)<sub>2</sub>**, respectively (Figure 5-11), and with an emission band shape that looks extremely similar to those of the iridium(III) corroles.<sup>12</sup> The luminescence lifetimes of the complexes are on the order of hundreds of nanoseconds, implying that the emission is phosphorescence from a triplet state.

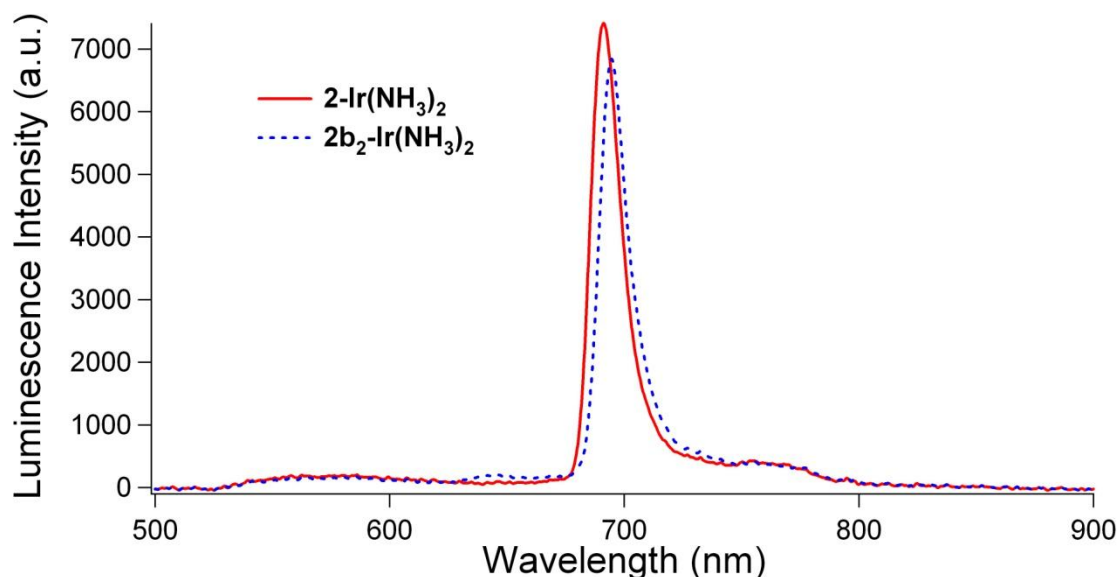


Figure 5-11: Emission spectra of **2-Ir(NH<sub>3</sub>)<sub>2</sub>** (solid) and **2b<sub>2</sub>-Ir(NH<sub>3</sub>)<sub>2</sub>** (dashed) at 77K in frozen CH<sub>3</sub>CN. Room temperature emission spectra can be viewed in Supporting Information.

Future work in our laboratories will focus on the development of more efficient syntheses for azaporphyrin complexes starting from a variety of meso-substituted corroles, as well as the expansion of the reaction to include corrole complexes of metals other than iridium. Monoazaporphyrin complexes of iron(III) have been studied to some extent as biomimetic

heme complexes, but always with significant  $\beta$ -substitution and without meso-substituents; so the development of new iron(III) MAzP complexes from the parent corroles could produce an interesting new family of compounds. Additionally, we will further study the photophysics of the Ir(III) monoazaporphyrins, whose quantum yields of emission appear in preliminary experiments to be slightly higher than those of their parent corroles.

---

## References

- (1) Gross, Z.; Gray, H. B. *Comm. Inorg. Chem.* **2006**, *27*, 61–72.
- (2) a) Golubkov, G.; Gross, Z. *Angew. Chem. Int. Ed.* **2003**, *42*, 4507–4510. b) Golubkov, G.; Gross, Z. *J. Am. Chem. Soc.* **2005**, *127*, 3258–3259. c) Mahammed, A.; Gray, H. B.; Meier–Callahan, A. E.; Gross, Z. *J. Am. Chem. Soc.* **2003**, *125*, 1162–1163. d) Gross, Z.; Golubkov, G.; Simkhovich, L. *Angew. Chem. Int. Ed. Eng.* **2000**, *39*, 4045–4047. e) Golubkov, G.; Bendix, J.; Gray, H. B.; Mahammed, A.; Goldberg, I.; DiBilio, A. J.; Gross, Z. *Angew. Chem. Int. Ed. Eng.* **2001**, *40*, 2132–2134. f) Mandimutsira, B. S.; Ramdhanie, B.; Todd, R. C.; Wang, H. L.; Zareba, A. A.; Czernuszewicz, R. S.; Goldberg, D. P. *J. Am. Chem. Soc.* **2002**, *124*, 15170–15171.
- (3) Simkhovich, L.; Gross, Z. *Tet. Lett.* **2001**, *42*, 8089–8092.
- (4) a) Adamian, V. A.; D'Souza, F.; Licocchia, S.; Di Vona, M. L.; Tassoni, E.; Paolesse, R.; Boschi, T.; Kadish, K. M. *Inorg. Chem.* **1995**, *34*, 532–540. b) Kadish, K. M.; Adamian, V. A.; Van Caemelbecke, E.; Gueletti, E.; Will, S.; Erben, C.; Vogel, E. *J. Am. Chem. Soc.* **1998**, *120*, 11986–11993.
- (5) Zakharieva, O.; Schunemann V.; Gerdan M.; Licocchia S.; Cai S.; Walker F. A.; Trautwein A. X. *J. Am. Chem. Soc.* **2002**, *124*, 6636–6648. b) Kadish, K. M.; Shen, J.; Fremont, L.; Chen, P.; El Ojaimi, M.; Chkounda, M.; Gros, C. P.; Barbe, J. M.; Ohkubo, K.; Fukuzumi, S.; Guillard, R. *Inorg. Chem.* **2008**, *47*, 6726–6737.
- (6) Palmer, J. H.; Day, M. W.; Wilson, A. D.; Henling, L. M.; Gross, Z.; Gray, H. B. *J. Am. Chem. Soc.* **2008**, *130*, 7786–7787.
- (7) Palmer, J. H.; Mahammed, A.; Lancaster, K. M.; Gross, Z.; Gray, H. B. *Inorg. Chem.* **2009**, *48*, 9308–9315.
- (8) Dong, S. S.; Nielsen, R. J.; Palmer, J. H.; Gray, H. B.; Gross, Z.; Dasgupta, S.; Goddard, W. A. III. *Inorg. Chem.* **2011**, ASAP.
- (9) Palmer, J. H.; Lancaster, K. M.; DeBeer, S.; Gray, H. B. *manuscript in preparation*.
- (10) a) Nakamura, K.; Ikezaki, A.; Ohgo, Y.; Ikeue, T.; Neya, S.; Nakamura, M. *Inorg. Chem.* **2008**, *47*, 10299–10307. b) Balch, A. L.; Olmstead, M. M.; Safari, N. *Inorg. Chem.* **1993**, *32*, 219–296. c) Saito, S.; Tamura, N.; *Bull. Chem. Soc. Jpn.* **1987**, *60*, 4037–4049. d) Saito, S.; Sumita, S.; Iwai, K.; Sano, H. *Bull. Chem. Soc. Jpn.* **1988**, *61*, 3539–3547. e) For a somewhat dated but still relevant review, see: Kobayashi, N. In *The Porphyrin Handbook*; Kadish, K. M., Smith, K. M., Guillard, R., Eds.; Academic Press: San Diego, CA, **2000**, *2*, 301–360.
- (11) Stuzhin, P. A.; Kabeshcheva, E. V.; Khelevina, O. G. *Russ. J. Coord. Chem.* **2003**, *29*, 377–381.
- (12) Palmer, J. H.; Durrell, A. C.; Winkler, J. R.; Gross, Z.; Gray, H. B. *J. Am. Chem. Soc.* **2010**, *132*, 9230–9231.

*E p i l o g u e*

## A BRIEF DESCRIPTION OF ONGOING WORK

Throughout the work presented in this thesis, I've attempted to discern the character of one-electron oxidized Ir(III) corroles with a battery of techniques and theoretical treatments. This might seem like the foolhardy overemphasis of the blinkered specialist, but there are plenty of broad reasons to continually revisit the issue of electronic structure in non-innocent systems. The ongoing work of scientists like Karl Wieghardt<sup>1</sup> and Edward Solomon<sup>2</sup> has slowly painted a picture of the bonding and electronic structure of coordination compounds wherein the "formal" and "physical" oxidation states of the metal (and of the ligands) can be vastly different. A good example is the neutral, hexacoordinate metal complex  $V(pdt)_3$ ,<sup>3</sup> where  $pdt = [cis-1,2-diphenylethene-1,2-dithiolate]^{2-}$ . This is formally a V(VI) compound, but of course vanadium is a  $d^5$  metal, and in fact this complex has been assigned as having a V(IV) center with two additional holes distributed across the highly redox-active ligands. In a natural extension of this work to the realm of catalysis, Paul Chirik,<sup>4</sup> Pat Holland,<sup>5</sup> Craig Grapperhaus,<sup>6</sup> and many other chemists have sought to use non-innocent ligands to temporarily dock holes or electrons, so ligand redox activity, once thought of primarily as a difficulty to be surmounted by clever design, has been co-opted into practical catalyst design.

With my increasingly detailed work on the electronic structure of the formal iridium(IV) corrole systems, I have sought to find out if the incorporation of 5d metals, with the high electropositivity and relativistic effects they bring to the table, could allow for clean oxidation of neutral metallocorroles to metal-based radicals by stabilizing the state with

spin on the metal more effectively than has been seen in the past with lighter metals. Corroles are famously non-innocent, and extreme metal-ligand covalency has been well-documented for iron<sup>7</sup> and copper<sup>8</sup> corroles. At first, I felt certain this was the case based on our early EPR and UV-vis experiments.<sup>9</sup> However, the computational work I did in collaboration with Sijia, Smith, and Bill Goddard gave me significant pause, as it seemed to suggest that ligand-based oxidation would be favored in a simple model case.<sup>10</sup> Additionally, XAS data from SSRL (collected in collaboration with Serena DeBeer, now of Cornell University) also suggested that oxidation was mostly ligand-based.

We have recently run a series of highly sophisticated DFT calculations that include spin-orbit effects and utilize large basis sets as well as a number of perturbative correction factors, and that I believe give a fairly accurate picture of the “true” electronic structure of my one-electron oxidized, formally Ir(IV) iridium corrole complexes. Remarkably accurate EPR parameters have been calculated based on these ground state electronic structures, suggesting as strongly as possible that the calculated spin density mimics the real distribution of electron spin in the oxidized molecules. Perhaps unsurprisingly, the calculated ground states of the “Ir(IV)” corroles are highly delocalized, with spin both on the iridium and on the ligand. These computed electronic states appear to correspond accurately to the experimental parameters of the complexes; therefore, I postulate that, after extensive experimental and theoretical studies on the subject of iridium corrole non-innocence, we have finally zeroed in on the real electronic structure of the one-electron oxidized  $[\text{Ir}(\text{tpfc})\text{L}_2]^+$  family of complexes.

My original outline of this thesis included a chapter presenting these calculations, comparing them to our experimental EPR spectra, and discussing the XAS parameters as well. Unfortunately, both experimental and computational data were still being collected in the final days of thesis composition, and I don't feel that the project is yet quite at the stage where I can do it justice here. That said, it currently appears that when spin-orbit coupling is explicitly included in the calculations of the iridium(IV) ground state, a small amount of spin density, between 10 and 19% depending on the axial ligand, is transferred from the ring (where all of it resides in our earlier calculations) to the metal. What is more, we can then use these calculated ground states to model the EPR parameters of the oxidized corroles, and we receive very accurate numbers. We have found that the amount of anisotropy ( $\Delta g$ ) in the experimental g tensor components scales with the electron-donating strength of the ligand, such that **[1-Ir(meopy)<sub>2</sub>]<sup>+</sup>** and **[1-Ir(dmap)<sub>2</sub>]<sup>+</sup>** have broad EPR spectra with highly anisotropic signal, and **[1-Ir(cfpy)<sub>2</sub>]<sup>+</sup>** has a relatively narrow spectrum with a  $\Delta g$  that is not nearly as large as in the cases where the ligands are electronically rich.

The theoretical calculations we have done model this trend in  $\Delta g$  accurately, and also suggest an explanation for the experimental results. As the axial ligands become more electron-donating, the percentage of spin on the metal increases from 10% in the case of **[1-Ir(cfpy)<sub>2</sub>]<sup>+</sup>** to 19% for **[1-Ir(dmap)<sub>2</sub>]<sup>+</sup>**, suggesting that the anisotropy of the EPR signal is owing to mixing of small amounts of  $d_{xy}$  ( $C_{2v}$  symmetry) into an orbital that is of primarily corrole ligand character. The calculated spin on the iridium  $d_{xy}$  orbital in **[1-Ir(py)<sub>2</sub>]<sup>+</sup>** is 14%, whereas the  $d_{xy}$  spin in **[1-Ir(tma)<sub>2</sub>]<sup>+</sup>** is 20%, so these results also help to explain the extremely rhombic EPR spectrum observed for the tma-ligated complex. I hope to expand

on these results in an article very shortly, but there a few loose ends to wrap up, such as modeling and interpretation of my XAS data, before that can happen.

Two years on from my initial publication of the iridium corroles, there has been no further examination of third-row metallocorrole complexes, leaving our iridium and the oxorhenium corrole of K. S. Chan as the only examples in the literature.<sup>11</sup> I am currently in the process of finishing the characterization of a platinum corrole dimer which I hope can remedy this sad situation. Additionally, I plan to finish my study of the iridium azaporphyrins described in Chapter 5, which should add a new chapter to the increasingly lengthy tome of corrole reactivity.

- 
- (1) Sproules, S.; Benedito, F. L.; Bill, E.; Weyhermüller, T. George, S. D.; Wieghardt, K. *Inorg. Chem.* **2009**, *48*, 10926–10941.
  - (2) Hocking, R. K.; George, S. D.; Gross, Z.; Walker, F. A.; Hodgson, K. O.; Hedman, B.; Solomon, E. I. *Inorg. Chem.* **2009**, *48*, 1678–1688.
  - (3) Sproules, S.; Weyhermüller, T.; DeBeer, S.; Wieghardt, K. *Inorg. Chem.* **2010**, *49*, 5241–5261.
  - (4) Chirik, P. J.; Wieghardt, K. *Science*. **2010**, *327*, 794–795.
  - (5) Holland, P. L. *Acc. Chem. Res.* **2008**, *41*, 905–914.
  - (6) Grapperhaus, C. A.; Kozłowski, P. M.; Kumar, D.; Frye, H. N.; Venna, K. B.; Poturovic, S. *Angew. Chem. Int. Ed.* **2007**, *46*, 4085–4088.
  - (7) Zakharieva, O.; Schünemann, V.; Gerdan, M.; Licoccia, S.; Cai, S.; Walker, F. A.; Trautwein, A. X.. *J. Am. Chem. Soc.* **2002**, *124*, 6636–6648.
  - (8) a) Alemayehu, A. B.; Hansen, L. K.; Ghosh, A. *Inorg. Chem.* **2010**, *49*, 7608–7610. b) Pierloot, K.; Zhao, H.; Vancoillie, S. *Inorg. Chem.* **2010**, *49*, 10316–10329.
  - (9) Palmer, J. H.; Mahammed, A.; Lancaster, K. M.; Gross, Z.; Gray, H. B. *Inorg. Chem.* **2009**, *48*, 9308–9315.
  - (10) Dong, S. S.; Nielsen, R. J.; Palmer, J. H.; Gray, H. B.; Gross, Z.; Dasgupta, S.; Goddard, W. A., III. *Inorg. Chem.* **2011**, ASAP.
  - (11) a) Palmer, J. H.; Day, M. W.; Wilson, A. D.; Henling, L. M.; Gross, Z.; Gray, H. B. *J. Am. Chem. Soc.* **2008**, *130*, 7786–7787. b) Tse, M. K.; Zhang, Z.; Mak, T. C. W.; Chan, K. S. *Chem. Commun.* 1998, 1199–1200.

*A p p e n d i x A*

## METHODOLOGY AND INSTRUMENTATION

**Materials:** Solvents, including dichloromethane, acetonitrile, acetone, methanol, ethyl acetate, tetrahydrofuran, benzene, and toluene were purchased from the Caltech VWR stockroom, generally through EMD Chemicals, and were used without further purification in most cases. Solvents used for air- and moisture-sensitive reactions were degassed with argon and dried on columns of activated alumina in a glove box. Solvents for air-sensitive photophysical measurements were subjected to three freeze-pump-thaw cycles after being purged with dry nitrogen gas. Deuterated NMR solvents were purchased from the Caltech chemistry stockroom through Cambridge Isotope Laboratories (or occasionally Sigma-Aldrich) and were used as received. Reagents were purchased from Sigma-Aldrich, and largely used as received.  $[\text{Ir}(\text{cod})\text{Cl}]_2$  was occasionally purchased from Alfa Aesar instead. Crystallization of the discussed complexes was achieved by slow evaporation of concentrated methylene chloride solutions with small amounts of methanol and/or hexanes added.

**Nuclear Magnetic Resonance Spectroscopy:** One-dimensional proton NMR experiments were performed on two different Varian Mercury 300 MHz NMR spectrometers and one Varian Mercury 600 MHz NMR spectrometers. All  $^{19}\text{F}$  1D NMR experiments were performed on one of the 300 MHz spectrometers because of the lack of an appropriate probe on the 600 MHz instrument. Two-dimensional experiments, including  $^1\text{H}$ - $^1\text{H}$  COSY,  $^1\text{H}$ - $^{13}\text{C}$  HSQC,  $^1\text{H}$ - $^{13}\text{C}$  HMBC,  $^1\text{H}$ - $^{13}\text{C}$  H2BC,  $^1\text{H}$ - $^{15}\text{N}$  HSQC,

and  $^1\text{H}$ - $^{15}\text{N}$  HMBC, were performed exclusively on the 600 MHz instrument. COSY refers to COrrrelation SpectroscopY and detects interactions between two vicinal nuclei of identical type. HSQC stands for Heteronuclear Single Quantum Correlation, and detects one-bond interactions between two different types of nuclei. HMBC is an acronym for Heteronuclear Multiple Bond Correlation, and detects two- and three-bond couplings between two different types of nuclei. Finally, H2BC, which stands for Heteronuclear Two Bond Correlation, acts as a variant of HMBC wherein the three-bond interactions are attenuated dramatically and the signal corresponds primarily to two-bond coupling.

**Mass spectrometry:** MS was performed by electrospray ionization into a Thermofinnigan LCQ ion trap mass spectrometer. Solutions of 1–10  $\mu\text{M}$  analyte concentration were prepared in  $\text{CH}_3\text{OH}$  for injection when possible; in the case of material less soluble in methanol, a mix of 7:3  $\text{CH}_3\text{OH}/\text{CHCl}_3$  was employed instead. Ions were examined primarily in positive mode.

**UV-visible spectroscopy:** For the work presented in Chapters 1 and 2, UV-vis spectra were obtained on a Hewlett-Packard 8452A Diode Array Photospectrometer. Titrations of corrole compounds by oxidants were performed by adding small amounts of stock oxidant solution to corrole solutions in  $\text{CH}_2\text{Cl}_2$ . For the rest of the work presented here, UV-vis spectra were obtained on a Varian Cary 50 Scanning Photospectrometer. In all cases, the error in reported wavelength values is at most  $\pm 0.5$  nm. Extinction coefficients were measured for gravimetrically prepared solutions, and should be accurate to  $\pm 10\%$ .



**Cyclic voltammetry:** The data presented in Chapter 2 were collected on a WaveNow USB Potentiostat/Galvanostat (Pine Research Instrumentation) using Pine AfterMath Data Organizer software. All other CV experiments were performed using a BAS100B/W Electrochemical Analyzer. For the experiments presented in Chapter 1, tetraethylammonium hexafluorophosphate (0.3 M) was employed as the electrolyte; for all other experiments tetrabutylammonium hexafluorophosphate (0.1–0.5 M) was used instead. All electrochemical experiments involving the corroles were performed in  $\text{CH}_2\text{Cl}_2$  to avoid the ligand substitution problems that occasionally appeared when  $\text{CH}_3\text{CN}$  (a more traditional electrochemistry solvent with a larger non-redox-active window) was used instead. All CV measurements were referenced to the ferrocenium/ferrocene ( $\text{Fc}^+/\text{Fc}^0$ ) reduction potential and then back-converted to potentials vs. the standard saturated calomel electrode (SCE) by addition of 0.465 V to the values vs.  $\text{Fc}^+/\text{Fc}^0$ . A three-electrode setup was employed for CV measurements, with a glassy carbon disc working electrode, a platinum wire counter electrode, and a Ag/AgCl quasi-reference electrode prepared by dipping a silver wire into HCl for four hours and then inserting it into a tube filled with electrolyte solution (separated from the bulk CV solution by a Vykor frit).

**Spectroelectrochemistry:** Spectroelectrochemical measurements were performed, using a Varian Cary 50 Scanning Photospectrometer (with attached software scanning kinetics package), in a homemade cuvet with a one mm path length at the beam and a one cm well at the top. Optically transparent platinum mesh was employed as the working electrode and a platinum wire was used as the auxiliary electrode. A silver wire, coated in AgCl by a four-hour stay in a concentrated HCl bath and then immersed in electrolyte solution,

was separated by a Vykro frit from the bulk solution and allowed to act as a quasi-reference electrode. Tetrabutylammonium hexafluorophosphate (0.1 M in  $\text{CH}_2\text{Cl}_2$ ) was employed as the electrolyte.

**Electron Paramagnetic Resonance:** EPR measurements were performed using a Bruker EMX Biospin instrument, with a Gunn diode microwave source. Most EPR was performed in  $\text{CH}_2\text{Cl}_2$ , which does not generally glass as well as toluene but which gave us better results in general and which can dissolve both of the oxidants we employed in experiments (iodine and (tris)-4-bromophenylaminium hexachloroantimonate). Solutions were pre-cooled by rapid freezing in liquid nitrogen; spectra of samples at 20 K, where signal was found to be optimal for these systems, were obtained using liquid helium as a coolant. The SPINCOUNT package by Michael Hendrich was used to simulate EPR parameters.

**Quantum Yield, Lifetime, and Emission Measurements:** Steady-state and time-resolved emission measurements were conducted at the Beckman Institute Laser Resource Center. Emission spectra were recorded on samples dissolved in solution (room temperature) or frozen glass (77 K). Samples were degassed by three freeze-pump-thaw cycles. For steady-state emission spectra, the 496.5 nm line of an argon ion laser (Coherent Inova 70) was used to excite samples. Right angle emission was collected *via* a Melles Griot Fiber Optic Spectrometer (MGSPEC-2048-SPU). Quantum yields were obtained by comparing signal intensity (corrected through use of a pre-made software file) to a tetraphenylporphyrin standard. Absorption values for the samples at 496.5 nm were recorded on a Hewlett-Packard 8451A diode array spectrophotometer. For time-

resolved measurements, samples were excited at 440 nm. Pulses of 8 ns duration from the third harmonic of a Q-switched Nd:YAG laser (Spectra-Physics Quanta-Ray PRO-Series) operating at 10 Hz were used to pump an optical parametric oscillator (OPO, Spectra-Physics Quanta-Ray MOPO-700) to provide laser pulses at 440 nm. Emitted light was detected with a photomultiplier tube (PMT, Hamamatsu R928). PMT current was amplified and recorded using a transient digitizer (Tektronix DSA 602).

**Computational Methods:** The calculations presented in Chapter 4 were performed using Jaguar 7.0 (Schrödinger, L.L.C.), employing the hybrid functional B3LYP (Becke 3 Parameter, Lee, Yang, and Parr). The pseudopotentials of Hay and Wadt were used to model core electrons, which were not treated explicitly due to the computational costs involved. Geometries were computed with 2- $\zeta$  valence functions on the metal and 6-31G\*\* for all other atoms. Meanwhile, single point energies were computed with 3- $\zeta$  valence functions on the metal and 6-31G\*\*\*<sup>++</sup> for all other atoms. Solvation energies were obtained using the Poisson-Boltzmann continuum solvation model, with a dielectric constant of  $\epsilon = 8.93$  and probe radius of 2.33 Å to represent dichloromethane. The work described in the Epilogue employed the ORCA program, developed by Frank Neese at the University of Bonn in Germany.

## Appendix B

### SYNTHESIS AND CHARACTERIZATION

The following is a representative, but not completely comprehensive, list of the corrole and azaporphyrin syntheses I developed while at Caltech. It should give the reader a good idea of how these compounds are made without a lot of tedious reference to online Supporting Information files. Some NMR and/or UV-vis characterization data is included for each compound as well. X-ray structures for compounds **1-Ir(tma)<sub>2</sub>**, **1b-Ir(tma)<sub>2</sub>**, **1-Ir(py)<sub>2</sub>**, **1-Ir(dmap)<sub>2</sub>**, and **1-Ir(NH<sub>3</sub>)<sub>2</sub>** are included in Appendix C.

**5,10,15-(tris)Pentafluorophenylcorrolatoiridium(III) (bis)trimethylamine, 1-Ir(tma)<sub>2</sub>:** H<sub>3</sub>tpfc (80 mg), [Ir(cod)Cl]<sub>2</sub> (335 mg), and K<sub>2</sub>CO<sub>3</sub> (140 mg) were dissolved/suspended in 150 mL of degassed THF, and the mixture was heated at reflux under argon for 90 min (until corrole fluorescence was negligible to the eye upon long-wavelength irradiation with a hand-held lamp). Tma *N*-oxide (110 mg) was added, and the solution was allowed to slowly cool to room temperature while open to the laboratory atmosphere. Column chromatography of the black mixture (silica, 4:1 hexanes/CH<sub>2</sub>Cl<sub>2</sub>) provided an auburn solution, from which purple crystals of **1-Ir(tma)<sub>2</sub>** (30 mg, 27% yield) could be grown by slow evaporation. <sup>1</sup>H NMR (CDCl<sub>3</sub>): δ 8.99 (d, 2H, J = 5.4), 8.67 (d, 2H, J = 6.0), 8.55 (d, 2H, J = 6.0), 8.23 (d, 2H, J = 4.8), -2.95 (s, 18H). <sup>19</sup>F NMR (CDCl<sub>3</sub>): δ -138.38 (m, 6F), -154.89 (m, 3F), -163.27 (m, 6F). MS (ESI): 1105.1 ([M<sup>+</sup>]), 1046.0 ([M<sup>+</sup>-tma]), 986.5 ([M<sup>+</sup>-2tma]). UV-vis (toluene, nm, ε × 10<sup>-3</sup> M<sup>-1</sup> cm<sup>-1</sup>):

390 (51.9), 413 (64.3), 574 (15.9), 640 (5.64). Emission (toluene, nm): 788. XRD: See Appendix C.

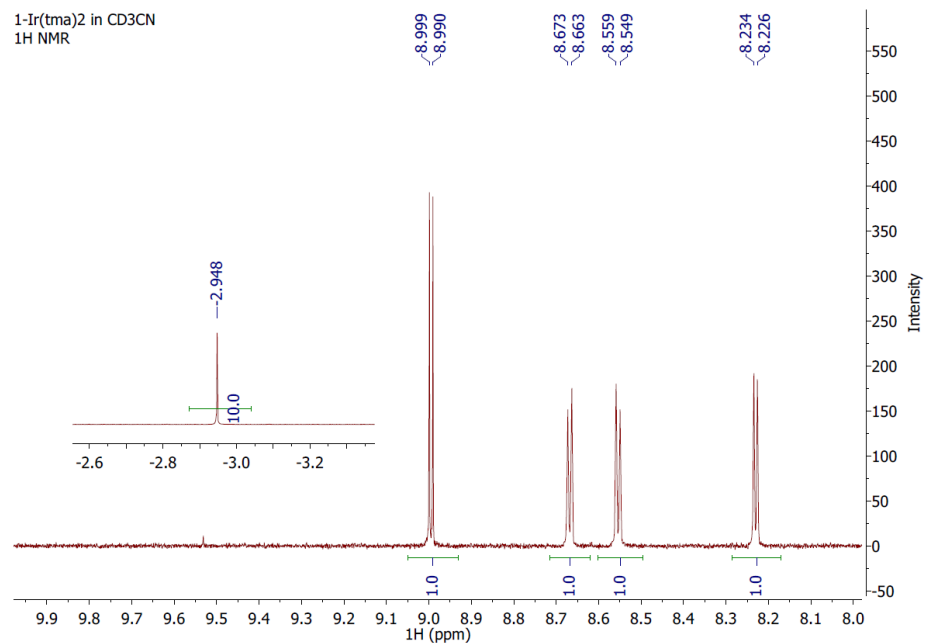


Figure B-1: <sup>1</sup>H NMR of **1-Ir(tma)<sub>2</sub>** in CD<sub>3</sub>CN

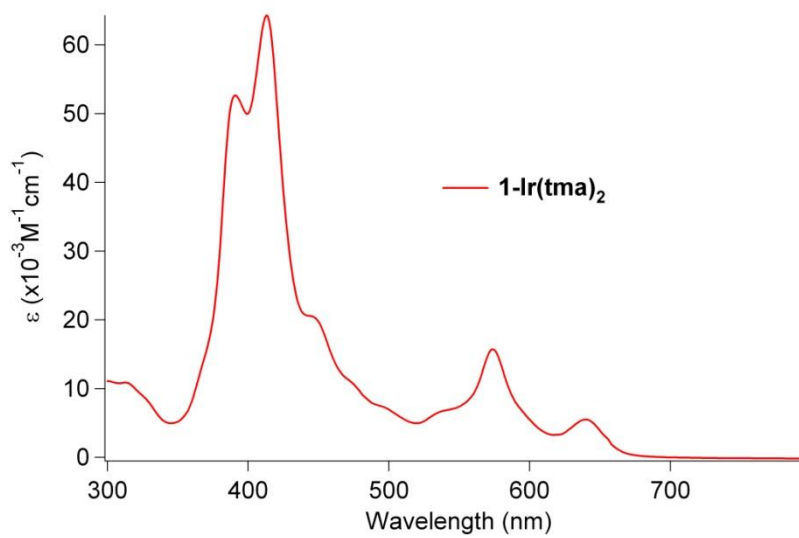


Figure B-2: UV-vis of **1-Ir(tma)<sub>2</sub>** in toluene

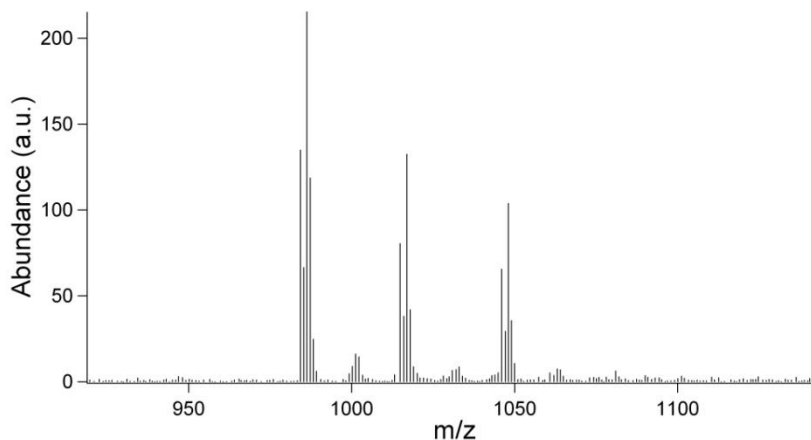
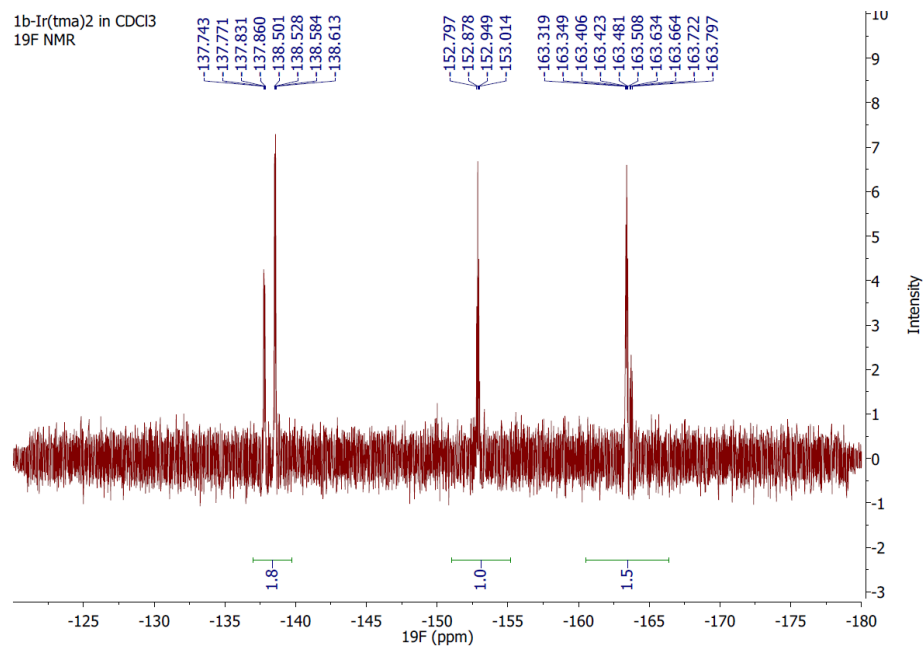
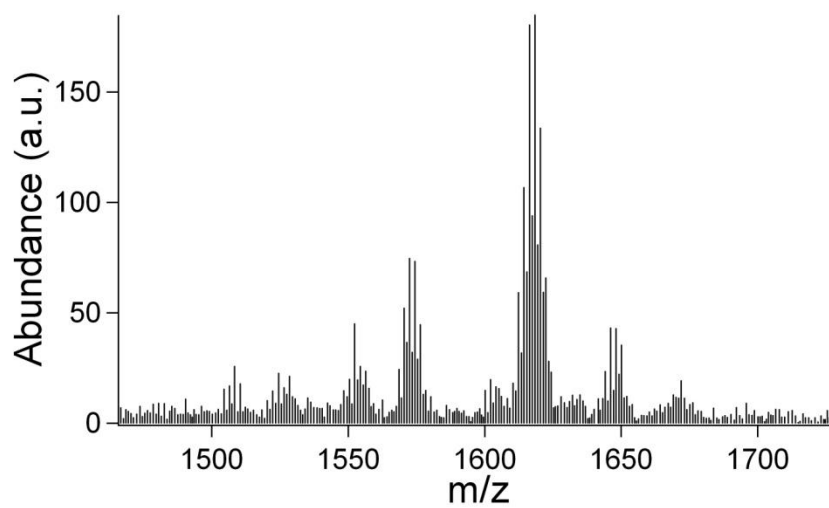


Figure B-3: ESI-MS of **1-Ir(tma)<sub>2</sub>**

**2,3,7,8,12,13,17,18-Octabromo-5,10,15-(tris)pentafluorophenylcorrolatoiridium(III) (bis)trimethylamine, 1b-Ir(tma)<sub>2</sub>:** Br<sub>2</sub> (70  $\mu$ L) and **1-Ir(tma)<sub>2</sub>** (15 mg) were dissolved in 20 mL of MeOH and stirred overnight. Column chromatography (silica, 4:1 hexanes/CH<sub>2</sub>Cl<sub>2</sub>) of the red mixture provided a ruddy solution from which purple crystals of **1b-Ir(tma)<sub>2</sub>** (15 mg, 63% yield) could be grown by addition of methanol followed by slow evaporation. <sup>1</sup>H NMR (CDCl<sub>3</sub>):  $\delta$  -2.60 (s, 18H). <sup>19</sup>F NMR (CDCl<sub>3</sub>):  $\delta$  -137.78 (d/d, 2F, <sup>3</sup>J = 35.1, <sup>4</sup>J = 18.3), -138.54 (d/d, 4F, <sup>3</sup>J = 33.9, <sup>4</sup>J = 17.1), -152.89 (m, 3F), -163.38 (m, 4F), -163.70 (m, 2F). MS (ESI): 1616.4 ([M<sup>+</sup> - 2tma]). UV-vis (toluene, nm,  $\epsilon \times 10^{-3} \text{ M}^{-1} \text{ cm}^{-1}$ ): 404 (54.0), 424 (62.8), 582 (13.9), 656 (6.15). Emission (toluene, nm): 795. XRD: See Appendix C.

Figure B-4: <sup>19</sup>F NMR of **1b-Ir(tma)<sub>2</sub>** in CDCl<sub>3</sub>Figure B-5: ESI-MS of **1b-Ir(tma)<sub>2</sub>**

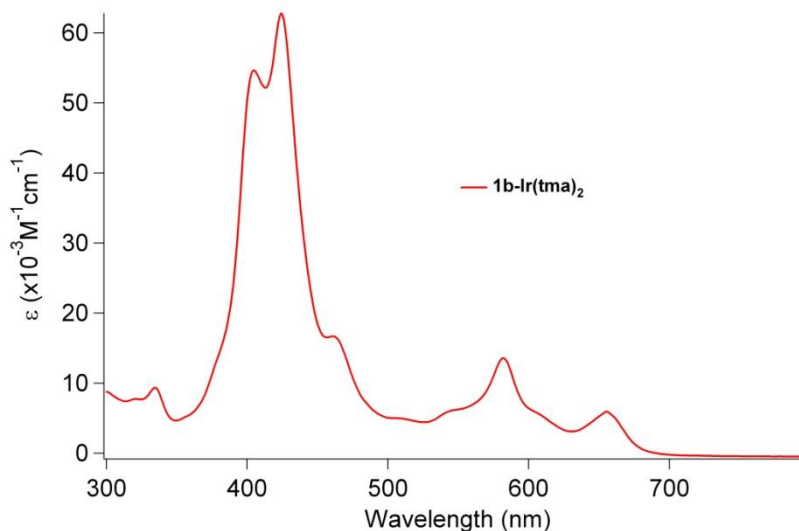
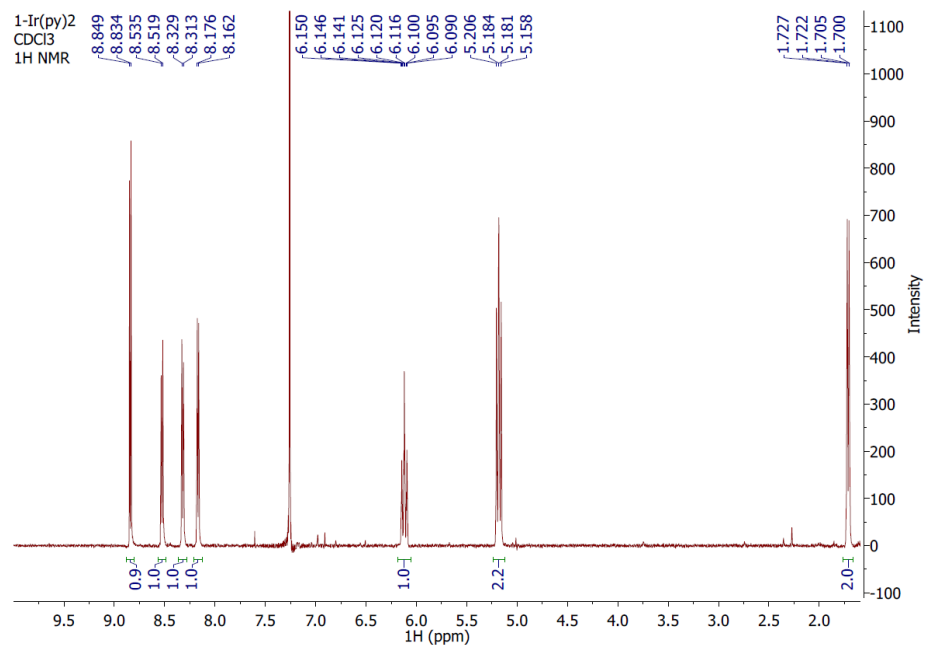
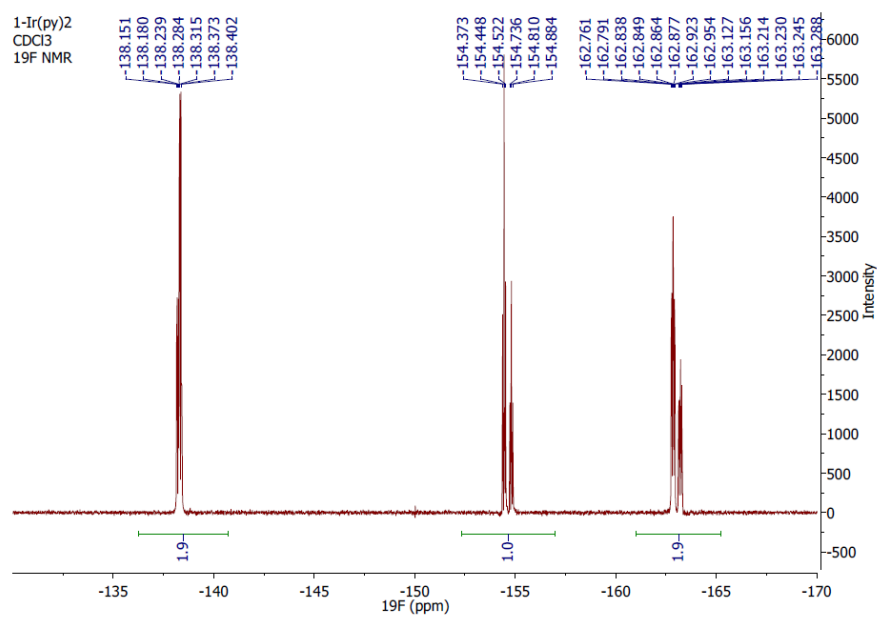
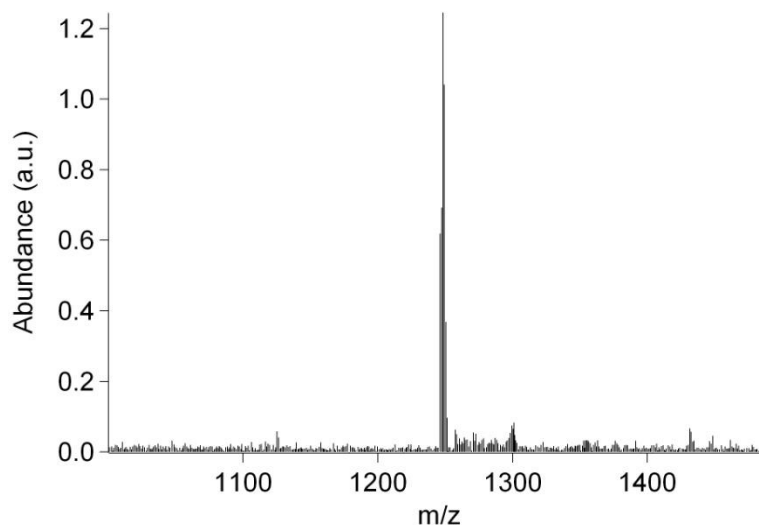
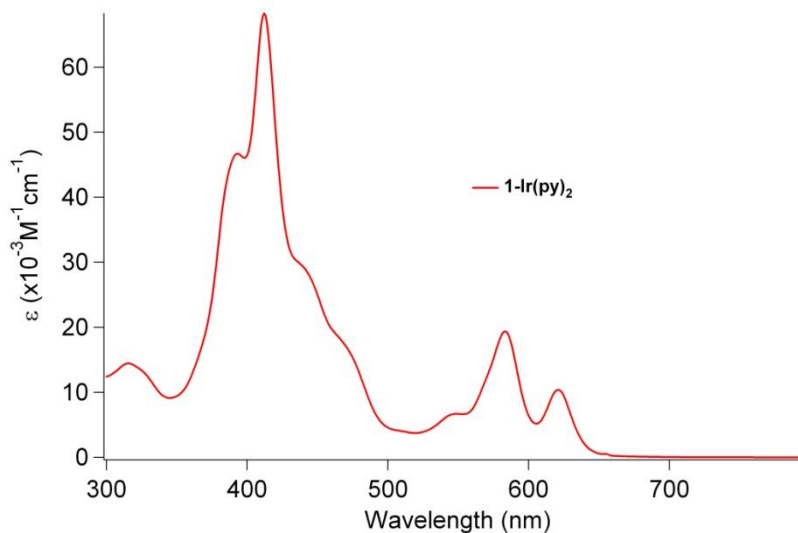


Figure B-6: UV-vis of **1b-Ir(tma)<sub>2</sub>** in toluene

**5,10,15-(tris)Pentafluorophenylcorrolatoiridium(III) (bis)pyridine, 1-Ir(py)<sub>2</sub>:** H<sub>3</sub>tpfc (40 mg), [Ir(cod)Cl]<sub>2</sub> (170 mg), and K<sub>2</sub>CO<sub>3</sub> (70 mg) were dissolved/suspended in 75 mL of degassed THF, and the mixture was heated at reflux under argon for 90 min. Pyridine (1 mL) was added, and the solution was allowed to slowly cool to room temperature while open to the laboratory atmosphere. Column chromatography of the forest green mixture (silica, 4:1 hexanes/CH<sub>2</sub>Cl<sub>2</sub> followed by 3:2 hexanes/CH<sub>2</sub>Cl<sub>2</sub>) afforded a bright green solution, from which thin, green crystals of **1-Ir(py)<sub>2</sub>** (26 mg, 50% yield) could be grown by addition of methanol followed by slow evaporation. <sup>1</sup>H NMR (CDCl<sub>3</sub>): δ 8.84 (d, 2H, J = 4.5), 8.53 (d, 2H, J = 4.8), 8.32 (d, 2H, J = 4.8), 8.17 (d, 2H, J = 4.5), 6.21 (t, 2H, J = 7.8), 5.19 (t, 4H, J = 7.0), 1.72 (d, 4H, J = 5.1). <sup>19</sup>F NMR (CDCl<sub>3</sub>): δ -138.68 (m, 6F), -154.84 (t, 2F, J = 22.2), -155.20 (t, 1F, J = 22.2), -163.28 (m, 4F), -163.65 (m, 2F). MS (ESI): 1144.1 ([M<sup>+</sup>]). UV-vis (toluene, nm, ε × 10<sup>-3</sup> M<sup>-1</sup> cm<sup>-1</sup>): 392 (46.1), 412 (68.3), 584 (19.4), 621 (10.6). Emission (toluene, nm): 792. XRD: See Appendix C.



Figure B-7: <sup>1</sup>H NMR of **1-Ir(py)<sub>2</sub>** in CDCl<sub>3</sub>Figure B-8: <sup>19</sup>F NMR of **1-Ir(py)<sub>2</sub>** in CDCl<sub>3</sub>

Figure B-9: ESI-MS of **1-Ir(py)<sub>2</sub>**Figure B-10: UV-vis of **1-Ir(py)<sub>2</sub>** in toluene

**5,10,15-(tris)Pentafluorophenylcorrolatoiridium(III) triphenylphosphine, 1-Ir(PPh<sub>3</sub>):** H<sub>3</sub>tpfc (40 mg), [Ir(cod)Cl]<sub>2</sub> (170 mg), and K<sub>2</sub>CO<sub>3</sub> (70 mg) were dissolved/suspended in 75 mL of degassed THF, and the mixture was heated at reflux under argon for 90 min. Triphenylphosphine (260 mg dissolved in 5 mL THF) was added, and the solution was heated at reflux for another half hour under laboratory atmosphere before being allowed to cool to room temperature. Column chromatography

of the deep green mixture (silica, 3:1 hexanes/ $\text{CH}_2\text{Cl}_2$ ) afforded a bright red-orange solution, which could be evaporated to give **1-Ir(PPh<sub>3</sub>)** (30 mg, 64% yield) as a ruby-colored solid.  $^1\text{H}$  NMR ( $\text{CDCl}_3$ ):  $\delta$  8.67 (d, 2H,  $J = 4.5$ ), 8.36 (d, 2H,  $J = 5.1$ ), 8.18 (d, 2H,  $J = 5.1$ ), 8.00 (d, 2H,  $J = 4.5$ ), 6.98 (t, 3H,  $J = 7.2$ ), 6.69 (t, 6H,  $J = 6.9$ ), 4.52 (d/d, 6H,  $^3J = 19.5$ ,  $^4J = 3.6$ ).  $^{19}\text{F}$  NMR ( $\text{CDCl}_3$ ):  $\delta$  -137.44 (m, 6F), -154.05 (m, 3F), -162.54 (m, 3F). MS (ESI): 1248.1 ( $[\text{M}^+]$ ). UV-vis ( $\text{CH}_2\text{Cl}_2$ , nm,  $\epsilon \times 10^{-3} \text{ M}^{-1} \text{ cm}^{-1}$ ): 398 (66), 554 (8.8), 588 (6.7)

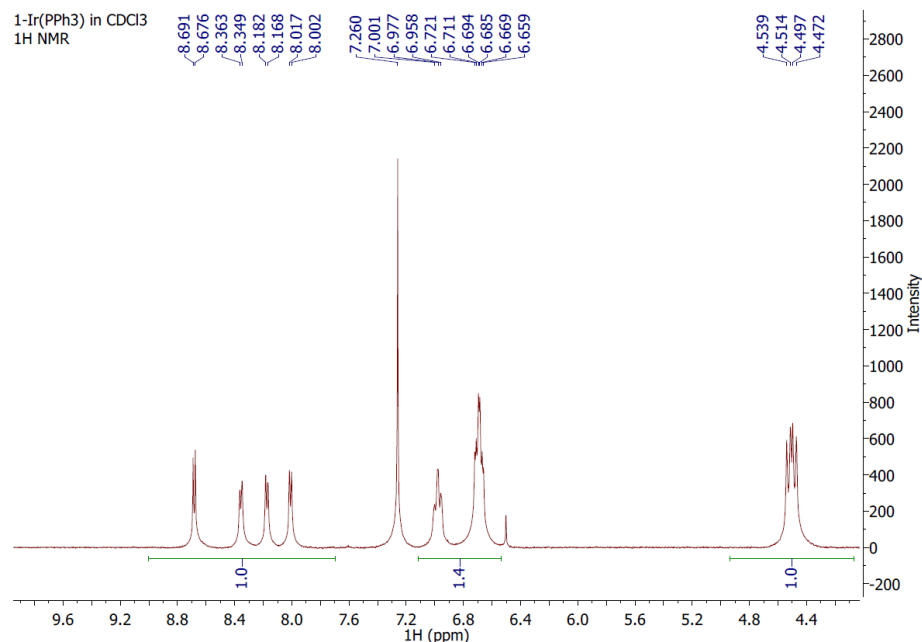


Figure B-11:  $^1\text{H}$  NMR of **1-Ir(PPh<sub>3</sub>)** in  $\text{CDCl}_3$

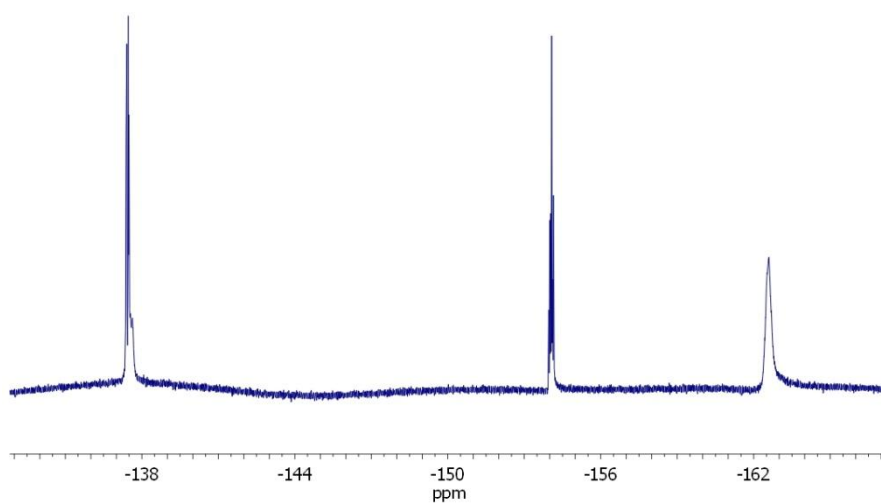


Figure B-12:  $^{19}\text{F}$  NMR of **1-Ir(PPh<sub>3</sub>)** in  $\text{CDCl}_3$

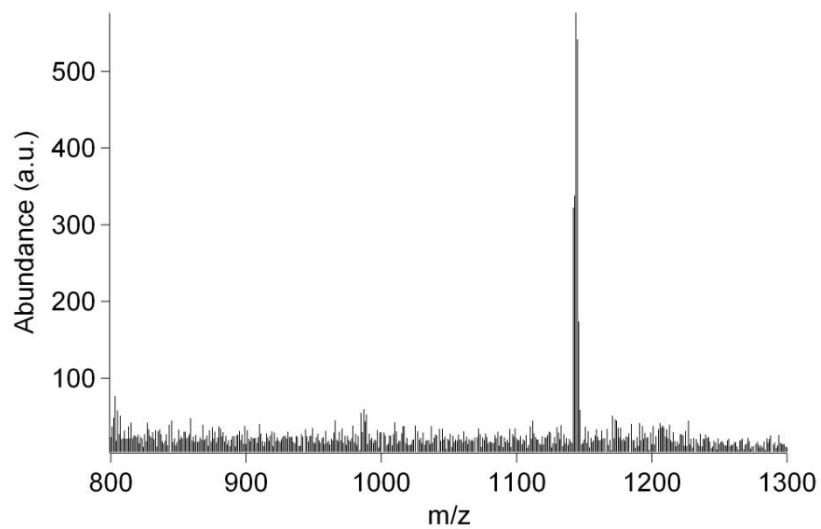


Figure B-13: ESI-MS of **1-Ir(PPh<sub>3</sub>)**

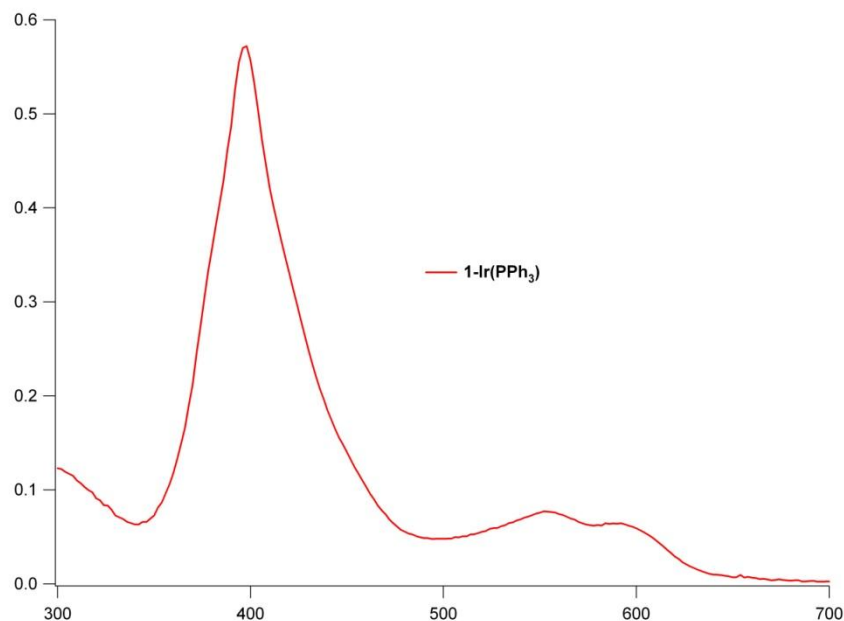


Figure B-14: UV-vis of **1-Ir(PPh<sub>3</sub>)** in CH<sub>2</sub>Cl<sub>2</sub>

**5,10,15-(tris)Pentafluorophenylcorrolatoiridium(III) (bis)-4-cyanopyridine, 1-Ir(cnpy)<sub>2</sub>:** H<sub>3</sub>tpfc (40 mg), [Ir(cod)Cl]<sub>2</sub> (170 mg), and K<sub>2</sub>CO<sub>3</sub> (70 mg) were dissolved/suspended in 75 mL of degassed THF, and the mixture was heated at reflux under argon for 90 min. 4-Cyanopyridine (105 mg) was added, and the solution was allowed to slowly cool to room temperature while open to the laboratory atmosphere. Column chromatography of the dichroic red/green mixture (silica, 4:1 hexanes/CH<sub>2</sub>Cl<sub>2</sub> followed by 2:3 hexanes/CH<sub>2</sub>Cl<sub>2</sub>) afforded a bright red solution, which upon evaporation yielded **1-Ir(cnpy)<sub>2</sub>** (36 mg, 66% yield) as a purple solid. <sup>1</sup>H NMR (CDCl<sub>3</sub>): δ 8.91 (d, 2H, J = 4.5), 8.60 (d, 2H, J = 5.1), 8.39 (d, 2H, J = 4.8), 8.26 (d, 2H, J = 4.5), 5.43 (d/d, 4H, <sup>3</sup>J = 6.9, <sup>4</sup>J = -4.2), 1.75 (d/d, 4H, <sup>3</sup>J = 6.9, <sup>4</sup>J = -3.9). <sup>19</sup>F NMR (CDCl<sub>3</sub>): δ -138.38 (d/d, 2F, <sup>3</sup>J = 34.8, <sup>4</sup>J = 17.4), -138.95 (d/d, 4F, <sup>3</sup>J = 34.8, <sup>4</sup>J = 17.4), -153.75 (t, 2F, J = 22.5), -154.11 (t, 1F, J = 22.2), -162.48 (m, 4F), -162.84 (m, 2F). MS (ESI): 1089.0

([M+cnpy]), 986.1 ([M+2(cnpy)]) UV-vis ( $\text{CH}_2\text{Cl}_2$ , nm,  $\epsilon \times 10^{-3} \text{ M}^{-1} \text{ cm}^{-1}$ ): 388 (8.8), 406 (14), 580 (4.2), 608 (2.8). Emission (toluene, nm): 788

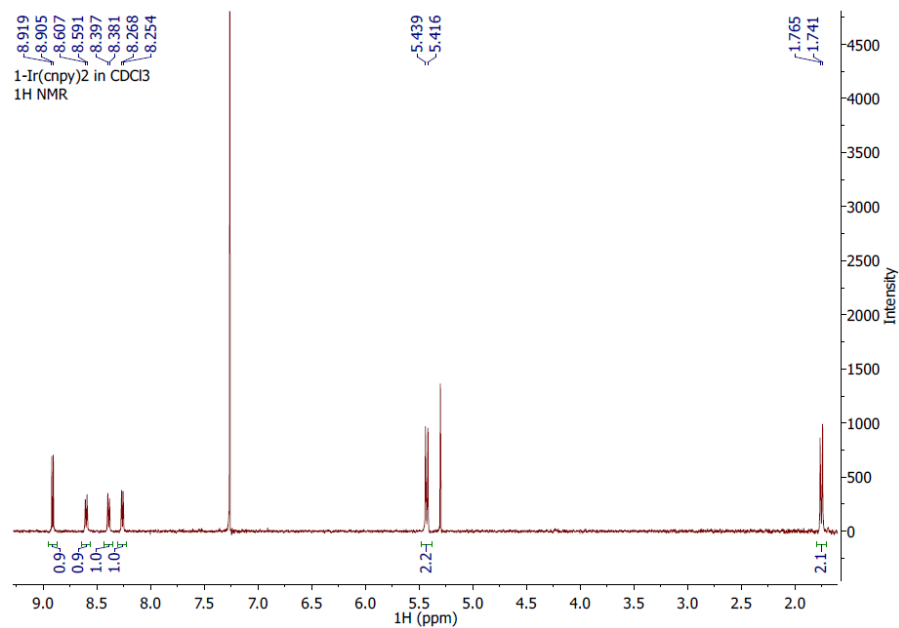


Figure B-15:  $^1\text{H}$  NMR of **1-Ir(cnpy)<sub>2</sub>** in  $\text{CDCl}_3$

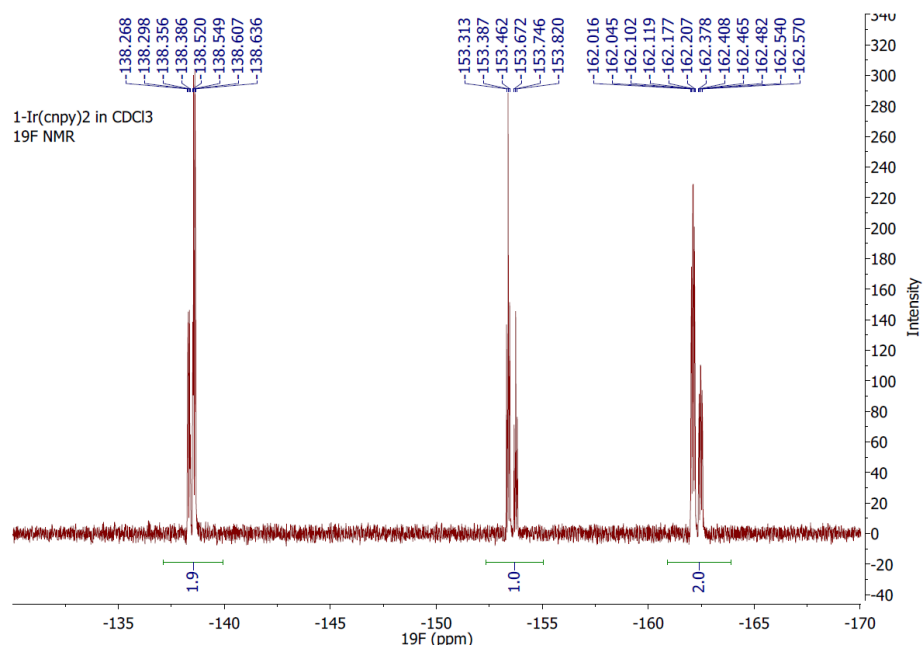
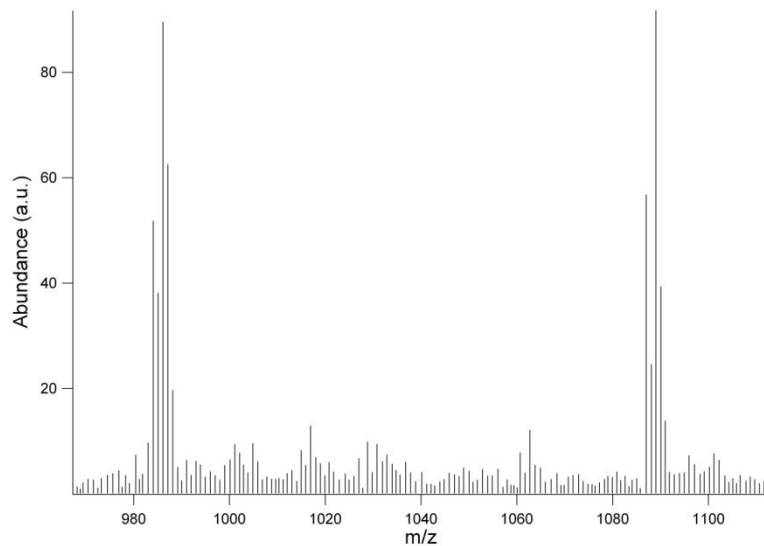
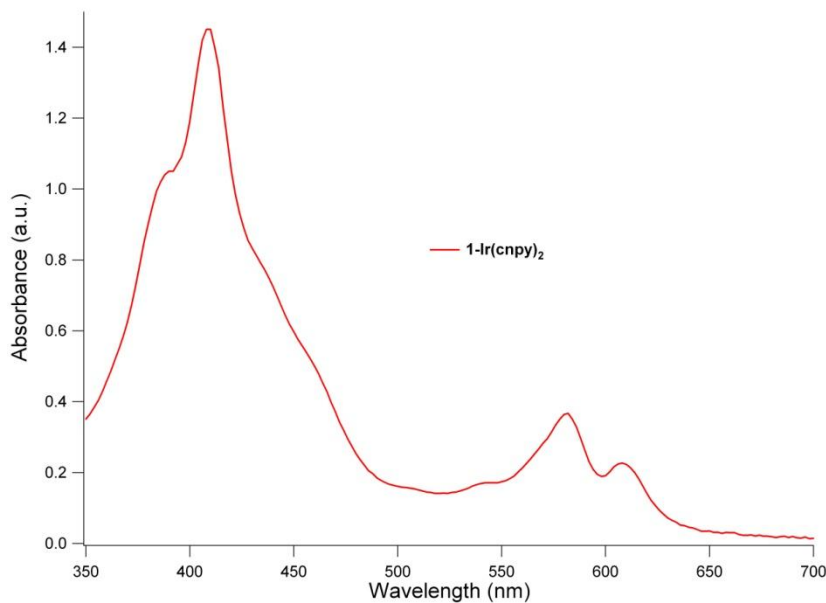


Figure B-16:  $^{19}\text{F}$  NMR of **1-Ir(cnpy)<sub>2</sub>** in  $\text{CDCl}_3$

Figure B-17: ESI-MS of **1-Ir(cnpy)<sub>2</sub>**Figure B-18: UV-vis of **1-Ir(cnpy)<sub>2</sub>** in CH<sub>2</sub>Cl<sub>2</sub>

**5,10,15-(tris)Pentafluorophenylcorrolatoiridium(III) (bis)-4-methoxypyridine, 1-Ir(meopy)<sub>2</sub>:** H<sub>3</sub>tpfc (40 mg), [Ir(cod)Cl]<sub>2</sub> (170 mg), and K<sub>2</sub>CO<sub>3</sub> (70 mg) were dissolved/suspended in 75 mL of degassed THF, and the mixture was heated at reflux under argon for 90 min. 4-Methoxypyridine (110 mg) was added, and the solution was allowed to slowly cool to room temperature while open to the laboratory atmosphere.

Column chromatography of the dark green mixture (silica, 4:1 hexanes/ $\text{CH}_2\text{Cl}_2$  followed by 2:3 hexanes/ $\text{CH}_2\text{Cl}_2$ ) afforded a bright red solution, which upon evaporation yielded **1-Ir(meopy) $_2$**  (28 mg, 50% yield) as a green solid.  $^1\text{H}$  NMR ( $\text{CDCl}_3$ ):  $\delta$  8.81 (d, 2H,  $J = 4.2$ ), 8.49 (d, 2H,  $J = 4.5$ ), 8.31 (d, 2H,  $J = 4.5$ ), 8.12 (d, 2H,  $J = 3.9$ ), 4.69 (d/d, 4H,  $^3J = 7.2$ ,  $^4J = -4.5$ ), 2.93 (s, 6H), 1.56 (m, 4H).  $^{19}\text{F}$  NMR ( $\text{CDCl}_3$ ):  $\delta$  -138.40 (d/d, 2F,  $^3J = 35.7$ ,  $^4J = 17.4$ ), -138.64 (d/d, 4F,  $^3J = 35.7$ ,  $^4J = 17.4$ ), -154.98 (t, 2F,  $J = 22.5$ ), -155.35 (t, 1F,  $J = 22.4$ ), -163.33 (m, 4F), -163.69 (m, 2F). UV-vis ( $\text{CH}_2\text{Cl}_2$ ): 394, 412, 584, 624

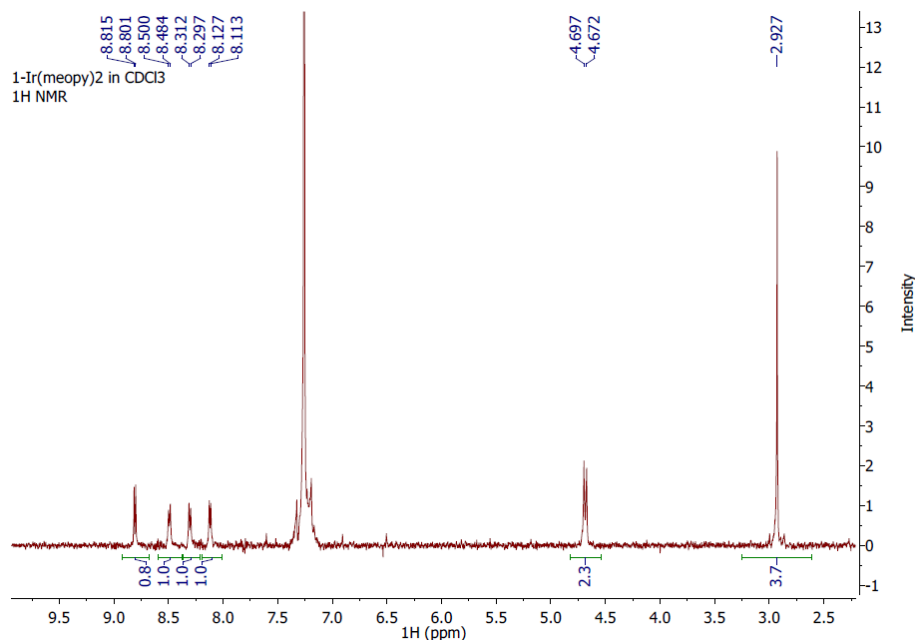


Figure B-19:  $^1\text{H}$  NMR of **1-Ir(meopy) $_2$**  in  $\text{CDCl}_3$



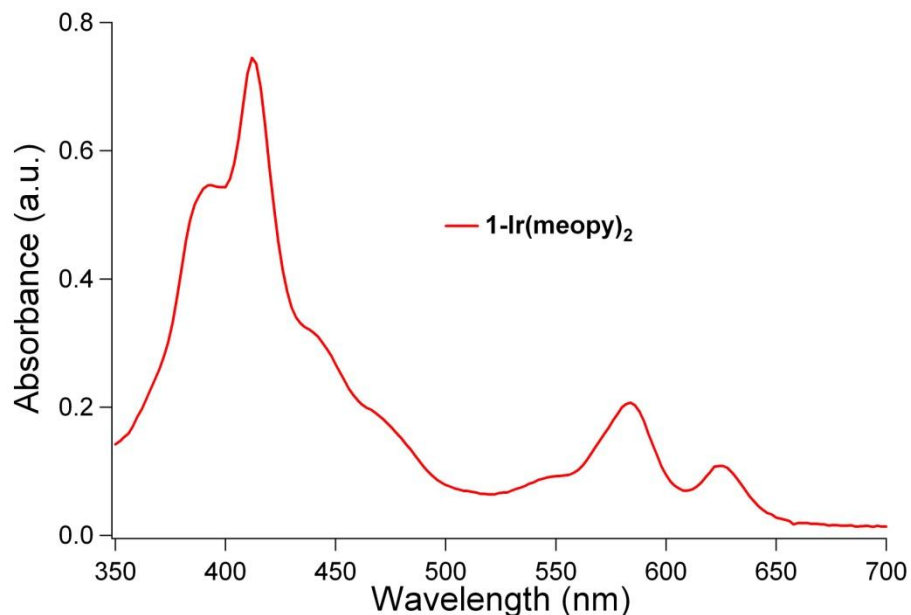


Figure B-20: UV-vis of **1-Ir(meopy)<sub>2</sub>** in CH<sub>2</sub>Cl<sub>2</sub>

**5,10,15-(tris)Pentafluorophenylcorrolatoiridium(III)**

**(bis)[3,5-**

**(bis)trifluoromethyl]pyridine, 1-Ir(cfpy)<sub>2</sub>**: H<sub>3</sub>tpfc (40 mg), [Ir(cod)Cl]<sub>2</sub> (170 mg), and K<sub>2</sub>CO<sub>3</sub> (70 mg) were dissolved/suspended in 75 mL of degassed THF, and the mixture was heated at reflux under argon for 90 min. 3,5-(bis)trifluoromethylpyridine (215 mg) was added, and the solution was allowed to slowly cool to room temperature while open to the laboratory atmosphere. Column chromatography of the deep green mixture (silica, 4:1 hexanes/CH<sub>2</sub>Cl<sub>2</sub> followed by 100% CH<sub>2</sub>Cl<sub>2</sub>) afforded a dichroic red/green solution, which upon evaporation yielded **1-Ir(cfpy)<sub>2</sub>** (13 mg, 20% yield) as a purple-red solid. <sup>1</sup>H NMR (CDCl<sub>3</sub>): δ 9.00 (d, 2H, J = 4.2), 8.70 (d, 2H, J = 4.8), 8.44 (d, 2H, J = 4.8), 8.38 (d, 2H, J = 4.2), 6.65 (s, 2H), 1.97 (s, 4H). <sup>19</sup>F NMR (CDCl<sub>3</sub>): δ = -64.29 (t, 12F, J = 7.5), -138.47 (m, 6F), -153.52 (t, 2F, J = 22.2), -153.82 (m, 1F), -162.35 (m, 6F). UV-vis (CH<sub>2</sub>Cl<sub>2</sub>, nm, ε x 10<sup>-3</sup> M<sup>-1</sup>cm<sup>-1</sup>): 384 (9.7), 406 (15), 580 (4.5), 602 (2.8)

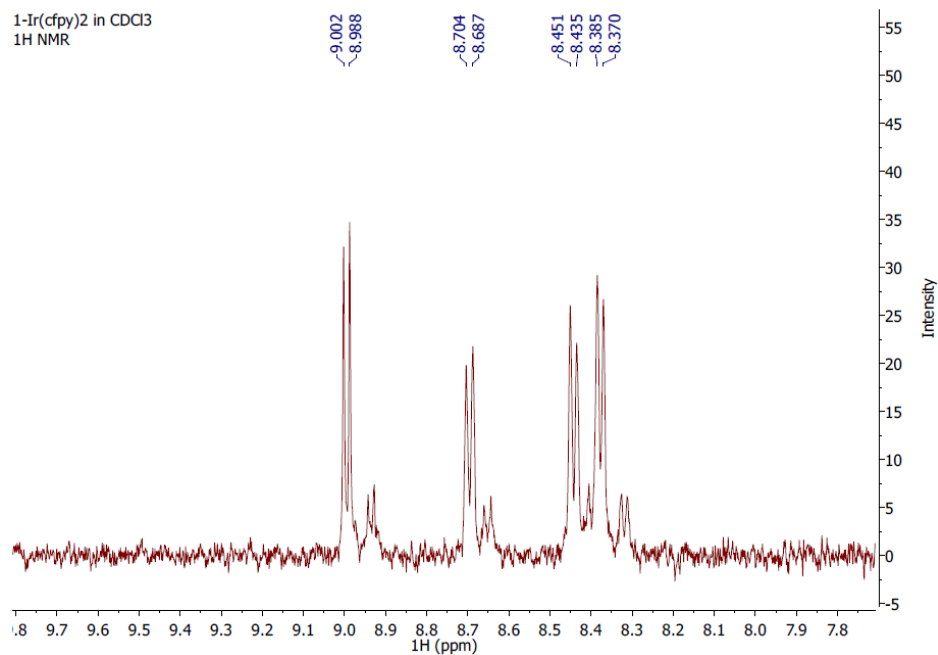


Figure B-21: <sup>1</sup>H NMR of **1-(cfpy)<sub>2</sub>** in CDCl<sub>3</sub>. There is a small impurity owing to what appears to be an equilibrium with the five-coordinate species **1-(cfpy)**.

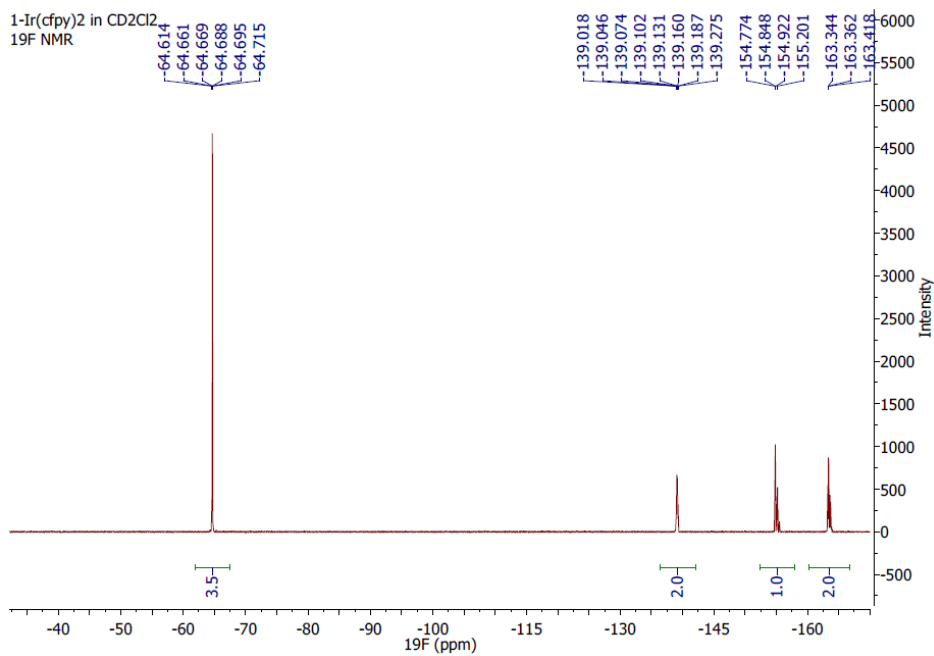


Figure B-22: <sup>19</sup>F NMR of **1-(cfpy)<sub>2</sub>** in CDCl<sub>3</sub>. The large downfield peak corresponds to the fluorine atoms in the –CF<sub>3</sub> groups on the axial ligands.

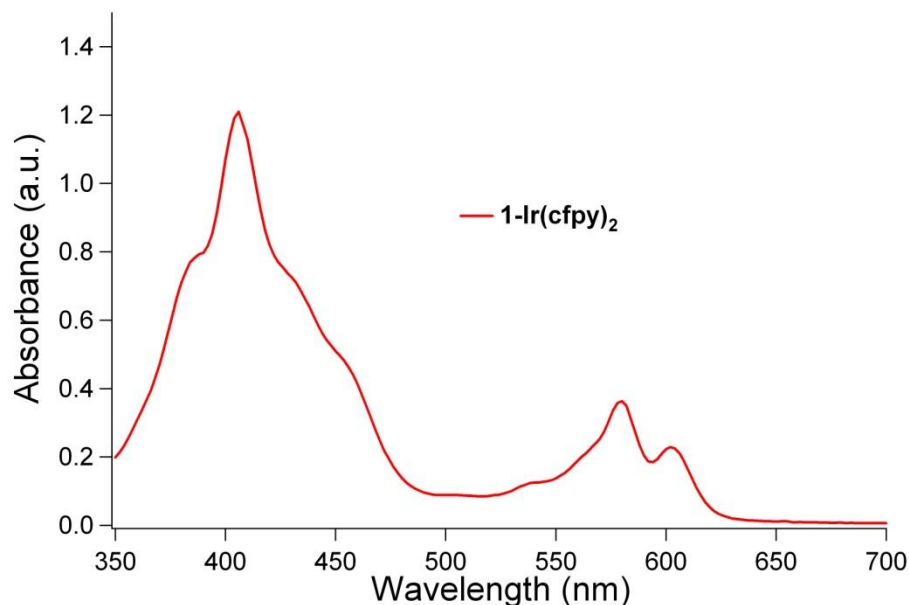
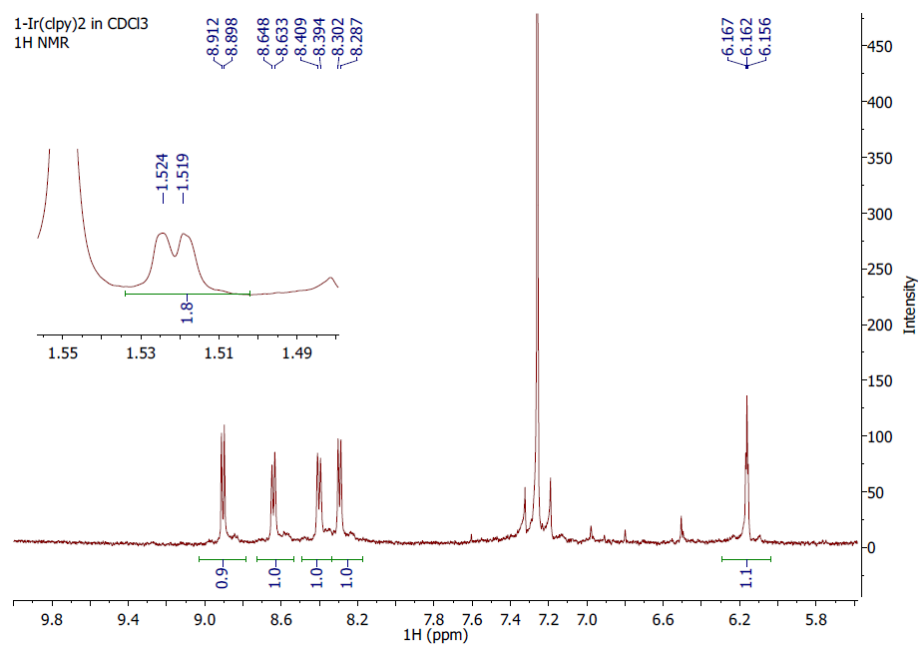
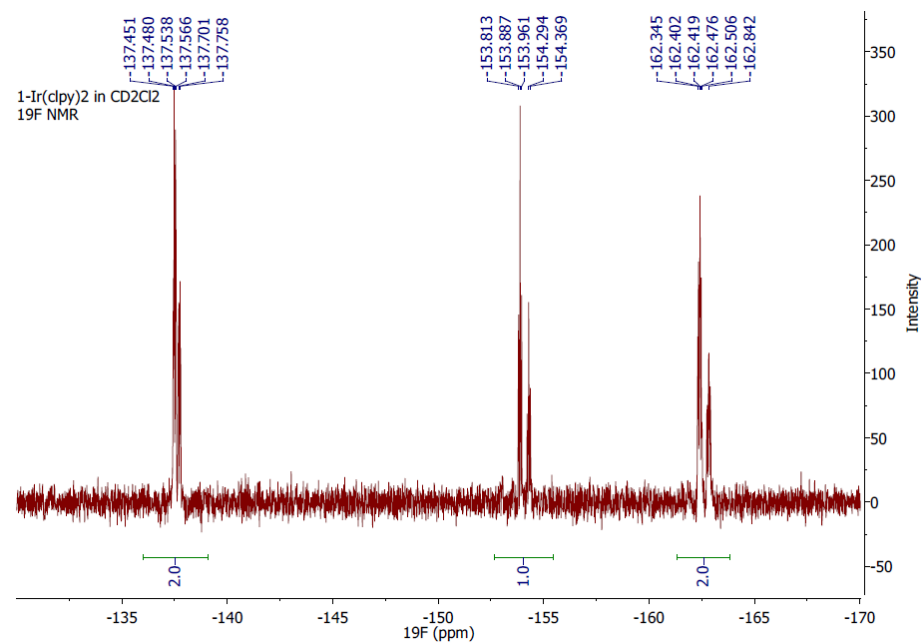


Figure B-23: UV-vis of **1-(cfpy)<sub>2</sub>** in CH<sub>2</sub>Cl<sub>2</sub>

**5,10,15-(tris)Pentafluorophenylcorrolatoiridium(III) (bis)-3,5-dichloropyridine, 1-Ir(clpy)<sub>2</sub>:** H<sub>3</sub>tpfc (40 mg), [Ir(cod)Cl]<sub>2</sub> (170 mg), and K<sub>2</sub>CO<sub>3</sub> (70 mg) were dissolved/suspended in 75 mL of degassed THF, and the mixture was heated at reflux under argon for 90 min. 3,5-Dichloropyridine (150 mg) was added, and the solution was allowed to slowly cool to room temperature while open to the laboratory atmosphere. Column chromatography of the dark green mixture (silica, 4:1 hexanes/CH<sub>2</sub>Cl<sub>2</sub> followed by 100% CH<sub>2</sub>Cl<sub>2</sub>) afforded a vivid green solution, which upon evaporation yielded **1-Ir(clpy)<sub>2</sub>** (27 mg, 47% yield) as a green microcrystalline solid. <sup>1</sup>H NMR (CDCl<sub>3</sub>): δ 8.91 (d, 2H, J = 4.2), 8.64 (d, 2H, J = 4.5), 8.40 (d, 2H, J = 4.5), 8.30 (d, 2H, J = 4.2), 6.16 (t, 2H, J = 1.8), 1.52 (d, 4H, J = 1.8). <sup>19</sup>F NMR (CDCl<sub>3</sub>): δ -137.49 (d/d, 2F, <sup>3</sup>J = 34.8, <sup>4</sup>J = 17.7), -137.71 (d/d, 4F, <sup>3</sup>J = 34.8, <sup>4</sup>J = 17.1), -153.87 (t, 2F, J = 22.5), -154.28 (t, 1F, J = 22.2), -162.39 (m, 4F), -162.82 (m, 2F). UV-vis (CH<sub>2</sub>Cl<sub>2</sub>, nm, ε x 10<sup>-3</sup> M<sup>-1</sup>cm<sup>-1</sup>): 390 (26), 406 (38), 580 (12), 608 (7.3)

Figure B-24: <sup>1</sup>H NMR of **1-(clpy)<sub>2</sub>** in CDCl<sub>3</sub>Figure B-25: <sup>19</sup>F NMR of **1-(clpy)<sub>2</sub>** in CDCl<sub>3</sub>

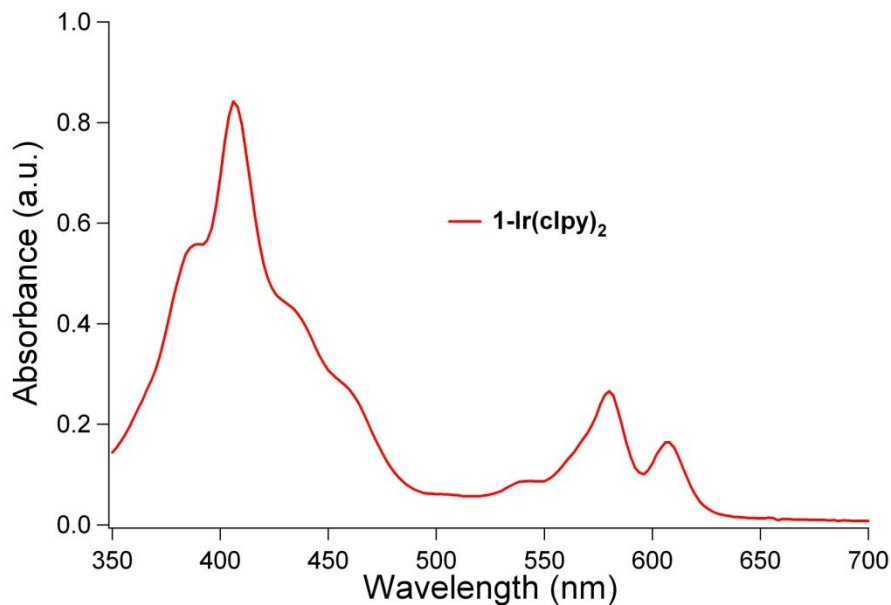
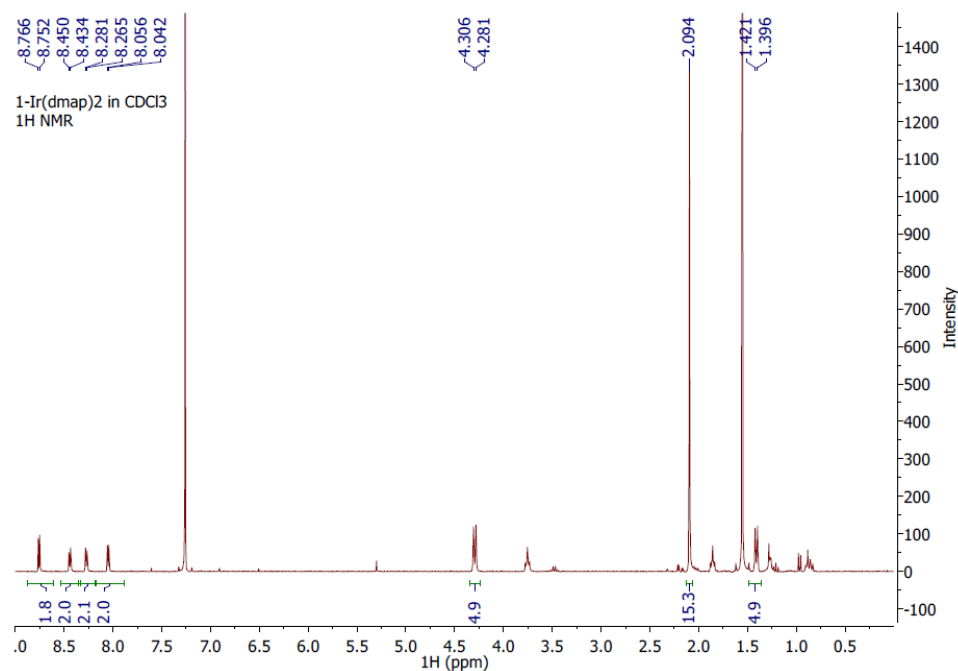
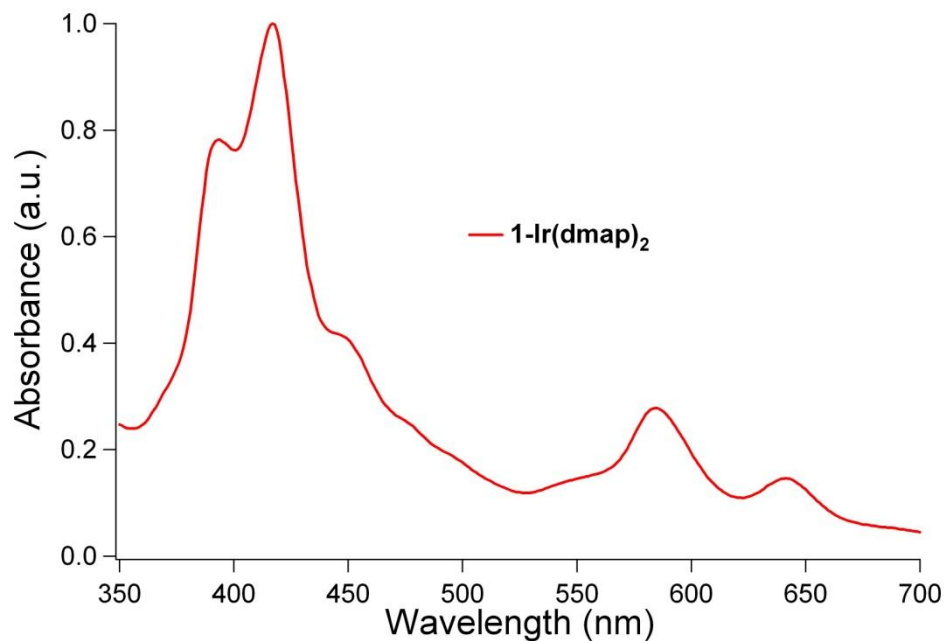


Figure B-26: UV-vis of **1-(clpy)<sub>2</sub>** in CH<sub>2</sub>Cl<sub>2</sub>

**5,10,15-(tris)Pentafluorophenylcorrolatoiridium(III) (bis)-4-(N,N-dimethylamino)pyridine, 1-Ir(dmap)<sub>2</sub>:** H<sub>3</sub>tpfc (40 mg), [Ir(cod)Cl]<sub>2</sub> (170 mg), and K<sub>2</sub>CO<sub>3</sub> (70 mg) were dissolved/suspended in 75 mL of degassed THF, and the mixture was heated at reflux under argon for 90 min. 4-dimethylaminopyridine (220 mg) was added, and the solution was allowed to slowly cool to room temperature while open to the laboratory atmosphere. Column chromatography of the dark green mixture (silica, 4:1 hexanes/CH<sub>2</sub>Cl<sub>2</sub> followed by 2:3 hexanes/CH<sub>2</sub>Cl<sub>2</sub>) afforded a green solution, which upon evaporation yielded **1-Ir(dmap)<sub>2</sub>** (30 mg, 49% yield) as a green solid. <sup>1</sup>H NMR (CDCl<sub>3</sub>): δ 8.76 (d, 2H, J = 4.2), 8.44 (d, 2H, J = 4.8), 8.27 (d, 2H, J = 4.2), 8.05 (d, 2H, J = 4.2), 4.25 (d, 4H, J = 7.5), 2.09 (s, 12H), 1.41 (d, 4H, J = 7.5). UV-vis (CH<sub>2</sub>Cl<sub>2</sub>, nm): 393, 417, 585, 642. Emission (toluene, nm): 788. XRD: See Appendix C.

Figure B-27: <sup>1</sup>H NMR of **1-Ir(dmap)<sub>2</sub>** in CDCl<sub>3</sub>Figure B-28: UV-vis of **1-Ir(dmap)<sub>2</sub>** in CH<sub>2</sub>Cl<sub>2</sub>

**5,10,15-(tris)Pentafluorophenylcorrolatoiridium(III) (bis)ammine, 1-Ir(NH<sub>3</sub>)<sub>2</sub>:**

H<sub>3</sub>tpfc (40 mg), [Ir(cod)Cl]<sub>2</sub> (170 mg), and K<sub>2</sub>CO<sub>3</sub> (70 mg) were dissolved/suspended in

75 mL of degassed THF, and the mixture was heated at reflux under argon for 90 min. The solution was then exposed to the atmosphere, followed by saturation with gaseous ammonia for 15 minutes while cooling occurred. Column chromatography of the turbid green mixture (silica, 3:1 hexanes/ $\text{CH}_2\text{Cl}_2$  followed by 1:1 hexanes/ $\text{CH}_2\text{Cl}_2$ ) afforded a dark green solution, which upon evaporation yielded **1-Ir(NH<sub>3</sub>)<sub>2</sub>** (20 mg, 39% yield) as a green microcrystalline solid.  $^1\text{H}$  NMR ( $\text{d}^6$ -DMSO):  $\delta$  8.72 (d, 2H,  $J = 4.2$ ), 8.47 (d, 2H,  $J = 4.8$ ), 8.37 (d, 2H,  $J = 4.8$ ), 8.01 (d, 2H,  $J = 4.2$ ), -4.057 (s, 6H). MS (ESI): 1019.7 ( $[\text{M}^+]$ ), 1001.7 ( $[\text{M}^+ - 1\text{NH}_3]$ ), 986.0 ( $[\text{M}^+ - 2\text{NH}_3]$ ). UV-vis ( $\text{CH}_2\text{Cl}_2$ , nm): 394, 413, 584, 624. Emission (toluene, nm): 801. XRD: See Appendix C.

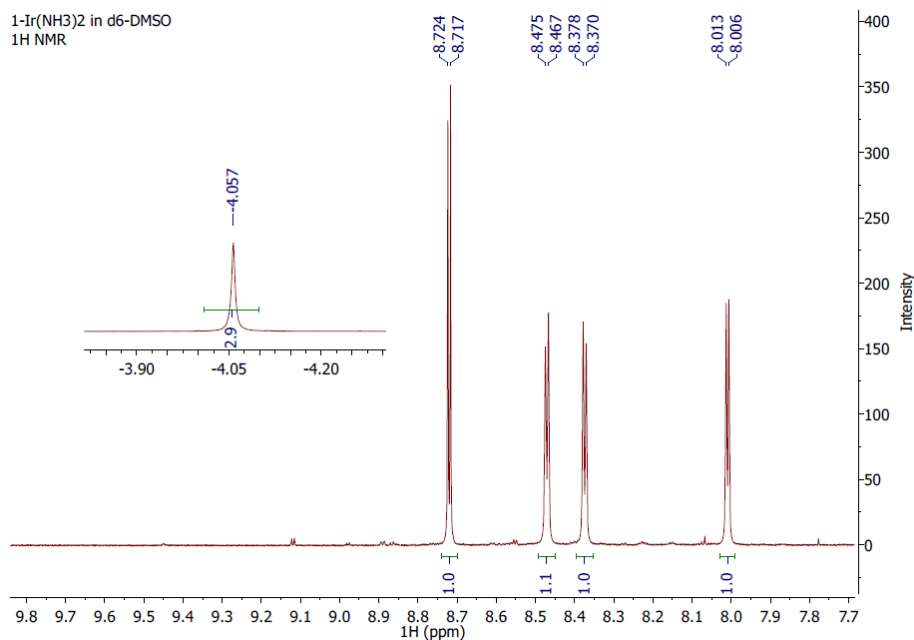


Figure B-29:  $^1\text{H}$  NMR of **1-Ir(NH<sub>3</sub>)<sub>2</sub>** in  $\text{d}^6$ -DMSO

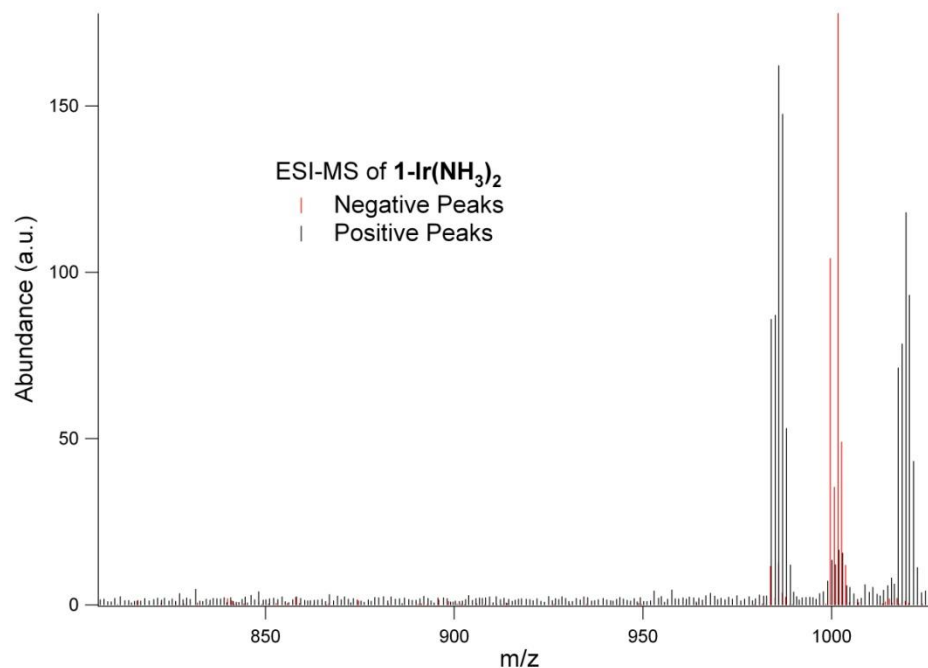


Figure B-30: ESI-MS of **1-Ir(NH<sub>3</sub>)<sub>2</sub>**. Positive and negative peaks overlaid so all three peaks are visible

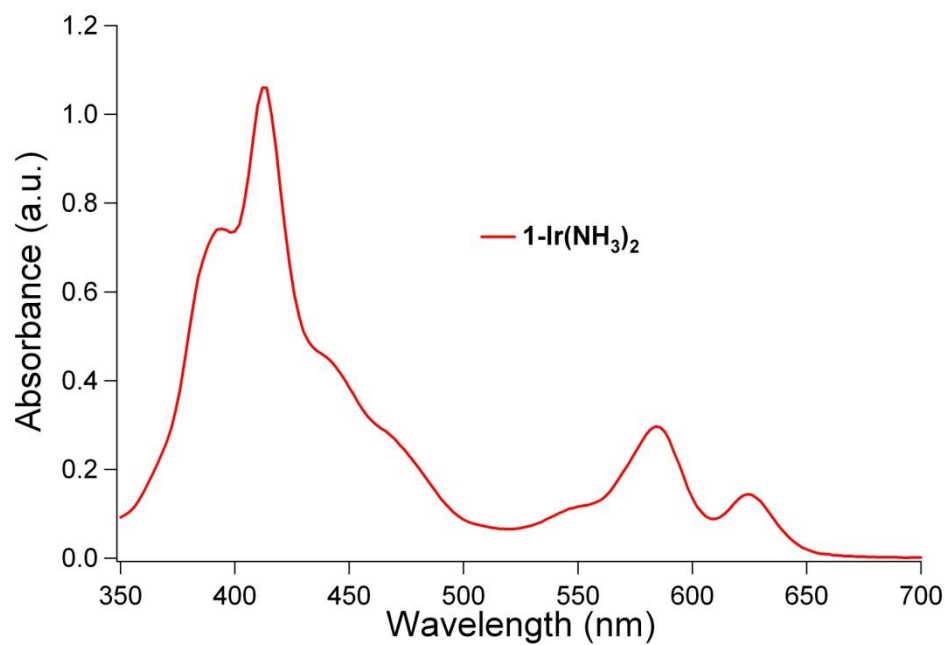


Figure B-31: UV-vis of **1-Ir(NH<sub>3</sub>)<sub>2</sub>** in CH<sub>2</sub>Cl<sub>2</sub>

**2,3,7,8,12,13,17,18-octabromo-5,10,15-(tris)Pentafluorophenylcorrolatoiridium(III)**

**(bis)amine, 1b-Ir(NH<sub>3</sub>)<sub>2</sub>:** Br<sub>2</sub> (30 μL) and **1-Ir(NH<sub>3</sub>)<sub>2</sub>** (50 mg) were dissolved in 50



mL of  $\text{C}_6\text{H}_6$  and stirred overnight. Column chromatography (silica, 1:1 hexanes/ $\text{CH}_2\text{Cl}_2$ ) of the dark green mixture provided a green solution from which green microcrystals of **1b-Ir(NH<sub>3</sub>)<sub>2</sub>** could be recovered in essentially quantitative yield by slow evaporation.  $^1\text{H}$  NMR ( $\text{CD}_2\text{Cl}_2$ ):  $\delta$  -4.03 (s, 6H,  $J(^{15}\text{N}) = 71$  Hz). UV-vis ( $\text{CH}_2\text{Cl}_2$ , nm): 408, 427, 594, 640. Emission (toluene, nm): 808

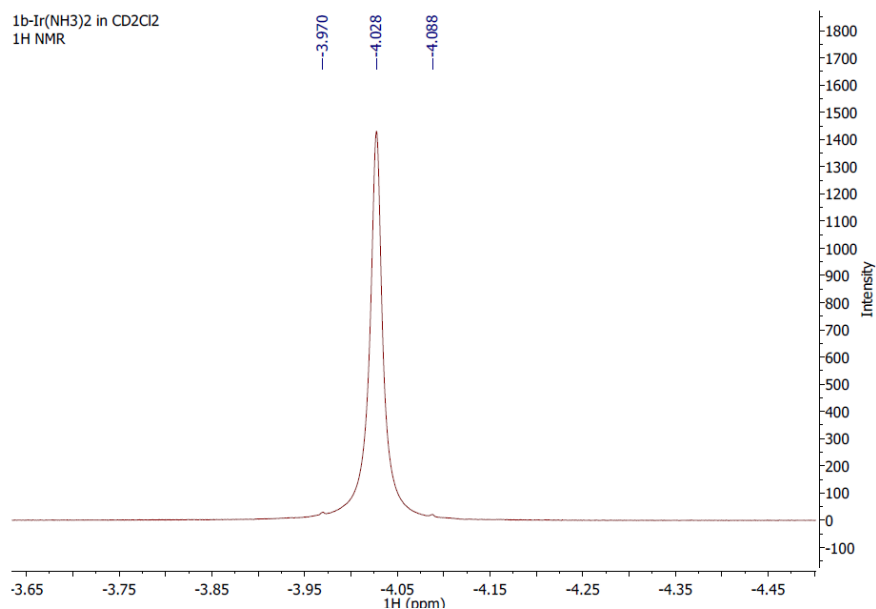


Figure B-32:  $^1\text{H}$  NMR of **1b-Ir(NH<sub>3</sub>)<sub>2</sub>** in  $\text{CD}_2\text{Cl}_2$

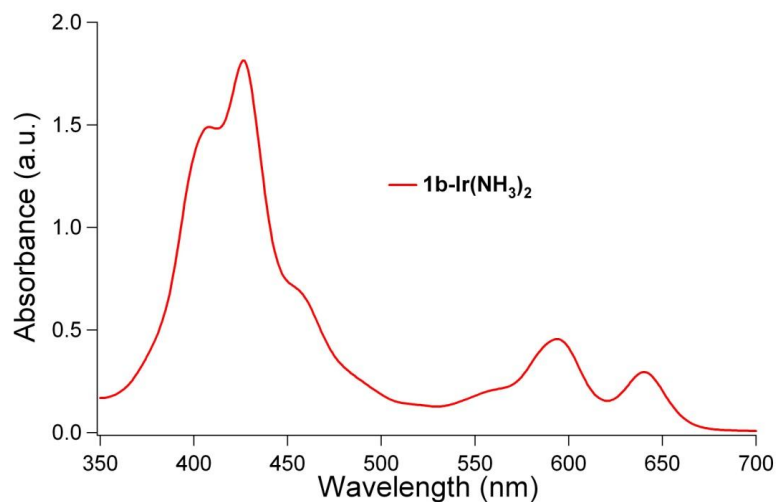


Figure B-33: UV-vis of **1b-Ir(NH<sub>3</sub>)<sub>2</sub>** in  $\text{CH}_2\text{Cl}_2$

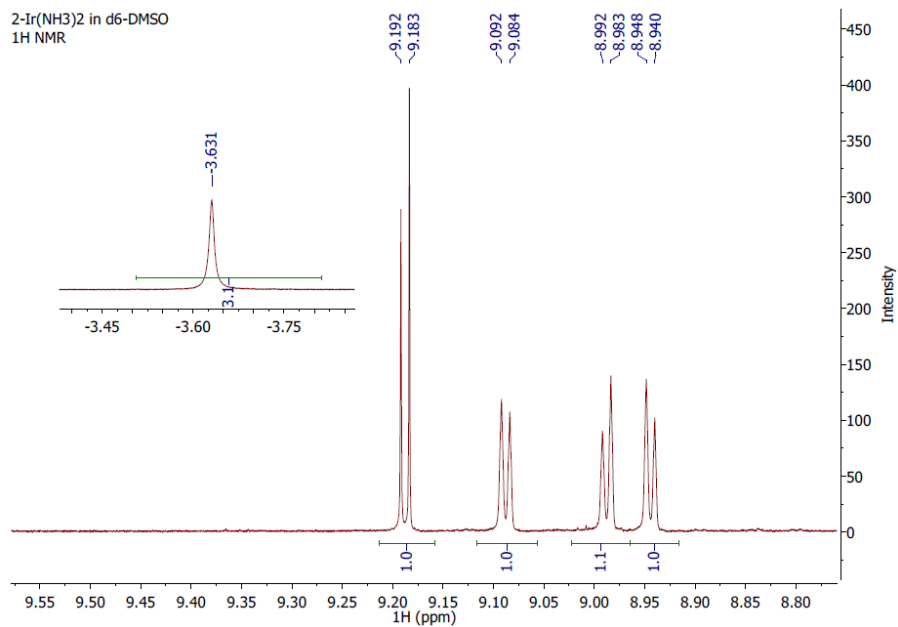
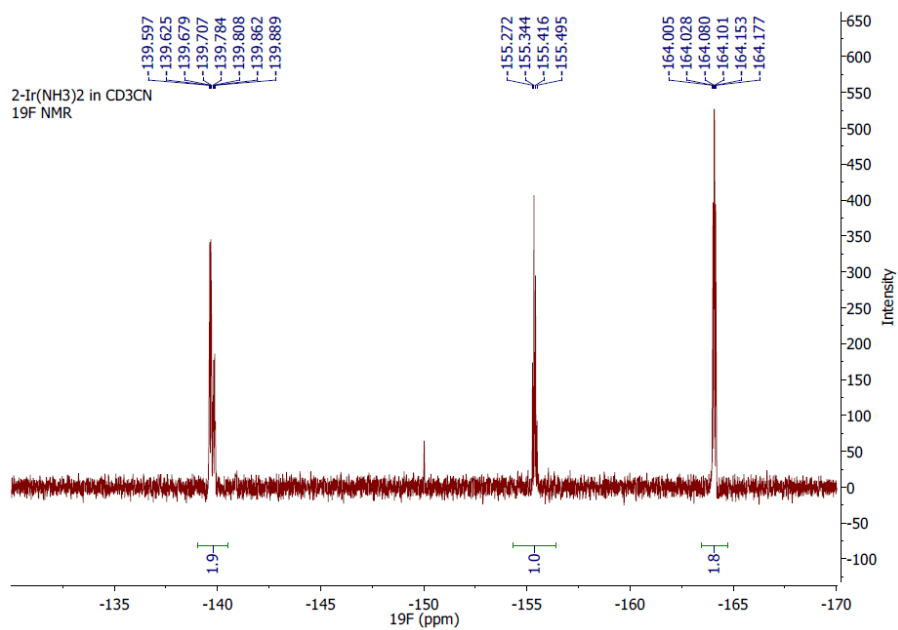
**3,17-dibromo-5,10,15-(tris)pentafluorophenylmonoazaporphyrinatoiridium(III)**

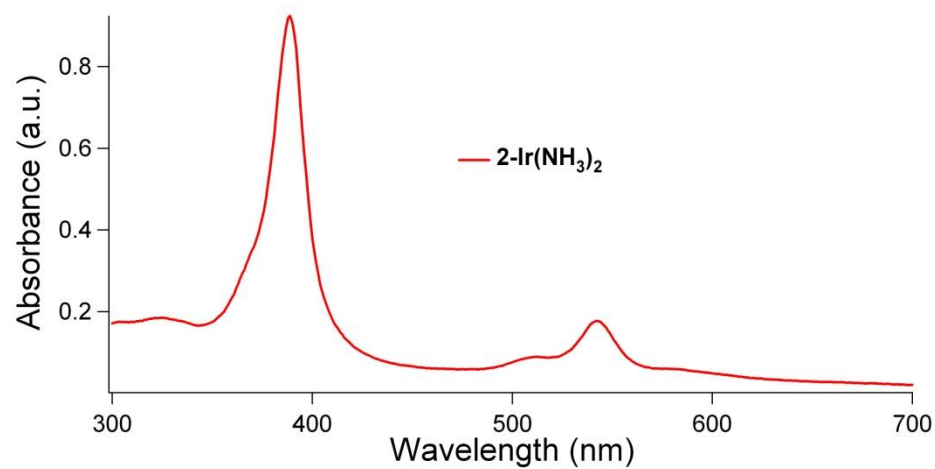
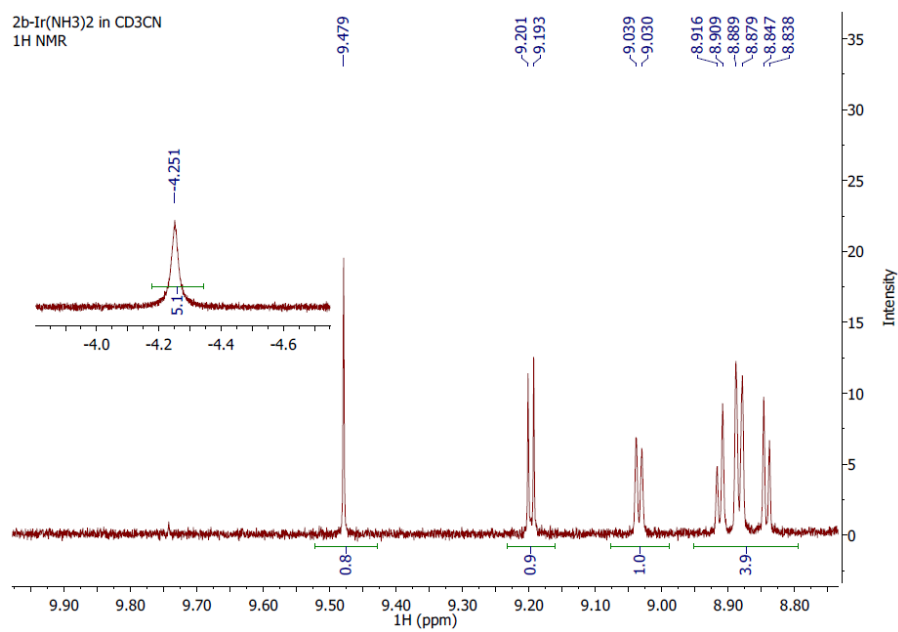
**(bis)amine, 2b<sub>2</sub>-Ir(NH<sub>3</sub>)<sub>2</sub>, 3-bromo-5,10,15-**

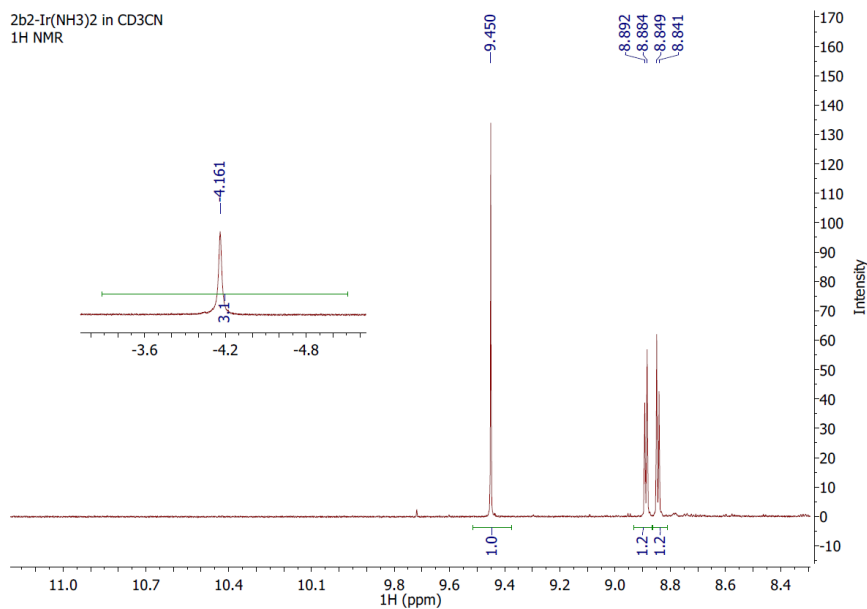
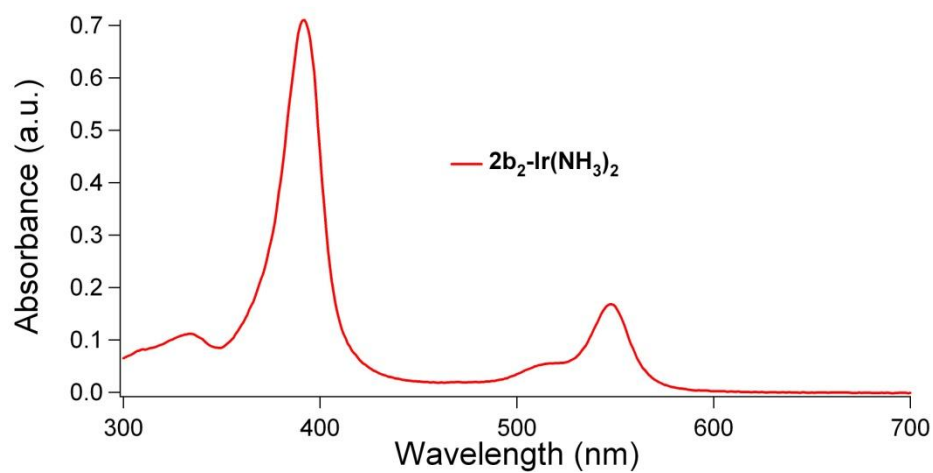
**(tris)pentafluorophenylmonoazaporphyrinatoiridium(III) (bis)amine, 2b-**

**Ir(NH<sub>3</sub>)<sub>2</sub>, and 5,10,15-(tris)pentafluorophenylmonoazaporphyrinatoiridium(III)**

**(bis)amine, 2-Ir(NH<sub>3</sub>)<sub>2</sub>:** To a rapidly stirring solution of **1-Ir(NH<sub>3</sub>)<sub>2</sub>** (22 mg) in methanol was added 250  $\mu$ L of aqueous 6 N NH<sub>4</sub>OH. Shortly after, 104 mg N-bromosuccinimide was added and the reaction mixture immediately turned from green to purple and began to evolve gas. After five minutes, a new pink spot could be observed by TLC, and the reaction was allowed to stir for ten more minutes before being concentrated onto silica and subjected to column chromatography on silica. CH<sub>2</sub>Cl<sub>2</sub> was first used to elute any remaining corrole, followed by 2% MeOH in CH<sub>2</sub>Cl<sub>2</sub> to elute pink solutions of **2b<sub>2</sub>-Ir(NH<sub>3</sub>)<sub>2</sub>** (9 mg, 35% yield), 3% MeOH in CH<sub>2</sub>Cl<sub>2</sub> to elute **2b-Ir(NH<sub>3</sub>)<sub>2</sub>** (2 mg, 8% yield), and 4% MeOH in CH<sub>2</sub>Cl<sub>2</sub> to elute **2-Ir(NH<sub>3</sub>)<sub>2</sub>** (1 mg, 4% yield), all of which could be evaporated to yield red solid products. Characterization data: **2b<sub>2</sub>-Ir(NH<sub>3</sub>)<sub>2</sub>**. <sup>1</sup>H NMR (CD<sub>3</sub>CN):  $\delta$  9.45 (s, 2H), 8.89 (d, 2H, J = 4.8), 8.85 (d, 2H, J = 4.8), -4.161 (s, 6H). UV-vis (CH<sub>3</sub>CN, nm): 392, 513 (sh), 548. Emission (CH<sub>3</sub>CN, nm): 695. **2b-Ir(NH<sub>3</sub>)<sub>2</sub>**. <sup>1</sup>H NMR (CD<sub>3</sub>CN):  $\delta$  9.48 (s, 1H), 9.20 (d, 1H, J = 4.8), 9.03 (d, 1H, J = 5.4), 8.91 (d, 1H, J = 4.2), 8.88 (d, 2H, J = 6.0), 8.84 (d, 1H, J = 5.4), -4.251 (s, 6H). **2-Ir(NH<sub>3</sub>)<sub>2</sub>**. <sup>1</sup>H NMR (d<sup>6</sup>-DMSO):  $\delta$  9.19 (d, 2H, J = 5.4), 9.09 (d, 2H, J = 4.8), 8.99 (d, 2H, J = 5.4), 8.94 (d, 2H, J = 4.8), -3.361 (s, 6H). UV-vis (CH<sub>3</sub>CN, nm): 389, 506 (sh), 542. Emission (CH<sub>3</sub>CN, nm): 691

Figure B-34: <sup>1</sup>H NMR of **2-Ir(NH<sub>3</sub>)<sub>2</sub>** in d<sup>6</sup>-DMSOFigure B-35: <sup>19</sup>F NMR of **2-Ir(NH<sub>3</sub>)<sub>2</sub>** in CD<sub>3</sub>CN

Figure B-36: UV-vis of **2-Ir(NH<sub>3</sub>)<sub>2</sub>** in CD<sub>3</sub>CNFigure B-37: <sup>1</sup>H NMR of **2b-Ir(NH<sub>3</sub>)<sub>2</sub>** in CD<sub>3</sub>CN

Figure B-38: <sup>1</sup>H NMR of **2b<sub>2</sub>-Ir(NH<sub>3</sub>)<sub>2</sub>** in CD<sub>3</sub>CNFigure B-39: UV-vis of **2b<sub>2</sub>-Ir(NH<sub>3</sub>)<sub>2</sub>** in CD<sub>3</sub>CN

*A p p e n d i x C*

## X-RAY DIFFRACTION REPORTS FROM THE BECKMAN INSTITUTE

X-ray structures for compounds **1-Ir(tma)<sub>2</sub>**, **1b-Ir(tma)<sub>2</sub>**, **1-Ir(py)<sub>2</sub>**, **1-Ir(dmap)<sub>2</sub>**, and **1-Ir(NH<sub>3</sub>)<sub>2</sub>** are listed below, along with full reports and analysis, including experimental setup, selected bond lengths, and other relevant parameters. These reports were produced by Michael W. Day at the Beckman Institute. The reports for **1-Ir(tma)<sub>2</sub>**, **1b-Ir(tma)<sub>2</sub>**, **1-Ir(py)<sub>2</sub>**, which were originally PDF files, have been reformatted for the Microsoft Word program, while the reports for **1-Ir(dmap)<sub>2</sub>**, and **1-Ir(NH<sub>3</sub>)<sub>2</sub>**, which were produced in Word format, have largely just been edited in small ways, and therefore appear somewhat different from the former three reports. The nomenclature in all cases has been altered to match that of the thesis.

CALIFORNIA INSTITUTE OF TECHNOLOGY  
BECKMAN INSTITUTE  
X-RAY CRYSTALLOGRAPHY LABORATORY

Date 18 December 2007

**Crystal Structure Analysis of:**

**1-Ir(tma)<sub>2</sub>**

(shown below)

**For** Investigator: Joshua Palmer ext. 6332

Advisor: H. B. Gray ext. 6500

Account Number: HBG.BP-1-BP.AMOCO

**By** Michael W. Day 116 Beckman ext. 2734

e-mail: mikeday@caltech.edu

Contents

Table 1. Crystal data

Figures Minimum overlap

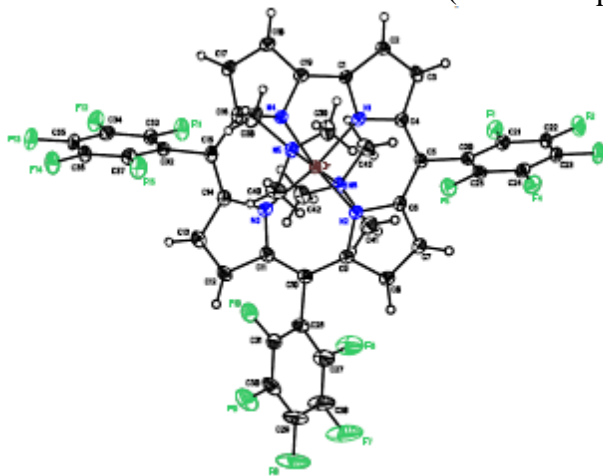
Table 2. Atomic Coordinates

Table 3. Selected bond distances and angles

Table 4. Full bond distances and angles

Table 5. Anisotropic displacement parameters

Table 6. Observed and calculated structure factors (available upon request)



**1-Ir(tma)<sub>2</sub>**

**Note:** The crystallographic data have been deposited in the Cambridge Database (CCDC) and have been placed on hold pending further instructions from me. The deposition number is 671270. Ideally the CCDC would like the publication to contain a footnote of the type: "Crystallographic data have been deposited at the CCDC, 12 Union Road,

Cambridge CB2 1EZ, UK, and copies can be obtained on request, free of charge, by quoting the publication citation and the deposition number 671270”.



Table C-1-1. Crystal data and structure refinement for **1-Ir(tma)<sub>2</sub>** (CCDC 671270)

Empirical formula	C <sub>43</sub> H <sub>26</sub> N <sub>6</sub> F <sub>15</sub> Ir • 0.185(CH <sub>2</sub> Cl <sub>2</sub> )		
Formula weight	1119.61		
Crystallization Solvent	Dichloromethane		
Crystal Habit	Needle		
Crystal size	0.32 x 0.07 x 0.02 mm <sup>3</sup>		
Crystal color	Blue		
<b>Data Collection</b>			
Type of diffractometer	Bruker KAPPA APEX II		
Wavelength	0.71073 Å MoKα		
Data Collection Temperature	100(2) K		
θ range for 9398 reflections used in lattice determination	2.54 to 28.61°		
Unit cell dimensions	a = 8.1456(4) Å	α = 80.628(3)°	
	b = 13.1188(6) Å	β = 80.543(3)°	
	c = 19.8366(8) Å	γ = 89.488(3)°	
Volume	2062.68(16) Å <sup>3</sup>		
Z	2		
Crystal system	Triclinic		
Space group	P-1		
Density (calculated)	1.803 Mg/m <sup>3</sup>		
F(000)	1092		
θ range for data collection	1.57 to 28.65°		
Completeness to θ = 28.65°	99.2 %		
Index ranges	-10 ≤ h ≤ 10, -17 ≤ k ≤ 17, -26 ≤ l ≤ 26		
Data collection scan type	ω scans; 22 settings		
Reflections collected	70274		
Independent reflections	10507 [R <sub>int</sub> = 0.0628]		
Absorption coefficient	3.370 mm <sup>-1</sup>		
Absorption correction	Semi-empirical from equivalents		
Max. and min. transmission	0.7457 and 0.6119		

Table C-1-1 (cont.)

### Structure Solution and Refinement

Structure solution program	SHELXS-97 (Sheldrick, 1990)
Primary solution method	Direct methods
Secondary solution method	Difference Fourier map
Hydrogen placement	Geometric positions
Structure refinement program	SHELXL-97 (Sheldrick, 1997)
Refinement method	Full matrix least-squares on $F^2$
Data / restraints / parameters	10507 / 0 / 620
Treatment of hydrogen atoms	Riding
Goodness-of-fit on $F^2$	1.818
Final R indices [ $I > 2\sigma(I)$ , 9104 reflections]	$R1 = 0.0330$ , $wR2 = 0.0548$
R indices (all data)	$R1 = 0.0458$ , $wR2 = 0.0561$
Type of weighting scheme used	Sigma
Weighting scheme used	$w = 1/\sigma^2(F_o^2)$
Max shift/error	0.001
Average shift/error	0.000
Largest diff. peak and hole	1.996 and -1.834 e.Å <sup>-3</sup>

### Special Refinement Details

Crystals were mounted on a glass fiber using Paratone oil then placed on the diffractometer under a nitrogen stream at 100K.

The crystals contain dichloromethane as a solvent of crystallization. It was refined with partial occupancy in the asymmetric unit with a final refined value of Occ = 0.185.

Refinement of  $F^2$  against ALL reflections. The weighted R-factor ( $wR$ ) and goodness of fit ( $S$ ) are based on  $F^2$ , conventional R-factors ( $R$ ) are based on  $F$ , with  $F$  set to zero for negative  $F^2$ . The threshold expression of  $F^2 > 2\sigma(F^2)$  is used only for calculating R-factors(gt), etc., and is not relevant to the choice of reflections for refinement. R-factors based on  $F^2$  are statistically about twice as large as those based on  $F$ , and R-factors based on ALL data will be even larger.

All esds (except the esd in the dihedral angle between two l.s. planes) are estimated using the full covariance matrix. The cell esds are taken into account individually in the estimation of esds in distances, angles, and torsion angles; correlations between esds in cell parameters are only used when they are defined by crystal symmetry. An approximate (isotropic) treatment of cell esds is used for estimating esds involving l.s. planes.

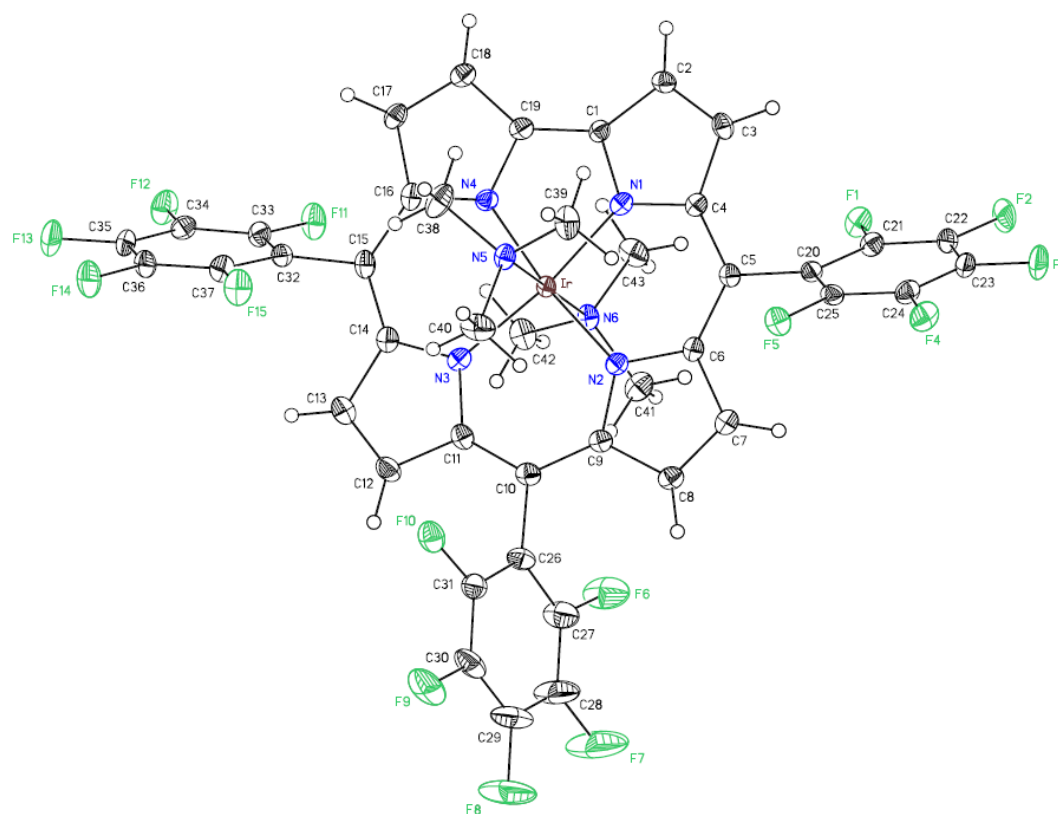


Table C-1-2. Atomic coordinates ( $\times 10^4$ ) and equivalent isotropic displacement parameters ( $\text{\AA}^2 \times 10^3$ ) for **1-Ir(tma)<sub>2</sub>** (CCDC 671270).  $U_{eq}$  is defined as the trace of the orthogonalized  $U_{ij}$  tensor.

	x	y	z	$U_{eq}$	Occ
Ir	1324(1)	2479(1)	7024(1)	12(1)	1
F(1)	2573(2)	6662(2)	6126(1)	22(1)	1
F(2)	1653(3)	8597(2)	5712(1)	29(1)	1
F(3)	-1593(3)	9019(2)	5636(1)	30(1)	1
F(4)	-3922(2)	7467(2)	5984(1)	24(1)	1
F(5)	-3029(2)	5525(2)	6378(1)	20(1)	1
F(6)	-857(3)	3257(2)	9648(1)	47(1)	1
F(7)	-3076(4)	3111(3)	10825(1)	77(1)	1
F(8)	-5838(4)	1883(3)	11010(1)	68(1)	1
F(9)	-6354(3)	799(2)	10003(1)	41(1)	1
F(10)	-4104(2)	887(2)	8849(1)	25(1)	1
F(11)	6068(2)	-569(2)	7429(1)	26(1)	1
F(12)	6967(2)	-2552(2)	7641(1)	27(1)	1
F(13)	4673(3)	-4087(2)	7761(1)	29(1)	1
F(14)	1475(3)	-3621(2)	7630(1)	28(1)	1
F(15)	577(2)	-1642(2)	7363(1)	26(1)	1
N(1)	2027(3)	3495(2)	6203(1)	14(1)	1
N(2)	-342(3)	3405(2)	7438(1)	15(1)	1
N(3)	807(3)	1315(2)	7794(1)	14(1)	1
N(4)	3056(3)	1707(2)	6516(1)	15(1)	1
N(5)	-560(3)	1907(2)	6503(1)	15(1)	1
N(6)	3187(3)	3064(2)	7548(1)	15(1)	1
C(1)	3191(4)	3214(2)	5691(2)	14(1)	1
C(2)	3443(4)	4078(3)	5149(2)	16(1)	1
C(3)	2414(4)	4851(3)	5346(2)	17(1)	1
C(4)	1519(4)	4486(2)	6029(2)	14(1)	1
C(5)	295(4)	4921(2)	6494(2)	14(1)	1
C(6)	-536(4)	4425(3)	7153(2)	14(1)	1
C(7)	-1670(4)	4855(3)	7659(2)	16(1)	1
C(8)	-2129(4)	4108(3)	8221(2)	17(1)	1
C(9)	-1263(4)	3180(3)	8087(2)	14(1)	1
C(10)	-1247(4)	2211(3)	8522(2)	16(1)	1
C(11)	-262(4)	1344(3)	8396(2)	16(1)	1
C(12)	-200(4)	356(3)	8833(2)	20(1)	1
C(13)	890(4)	-230(3)	8481(2)	21(1)	1
C(14)	1562(4)	364(3)	7815(2)	16(1)	1
C(15)	2758(4)	78(3)	7282(2)	17(1)	1
C(16)	3479(4)	701(3)	6654(2)	16(1)	1
C(17)	4585(4)	507(3)	6045(2)	17(1)	1
C(18)	4750(4)	1408(3)	5568(2)	17(1)	1
C(19)	3759(4)	2178(3)	5863(2)	16(1)	1
C(20)	-188(4)	6007(2)	6265(2)	14(1)	1
C(21)	952(4)	6826(3)	6082(2)	17(1)	1
C(22)	504(5)	7828(3)	5870(2)	20(1)	1
C(23)	-1140(5)	8048(3)	5836(2)	20(1)	1
C(24)	-2305(4)	7261(3)	6011(2)	18(1)	1
C(25)	-1832(4)	6264(3)	6217(2)	16(1)	1

C(26)	-2414(4)	2103(3)	9196(2)	20(1)	1
C(27)	-2212(5)	2640(3)	9724(2)	31(1)	1
C(28)	-3327(6)	2570(4)	10326(2)	45(1)	1
C(29)	-4733(6)	1952(4)	10428(2)	41(1)	1
C(30)	-4987(5)	1392(3)	9917(2)	28(1)	1
C(31)	-3829(4)	1461(3)	9321(2)	21(1)	1
C(32)	3288(4)	-1025(3)	7392(2)	15(1)	1
C(33)	4912(4)	-1306(3)	7460(2)	18(1)	1
C(34)	5384(4)	-2315(3)	7577(2)	18(1)	1
C(35)	4227(4)	-3099(3)	7635(2)	19(1)	1
C(36)	2605(4)	-2857(3)	7570(2)	19(1)	1
C(37)	2171(4)	-1838(3)	7440(2)	18(1)	1
C(38)	12(5)	1039(3)	6131(2)	26(1)	1
C(39)	-1127(5)	2734(3)	5990(2)	23(1)	1
C(40)	-2065(4)	1530(3)	7013(2)	26(1)	1
C(41)	2496(4)	3734(3)	8061(2)	22(1)	1
C(42)	4013(4)	2201(3)	7937(2)	21(1)	1
C(43)	4516(4)	3688(3)	7045(2)	23(1)	1
<hr/>					
Cl(1)	6878(13)	5635(7)	9770(5)	95(4)	0.185(3)
Cl(2)	9171(10)	7272(6)	9083(4)	71(3)	0.185(3)
C(51)	8800(40)	5970(20)	9329(15)	58(8)	0.185(3)

Table C-1-3. Selected bond lengths [Å] and angles [°] for **1-Ir(tma)<sub>2</sub>** (CCDC 671270)

Ir-N(1)	1.940(3)	N(1)-Ir-N(4)	79.57(11)
Ir-N(4)	1.968(3)	N(1)-Ir-N(3)	172.20(12)
Ir-N(3)	1.970(3)	N(4)-Ir-N(3)	92.69(11)
Ir-N(2)	1.981(3)	N(1)-Ir-N(2)	93.09(11)
Ir-N(6)	2.184(3)	N(4)-Ir-N(2)	172.66(11)
Ir-N(5)	2.186(3)	N(3)-Ir-N(2)	94.64(11)
		N(1)-Ir-N(6)	90.92(11)
		N(4)-Ir-N(6)	89.98(11)
		N(3)-Ir-N(6)	90.11(10)
		N(2)-Ir-N(6)	89.78(11)
		N(1)-Ir-N(5)	89.02(11)
		N(4)-Ir-N(5)	90.67(11)
		N(3)-Ir-N(5)	90.04(11)
		N(2)-Ir-N(5)	89.55(11)
		N(6)-Ir-N(5)	179.32(12)

Table C-1-4. Bond lengths [Å] and angles [°] for **1-Ir(tma)<sub>2</sub>** (CCDC 671270)

Ir-N(1)	1.940(3)	C(14)-C(15)	1.411(5)
Ir-N(4)	1.968(3)	C(15)-C(16)	1.415(5)
Ir-N(3)	1.970(3)	C(15)-C(32)	1.499(5)
Ir-N(2)	1.981(3)	C(16)-C(17)	1.439(5)
Ir-N(6)	2.184(3)	C(17)-C(18)	1.381(5)
Ir-N(5)	2.186(3)	C(18)-C(19)	1.427(5)
F(1)-C(21)	1.351(4)	C(20)-C(21)	1.389(5)
F(2)-C(22)	1.345(4)	C(20)-C(25)	1.392(4)
F(3)-C(23)	1.338(4)	C(21)-C(22)	1.378(5)
F(4)-C(24)	1.350(4)	C(22)-C(23)	1.378(5)
F(5)-C(25)	1.343(4)	C(23)-C(24)	1.371(5)
F(6)-C(27)	1.348(5)	C(24)-C(25)	1.378(5)
F(7)-C(28)	1.349(5)	C(26)-C(27)	1.386(5)
F(8)-C(29)	1.333(5)	C(26)-C(31)	1.398(5)
F(9)-C(30)	1.336(5)	C(27)-C(28)	1.368(6)
F(10)-C(31)	1.340(4)	C(28)-C(29)	1.378(7)
F(11)-C(33)	1.342(4)	C(29)-C(30)	1.387(6)
F(12)-C(34)	1.346(4)	C(30)-C(31)	1.377(5)
F(13)-C(35)	1.338(4)	C(32)-C(37)	1.389(5)
F(14)-C(36)	1.344(4)	C(32)-C(33)	1.392(5)
F(15)-C(37)	1.350(4)	C(33)-C(34)	1.369(5)
N(1)-C(1)	1.366(4)	C(34)-C(35)	1.379(5)
N(1)-C(4)	1.368(4)	C(35)-C(36)	1.378(5)
N(2)-C(9)	1.368(4)	C(36)-C(37)	1.374(5)
N(2)-C(6)	1.383(4)	Cl(1)-C(51)	1.68(3)
N(3)-C(11)	1.363(4)	Cl(2)-C(51)	1.72(3)
N(3)-C(14)	1.383(4)		
N(4)-C(16)	1.357(4)	N(1)-Ir-N(4)	79.57(11)
N(4)-C(19)	1.375(4)	N(1)-Ir-N(3)	172.20(12)
N(5)-C(40)	1.487(4)	N(4)-Ir-N(3)	92.69(11)
N(5)-C(38)	1.487(5)	N(1)-Ir-N(2)	93.09(11)
N(5)-C(39)	1.487(4)	N(4)-Ir-N(2)	172.66(11)
N(6)-C(42)	1.483(4)	N(3)-Ir-N(2)	94.64(11)
N(6)-C(41)	1.489(5)	N(1)-Ir-N(6)	90.92(11)
N(6)-C(43)	1.495(4)	N(4)-Ir-N(6)	89.98(11)
C(1)-C(2)	1.420(4)	N(3)-Ir-N(6)	90.11(10)
C(1)-C(19)	1.437(5)	N(2)-Ir-N(6)	89.78(11)
C(2)-C(3)	1.375(5)	N(1)-Ir-N(5)	89.02(11)
C(3)-C(4)	1.438(5)	N(4)-Ir-N(5)	90.67(11)
C(4)-C(5)	1.424(5)	N(3)-Ir-N(5)	90.04(11)
C(5)-C(6)	1.425(4)	N(2)-Ir-N(5)	89.55(11)
C(5)-C(20)	1.493(4)	N(6)-Ir-N(5)	179.32(12)
C(6)-C(7)	1.431(5)	C(1)-N(1)-C(4)	111.6(3)
C(7)-C(8)	1.364(5)	C(1)-N(1)-Ir	118.0(2)
C(8)-C(9)	1.442(5)	C(4)-N(1)-Ir	130.4(2)
C(9)-C(10)	1.416(4)	C(9)-N(2)-C(6)	110.8(3)
C(10)-C(11)	1.418(5)	C(9)-N(2)-Ir	124.6(2)
C(10)-C(26)	1.494(5)	C(6)-N(2)-Ir	123.9(2)
C(11)-C(12)	1.443(4)	C(11)-N(3)-C(14)	110.2(3)
C(12)-C(13)	1.352(5)	C(11)-N(3)-Ir	125.4(2)
C(13)-C(14)	1.444(5)	C(14)-N(3)-Ir	124.3(2)



C(16)-N(4)-C(19)	112.7(3)	N(4)-C(19)-C(1)	112.8(3)
C(16)-N(4)-Ir	129.7(2)	C(18)-C(19)-C(1)	141.6(3)
C(19)-N(4)-Ir	116.5(2)	C(21)-C(20)-C(25)	115.4(3)
C(40)-N(5)-C(38)	107.0(3)	C(21)-C(20)-C(5)	122.9(3)
C(40)-N(5)-C(39)	106.3(3)	C(25)-C(20)-C(5)	121.7(3)
C(38)-N(5)-C(39)	107.2(3)	F(1)-C(21)-C(22)	117.1(3)
C(40)-N(5)-Ir	110.4(2)	F(1)-C(21)-C(20)	120.0(3)
C(38)-N(5)-Ir	113.6(2)	C(22)-C(21)-C(20)	122.9(3)
C(39)-N(5)-Ir	111.9(2)	F(2)-C(22)-C(23)	119.7(3)
C(42)-N(6)-C(41)	106.2(3)	F(2)-C(22)-C(21)	120.5(3)
C(42)-N(6)-C(43)	107.3(3)	C(23)-C(22)-C(21)	119.8(3)
C(41)-N(6)-C(43)	106.6(3)	F(3)-C(23)-C(24)	120.5(3)
C(42)-N(6)-Ir	110.9(2)	F(3)-C(23)-C(22)	120.3(3)
C(41)-N(6)-Ir	113.9(2)	C(24)-C(23)-C(22)	119.2(3)
C(43)-N(6)-Ir	111.6(2)	F(4)-C(24)-C(23)	119.8(3)
N(1)-C(1)-C(2)	106.5(3)	F(4)-C(24)-C(25)	120.0(3)
N(1)-C(1)-C(19)	112.8(3)	C(23)-C(24)-C(25)	120.2(3)
C(2)-C(1)-C(19)	140.7(3)	F(5)-C(25)-C(24)	117.4(3)
C(3)-C(2)-C(1)	108.2(3)	F(5)-C(25)-C(20)	120.0(3)
C(2)-C(3)-C(4)	108.0(3)	C(24)-C(25)-C(20)	122.6(3)
N(1)-C(4)-C(5)	120.2(3)	C(27)-C(26)-C(31)	115.6(3)
N(1)-C(4)-C(3)	105.7(3)	C(27)-C(26)-C(10)	123.4(3)
C(5)-C(4)-C(3)	134.1(3)	C(31)-C(26)-C(10)	121.0(3)
C(4)-C(5)-C(6)	126.9(3)	F(6)-C(27)-C(28)	117.9(4)
C(4)-C(5)-C(20)	116.8(3)	F(6)-C(27)-C(26)	119.1(3)
C(6)-C(5)-C(20)	116.3(3)	C(28)-C(27)-C(26)	123.0(4)
N(2)-C(6)-C(5)	125.2(3)	F(7)-C(28)-C(27)	120.7(4)
N(2)-C(6)-C(7)	106.0(3)	F(7)-C(28)-C(29)	119.2(4)
C(5)-C(6)-C(7)	128.7(3)	C(27)-C(28)-C(29)	120.1(4)
C(8)-C(7)-C(6)	108.8(3)	F(8)-C(29)-C(28)	120.9(4)
C(7)-C(8)-C(9)	107.7(3)	F(8)-C(29)-C(30)	120.0(4)
N(2)-C(9)-C(10)	123.7(3)	C(28)-C(29)-C(30)	119.2(4)
N(2)-C(9)-C(8)	106.7(3)	F(9)-C(30)-C(31)	120.5(4)
C(10)-C(9)-C(8)	129.6(3)	F(9)-C(30)-C(29)	120.0(4)
C(9)-C(10)-C(11)	128.0(3)	C(31)-C(30)-C(29)	119.5(4)
C(9)-C(10)-C(26)	115.3(3)	F(10)-C(31)-C(30)	117.5(3)
C(11)-C(10)-C(26)	116.7(3)	F(10)-C(31)-C(26)	119.9(3)
N(3)-C(11)-C(10)	123.3(3)	C(30)-C(31)-C(26)	122.6(4)
N(3)-C(11)-C(12)	107.5(3)	C(37)-C(32)-C(33)	115.6(3)
C(10)-C(11)-C(12)	129.2(3)	C(37)-C(32)-C(15)	121.7(3)
C(13)-C(12)-C(11)	107.4(3)	C(33)-C(32)-C(15)	122.7(3)
C(12)-C(13)-C(14)	108.9(3)	F(11)-C(33)-C(34)	117.8(3)
N(3)-C(14)-C(15)	125.0(3)	F(11)-C(33)-C(32)	119.6(3)
N(3)-C(14)-C(13)	106.0(3)	C(34)-C(33)-C(32)	122.6(3)
C(15)-C(14)-C(13)	129.0(3)	F(12)-C(34)-C(33)	120.6(3)
C(14)-C(15)-C(16)	127.8(3)	F(12)-C(34)-C(35)	119.4(3)
C(14)-C(15)-C(32)	115.6(3)	C(33)-C(34)-C(35)	120.0(3)
C(16)-C(15)-C(32)	116.6(3)	F(13)-C(35)-C(36)	120.3(3)
N(4)-C(16)-C(15)	120.0(3)	F(13)-C(35)-C(34)	120.3(3)
N(4)-C(16)-C(17)	105.6(3)	C(36)-C(35)-C(34)	119.5(3)
C(15)-C(16)-C(17)	134.3(3)	F(14)-C(36)-C(37)	121.1(3)
C(18)-C(17)-C(16)	107.9(3)	F(14)-C(36)-C(35)	119.5(3)
C(17)-C(18)-C(19)	108.4(3)	C(37)-C(36)-C(35)	119.4(3)
N(4)-C(19)-C(18)	105.4(3)	F(15)-C(37)-C(36)	117.1(3)
F(15)-C(37)-C(32)	119.9(3)	Cl(1)-C(51)-Cl(2)	115.1(16)
C(36)-C(37)-C(32)	122.9(3)		

Table C-1-5. Anisotropic displacement parameters ( $\text{\AA}^2 \times 10^4$ ) for **1-Ir(tma)<sub>2</sub>** (CCDC 671270). The anisotropic displacement factor exponent takes the form:  $-2\pi^2 [h^2 a^{*2} U^{11} + \dots + 2 h k a^* b^* U^{12}]$ .

	U <sup>11</sup>	U <sup>22</sup>	U <sup>33</sup>	U <sup>23</sup>	U <sup>13</sup>	U <sup>12</sup>
Ir	84(1)	112(1)	151(1)	-24(1)	-12(1)	-12(1)
F(1)	125(11)	215(11)	329(12)	-94(9)	-24(9)	-44(8)
F(2)	288(13)	160(11)	402(13)	-42(9)	19(10)	-112(9)
F(3)	410(14)	118(10)	357(13)	-29(9)	-72(11)	63(9)
F(4)	184(11)	255(11)	285(12)	-61(9)	-66(9)	95(9)
F(5)	136(10)	204(11)	250(11)	-13(9)	-45(9)	-31(8)
F(6)	426(16)	668(18)	344(14)	-232(13)	-7(12)	-238(13)
F(7)	790(20)	1220(30)	327(15)	-425(17)	121(15)	-290(20)
F(8)	552(19)	1040(30)	328(15)	-117(16)	267(14)	-123(17)
F(9)	187(12)	430(15)	494(15)	108(12)	95(11)	-67(11)
F(10)	196(11)	218(11)	311(12)	-6(9)	-33(9)	-39(9)
F(11)	145(11)	183(11)	453(14)	-42(10)	-62(10)	-45(9)
F(12)	154(11)	225(11)	423(13)	-77(10)	-45(10)	63(9)
F(13)	290(13)	137(11)	448(14)	-61(10)	-51(10)	37(9)
F(14)	257(12)	173(11)	417(13)	-45(10)	-85(10)	-85(9)
F(15)	154(11)	235(11)	405(13)	-49(10)	-111(10)	-17(9)
N(1)	89(15)	161(15)	172(15)	-51(12)	-29(12)	12(12)
N(2)	128(15)	154(15)	159(15)	-35(12)	-24(12)	10(12)
N(3)	73(14)	172(15)	185(15)	-57(12)	-18(12)	-5(12)
N(4)	122(15)	155(15)	160(15)	-36(12)	0(12)	7(12)
N(5)	119(15)	136(15)	214(16)	-43(12)	-37(13)	-17(12)
N(6)	114(15)	139(15)	198(16)	-15(12)	-38(12)	-12(12)
C(1)	124(18)	136(17)	165(17)	-48(14)	-16(14)	-16(14)
C(2)	134(18)	179(18)	151(17)	-30(14)	-9(14)	-48(14)
C(3)	151(19)	144(17)	214(19)	0(14)	-32(15)	-37(14)
C(4)	105(17)	147(17)	169(17)	-47(14)	-34(14)	-18(13)
C(5)	108(17)	137(16)	171(18)	-22(14)	-31(14)	-18(13)
C(6)	115(17)	135(17)	188(18)	-37(14)	-38(14)	-3(13)
C(7)	119(17)	170(17)	199(18)	-56(14)	-51(14)	9(14)
C(8)	114(18)	202(19)	190(18)	-50(15)	-9(14)	-3(14)
C(9)	96(17)	173(17)	161(17)	-38(14)	-22(14)	-21(14)
C(10)	117(18)	198(18)	174(18)	-33(14)	-10(14)	-38(14)
C(11)	111(17)	166(18)	202(18)	-5(14)	-28(14)	-26(14)
C(12)	171(19)	192(19)	205(19)	20(15)	11(15)	-13(15)
C(13)	190(20)	183(18)	225(19)	13(15)	-42(16)	-21(15)
C(14)	117(18)	151(17)	216(19)	-27(14)	-39(15)	-3(14)
C(15)	132(18)	131(17)	245(19)	-29(15)	-65(15)	-23(14)
C(16)	125(18)	128(17)	237(19)	-37(14)	-64(15)	5(14)
C(17)	132(18)	166(18)	225(19)	-72(15)	-29(15)	23(14)
C(18)	125(18)	199(18)	197(18)	-66(15)	-13(14)	-8(14)
C(19)	103(17)	183(18)	180(18)	-54(14)	-1(14)	-34(14)
C(20)	162(18)	141(17)	129(17)	-26(13)	-23(14)	-9(14)
C(21)	152(18)	172(17)	184(18)	-50(14)	-34(15)	-10(14)
C(22)	260(20)	129(17)	191(18)	-47(14)	-3(16)	-61(15)
C(23)	300(20)	125(17)	177(18)	-31(14)	-35(16)	33(15)
C(24)	166(19)	194(18)	189(18)	-49(15)	-36(15)	58(15)
C(25)	148(18)	170(17)	143(17)	-30(14)	1(14)	-39(14)



C(26)	152(19)	252(19)	163(18)	-15(15)	8(15)	-7(15)
C(27)	290(20)	390(20)	230(20)	-68(18)	0(18)	-77(19)
C(28)	500(30)	670(30)	190(20)	-170(20)	30(20)	-70(30)
C(29)	390(30)	570(30)	200(20)	-20(20)	100(20)	-10(20)
C(30)	190(20)	300(20)	290(20)	80(18)	37(17)	-39(17)
C(31)	210(20)	204(19)	199(19)	-7(15)	-19(16)	54(15)
C(32)	159(18)	140(17)	159(17)	-24(14)	-21(14)	-11(14)
C(33)	166(19)	153(17)	214(19)	-52(14)	-13(15)	-46(14)
C(34)	140(18)	200(18)	200(18)	-48(15)	-10(15)	33(14)
C(35)	220(20)	120(17)	228(19)	-35(14)	-30(16)	38(14)
C(36)	210(20)	146(17)	232(19)	-41(14)	-33(16)	-78(15)
C(37)	130(18)	190(18)	239(19)	-47(15)	-40(15)	12(14)
C(38)	220(20)	250(20)	380(20)	-172(18)	-117(18)	15(16)
C(39)	210(20)	191(19)	320(20)	-32(16)	-135(17)	-18(16)
C(40)	160(20)	380(20)	250(20)	-63(17)	-10(16)	-108(17)
C(41)	190(20)	250(20)	270(20)	-104(16)	-77(16)	-18(16)
C(42)	150(20)	220(20)	280(20)	-6(16)	-93(16)	-12(15)
C(43)	163(19)	270(20)	240(20)	-18(16)	-47(16)	-91(16)
<hr/>						
Cl(1)	1080(80)	550(50)	1040(70)	-190(50)	450(60)	-70(50)
Cl(2)	560(50)	710(60)	840(60)	70(40)	-220(40)	-20(40)
C(51)	600(200)	500(170)	700(200)	-430(150)	-200(160)	20(140)

CALIFORNIA INSTITUTE OF TECHNOLOGY  
BECKMAN INSTITUTE  
X-RAY CRYSTALLOGRAPHY LABORATORY

Date 24 January 2008

**Crystal Structure Analysis of:**

**1b-Ir(tma)<sub>2</sub>**

(shown below)

**For** Investigator: Joshua Palmer ext. 6332

Advisor: H. B. Gray ext. 6500

Account Number: HGB.BP-1-BP.AMOCO

**By** Michael W. Day 116 Beckman ext. 2734

e-mail: mikeday@caltech.edu

Contents

Table 1. Crystal data

Figures Minimum overlap

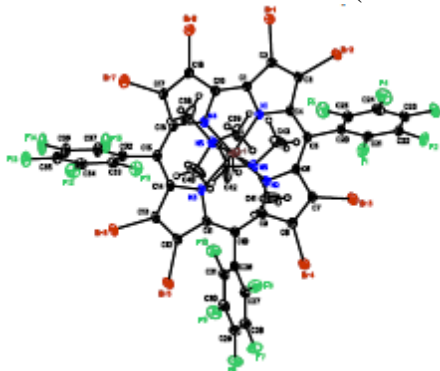
Table 2. Atomic Coordinates

Table 3. Selected bond distances and angles

Table 4. Full bond distances and angles

Table 5. Anisotropic displacement parameters

Table 6. Observed and calculated structure factors (available upon request)



**1b-Ir(tma)<sub>2</sub>**

**Note:** The crystallographic data have been deposited in the Cambridge Database (CCDC) and have been placed on hold pending further instructions from me. The deposition number is 675602. Ideally the CCDC would like the publication to contain a footnote of the type: "Crystallographic data have been deposited at the CCDC, 12 Union Road, Cambridge CB2 1EZ, UK, and copies can be obtained on request, free of charge, by quoting the publication citation and the deposition number 657602".

Table C-2-1. Crystal data and structure refinement for **1b-Ir(tma)<sub>2</sub>** (CCDC 675602)

Empirical formula	C <sub>43</sub> H <sub>18</sub> N <sub>6</sub> Br <sub>3</sub> F <sub>15</sub> Ir, 3(CH <sub>2</sub> Cl <sub>2</sub> )		
Formula weight	1989.89		
Crystallization Solvent	Dichloromethane		
Crystal Habit	Block		
Crystal size	0.46 x 0.25 x 0.14 mm <sup>3</sup>		
Crystal color	Dark green		
<b>Data Collection</b>			
Type of diffractometer	Bruker KAPPA APEX II		
Wavelength	0.71073 Å MoKα		
Data Collection Temperature	100(2) K		
θ range for 9503 reflections used in lattice determination	2.58 to 43.28°		
Unit cell dimensions	a = 10.5456(5) Å b = 12.9293(6) Å c = 21.2776(9) Å	α = 81.591(3)° β = 76.344(3)° γ = 86.714(3)°	
Volume	2788.0(2) Å <sup>3</sup>		
Z	2		
Crystal system	Triclinic		
Space group	P-1		
Density (calculated)	2.370 Mg/m <sup>3</sup>		
F(000)	1872		
θ range for data collection	1.76 to 43.48°		
Completeness to θ = 43.48°	96.6 %		
Index ranges	-20 ≤ h ≤ 20, -24 ≤ k ≤ 22, -41 ≤ l ≤ 40		
Data collection scan type	ω scans; 24 settings		
Reflections collected	177276		
Independent reflections	40945 [R <sub>int</sub> = 0.0501]		
Absorption coefficient	8.508 mm <sup>-1</sup>		
Absorption correction	Semi-empirical from equivalents		
Max. and min. transmission	0.7485 and 0.4771		

Table C-2-1 (cont.)

### Structure Solution and Refinement

Structure solution program	SHELXS-97 (Sheldrick, 1990)
Primary solution method	Direct methods
Secondary solution method	Difference Fourier map
Hydrogen placement	Geometric positions
Structure refinement program	SHELXL-97 (Sheldrick, 1997)
Refinement method	Full matrix least-squares on $F^2$
Data / restraints / parameters	40945 / 0 / 764
Treatment of hydrogen atoms	Riding
Goodness-of-fit on $F^2$	1.534
Final R indices [ $I > 2\sigma(I)$ , 28576 reflections]	$R1 = 0.0412$ , $wR2 = 0.0606$
R indices (all data)	$R1 = 0.0793$ , $wR2 = 0.0634$
Type of weighting scheme used	Sigma
Weighting scheme used	$w = 1/\sigma^2(F_o^2)$
Max shift/error	0.004
Average shift/error	0.000
Largest diff. peak and hole	4.350 and -2.801 $e \cdot \text{\AA}^{-3}$

### Special Refinement Details

Crystals were mounted on a glass fiber using Paratone oil then placed on the diffractometer under a nitrogen stream at 100K.

The crystals contain dichloromethane as a solvent of crystallization—three in the asymmetric unit. One of those three is disordered with the chlorine atoms occupying two orientations while sharing a common carbon atom. The disorder was modeled without restraint, except that the total chlorine population was restrained so that the orientations' occupancy summed to one.

Refinement of  $F^2$  against ALL reflections. The weighted R-factor ( $wR$ ) and goodness of fit ( $S$ ) are based on  $F^2$ , conventional R-factors ( $R$ ) are based on  $F$ , with  $F$  set to zero for negative  $F^2$ . The threshold expression of  $F^2 > 2\sigma(F^2)$  is used only for calculating R-factors(gt), etc., and is not relevant to the choice of reflections for refinement. R-factors based on  $F^2$  are statistically about twice as large as those based on  $F$ , and R-factors based on ALL data will be even larger.

All esds (except the esd in the dihedral angle between two l.s. planes) are estimated using the full covariance matrix. The cell esds are taken into account individually in the estimation of esds in distances, angles, and torsion angles; correlations between esds in cell parameters are only used when they are defined by crystal symmetry. An approximate (isotropic) treatment of cell esds is used for estimating esds involving l.s. planes.

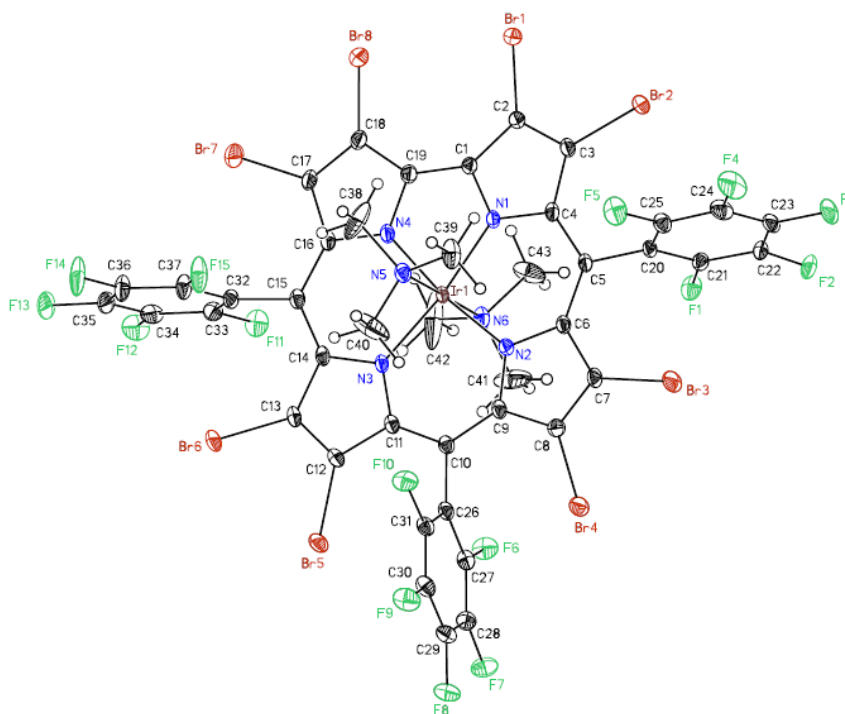


Table 2. Atomic coordinates ( $\times 10^4$ ) and equivalent isotropic displacement parameters ( $\text{\AA}^2 \times 10^3$ ) for **1b-Ir(tma)<sub>2</sub>** (CCDC 675602).  $U(\text{eq})$  is defined as the trace of the orthogonalized  $U_{ij}$  tensor.

	x	y	z	$U_{\text{eq}}$	Occ
Ir(1)	5600(1)	2707(1)	2759(1)	11(1)	1
Br(1)	3909(1)	1493(1)	5558(1)	21(1)	1
Br(2)	2518(1)	-307(1)	4875(1)	21(1)	1
Br(3)	2815(1)	-505(1)	1893(1)	24(1)	1
Br(4)	4474(1)	911(1)	528(1)	20(1)	1
Br(5)	8185(1)	4625(1)	73(1)	19(1)	1
Br(6)	8884(1)	6129(1)	1101(1)	20(1)	1
Br(7)	7691(1)	5625(1)	4165(1)	25(1)	1
Br(8)	5967(1)	3715(1)	5284(1)	21(1)	1
F(1)	4745(1)	-1423(1)	3164(1)	23(1)	1
F(2)	3299(1)	-3156(1)	3442(1)	27(1)	1
F(3)	664(1)	-2985(1)	3816(1)	31(1)	1
F(4)	-531(1)	-1066(1)	3821(1)	33(1)	1
F(5)	909(1)	668(1)	3487(1)	28(1)	1
F(6)	8099(1)	1767(1)	282(1)	23(1)	1
F(7)	8270(1)	1915(1)	-1015(1)	24(1)	1
F(8)	6419(1)	3027(1)	-1548(1)	25(1)	1
F(9)	4470(1)	4040(1)	-792(1)	26(1)	1
F(10)	4310(1)	3925(1)	500(1)	22(1)	1
F(11)	10087(1)	4930(1)	2599(1)	25(1)	1
F(12)	11309(1)	6752(1)	2474(1)	29(1)	1
F(13)	9936(1)	8587(1)	2426(1)	31(1)	1
F(14)	7336(1)	8600(1)	2531(1)	42(1)	1
F(15)	6107(1)	6777(1)	2626(1)	33(1)	1
N(1)	4654(2)	1931(1)	3581(1)	13(1)	1
N(2)	4941(2)	1826(1)	2219(1)	14(1)	1
N(3)	6639(1)	3618(1)	2001(1)	13(1)	1
N(4)	6125(2)	3447(1)	3397(1)	14(1)	1
N(5)	3890(2)	3752(1)	2756(1)	16(1)	1
N(6)	7308(2)	1662(1)	2749(1)	17(1)	1
C(1)	4824(2)	2224(1)	4151(1)	14(1)	1
C(2)	4113(2)	1495(1)	4663(1)	15(1)	1
C(3)	3560(2)	784(1)	4385(1)	15(1)	1
C(4)	3926(2)	1065(1)	3685(1)	13(1)	1
C(5)	3677(2)	624(1)	3152(1)	13(1)	1
C(6)	4142(2)	987(1)	2479(1)	14(1)	1
C(7)	3882(2)	585(1)	1915(1)	16(1)	1
C(8)	4529(2)	1174(1)	1364(1)	15(1)	1
C(9)	5232(2)	1975(1)	1547(1)	14(1)	1
C(10)	6058(2)	2754(1)	1153(1)	14(1)	1
C(11)	6738(2)	3512(1)	1358(1)	13(1)	1
C(12)	7557(2)	4341(1)	979(1)	14(1)	1
C(13)	7880(2)	4931(1)	1397(1)	14(1)	1
C(14)	7305(2)	4479(1)	2058(1)	13(1)	1
C(15)	7380(2)	4814(1)	2654(1)	15(1)	1
C(16)	6835(2)	4323(1)	3292(1)	15(1)	1
C(17)	6849(2)	4550(1)	3935(1)	16(1)	1

C(18)	6142(2)	3799(1)	4387(1)	16(1)	1
C(19)	5653(2)	3094(1)	4043(1)	15(1)	1
C(20)	2869(2)	-329(1)	3331(1)	13(1)	1
C(21)	3447(2)	-1321(1)	3334(1)	15(1)	1
C(22)	2711(2)	-2209(1)	3483(1)	18(1)	1
C(23)	1378(2)	-2127(2)	3662(1)	21(1)	1
C(24)	771(2)	-1146(2)	3665(1)	22(1)	1
C(25)	1523(2)	-275(2)	3496(1)	17(1)	1
C(26)	6188(2)	2829(1)	433(1)	14(1)	1
C(27)	7183(2)	2327(1)	28(1)	16(1)	1
C(28)	7280(2)	2390(2)	-635(1)	17(1)	1
C(29)	6358(2)	2968(2)	-911(1)	18(1)	1
C(30)	5365(2)	3485(2)	-520(1)	18(1)	1
C(31)	5296(2)	3414(1)	136(1)	16(1)	1
C(32)	8063(2)	5808(1)	2612(1)	15(1)	1
C(33)	9384(2)	5832(2)	2583(1)	17(1)	1
C(34)	10026(2)	6748(2)	2517(1)	20(1)	1
C(35)	9323(2)	7686(2)	2494(1)	22(1)	1
C(36)	8009(2)	7688(2)	2544(1)	24(1)	1
C(37)	7387(2)	6761(2)	2597(1)	20(1)	1
C(38)	3731(2)	4500(2)	3240(2)	39(1)	1
C(39)	2666(2)	3168(2)	2920(1)	25(1)	1
C(40)	3956(3)	4381(2)	2113(1)	47(1)	1
C(41)	7656(3)	1137(2)	2154(1)	41(1)	1
C(42)	8466(3)	2229(2)	2770(2)	72(1)	1
C(43)	7110(2)	815(2)	3308(1)	32(1)	1
C(51)	2473(3)	626(2)	9260(1)	36(1)	1
Cl(1)	926(1)	936(1)	9104(1)	40(1)	1
Cl(2)	3616(1)	1580(1)	8896(1)	57(1)	1
C(52)	1202(4)	2774(2)	707(1)	53(1)	1
Cl(3)	1075(1)	3496(1)	1378(1)	50(1)	1
Cl(4)	773(1)	1482(1)	931(1)	58(1)	1
C(53)	10193(4)	6577(2)	5492(2)	53(1)	1
Cl(5A)	9121(2)	5785(1)	5443(1)	54(1)	0.526(2)
Cl(6A)	9884(2)	7892(1)	5425(1)	55(1)	0.526(2)
Cl(5B)	8684(1)	7181(1)	5220(1)	41(1)	0.474(2)
Cl(6B)	10756(2)	7409(1)	5851(1)	54(1)	0.474(2)

---

Table C-2-3. Selected bond lengths [Å] and angles [°] for **1b-Ir(tma)<sub>2</sub>** (CCDC 675602)

Ir(1)-N(1)	1.9585(16)	N(1)-Ir(1)-N(4)	79.08(6)
Ir(1)-N(4)	1.9630(14)	N(1)-Ir(1)-N(3)	172.15(6)
Ir(1)-N(3)	1.9870(15)	N(4)-Ir(1)-N(3)	93.08(6)
Ir(1)-N(2)	1.9893(14)	N(1)-Ir(1)-N(2)	93.07(6)
Ir(1)-N(6)	2.1865(15)	N(4)-Ir(1)-N(2)	172.13(6)
Ir(1)-N(5)	2.1918(14)	N(3)-Ir(1)-N(2)	94.77(6)
		N(1)-Ir(1)-N(6)	91.33(6)
		N(4)-Ir(1)-N(6)	89.55(6)
		N(3)-Ir(1)-N(6)	88.99(6)
		N(2)-Ir(1)-N(6)	90.10(6)
		N(1)-Ir(1)-N(5)	89.15(6)
		N(4)-Ir(1)-N(5)	91.07(6)
		N(3)-Ir(1)-N(5)	90.61(6)
		N(2)-Ir(1)-N(5)	89.33(6)
		N(6)-Ir(1)-N(5)	179.27(6)



Table C-2-4. Bond lengths [Å] and angles [°] for **1b-Ir(tma)<sub>2</sub>** (CCDC 675602)

Ir(1)-N(1)	1.9585(16)	C(7)-C(8)	1.358(3)
Ir(1)-N(4)	1.9630(14)	C(8)-C(9)	1.456(2)
Ir(1)-N(3)	1.9870(15)	C(9)-C(10)	1.409(3)
Ir(1)-N(2)	1.9893(14)	C(10)-C(11)	1.421(2)
Ir(1)-N(6)	2.1865(15)	C(10)-C(26)	1.495(2)
Ir(1)-N(5)	2.1918(14)	C(11)-C(12)	1.439(3)
Br(1)-C(2)	1.8634(17)	C(12)-C(13)	1.363(2)
Br(2)-C(3)	1.8684(19)	C(13)-C(14)	1.445(3)
Br(3)-C(7)	1.8656(18)	C(14)-C(15)	1.419(2)
Br(4)-C(8)	1.8733(16)	C(15)-C(16)	1.414(3)
Br(5)-C(12)	1.8721(17)	C(15)-C(32)	1.490(3)
Br(6)-C(13)	1.8726(19)	C(16)-C(17)	1.444(2)
Br(7)-C(17)	1.8717(18)	C(17)-C(18)	1.377(3)
Br(8)-C(18)	1.8603(18)	C(18)-C(19)	1.436(2)
F(1)-C(21)	1.335(2)	C(20)-C(25)	1.379(3)
F(2)-C(22)	1.345(2)	C(20)-C(21)	1.388(2)
F(3)-C(23)	1.333(2)	C(21)-C(22)	1.378(3)
F(4)-C(24)	1.335(2)	C(22)-C(23)	1.369(3)
F(5)-C(25)	1.347(2)	C(23)-C(24)	1.387(3)
F(6)-C(27)	1.343(2)	C(24)-C(25)	1.371(3)
F(7)-C(28)	1.3392(19)	C(26)-C(31)	1.384(2)
F(8)-C(29)	1.332(2)	C(26)-C(27)	1.387(2)
F(9)-C(30)	1.341(2)	C(27)-C(28)	1.380(2)
F(10)-C(31)	1.3449(19)	C(28)-C(29)	1.381(3)
F(11)-C(33)	1.346(2)	C(29)-C(30)	1.381(2)
F(12)-C(34)	1.335(2)	C(30)-C(31)	1.372(2)
F(13)-C(35)	1.337(2)	C(32)-C(33)	1.382(3)
F(14)-C(36)	1.341(2)	C(32)-C(37)	1.389(2)
F(15)-C(37)	1.336(2)	C(33)-C(34)	1.372(3)
N(1)-C(4)	1.357(2)	C(34)-C(35)	1.385(3)
N(1)-C(1)	1.375(2)	C(35)-C(36)	1.364(3)
N(2)-C(9)	1.375(2)	C(36)-C(37)	1.376(3)
N(2)-C(6)	1.378(2)	C(51)-Cl(2)	1.739(3)
N(3)-C(11)	1.373(2)	C(51)-Cl(1)	1.753(2)
N(3)-C(14)	1.384(2)	C(52)-Cl(4)	1.725(3)
N(4)-C(16)	1.356(2)	C(52)-Cl(3)	1.793(3)
N(4)-C(19)	1.367(2)	C(53)-Cl(5A)	1.599(4)
N(5)-C(40)	1.475(3)	C(53)-Cl(6B)	1.618(4)
N(5)-C(39)	1.476(3)	C(53)-Cl(6A)	1.704(3)
N(5)-C(38)	1.488(2)	C(53)-Cl(5B)	1.907(4)
N(6)-C(42)	1.472(3)		
N(6)-C(43)	1.478(3)	N(1)-Ir(1)-N(4)	79.08(6)
N(6)-C(41)	1.484(2)	N(1)-Ir(1)-N(3)	172.15(6)
C(1)-C(19)	1.423(3)	N(4)-Ir(1)-N(3)	93.08(6)
C(1)-C(2)	1.426(3)	N(1)-Ir(1)-N(2)	93.07(6)
C(2)-C(3)	1.386(2)	N(4)-Ir(1)-N(2)	172.13(6)
C(3)-C(4)	1.445(2)	N(3)-Ir(1)-N(2)	94.77(6)
C(4)-C(5)	1.423(2)	N(1)-Ir(1)-N(6)	91.33(6)
C(5)-C(6)	1.419(2)	N(4)-Ir(1)-N(6)	89.55(6)
C(5)-C(20)	1.490(3)	N(3)-Ir(1)-N(6)	88.99(6)
C(6)-C(7)	1.461(2)	N(2)-Ir(1)-N(6)	90.10(6)

N(1)-Ir(1)-N(5)	89.15(6)	N(2)-C(9)-C(8)	105.35(16)
N(4)-Ir(1)-N(5)	91.07(6)	C(10)-C(9)-C(8)	130.06(15)
N(3)-Ir(1)-N(5)	90.61(6)	C(9)-C(10)-C(11)	127.82(15)
N(2)-Ir(1)-N(5)	89.33(6)	C(9)-C(10)-C(26)	116.35(15)
N(6)-Ir(1)-N(5)	179.27(6)	C(11)-C(10)-C(26)	115.76(16)
C(4)-N(1)-C(1)	112.63(15)	N(3)-C(11)-C(10)	123.67(16)
C(4)-N(1)-Ir(1)	129.68(11)	N(3)-C(11)-C(12)	106.17(14)
C(1)-N(1)-Ir(1)	117.38(12)	C(10)-C(11)-C(12)	130.03(15)
C(9)-N(2)-C(6)	112.37(14)	C(13)-C(12)-C(11)	108.37(15)
C(9)-N(2)-Ir(1)	124.19(13)	C(13)-C(12)-Br(5)	122.03(15)
C(6)-N(2)-Ir(1)	123.44(11)	C(11)-C(12)-Br(5)	129.58(13)
C(11)-N(3)-C(14)	111.38(15)	C(12)-C(13)-C(14)	108.59(16)
C(11)-N(3)-Ir(1)	124.90(12)	C(12)-C(13)-Br(6)	122.26(14)
C(14)-N(3)-Ir(1)	123.64(11)	C(14)-C(13)-Br(6)	129.15(13)
C(16)-N(4)-C(19)	113.34(14)	N(3)-C(14)-C(15)	125.53(17)
C(16)-N(4)-Ir(1)	129.08(13)	N(3)-C(14)-C(13)	105.44(14)
C(19)-N(4)-Ir(1)	117.42(12)	C(15)-C(14)-C(13)	129.03(17)
C(40)-N(5)-C(39)	106.81(19)	C(16)-C(15)-C(14)	126.93(17)
C(40)-N(5)-C(38)	106.9(2)	C(16)-C(15)-C(32)	115.67(15)
C(39)-N(5)-C(38)	106.20(17)	C(14)-C(15)-C(32)	117.36(16)
C(40)-N(5)-Ir(1)	112.08(12)	N(4)-C(16)-C(15)	121.45(15)
C(39)-N(5)-Ir(1)	111.87(11)	N(4)-C(16)-C(17)	105.17(16)
C(38)-N(5)-Ir(1)	112.58(12)	C(15)-C(16)-C(17)	133.39(17)
C(42)-N(6)-C(43)	106.8(2)	C(18)-C(17)-C(16)	108.05(15)
C(42)-N(6)-C(41)	107.0(2)	C(18)-C(17)-Br(7)	123.09(13)
C(43)-N(6)-C(41)	106.00(17)	C(16)-C(17)-Br(7)	128.83(15)
C(42)-N(6)-Ir(1)	111.72(12)	C(17)-C(18)-C(19)	108.27(15)
C(43)-N(6)-Ir(1)	112.88(12)	C(17)-C(18)-Br(8)	123.95(13)
C(41)-N(6)-Ir(1)	112.03(12)	C(19)-C(18)-Br(8)	127.70(15)
N(1)-C(1)-C(19)	112.90(16)	N(4)-C(19)-C(1)	113.19(15)
N(1)-C(1)-C(2)	105.70(15)	N(4)-C(19)-C(18)	105.14(16)
C(19)-C(1)-C(2)	141.36(16)	C(1)-C(19)-C(18)	141.56(17)
C(3)-C(2)-C(1)	108.27(15)	C(25)-C(20)-C(21)	116.82(17)
C(3)-C(2)-Br(1)	124.84(15)	C(25)-C(20)-C(5)	122.19(15)
C(1)-C(2)-Br(1)	126.89(13)	C(21)-C(20)-C(5)	120.99(16)
C(2)-C(3)-C(4)	107.76(16)	F(1)-C(21)-C(22)	118.77(16)
C(2)-C(3)-Br(2)	123.21(13)	F(1)-C(21)-C(20)	119.55(17)
C(4)-C(3)-Br(2)	129.02(13)	C(22)-C(21)-C(20)	121.63(17)
N(1)-C(4)-C(5)	120.88(16)	F(2)-C(22)-C(23)	119.87(18)
N(1)-C(4)-C(3)	105.61(14)	F(2)-C(22)-C(21)	120.17(18)
C(5)-C(4)-C(3)	133.51(17)	C(23)-C(22)-C(21)	119.94(17)
C(6)-C(5)-C(4)	126.60(17)	F(3)-C(23)-C(22)	120.14(18)
C(6)-C(5)-C(20)	117.69(15)	F(3)-C(23)-C(24)	120.06(19)
C(4)-C(5)-C(20)	115.70(15)	C(22)-C(23)-C(24)	119.78(18)
N(2)-C(6)-C(5)	126.18(15)	F(4)-C(24)-C(25)	121.18(18)
N(2)-C(6)-C(7)	105.08(15)	F(4)-C(24)-C(23)	119.73(19)
C(5)-C(6)-C(7)	128.74(17)	C(25)-C(24)-C(23)	119.08(18)
C(8)-C(7)-C(6)	108.54(16)	F(5)-C(25)-C(24)	117.90(17)
C(8)-C(7)-Br(3)	122.16(13)	F(5)-C(25)-C(20)	119.40(17)
C(6)-C(7)-Br(3)	129.26(14)	C(24)-C(25)-C(20)	122.69(17)
C(7)-C(8)-C(9)	108.64(15)	C(31)-C(26)-C(27)	116.39(16)
C(7)-C(8)-Br(4)	122.43(14)	C(31)-C(26)-C(10)	120.65(15)
C(9)-C(8)-Br(4)	128.92(14)	C(27)-C(26)-C(10)	122.96(15)
N(2)-C(9)-C(10)	124.59(15)	F(6)-C(27)-C(28)	118.20(15)

F(6)-C(27)-C(26)	119.42(15)	F(12)-C(34)-C(33)	121.32(17)
C(28)-C(27)-C(26)	122.38(16)	F(12)-C(34)-C(35)	119.68(18)
F(7)-C(28)-C(27)	120.86(16)	C(33)-C(34)-C(35)	119.00(18)
F(7)-C(28)-C(29)	119.62(16)	F(13)-C(35)-C(36)	120.29(18)
C(27)-C(28)-C(29)	119.51(16)	F(13)-C(35)-C(34)	119.72(19)
F(8)-C(29)-C(28)	120.62(16)	C(36)-C(35)-C(34)	119.99(19)
F(8)-C(29)-C(30)	120.02(16)	F(14)-C(36)-C(35)	119.39(19)
C(28)-C(29)-C(30)	119.36(16)	F(14)-C(36)-C(37)	120.47(19)
F(9)-C(30)-C(31)	121.11(16)	C(35)-C(36)-C(37)	120.13(18)
F(9)-C(30)-C(29)	118.98(16)	F(15)-C(37)-C(36)	119.48(16)
C(31)-C(30)-C(29)	119.90(16)	F(15)-C(37)-C(32)	119.03(17)
F(10)-C(31)-C(30)	117.99(15)	C(36)-C(37)-C(32)	121.48(18)
F(10)-C(31)-C(26)	119.55(15)	Cl(2)-C(51)-Cl(1)	113.23(14)
C(30)-C(31)-C(26)	122.45(16)	Cl(4)-C(52)-Cl(3)	114.43(17)
C(33)-C(32)-C(37)	116.86(17)	Cl(5A)-C(53)-Cl(6B)	153.0(2)
C(33)-C(32)-C(15)	122.33(16)	Cl(5A)-C(53)-Cl(6A)	121.1(2)
C(37)-C(32)-C(15)	120.81(16)	Cl(6B)-C(53)-Cl(6A)	53.20(12)
F(11)-C(33)-C(34)	118.05(17)	Cl(5A)-C(53)-Cl(5B)	63.30(15)
F(11)-C(33)-C(32)	119.44(17)	Cl(6B)-C(53)-Cl(5B)	108.72(16)
C(34)-C(33)-C(32)	122.48(17)	Cl(6A)-C(53)-Cl(5B)	58.54(12)

---

Table C-2-5. Anisotropic displacement parameters ( $\text{\AA}^2 \times 10^4$ ) for **1b-Ir(tma)<sub>2</sub>** (CCDC 675602). The anisotropic displacement factor exponent takes the form:  $-2\pi^2 [h^2 a^{*2} U^{11} + \dots + 2 h k a^* b^* U^{12}]$ .

	U <sup>11</sup>	U <sup>22</sup>	U <sup>33</sup>	U <sup>23</sup>	U <sup>13</sup>	U <sup>12</sup>
Ir(1)	107(1)	77(1)	142(1)	-10(1)	-5(1)	-15(1)
Br(1)	276(1)	182(1)	147(1)	-38(1)	18(1)	-67(1)
Br(2)	254(1)	174(1)	170(1)	-11(1)	22(1)	-93(1)
Br(3)	279(1)	253(1)	190(1)	-6(1)	-46(1)	-175(1)
Br(4)	212(1)	223(1)	160(1)	-10(1)	-49(1)	-91(1)
Br(5)	169(1)	202(1)	168(1)	8(1)	4(1)	-76(1)
Br(6)	212(1)	155(1)	208(1)	17(1)	-16(1)	-93(1)
Br(7)	262(1)	216(1)	281(1)	-65(1)	-47(1)	-90(1)
Br(8)	251(1)	195(1)	177(1)	-45(1)	-37(1)	-44(1)
F(1)	154(5)	187(6)	337(6)	-80(5)	-16(5)	28(5)
F(2)	429(8)	105(5)	273(6)	-58(5)	-81(6)	-2(5)
F(3)	395(8)	264(7)	271(6)	11(5)	-39(6)	-252(6)
F(4)	129(6)	456(8)	385(7)	-15(6)	-2(5)	-118(5)
F(5)	172(6)	221(6)	404(7)	-18(5)	-27(5)	56(5)
F(6)	182(6)	279(7)	237(6)	-47(5)	-62(5)	89(5)
F(7)	168(6)	330(7)	220(5)	-92(5)	-4(4)	55(5)
F(8)	256(6)	321(7)	135(5)	4(5)	-19(4)	4(5)
F(9)	243(7)	295(7)	223(6)	25(5)	-87(5)	94(5)
F(10)	166(6)	262(6)	209(5)	-33(5)	-12(4)	89(5)
F(11)	170(6)	234(6)	355(7)	-48(5)	-83(5)	51(5)
F(12)	122(5)	433(8)	319(6)	-62(6)	-43(5)	-108(5)
F(13)	299(7)	249(7)	388(7)	-80(6)	-8(6)	-194(5)
F(14)	266(7)	110(6)	821(11)	-118(7)	11(7)	-20(5)
F(15)	110(5)	137(6)	690(10)	-72(6)	-6(6)	-14(4)
N(1)	141(7)	89(6)	150(6)	-11(5)	-20(5)	-20(5)
N(2)	142(7)	113(7)	143(6)	-15(5)	3(5)	-28(5)
N(3)	107(6)	88(6)	165(6)	-14(5)	0(5)	-23(5)
N(4)	145(7)	103(7)	171(6)	-10(5)	-22(5)	-31(5)
N(5)	138(7)	118(7)	189(7)	-11(5)	-2(5)	7(5)
N(6)	146(7)	112(7)	227(7)	-11(6)	-28(6)	-3(6)
C(1)	150(8)	109(8)	147(7)	-21(6)	-4(6)	-4(6)
C(2)	172(8)	124(8)	148(7)	-19(6)	1(6)	-14(6)
C(3)	140(8)	107(8)	180(8)	-8(6)	6(6)	-16(6)
C(4)	116(7)	86(7)	185(7)	-16(6)	-9(6)	-3(6)
C(5)	110(7)	88(7)	179(7)	-15(6)	12(6)	-6(6)
C(6)	126(7)	107(8)	165(7)	-15(6)	-9(6)	-23(6)
C(7)	142(8)	130(8)	189(8)	-18(6)	-23(6)	-54(6)
C(8)	150(8)	160(9)	154(7)	-27(6)	-29(6)	-25(6)
C(9)	113(7)	112(8)	175(7)	-9(6)	-14(6)	-23(6)
C(10)	114(7)	118(8)	159(7)	-5(6)	-16(6)	-3(6)
C(11)	98(7)	99(8)	174(7)	0(6)	-7(6)	3(6)
C(12)	119(7)	125(8)	159(7)	20(6)	-10(6)	-2(6)
C(13)	105(7)	90(7)	208(8)	6(6)	-21(6)	-9(6)
C(14)	104(7)	85(7)	193(8)	-8(6)	-14(6)	5(6)
C(15)	111(7)	106(8)	203(8)	-22(6)	-5(6)	1(6)
C(16)	123(7)	106(8)	197(8)	-20(6)	-15(6)	-11(6)
C(17)	156(8)	123(8)	213(8)	-56(7)	-20(6)	-26(6)



C(18)	178(8)	122(8)	190(8)	-48(6)	-25(6)	-5(7)
C(19)	155(8)	123(8)	170(7)	-25(6)	-18(6)	-8(6)
C(20)	124(7)	109(8)	151(7)	-18(6)	-2(6)	-37(6)
C(21)	138(8)	140(8)	169(7)	-41(6)	-7(6)	-22(6)
C(22)	274(10)	108(8)	162(8)	-23(6)	-51(7)	-39(7)
C(23)	272(10)	208(10)	144(8)	0(7)	-35(7)	-148(8)
C(24)	148(8)	296(11)	196(8)	-14(8)	-4(7)	-78(7)
C(25)	143(8)	160(9)	193(8)	-9(7)	-12(6)	-13(7)
C(26)	124(7)	124(8)	163(7)	-3(6)	-8(6)	-27(6)
C(27)	123(7)	146(8)	191(8)	-7(6)	-29(6)	2(6)
C(28)	126(8)	191(9)	186(8)	-37(7)	9(6)	-7(7)
C(29)	168(8)	205(9)	147(7)	4(6)	-11(6)	-30(7)
C(30)	146(8)	164(9)	196(8)	25(7)	-40(6)	11(7)
C(31)	127(8)	136(8)	178(7)	5(6)	-2(6)	6(6)
C(32)	120(7)	131(8)	193(8)	-36(6)	-2(6)	-36(6)
C(33)	124(8)	187(9)	189(8)	-39(7)	-7(6)	-14(7)
C(34)	121(8)	295(11)	185(8)	-54(7)	-10(6)	-69(7)
C(35)	216(9)	200(10)	248(9)	-66(8)	8(7)	-125(7)
C(36)	174(9)	132(9)	390(11)	-78(8)	25(8)	-39(7)
C(37)	101(7)	137(9)	342(10)	-61(7)	11(7)	-30(6)
C(38)	255(12)	306(13)	744(19)	-363(13)	-220(13)	142(10)
C(39)	141(9)	173(10)	442(12)	-25(9)	-81(8)	-12(7)
C(40)	314(14)	501(16)	371(13)	260(11)	116(10)	263(13)
C(41)	484(16)	506(16)	183(9)	-82(10)	-62(10)	369(14)
C(42)	148(11)	165(12)	1890(40)	-226(19)	-310(19)	36(9)
C(43)	299(12)	375(13)	201(9)	89(9)	3(8)	183(10)
C(51)	294(13)	344(13)	441(14)	38(11)	-160(11)	-26(10)
Cl(1)	263(3)	385(3)	561(4)	75(3)	-177(3)	-59(2)
Cl(2)	357(4)	439(4)	939(6)	212(4)	-351(4)	-142(3)
C(52)	730(20)	363(16)	400(15)	20(12)	28(14)	-6(15)
Cl(3)	510(4)	625(5)	329(3)	-29(3)	-55(3)	-61(4)
Cl(4)	449(4)	512(5)	669(5)	-5(4)	97(4)	-144(3)
C(53)	680(20)	389(17)	439(16)	-86(13)	63(15)	61(15)
Cl(5A)	495(9)	594(10)	576(9)	-269(7)	-42(7)	-169(7)
Cl(6A)	584(10)	370(8)	548(8)	-87(6)	185(7)	-46(6)
Cl(5B)	313(7)	568(9)	330(6)	-77(6)	-73(5)	78(6)
Cl(6B)	396(8)	577(10)	763(11)	-344(9)	-234(8)	84(7)

---

CALIFORNIA INSTITUTE OF TECHNOLOGY  
BECKMAN INSTITUTE  
X-RAY CRYSTALLOGRAPHY LABORATORY

Date 24 January 2008

**Crystal Structure Analysis of:**

**1-Ir(py)<sub>2</sub>**

(shown below)

**For** Investigator: Joshua Palmer ext. 6332

Advisor: H. B. Gray ext. 6500

Account Number: HGB.BP-1-BP.AMOCO

**By** Michael W. Day 116 Beckman ext. 2734

e-mail: mikeday@caltech.edu

Contents

Table 1. Crystal data

Figures Minimum overlap

Table 2. Atomic Coordinates

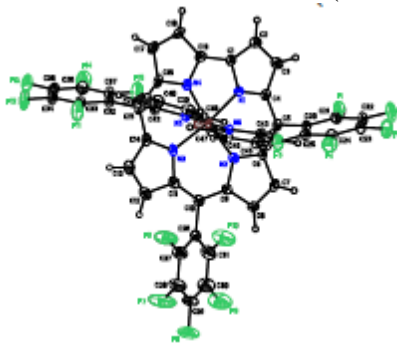
Table 3. Selected bond distances and angles

Table 4. Full bond distances and angles

Table 5. Anisotropic displacement parameters

Table 6. Hydrogen bond distances and angles

Table 7. Observed and calculated structure factors (available upon request)



**1-Ir(py)<sub>2</sub>**

**Note:** The crystallographic data have been deposited in the Cambridge Database (CCDC) and have been placed on hold pending further instructions from me. The deposition number is 657603. Ideally the CCDC would like the publication to contain a footnote of the type: "Crystallographic data have been deposited at the CCDC, 12 Union Road, Cambridge CB2 1EZ, UK, and copies can be obtained on request, free of charge, by quoting the publication citation and the deposition number 657603".

Table C-3-1. Crystal data and structure refinement for **1-Ir(py)<sub>2</sub>** (CCDC 657603)

Empirical formula	C <sub>47</sub> H <sub>18</sub> N <sub>6</sub> F <sub>15</sub> Ir, 3(CH <sub>4</sub> O)	
Formula weight	1240.00	
Crystallization Solvent	Methanol	
Crystal Habit	Column	
Crystal size	0.31 x 0.12 x 0.07 mm <sup>3</sup>	
Crystal color	Dark red	
<b>Data Collection</b>		
Type of diffractometer	Bruker KAPPA APEX II	
Wavelength	0.71073 Å MoKα	
Data Collection Temperature	100(2) K	
θ range for 9608 reflections used in lattice determination	2.39 to 32.74°	
Unit cell dimensions	a = 48.016(2) Å b = 8.7249(4) Å c = 27.2703(13) Å	β = 124.247(2)°
Volume	9443.7(8) Å <sup>3</sup>	
Z	8	
Crystal system	Monoclinic	
Space group	C2/c	
Density (calculated)	1.744 Mg/m <sup>3</sup>	
F(000)	4864	
θ range for data collection	1.81 to 32.95°	
Completeness to θ = 32.95°	98.5 %	
Index ranges	-73 ≤ h ≤ 72, -11 ≤ k ≤ 13, -40 ≤ l ≤ 41	
Data collection scan type	ω scans; 21 settings	
Reflections collected	112588	
Independent reflections	17484 [R <sub>int</sub> = 0.0721]	
Absorption coefficient	2.938 mm <sup>-1</sup>	
Absorption correction	None	
Max. and min. transmission (calc)	0.8208 and 0.4628	

Table C-3-1 cont.

### Structure Solution and Refinement

Structure solution program	SHELXS-97 (Sheldrick, 1990)
Primary solution method	Patterson method
Secondary solution method	Difference Fourier map
Hydrogen placement	Geometric positions
Structure refinement program	SHELXL-97 (Sheldrick, 1997)
Refinement method	Full matrix least-squares on $F^2$
Data / restraints / parameters	17484 / 54 / 695
Treatment of hydrogen atoms	Riding
Goodness-of-fit on $F^2$	1.520
Final R indices [ $I > 2\sigma(I)$ , 12341 reflections]	$R1 = 0.0441$ , $wR2 = 0.0563$
R indices (all data)	$R1 = 0.0761$ , $wR2 = 0.0580$
Type of weighting scheme used	Sigma
Weighting scheme used	$w = 1/\sigma^2(F_o^2)$
Max shift/error	0.007
Average shift/error	0.000
Largest diff. peak and hole	4.237 and -2.827 e.Å <sup>-3</sup>

### Special Refinement Details

Crystals were mounted on a glass fiber using Paratone oil then placed on the diffractometer under a nitrogen stream at 100K.

The crystals contain methanol as a solvent of crystallization—three in the asymmetric unit. One of those three is disordered between two positions. The disorder was modeled with restraint on the C-O bond distances and on the anisotropic displacement parameters (ADP). In the solvent only C-O distances were restrained to have similar distances, the ADPs were restrained to mimic isotropic behavior, and for the disordered site the population was restrained so the occupancies summed to one.

Refinement of  $F^2$  against ALL reflections. The weighted R-factor ( $wR$ ) and goodness of fit ( $S$ ) are based on  $F^2$ , conventional R-factors ( $R$ ) are based on  $F$ , with  $F$  set to zero for



negative  $F^2$ . The threshold expression of  $F^2 > 2\sigma(F^2)$  is used only for calculating R-factors(gt), etc., and is not relevant to the choice of reflections for refinement. R-factors based on  $F^2$  are statistically about twice as large as those based on  $F$ , and R-factors based on ALL data will be even larger.

All esds (except the esd in the dihedral angle between two l.s. planes) are estimated using the full covariance matrix. The cell esds are taken into account individually in the estimation of esds in distances, angles, and torsion angles; correlations between esds in cell parameters are only used when they are defined by crystal symmetry. An approximate (isotropic) treatment of cell esds is used for estimating esds involving l.s. planes.

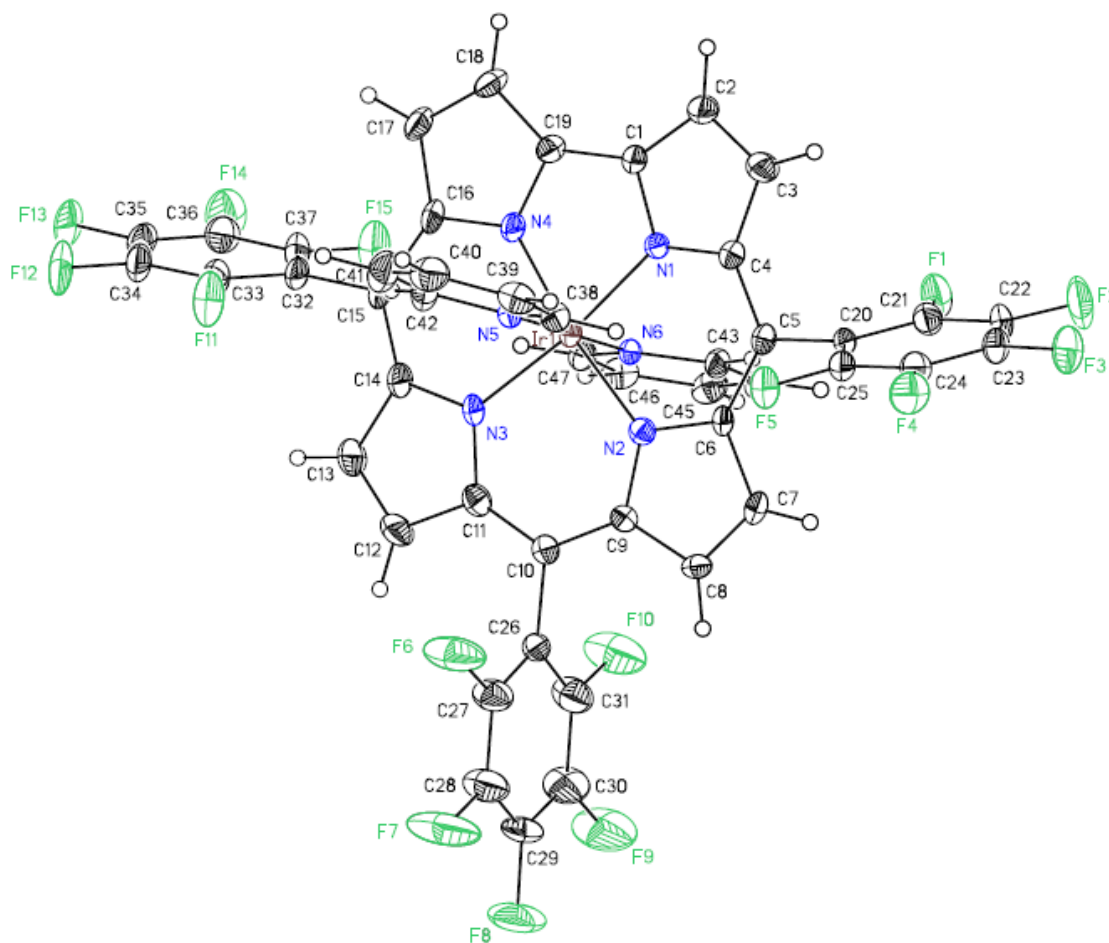


Table C-3-2. Atomic coordinates ( $\times 10^4$ ) and equivalent isotropic displacement parameters ( $\text{\AA}^2 \times 10^3$ ) for **1-Ir(py)<sub>2</sub>** (CCDC 657603).  $U_{eq}$  is defined as the trace of the orthogonalized  $U_{ij}$  tensor.

	x	y	z		$U_{eq}$
Ir(1)	5966(1)	2657(1)	37(1)	17(1)	1
F(1)	5516(1)	3864(2)	1516(1)	36(1)	1
F(2)	5321(1)	2868(2)	2209(1)	50(1)	1
F(3)	5304(1)	-171(2)	2394(1)	45(1)	1
F(4)	5495(1)	-2227(2)	1892(1)	36(1)	1
F(5)	5695(1)	-1256(2)	1201(1)	29(1)	1
F(6)	7064(1)	-1186(2)	1111(1)	60(1)	1
F(7)	7708(1)	-1870(2)	1935(1)	79(1)	1
F(8)	8128(1)	299(2)	2706(1)	67(1)	1
F(9)	7893(1)	3140(2)	2662(1)	79(1)	1
F(10)	7246(1)	3836(2)	1831(1)	66(1)	1
F(11)	6131(1)	1475(2)	-1786(1)	44(1)	1
F(12)	6229(1)	2374(2)	-2618(1)	48(1)	1
F(13)	6261(1)	5398(2)	-2813(1)	44(1)	1
F(14)	6212(1)	7524(2)	-2139(1)	50(1)	1
F(15)	6118(1)	6640(2)	-1299(1)	44(1)	1
N(1)	5548(1)	2875(2)	-7(1)	18(1)	1
N(2)	6212(1)	1834(2)	853(1)	17(1)	1
N(3)	6356(1)	2535(3)	-27(1)	21(1)	1
N(4)	5672(1)	3499(2)	-758(1)	19(1)	1
N(5)	5804(1)	504(2)	-333(1)	19(1)	1
N(6)	6125(1)	4806(2)	395(1)	17(1)	1
C(1)	5268(1)	3338(3)	-542(1)	20(1)	1
C(2)	4995(1)	3231(3)	-476(2)	26(1)	1
C(3)	5117(1)	2679(3)	84(1)	27(1)	1
C(4)	5474(1)	2447(3)	381(1)	19(1)	1
C(5)	5725(1)	1839(3)	948(1)	19(1)	1
C(6)	6070(1)	1600(3)	1170(1)	16(1)	1
C(7)	6342(1)	1145(3)	1757(1)	19(1)	1
C(8)	6631(1)	1139(3)	1778(1)	19(1)	1
C(9)	6552(1)	1570(3)	1205(1)	16(1)	1
C(10)	6765(1)	1702(3)	1000(1)	21(1)	1
C(11)	6678(1)	2154(3)	440(2)	25(1)	1
C(12)	6893(1)	2367(4)	223(2)	38(1)	1
C(13)	6694(1)	2873(3)	-344(2)	35(1)	1
C(14)	6351(1)	2996(3)	-511(2)	26(1)	1
C(15)	6066(1)	3559(3)	-1046(1)	24(1)	1
C(16)	5735(1)	3776(3)	-1179(1)	21(1)	1
C(17)	5416(1)	4175(3)	-1707(1)	25(1)	1
C(18)	5178(1)	4109(3)	-1579(1)	24(1)	1
C(19)	5340(1)	3684(3)	-977(1)	19(1)	1
C(20)	5612(1)	1341(3)	1330(1)	19(1)	1
C(21)	5509(1)	2351(3)	1595(1)	24(1)	1
C(22)	5406(1)	1847(3)	1947(2)	30(1)	1
C(23)	5399(1)	318(4)	2045(2)	30(1)	1
C(24)	5497(1)	-717(3)	1791(2)	25(1)	1
C(25)	5602(1)	-200(3)	1442(1)	23(1)	1

C(26)	7129(1)	1337(3)	1446(1)	21(1)	1
C(27)	7262(1)	-81(3)	1490(2)	33(1)	1
C(28)	7595(1)	-444(4)	1909(2)	42(1)	1
C(29)	7804(1)	637(4)	2292(2)	40(1)	1
C(30)	7686(1)	2067(4)	2269(2)	43(1)	1
C(31)	7352(1)	2408(4)	1847(2)	37(1)	1
C(32)	6117(1)	4024(3)	-1516(2)	24(1)	1
C(33)	6151(1)	2980(3)	-1861(2)	30(1)	1
C(34)	6201(1)	3435(4)	-2291(2)	32(1)	1
C(35)	6219(1)	4956(4)	-2390(2)	32(1)	1
C(36)	6187(1)	6030(4)	-2054(2)	32(1)	1
C(37)	6140(1)	5553(3)	-1626(2)	30(1)	1
C(38)	5692(1)	-525(3)	-113(2)	24(1)	1
C(39)	5561(1)	-1926(3)	-378(2)	29(1)	1
C(40)	5536(1)	-2285(3)	-893(2)	33(1)	1
C(41)	5648(1)	-1245(3)	-1120(2)	35(1)	1
C(42)	5780(1)	122(3)	-832(2)	29(1)	1
C(43)	6110(1)	5276(3)	851(1)	20(1)	1
C(44)	6235(1)	6665(3)	1127(1)	26(1)	1
C(45)	6378(1)	7628(3)	929(1)	27(1)	1
C(46)	6387(1)	7189(3)	451(2)	26(1)	1
C(47)	6258(1)	5777(3)	192(1)	22(1)	1
<hr/>					
C(51)	7183(5)	6190(20)	349(12)	179(11)	0.314(3)
O(51)	7428(5)	5226(18)	363(9)	202(8)	0.314(3)
<hr/>					
C(52)	7911(1)	9259(6)	1017(3)	122(2)	1
O(52)	7660(1)	10415(4)	759(2)	123(2)	1
<hr/>					
C(53)	6840(2)	8859(7)	9592(4)	84(2)	0.686(3)
O(53)	7116(1)	9625(4)	9631(2)	83(2)	0.686(3)
<hr/>					
C(54)	6988(2)	865(6)	8397(3)	131(2)	1
O(54)	7050(1)	1778(4)	8876(2)	133(2)	1

Table C-3-3. Selected bond lengths [Å] and angles [°] for **1-Ir(py)<sub>2</sub>** (CCDC 657603)

Ir(1)-N(4)	1.947(2)	N(4)-Ir(1)-N(1)	79.55(10)
Ir(1)-N(1)	1.953(2)	N(4)-Ir(1)-N(2)	172.23(10)
Ir(1)-N(2)	1.976(2)	N(1)-Ir(1)-N(2)	92.69(10)
Ir(1)-N(3)	1.979(2)	N(4)-Ir(1)-N(3)	92.92(10)
Ir(1)-N(6)	2.052(2)	N(1)-Ir(1)-N(3)	172.47(10)
Ir(1)-N(5)	2.066(2)	N(2)-Ir(1)-N(3)	94.84(10)
		N(4)-Ir(1)-N(6)	91.55(9)
		N(1)-Ir(1)-N(6)	91.87(9)
		N(2)-Ir(1)-N(6)	88.27(9)
		N(3)-Ir(1)-N(6)	88.60(9)
		N(4)-Ir(1)-N(5)	87.80(9)
		N(1)-Ir(1)-N(5)	88.04(9)
		N(2)-Ir(1)-N(5)	92.38(9)
		N(3)-Ir(1)-N(5)	91.41(9)
		N(6)-Ir(1)-N(5)	179.34(12)

Table C-3-4. Bond lengths [Å] and angles [°] for **1-Ir(tma)<sub>2</sub>** (CCDC 671270)

Ir(1)-N(4)	1.947(2)	C(15)-C(32)	1.494(4)
Ir(1)-N(1)	1.953(2)	C(16)-C(17)	1.434(4)
Ir(1)-N(2)	1.976(2)	C(17)-C(18)	1.370(4)
Ir(1)-N(3)	1.979(2)	C(18)-C(19)	1.416(4)
Ir(1)-N(6)	2.052(2)	C(20)-C(25)	1.386(4)
Ir(1)-N(5)	2.066(2)	C(20)-C(21)	1.396(4)
F(1)-C(21)	1.340(3)	C(21)-C(22)	1.376(4)
F(2)-C(22)	1.342(3)	C(22)-C(23)	1.366(4)
F(3)-C(23)	1.335(3)	C(23)-C(24)	1.372(4)
F(4)-C(24)	1.346(3)	C(24)-C(25)	1.382(4)
F(5)-C(25)	1.344(3)	C(26)-C(27)	1.365(4)
F(6)-C(27)	1.340(3)	C(26)-C(31)	1.377(4)
F(7)-C(28)	1.344(3)	C(27)-C(28)	1.381(5)
F(8)-C(29)	1.343(4)	C(28)-C(29)	1.345(5)
F(9)-C(30)	1.348(3)	C(29)-C(30)	1.358(4)
F(10)-C(31)	1.338(3)	C(30)-C(31)	1.381(5)
F(11)-C(33)	1.341(3)	C(32)-C(33)	1.383(4)
F(12)-C(34)	1.344(3)	C(32)-C(37)	1.384(4)
F(13)-C(35)	1.337(4)	C(33)-C(34)	1.383(4)
F(14)-C(36)	1.342(3)	C(34)-C(35)	1.365(4)
F(15)-C(37)	1.347(3)	C(35)-C(36)	1.378(4)
N(1)-C(4)	1.348(3)	C(36)-C(37)	1.369(4)
N(1)-C(1)	1.375(4)	C(38)-C(39)	1.378(4)
N(2)-C(9)	1.368(3)	C(39)-C(40)	1.374(5)
N(2)-C(6)	1.387(4)	C(40)-C(41)	1.368(4)
N(3)-C(14)	1.367(4)	C(41)-C(42)	1.371(4)
N(3)-C(11)	1.378(4)	C(43)-C(44)	1.373(4)
N(4)-C(19)	1.361(3)	C(44)-C(45)	1.373(4)
N(4)-C(16)	1.362(4)	C(45)-C(46)	1.383(4)
N(5)-C(42)	1.343(4)	C(46)-C(47)	1.381(4)
N(5)-C(38)	1.350(4)	C(51)-O(51)	1.425(5)
N(6)-C(43)	1.347(4)	C(52)-O(52)	1.418(4)
N(6)-C(47)	1.353(3)	C(53)-O(53)	1.432(4)
C(1)-C(2)	1.426(4)	C(54)-O(54)	1.410(4)
C(1)-C(19)	1.442(4)		
C(2)-C(3)	1.378(4)	N(4)-Ir(1)-N(1)	79.55(10)
C(3)-C(4)	1.437(4)	N(4)-Ir(1)-N(2)	172.23(10)
C(4)-C(5)	1.424(4)	N(1)-Ir(1)-N(2)	92.69(10)
C(5)-C(6)	1.422(4)	N(4)-Ir(1)-N(3)	92.92(10)
C(5)-C(20)	1.482(4)	N(1)-Ir(1)-N(3)	172.47(10)
C(6)-C(7)	1.440(4)	N(2)-Ir(1)-N(3)	94.84(10)
C(7)-C(8)	1.359(4)	N(4)-Ir(1)-N(6)	91.55(9)
C(8)-C(9)	1.433(4)	N(1)-Ir(1)-N(6)	91.87(9)
C(9)-C(10)	1.421(4)	N(2)-Ir(1)-N(6)	88.27(9)
C(10)-C(11)	1.395(4)	N(3)-Ir(1)-N(6)	88.60(9)
C(10)-C(26)	1.497(4)	N(4)-Ir(1)-N(5)	87.80(9)
C(11)-C(12)	1.462(4)	N(1)-Ir(1)-N(5)	88.04(9)
C(12)-C(13)	1.354(5)	N(2)-Ir(1)-N(5)	92.38(9)
C(13)-C(14)	1.445(4)	N(3)-Ir(1)-N(5)	91.41(9)
C(14)-C(15)	1.413(4)	N(6)-Ir(1)-N(5)	179.34(12)
C(15)-C(16)	1.427(4)	C(4)-N(1)-C(1)	112.4(2)



C(4)-N(1)-Ir(1)	130.07(19)	C(17)-C(18)-C(19)	108.2(3)
C(1)-N(1)-Ir(1)	116.8(2)	N(4)-C(19)-C(18)	106.4(3)
C(9)-N(2)-C(6)	110.5(2)	N(4)-C(19)-C(1)	112.3(3)
C(9)-N(2)-Ir(1)	124.9(2)	C(18)-C(19)-C(1)	141.2(3)
C(6)-N(2)-Ir(1)	124.27(19)	C(25)-C(20)-C(21)	115.5(3)
C(14)-N(3)-C(11)	111.4(2)	C(25)-C(20)-C(5)	120.8(3)
C(14)-N(3)-Ir(1)	124.5(2)	C(21)-C(20)-C(5)	123.7(2)
C(11)-N(3)-Ir(1)	123.62(19)	F(1)-C(21)-C(22)	118.5(3)
C(19)-N(4)-C(16)	111.8(3)	F(1)-C(21)-C(20)	119.4(3)
C(19)-N(4)-Ir(1)	118.0(2)	C(22)-C(21)-C(20)	122.1(3)
C(16)-N(4)-Ir(1)	129.7(2)	F(2)-C(22)-C(23)	119.6(3)
C(42)-N(5)-C(38)	117.3(3)	F(2)-C(22)-C(21)	119.8(3)
C(42)-N(5)-Ir(1)	120.9(2)	C(23)-C(22)-C(21)	120.6(3)
C(38)-N(5)-Ir(1)	121.6(2)	F(3)-C(23)-C(22)	120.6(3)
C(43)-N(6)-C(47)	117.9(2)	F(3)-C(23)-C(24)	120.1(3)
C(43)-N(6)-Ir(1)	121.29(19)	C(22)-C(23)-C(24)	119.3(3)
C(47)-N(6)-Ir(1)	120.8(2)	F(4)-C(24)-C(23)	119.9(3)
N(1)-C(1)-C(2)	105.5(3)	F(4)-C(24)-C(25)	120.4(3)
N(1)-C(1)-C(19)	113.0(3)	C(23)-C(24)-C(25)	119.7(3)
C(2)-C(1)-C(19)	141.4(3)	F(5)-C(25)-C(24)	117.6(2)
C(3)-C(2)-C(1)	108.2(3)	F(5)-C(25)-C(20)	119.7(3)
C(2)-C(3)-C(4)	107.8(3)	C(24)-C(25)-C(20)	122.8(3)
N(1)-C(4)-C(5)	121.2(3)	C(27)-C(26)-C(31)	115.5(3)
N(1)-C(4)-C(3)	106.0(3)	C(27)-C(26)-C(10)	122.6(3)
C(5)-C(4)-C(3)	132.7(3)	C(31)-C(26)-C(10)	122.0(3)
C(6)-C(5)-C(4)	126.1(3)	F(6)-C(27)-C(26)	119.3(3)
C(6)-C(5)-C(20)	117.1(3)	F(6)-C(27)-C(28)	117.6(3)
C(4)-C(5)-C(20)	116.7(3)	C(26)-C(27)-C(28)	123.1(3)
N(2)-C(6)-C(5)	125.4(3)	F(7)-C(28)-C(29)	120.4(3)
N(2)-C(6)-C(7)	106.0(2)	F(7)-C(28)-C(27)	120.1(3)
C(5)-C(6)-C(7)	128.6(3)	C(29)-C(28)-C(27)	119.5(3)
C(8)-C(7)-C(6)	108.4(3)	F(8)-C(29)-C(28)	120.3(3)
C(7)-C(8)-C(9)	108.3(3)	F(8)-C(29)-C(30)	119.8(3)
N(2)-C(9)-C(10)	123.3(3)	C(28)-C(29)-C(30)	119.8(3)
N(2)-C(9)-C(8)	106.8(2)	F(9)-C(30)-C(29)	119.9(3)
C(10)-C(9)-C(8)	129.9(3)	F(9)-C(30)-C(31)	120.3(3)
C(11)-C(10)-C(9)	127.9(3)	C(29)-C(30)-C(31)	119.8(3)
C(11)-C(10)-C(26)	116.4(3)	F(10)-C(31)-C(26)	119.7(3)
C(9)-C(10)-C(26)	115.7(3)	F(10)-C(31)-C(30)	118.0(3)
N(3)-C(11)-C(10)	124.8(3)	C(26)-C(31)-C(30)	122.3(3)
N(3)-C(11)-C(12)	105.9(3)	C(33)-C(32)-C(37)	115.7(3)
C(10)-C(11)-C(12)	129.3(3)	C(33)-C(32)-C(15)	123.0(3)
C(13)-C(12)-C(11)	107.5(3)	C(37)-C(32)-C(15)	121.3(3)
C(12)-C(13)-C(14)	109.1(3)	F(11)-C(33)-C(34)	118.2(3)
N(3)-C(14)-C(15)	125.3(3)	F(11)-C(33)-C(32)	119.7(3)
N(3)-C(14)-C(13)	106.0(3)	C(34)-C(33)-C(32)	122.1(3)
C(15)-C(14)-C(13)	128.6(3)	F(12)-C(34)-C(35)	120.0(3)
C(14)-C(15)-C(16)	127.1(3)	F(12)-C(34)-C(33)	119.7(3)
C(14)-C(15)-C(32)	116.5(3)	C(35)-C(34)-C(33)	120.3(3)
C(16)-C(15)-C(32)	116.4(3)	F(13)-C(35)-C(34)	120.3(3)
N(4)-C(16)-C(15)	120.3(3)	F(13)-C(35)-C(36)	120.4(3)
N(4)-C(16)-C(17)	105.7(3)	C(34)-C(35)-C(36)	119.3(3)
C(15)-C(16)-C(17)	133.9(3)	F(14)-C(36)-C(37)	121.2(3)
C(18)-C(17)-C(16)	107.9(3)	F(14)-C(36)-C(35)	119.4(3)

C(37)-C(36)-C(35)	119.4(3)	C(40)-C(41)-C(42)	119.4(3)
F(15)-C(37)-C(36)	117.5(3)	N(5)-C(42)-C(41)	122.9(3)
F(15)-C(37)-C(32)	119.3(3)	N(6)-C(43)-C(44)	122.8(3)
C(36)-C(37)-C(32)	123.3(3)	C(43)-C(44)-C(45)	119.0(3)
N(5)-C(38)-C(39)	122.2(3)	C(44)-C(45)-C(46)	119.2(3)
C(40)-C(39)-C(38)	119.4(3)	C(47)-C(46)-C(45)	119.2(3)
C(41)-C(40)-C(39)	118.7(3)	N(6)-C(47)-C(46)	121.9(3)

---

Table C-3-5. Anisotropic displacement parameters ( $\text{\AA}^2 \times 10^4$ ) for **1-Ir(py)<sub>2</sub>** (CCDC 657603). The anisotropic displacement factor exponent takes the form:  $-2\pi^2 [h^2 a^{*2} U^{11} + \dots + 2 h k a^* b^* U^{12}]$ .

	U <sup>11</sup>	U <sup>22</sup>	U <sup>33</sup>	U <sup>23</sup>	U <sup>13</sup>	U <sup>12</sup>
Ir(1)	170(1)	230(1)	136(1)	13(1)	103(1)	8(1)
F(1)	488(14)	323(10)	423(14)	21(8)	345(12)	83(8)
F(2)	695(16)	565(12)	531(15)	27(10)	528(14)	154(10)
F(3)	524(15)	679(13)	383(14)	115(10)	396(14)	18(10)
F(4)	411(12)	362(10)	380(12)	95(9)	266(11)	-37(9)
F(5)	405(12)	266(9)	325(12)	-23(8)	277(11)	-17(8)
F(6)	274(13)	413(12)	699(19)	-202(11)	25(13)	32(9)
F(7)	323(14)	533(13)	950(20)	-92(13)	21(15)	173(10)
F(8)	167(13)	908(16)	600(20)	-107(13)	19(13)	68(11)
F(9)	318(14)	775(15)	830(20)	-448(14)	53(15)	-113(11)
F(10)	357(14)	452(12)	840(20)	-272(12)	138(15)	1(10)
F(11)	701(16)	372(11)	456(15)	-71(9)	462(14)	-80(10)
F(12)	677(15)	607(12)	393(13)	-136(11)	444(13)	-73(11)
F(13)	524(15)	686(13)	313(13)	85(10)	359(13)	-10(10)
F(14)	695(15)	452(11)	523(15)	125(11)	451(14)	32(11)
F(15)	680(16)	386(10)	460(15)	-35(10)	447(14)	-17(10)
N(1)	145(13)	257(13)	150(13)	20(10)	94(12)	1(9)
N(2)	181(14)	153(11)	176(14)	-2(9)	101(12)	7(9)
N(3)	217(13)	287(13)	190(13)	-5(11)	158(12)	7(11)
N(4)	195(14)	243(12)	159(14)	11(10)	122(12)	-11(10)
N(5)	177(14)	258(13)	160(14)	16(10)	106(13)	44(10)
N(6)	155(14)	258(12)	133(13)	37(10)	99(12)	27(10)
C(1)	192(17)	252(15)	160(16)	-3(12)	109(15)	3(12)
C(2)	167(17)	393(17)	202(18)	-19(14)	89(16)	-22(13)
C(3)	190(16)	356(17)	261(17)	34(15)	134(15)	1(14)
C(4)	207(15)	223(14)	163(14)	12(13)	112(13)	12(13)
C(5)	230(17)	200(14)	167(16)	11(11)	136(15)	-12(11)
C(6)	220(17)	155(13)	165(16)	-3(11)	143(14)	1(11)
C(7)	283(19)	176(14)	150(16)	-16(11)	139(16)	-8(12)
C(8)	152(16)	200(14)	165(17)	11(11)	57(14)	17(11)
C(9)	160(16)	145(13)	185(16)	1(11)	101(14)	-12(11)
C(10)	197(17)	264(15)	202(18)	8(12)	125(15)	11(12)
C(11)	210(17)	314(16)	266(18)	-1(13)	166(16)	-16(13)
C(12)	240(18)	640(20)	330(20)	114(19)	209(17)	117(18)
C(13)	320(20)	550(20)	300(20)	86(16)	257(19)	50(16)
C(14)	269(19)	370(18)	225(18)	19(13)	194(17)	-3(13)
C(15)	300(20)	293(16)	179(17)	-13(13)	174(17)	-16(13)
C(16)	275(19)	255(15)	157(17)	-21(12)	157(16)	-46(12)
C(17)	280(20)	327(17)	139(17)	4(13)	115(16)	-29(13)
C(18)	208(18)	318(16)	132(17)	21(12)	54(15)	-35(12)
C(19)	186(17)	208(14)	168(17)	-1(11)	87(15)	-15(11)
C(20)	148(16)	288(16)	151(16)	11(12)	104(14)	11(12)
C(21)	260(17)	262(16)	246(16)	27(14)	164(15)	39(13)
C(22)	300(20)	444(19)	260(20)	-14(14)	216(18)	77(14)
C(23)	290(20)	500(20)	240(20)	76(15)	215(18)	24(15)
C(24)	235(19)	313(17)	250(20)	61(13)	167(17)	-8(13)
C(25)	204(18)	321(17)	191(18)	-29(13)	123(16)	-1(13)

C(26)	162(17)	307(16)	191(18)	12(13)	111(15)	-13(12)
C(27)	210(20)	345(18)	360(20)	-69(15)	106(19)	-32(14)
C(28)	270(20)	390(20)	460(30)	-37(17)	120(20)	73(16)
C(29)	124(19)	600(20)	340(20)	-35(18)	58(19)	34(16)
C(30)	219(19)	480(20)	440(30)	-191(17)	96(19)	-136(16)
C(31)	266(19)	377(19)	440(20)	-70(18)	173(18)	-1(16)
C(32)	236(19)	384(18)	169(18)	6(13)	148(16)	-6(13)
C(33)	330(20)	390(19)	253(19)	-25(14)	209(18)	-59(14)
C(34)	320(20)	490(20)	230(20)	-60(16)	205(18)	-34(15)
C(35)	270(20)	550(20)	200(20)	58(16)	166(18)	-15(16)
C(36)	320(20)	393(19)	300(20)	83(15)	208(19)	12(15)
C(37)	360(20)	373(18)	250(20)	-11(14)	225(19)	37(15)
C(38)	231(19)	258(16)	233(19)	5(13)	140(16)	22(12)
C(39)	227(18)	268(17)	340(20)	1(14)	138(18)	15(13)
C(40)	299(19)	279(17)	320(20)	-65(16)	115(17)	12(15)
C(41)	470(20)	318(18)	280(20)	-36(15)	220(20)	33(15)
C(42)	390(20)	294(17)	240(20)	6(14)	213(19)	51(14)
C(43)	243(18)	232(15)	162(17)	45(12)	129(16)	58(12)
C(44)	330(20)	254(15)	170(17)	-19(13)	131(16)	32(13)
C(45)	298(17)	195(15)	237(17)	-36(14)	103(15)	-8(14)
C(46)	238(17)	230(16)	275(18)	31(13)	121(16)	-21(13)
C(47)	231(18)	266(16)	182(17)	36(12)	129(16)	16(12)
C(51)	1790(120)	1790(120)	1800(120)	-110(40)	1020(70)	30(40)
O(51)	2030(90)	1980(90)	2020(90)	0(40)	1130(60)	-20(40)
C(52)	990(30)	1390(30)	1380(40)	-20(30)	730(30)	260(30)
O(52)	1170(30)	1270(20)	1180(30)	50(20)	630(20)	240(20)
C(53)	990(40)	840(30)	820(40)	-120(30)	580(30)	-190(30)
O(53)	950(30)	880(30)	720(30)	-40(20)	500(30)	130(20)
C(54)	1430(40)	1350(40)	1220(40)	-90(30)	800(30)	-10(30)
O(54)	1610(30)	1240(20)	1190(30)	-120(20)	810(30)	180(20)

Table C-3-6. Hydrogen bonds for **1-Ir(py)<sub>2</sub>** (CCDC 657603) [Å and °]

D-H...A	d(D-H)	d(H...A)	d(D...A)	∠(DHA)
O(51)-H(51)...O(54)#1	0.84	2.25	2.791(19)	122.4
O(52)-H(52)...O(54)#2	0.84	1.89	2.714(6)	168.1
O(53)-H(53)...O(52)#3	0.84	2.04	2.777(7)	146.7
O(54)-H(54)...O(51)#1	0.84	2.25	2.791(19)	122.7

Symmetry transformations used to generate equivalent atoms:

#1 -x+3/2, -y+1/2, -z+1

#2 -x+3/2, -y+3/2, -z+1

#3 x, y, z+1

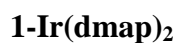


CALIFORNIA INSTITUTE OF TECHNOLOGY  
BECKMAN INSTITUTE  
X-RAY CRYSTALLOGRAPHY LABORATORY



Date 12 March 2010

**Crystal Structure Analysis of:**



(shown below)

**For** Investigator: Joshua Palmer ext. 6332  
Advisor: H. B. Gray ext. 6500  
Account Number: HGB.BP-1-BP.AMOCO  
**By** Michael W. Day 116 Beckman ext. 2734  
e-mail: mikeday@caltech.edu

Contents

Table 1. Crystal data

Figures Minimum overlap, unit cell contents

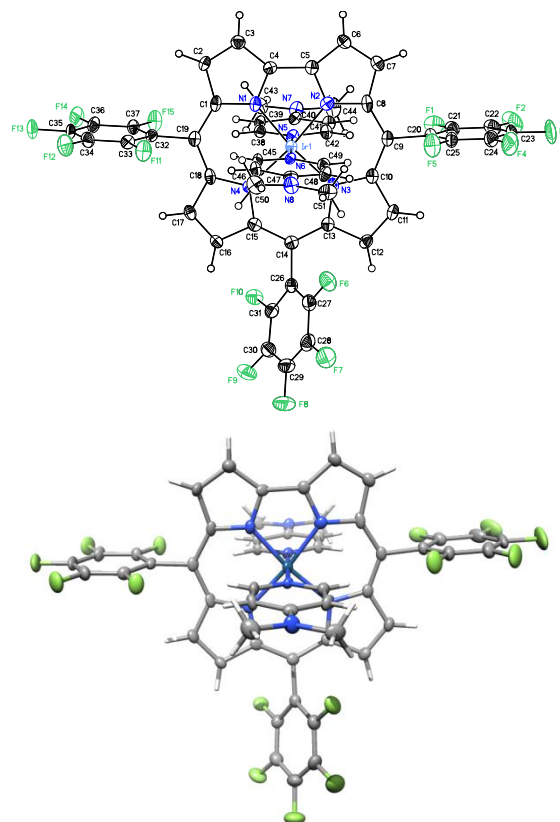
Table 2. Atomic coordinates

Table 3. Selected bond distances and angles

Table 4. Full bond distances and angles

Table 5. Anisotropic displacement parameters



Table 6. Observed and calculated structure factors (available upon request)



**1-Ir(dmap)<sub>2</sub>**

**Note:** The crystallographic data have been deposited in the Cambridge Database (CCDC) and have been placed on hold pending further instructions from me. The deposition number is 769414. Ideally the CCDC would like the publication to contain a footnote of the type: "Crystallographic data have been deposited at the CCDC, 12 Union Road, Cambridge CB2 1EZ, UK, and copies can be obtained on request, free of charge, by quoting the publication citation and the deposition number 769414".

Table C-4-1. Crystal data and structure refinement for **1-Ir(dmap)<sub>2</sub>** (CCDC 769414)

Empirical formula	C <sub>51</sub> H <sub>28</sub> F <sub>15</sub> N <sub>8</sub> Ir • 0.748(C <sub>6</sub> H <sub>12</sub> )	
Formula weight	1292.78	
Crystallization solvent	Dichloromethane/hexanes	
Crystal habit	Blade	
Crystal size	0.21 x 0.06 x 0.03 mm <sup>3</sup>	
Crystal color	Dichroic - green/red	
<b>Data Collection</b>		
Type of diffractometer	Bruker KAPPA APEX II	
Wavelength	0.71073 Å MoKa	
Data collection temperature	100(2) K	
q range for 9914 reflections used in lattice determination	2.19 to 29.48°	
Unit cell dimensions	a = 10.9258(5) Å	a= 70.957(2)°
	b = 14.9693(7) Å	b= 78.529(2)°
	c = 17.7416(8) Å	g = 69.831(2)°
Volume	2562.5(2) Å <sup>3</sup>	
Z	2	
Crystal system	Triclinic	
Space group	P-1	
Density (calculated)	1.676 Mg/m <sup>3</sup>	
F(000)	1276	
q range for data collection	1.22 to 30.41°	
Completeness to q = 30.41°	88.1 %	

Index ranges	$-14 \leq h \leq 15, -21 \leq k \leq 19, -24 \leq l \leq 24$
Data collection scan type	$\omega$ scans; 9 settings
Reflections collected	38630
Independent reflections	13679 [ $R_{\text{int}} = 0.0679$ ]
Absorption coefficient	$2.708 \text{ mm}^{-1}$
Absorption correction	None
Max. and min. transmission	0.9232 and 0.6002

Table C-3-1 cont.

<b>Structure Solution and Refinement</b>	
Structure solution program	SHELXS-97 (Sheldrick, 2008)
Primary solution method	Direct methods
Secondary solution method	Difference Fourier map
Hydrogen placement	Geometric positions
Structure refinement program	SHELXL-97 (Sheldrick, 2008)
Refinement method	Full matrix least-squares on $F^2$
Data / restraints / parameters	13679 / 0 / 705
Treatment of hydrogen atoms	Riding
Goodness-of-fit on $F^2$	1.537
Final R indices [ $I > 2s(I)$ , 10722 reflections] $R1 = 0.0488$ , $wR2 = 0.0732$	
R indices (all data)	$R1 = 0.0766$ , $wR2 = 0.0766$
Type of weighting scheme used	Sigma
Weighting scheme used	$w = 1/\sigma^2(F_o^2)$
Max shift/error	0.001
Average shift/error	0.000
Largest diff. peak and hole	3.371 and -2.654 e.Å <sup>-3</sup>

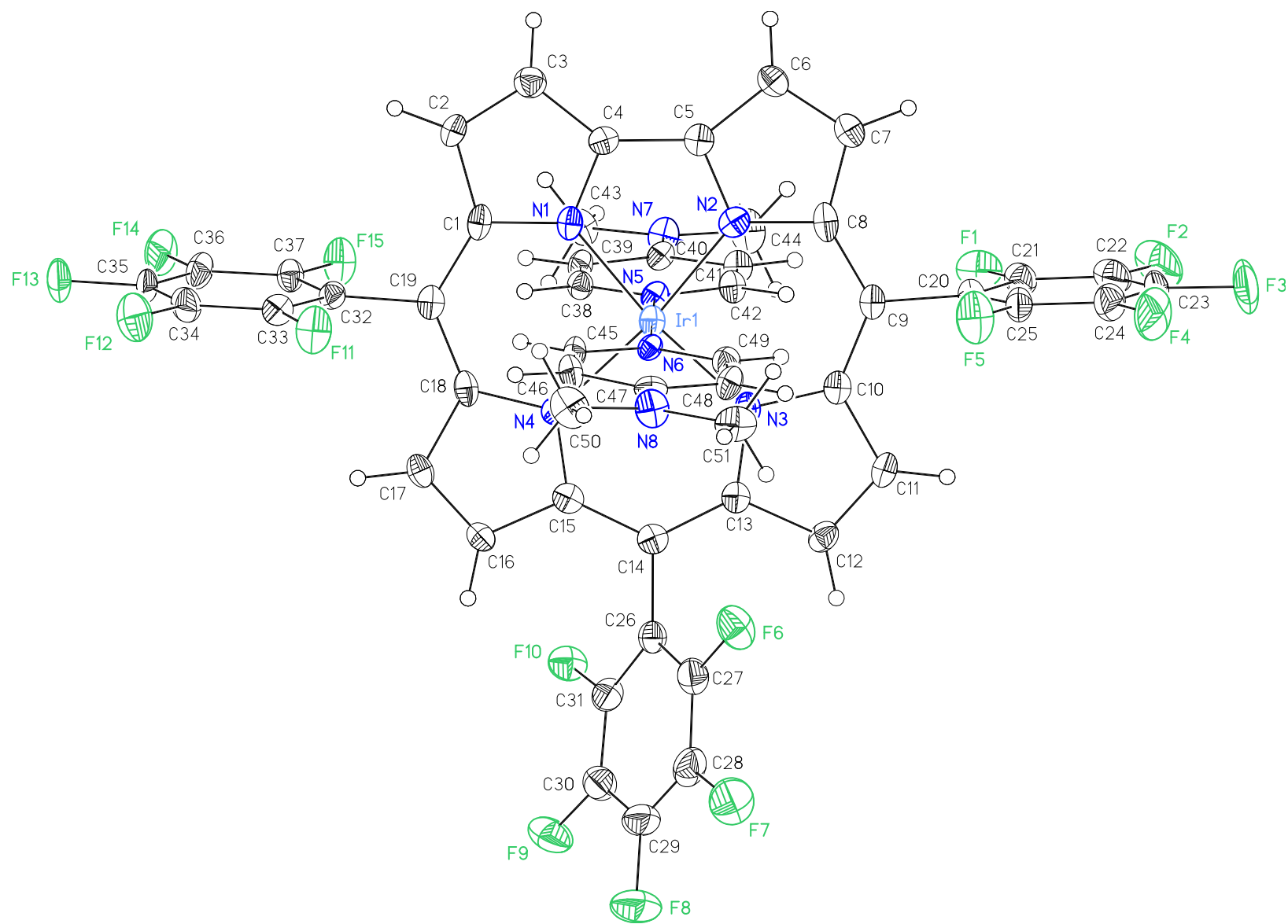
### Special Refinement Details

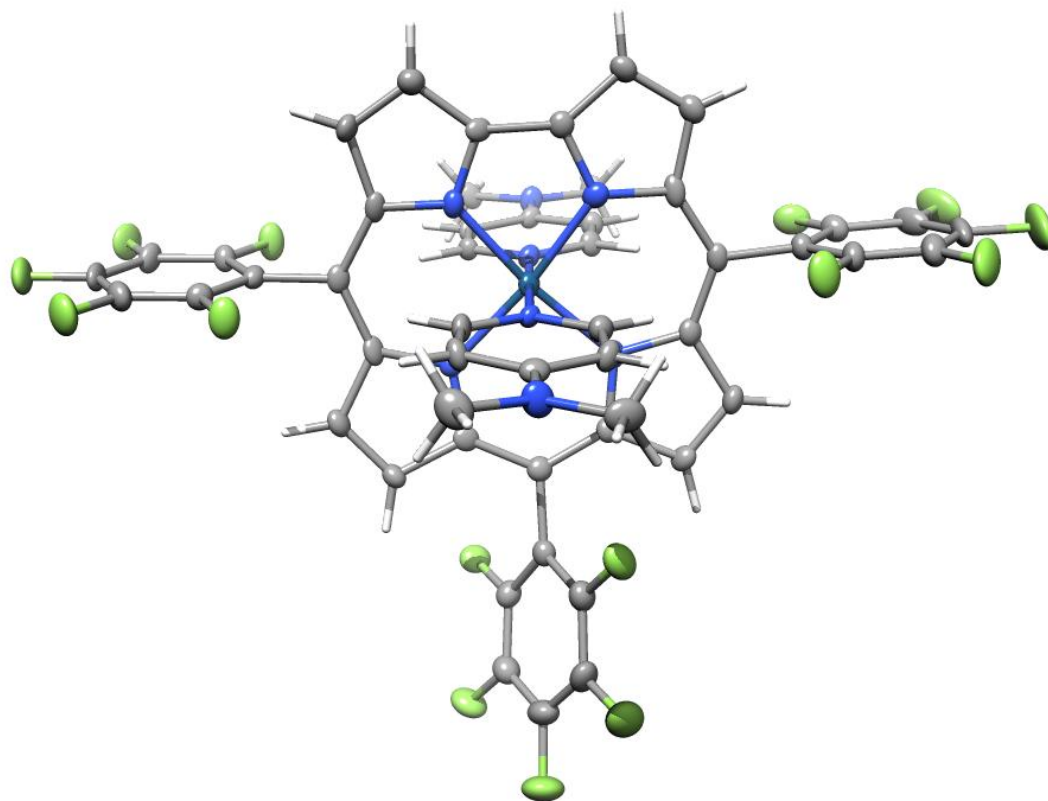
Crystals were mounted on a glass fiber using Paratone oil then placed on the diffractometer under a nitrogen stream at 100K.

The crystal contains methylcyclopentane as a solvent of crystallization. It was refined isotropically and without geometry restraints to a final occupancy of 0.748.

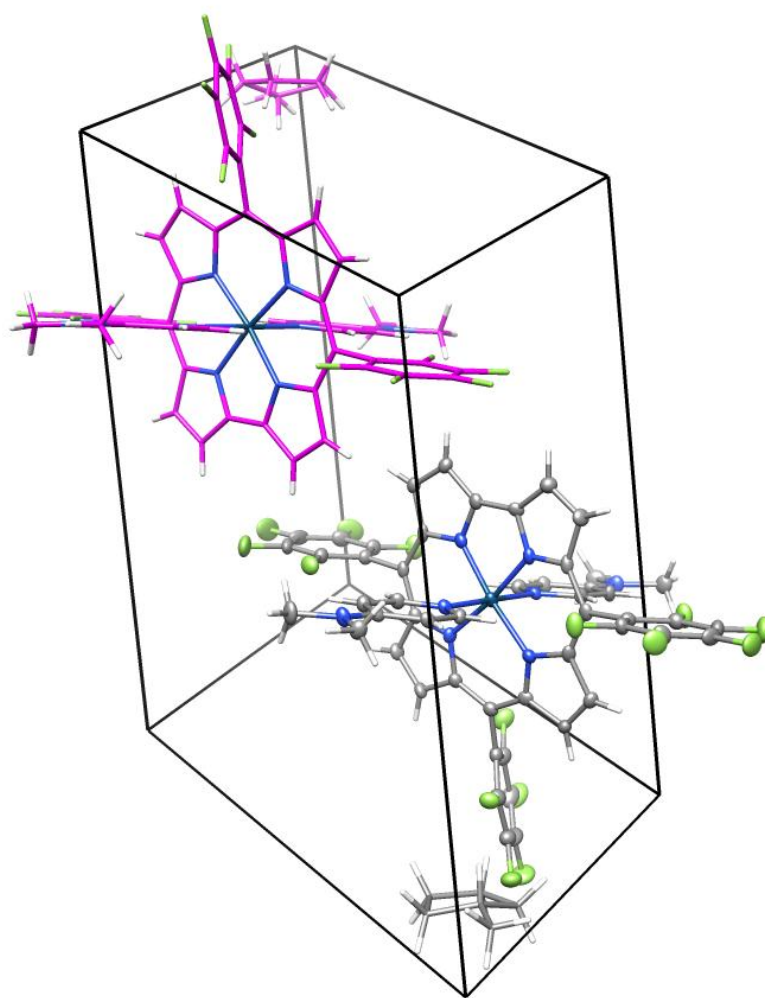
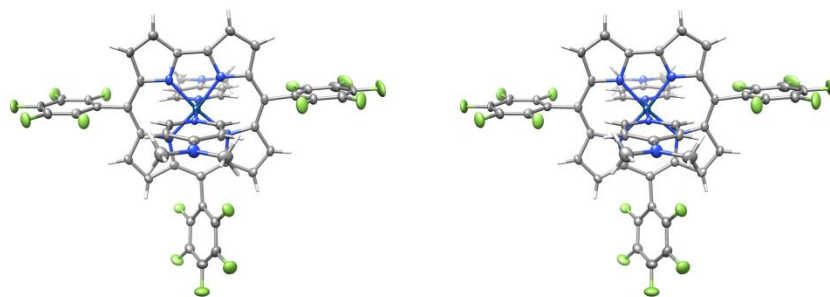
Refinement of  $F^2$  against ALL reflections. The weighted R-factor ( $wR$ ) and goodness of fit ( $S$ ) are based on  $F^2$ , conventional R-factors ( $R$ ) are based on  $F$ , with  $F$  set to zero for negative  $F^2$ . The threshold expression of  $F^2 > 2\sigma(F^2)$  is used only for calculating R-factors(gt), etc., and is not relevant to the choice of reflections for refinement. R-factors based on  $F^2$  are statistically about twice as large as those based on  $F$ , and R-factors based on ALL data will be even larger.

All esds (except the esd in the dihedral angle between two l.s. planes) are estimated using the full covariance matrix. The cell esds are taken into account individually in the estimation of esds in distances, angles, and torsion angles; correlations between esds in cell parameters are only used when they are defined by crystal symmetry. An approximate (isotropic) treatment of cell esds is used for estimating esds involving l.s. planes.









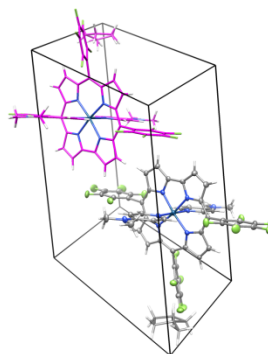
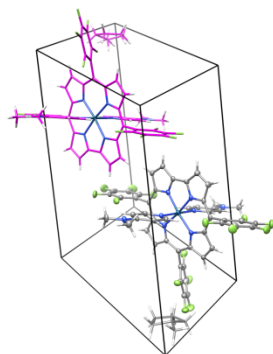


Table C-4-2. Atomic coordinates ( $\times 10^4$ ) and equivalent isotropic displacement parameters ( $\text{\AA}^2 \times 10^3$ ) for **1-Ir(dmap)<sub>2</sub>** (CCDC 769414).  $U(\text{eq})$  is defined as the trace of the orthogonalized  $U^{ij}$  tensor.

	x	y	z	$U_{\text{eq}}$	Occ
Ir(1)	7000(1)	2834(1)	2994(1)	17(1)	1
F(1)	3846(2)	6561(2)	3060(2)	35(1)	1
F(2)	3388(3)	8523(2)	2824(2)	58(1)	1
F(3)	5420(4)	9302(2)	2369(2)	66(1)	1
F(4)	7894(3)	8117(2)	2156(2)	54(1)	1
F(5)	8346(2)	6172(2)	2403(2)	40(1)	1
F(6)	8868(3)	4004(2)	32(2)	37(1)	1
F(7)	9381(3)	4161(2)	-1530(2)	51(1)	1
F(8)	8163(3)	3395(2)	-2235(2)	51(1)	1
F(9)	6284(3)	2549(2)	-1356(2)	40(1)	1
F(10)	5588(2)	2551(2)	172(1)	29(1)	1
F(11)	10107(2)	-1073(2)	3330(2)	33(1)	1
F(12)	10407(3)	-3040(2)	3732(2)	42(1)	1
F(13)	8311(3)	-3713(2)	4299(2)	40(1)	1
F(14)	5905(3)	-2437(2)	4498(2)	36(1)	1
F(15)	5588(2)	-474(2)	4129(2)	32(1)	1
N(1)	7377(3)	1775(3)	3983(2)	18(1)	1
N(2)	6913(3)	3582(3)	3736(2)	19(1)	1
N(3)	6605(3)	4025(3)	2075(2)	18(1)	1
N(4)	7158(3)	1914(3)	2355(2)	18(1)	1
N(5)	5023(3)	3008(3)	3314(2)	18(1)	1

N(6)	8973(3)	2667(3)	2660(2)	14(1)	1
N(7)	1046(3)	3381(3)	4045(2)	22(1)	1
N(8)	12936(4)	2411(3)	1905(2)	26(1)	1
C(1)	7589(4)	782(3)	4135(3)	19(1)	1
C(2)	7759(4)	358(4)	4984(3)	23(1)	1
C(3)	7591(4)	1125(4)	5289(3)	24(1)	1
C(4)	7340(4)	2021(3)	4661(2)	17(1)	1
C(5)	7047(4)	3073(3)	4520(2)	19(1)	1
C(6)	6835(4)	3802(3)	4926(3)	21(1)	1
C(7)	6555(4)	4719(4)	4371(2)	22(1)	1
C(8)	6600(4)	4593(3)	3596(3)	20(1)	1
C(9)	6377(4)	5229(3)	2819(2)	18(1)	1
C(10)	6388(4)	4976(3)	2118(2)	19(1)	1
C(11)	6236(4)	5614(3)	1314(2)	22(1)	1
C(12)	6397(4)	5041(3)	818(3)	22(1)	1
C(13)	6656(4)	4020(3)	1302(2)	19(1)	1
C(14)	6967(4)	3158(3)	1059(2)	20(1)	1
C(15)	7204(4)	2169(3)	1553(2)	18(1)	1
C(16)	7552(4)	1256(3)	1340(2)	19(1)	1
C(17)	7702(4)	497(3)	2022(2)	21(1)	1
C(18)	7473(4)	891(3)	2687(3)	19(1)	1
C(19)	7630(4)	375(3)	3504(2)	18(1)	1
C(20)	6103(4)	6306(3)	2728(2)	21(1)	1
C(21)	4858(4)	6925(4)	2847(3)	26(1)	1
C(22)	4612(5)	7931(4)	2731(3)	37(1)	1
C(23)	5650(6)	8325(4)	2498(3)	38(1)	1
C(24)	6896(5)	7729(4)	2385(3)	32(1)	1

C(25)	7114(4)	6739(3)	2507(3)	25(1)	1
C(26)	7205(4)	3275(3)	176(2)	21(1)	1
C(27)	8157(5)	3679(4)	-291(3)	28(1)	1
C(28)	8453(5)	3747(4)	-1106(3)	35(1)	1
C(29)	7841(5)	3359(4)	-1461(3)	36(1)	1
C(30)	6903(4)	2947(4)	-1015(3)	29(1)	1
C(31)	6573(4)	2934(3)	-225(3)	26(1)	1
C(32)	7836(4)	-714(3)	3724(2)	19(1)	1
C(33)	9053(4)	-1391(3)	3625(2)	21(1)	1
C(34)	9222(4)	-2398(4)	3818(3)	28(1)	1
C(35)	8156(5)	-2747(3)	4110(3)	27(1)	1
C(36)	6935(4)	-2090(3)	4217(3)	25(1)	1
C(37)	6790(4)	-1096(3)	4027(2)	21(1)	1
C(38)	4543(4)	2235(3)	3564(2)	17(1)	1
C(39)	3235(4)	2330(3)	3809(2)	18(1)	1
C(40)	2322(4)	3262(3)	3804(2)	17(1)	1
C(41)	2848(4)	4061(3)	3547(2)	21(1)	1
C(42)	4161(4)	3908(3)	3311(2)	18(1)	1
C(43)	528(4)	2539(3)	4286(3)	24(1)	1
C(44)	128(4)	4366(4)	3989(3)	30(1)	1
C(45)	9875(4)	1784(3)	2696(2)	20(1)	1
C(46)	11187(4)	1649(3)	2458(2)	21(1)	1
C(47)	11652(4)	2490(3)	2148(2)	20(1)	1
C(48)	10701(4)	3414(3)	2118(2)	21(1)	1
C(49)	9418(4)	3467(3)	2379(2)	21(1)	1
C(50)	13910(4)	1439(4)	2003(3)	33(1)	1
C(51)	13365(4)	3294(4)	1602(3)	30(1)	1

C(61)	1155(16)	-139(13)	718(9)	185(7)	0.748(6)
C(62)	1929(19)	650(14)	470(11)	173(7)	0.748(6)
C(63)	957(15)	1618(12)	205(9)	142(5)	0.748(6)
C(64)	1928(12)	2180(10)	-91(8)	119(5)	0.748(6)
C(65)	3279(11)	1524(10)	-168(7)	106(4)	0.748(6)
C(66)	3299(18)	479(15)	79(10)	194(8)	0.748(6)

---

Table C-4-3. Selected bond lengths [ $\text{\AA}$ ] and angles [ $^\circ$ ] for **1-Ir(dmap)<sub>2</sub>** (CCDC 769414)

Ir(1)-N(1)	1.946(3)	N(1)-Ir(1)-N(2)	78.76(15)
Ir(1)-N(2)	1.959(3)	N(1)-Ir(1)-N(3)	172.38(15)
Ir(1)-N(3)	1.968(4)	N(2)-Ir(1)-N(3)	93.62(14)
Ir(1)-N(4)	1.997(3)	N(1)-Ir(1)-N(4)	93.85(14)
Ir(1)-N(5)	2.067(3)	N(2)-Ir(1)-N(4)	172.60(15)
Ir(1)-N(6)	2.069(3)	N(3)-Ir(1)-N(4)	93.76(14)
		N(1)-Ir(1)-N(5)	89.16(13)
		N(2)-Ir(1)-N(5)	87.94(13)
		N(3)-Ir(1)-N(5)	90.74(13)
		N(4)-Ir(1)-N(5)	92.51(13)
		N(1)-Ir(1)-N(6)	91.45(13)
		N(2)-Ir(1)-N(6)	92.37(13)
		N(3)-Ir(1)-N(6)	88.69(13)
		N(4)-Ir(1)-N(6)	87.25(13)
		N(5)-Ir(1)-N(6)	179.36(15)

Table C-4-4. Bond lengths [Å] and angles [°] for **1-Ir(dmap)<sub>2</sub>** (CCDC 769414)

Ir(1)-N(1)	1.946(3)	N(3)-C(13)	1.364(5)
Ir(1)-N(2)	1.959(3)	N(3)-C(10)	1.386(5)
Ir(1)-N(3)	1.968(4)	N(4)-C(15)	1.343(5)
Ir(1)-N(4)	1.997(3)	N(4)-C(18)	1.392(5)
Ir(1)-N(5)	2.067(3)	N(5)-C(38)	1.342(5)
Ir(1)-N(6)	2.069(3)	N(5)-C(42)	1.351(6)
F(1)-C(21)	1.333(5)	N(6)-C(45)	1.340(6)
F(2)-C(22)	1.338(6)	N(6)-C(49)	1.354(5)
F(3)-C(23)	1.343(6)	N(7)-C(40)	1.341(5)
F(4)-C(24)	1.342(5)	N(7)-C(44)	1.454(6)
F(5)-C(25)	1.335(5)	N(7)-C(43)	1.462(5)
F(6)-C(27)	1.337(5)	N(8)-C(47)	1.359(5)
F(7)-C(28)	1.342(5)	N(8)-C(51)	1.456(5)
F(8)-C(29)	1.336(5)	N(8)-C(50)	1.457(6)
F(9)-C(30)	1.360(5)	C(1)-C(19)	1.427(6)
F(10)-C(31)	1.357(4)	C(1)-C(2)	1.454(6)
F(11)-C(33)	1.343(4)	C(2)-C(3)	1.367(6)
F(12)-C(34)	1.336(5)	C(3)-C(4)	1.417(6)
F(13)-C(35)	1.330(5)	C(4)-C(5)	1.439(6)
F(14)-C(36)	1.340(4)	C(5)-C(6)	1.426(6)
F(15)-C(37)	1.340(5)	C(6)-C(7)	1.377(6)
N(1)-C(4)	1.358(5)	C(7)-C(8)	1.437(6)
N(1)-C(1)	1.363(5)	C(8)-C(9)	1.408(6)
N(2)-C(5)	1.360(5)	C(9)-C(10)	1.410(6)
N(2)-C(8)	1.378(5)	C(9)-C(20)	1.494(6)



C(10)-C(11)	1.439(6)	C(35)-C(36)	1.378(7)
C(11)-C(12)	1.367(6)	C(36)-C(37)	1.372(6)
C(12)-C(13)	1.447(6)	C(38)-C(39)	1.380(5)
C(13)-C(14)	1.404(6)	C(39)-C(40)	1.405(6)
C(14)-C(15)	1.416(6)	C(40)-C(41)	1.409(5)
C(14)-C(26)	1.497(6)	C(41)-C(42)	1.372(5)
C(15)-C(16)	1.441(6)	C(45)-C(46)	1.375(5)
C(16)-C(17)	1.355(6)	C(46)-C(47)	1.421(6)
C(17)-C(18)	1.427(6)	C(47)-C(48)	1.407(6)
C(18)-C(19)	1.416(6)	C(48)-C(49)	1.370(5)
C(19)-C(32)	1.492(6)	C(61)-C(62)	1.583(17)
C(20)-C(21)	1.378(6)	C(62)-C(63)	1.46(2)
C(20)-C(25)	1.396(5)	C(62)-C(66)	1.49(2)
C(21)-C(22)	1.387(7)	C(63)-C(64)	1.489(14)
C(22)-C(23)	1.386(7)	C(64)-C(65)	1.473(16)
C(23)-C(24)	1.364(7)	C(65)-C(66)	1.474(18)
C(24)-C(25)	1.367(6)		
C(26)-C(27)	1.379(5)	N(1)-Ir(1)-N(2)	78.76(15)
C(26)-C(31)	1.385(6)	N(1)-Ir(1)-N(3)	172.38(15)
C(27)-C(28)	1.395(6)	N(2)-Ir(1)-N(3)	93.62(14)
C(28)-C(29)	1.363(7)	N(1)-Ir(1)-N(4)	93.85(14)
C(29)-C(30)	1.361(6)	N(2)-Ir(1)-N(4)	172.60(15)
C(30)-C(31)	1.372(6)	N(3)-Ir(1)-N(4)	93.76(14)
C(32)-C(33)	1.386(6)	N(1)-Ir(1)-N(5)	89.16(13)
C(32)-C(37)	1.388(5)	N(2)-Ir(1)-N(5)	87.94(13)
C(33)-C(34)	1.385(6)	N(3)-Ir(1)-N(5)	90.74(13)
C(34)-C(35)	1.378(6)	N(4)-Ir(1)-N(5)	92.51(13)

N(1)-Ir(1)-N(6)	91.45(13)	C(47)-N(8)-C(50)	120.3(4)
N(2)-Ir(1)-N(6)	92.37(13)	C(51)-N(8)-C(50)	119.2(4)
N(3)-Ir(1)-N(6)	88.69(13)	N(1)-C(1)-C(19)	120.4(4)
N(4)-Ir(1)-N(6)	87.25(13)	N(1)-C(1)-C(2)	105.8(4)
N(5)-Ir(1)-N(6)	179.36(15)	C(19)-C(1)-C(2)	133.8(4)
C(4)-N(1)-C(1)	111.6(4)	C(3)-C(2)-C(1)	107.1(4)
C(4)-N(1)-Ir(1)	118.5(3)	C(2)-C(3)-C(4)	108.8(4)
C(1)-N(1)-Ir(1)	129.8(3)	N(1)-C(4)-C(3)	106.7(4)
C(5)-N(2)-C(8)	113.1(4)	N(1)-C(4)-C(5)	112.3(4)
C(5)-N(2)-Ir(1)	117.7(3)	C(3)-C(4)-C(5)	141.0(4)
C(8)-N(2)-Ir(1)	128.9(3)	N(2)-C(5)-C(6)	105.7(4)
C(13)-N(3)-C(10)	110.8(4)	N(2)-C(5)-C(4)	112.6(4)
C(13)-N(3)-Ir(1)	125.0(3)	C(6)-C(5)-C(4)	141.7(4)
C(10)-N(3)-Ir(1)	123.8(3)	C(7)-C(6)-C(5)	108.1(4)
C(15)-N(4)-C(18)	111.8(4)	C(6)-C(7)-C(8)	108.9(4)
C(15)-N(4)-Ir(1)	124.8(3)	N(2)-C(8)-C(9)	120.1(4)
C(18)-N(4)-Ir(1)	122.4(3)	N(2)-C(8)-C(7)	104.3(4)
C(38)-N(5)-C(42)	116.9(4)	C(9)-C(8)-C(7)	135.6(4)
C(38)-N(5)-Ir(1)	122.0(3)	C(8)-C(9)-C(10)	128.2(4)
C(42)-N(5)-Ir(1)	121.0(3)	C(8)-C(9)-C(20)	115.7(4)
C(45)-N(6)-C(49)	116.3(4)	C(10)-C(9)-C(20)	116.1(4)
C(45)-N(6)-Ir(1)	123.0(3)	N(3)-C(10)-C(9)	125.3(4)
C(49)-N(6)-Ir(1)	120.7(3)	N(3)-C(10)-C(11)	106.1(4)
C(40)-N(7)-C(44)	120.6(4)	C(9)-C(10)-C(11)	128.5(4)
C(40)-N(7)-C(43)	120.7(4)	C(12)-C(11)-C(10)	108.4(4)
C(44)-N(7)-C(43)	118.4(4)	C(11)-C(12)-C(13)	107.8(4)
C(47)-N(8)-C(51)	120.3(4)	N(3)-C(13)-C(14)	124.1(4)

N(3)-C(13)-C(12)	106.7(4)	C(24)-C(23)-C(22)	120.2(5)
C(14)-C(13)-C(12)	129.1(4)	F(4)-C(24)-C(23)	119.9(5)
C(13)-C(14)-C(15)	127.5(4)	F(4)-C(24)-C(25)	120.6(5)
C(13)-C(14)-C(26)	116.8(4)	C(23)-C(24)-C(25)	119.5(4)
C(15)-C(14)-C(26)	115.4(4)	F(5)-C(25)-C(24)	118.1(4)
N(4)-C(15)-C(14)	123.9(4)	F(5)-C(25)-C(20)	119.3(4)
N(4)-C(15)-C(16)	106.1(4)	C(24)-C(25)-C(20)	122.6(4)
C(14)-C(15)-C(16)	130.1(4)	C(27)-C(26)-C(31)	114.8(4)
C(17)-C(16)-C(15)	108.3(4)	C(27)-C(26)-C(14)	121.2(4)
C(16)-C(17)-C(18)	108.7(4)	C(31)-C(26)-C(14)	123.9(4)
N(4)-C(18)-C(19)	126.1(4)	F(6)-C(27)-C(26)	120.5(4)
N(4)-C(18)-C(17)	105.1(4)	F(6)-C(27)-C(28)	116.9(4)
C(19)-C(18)-C(17)	128.6(4)	C(26)-C(27)-C(28)	122.6(4)
C(18)-C(19)-C(1)	127.3(4)	F(7)-C(28)-C(29)	120.3(4)
C(18)-C(19)-C(32)	115.8(4)	F(7)-C(28)-C(27)	119.6(4)
C(1)-C(19)-C(32)	116.9(4)	C(29)-C(28)-C(27)	120.0(4)
C(21)-C(20)-C(25)	116.5(4)	F(8)-C(29)-C(30)	121.5(4)
C(21)-C(20)-C(9)	122.5(4)	F(8)-C(29)-C(28)	119.7(4)
C(25)-C(20)-C(9)	120.9(4)	C(30)-C(29)-C(28)	118.8(4)
F(1)-C(21)-C(20)	119.7(4)	F(9)-C(30)-C(29)	119.8(4)
F(1)-C(21)-C(22)	118.4(4)	F(9)-C(30)-C(31)	119.8(4)
C(20)-C(21)-C(22)	121.9(4)	C(29)-C(30)-C(31)	120.4(4)
F(2)-C(22)-C(23)	120.0(5)	F(10)-C(31)-C(30)	117.1(4)
F(2)-C(22)-C(21)	120.8(5)	F(10)-C(31)-C(26)	119.7(4)
C(23)-C(22)-C(21)	119.2(5)	C(30)-C(31)-C(26)	123.2(4)
F(3)-C(23)-C(24)	120.1(5)	C(33)-C(32)-C(37)	116.6(4)
F(3)-C(23)-C(22)	119.7(5)	C(33)-C(32)-C(19)	122.7(4)

C(37)-C(32)-C(19)	120.7(4)	C(48)-C(47)-C(46)	115.9(4)
F(11)-C(33)-C(34)	118.3(4)	C(49)-C(48)-C(47)	120.3(4)
F(11)-C(33)-C(32)	119.8(4)	N(6)-C(49)-C(48)	123.8(4)
C(34)-C(33)-C(32)	121.9(4)	C(63)-C(62)-C(66)	119.5(16)
F(12)-C(34)-C(35)	119.3(4)	C(63)-C(62)-C(61)	105.9(15)
F(12)-C(34)-C(33)	120.9(4)	C(66)-C(62)-C(61)	124.1(17)
C(35)-C(34)-C(33)	119.8(4)	C(62)-C(63)-C(64)	95.2(13)
F(13)-C(35)-C(36)	120.4(4)	C(65)-C(64)-C(63)	112.2(12)
F(13)-C(35)-C(34)	120.1(4)	C(64)-C(65)-C(66)	110.6(12)
C(36)-C(35)-C(34)	119.5(4)	C(65)-C(66)-C(62)	96.1(15)
F(14)-C(36)-C(37)	121.2(4)		
F(14)-C(36)-C(35)	119.0(4)		
C(37)-C(36)-C(35)	119.8(4)		
F(15)-C(37)-C(36)	118.4(4)		
F(15)-C(37)-C(32)	119.1(4)		
C(36)-C(37)-C(32)	122.4(4)		
N(5)-C(38)-C(39)	123.0(4)		
C(38)-C(39)-C(40)	121.0(4)		
N(7)-C(40)-C(39)	122.7(4)		
N(7)-C(40)-C(41)	122.2(4)		
C(39)-C(40)-C(41)	115.2(4)		
C(42)-C(41)-C(40)	120.5(4)		
N(5)-C(42)-C(41)	123.5(4)		
N(6)-C(45)-C(46)	124.5(4)		
C(45)-C(46)-C(47)	119.3(4)		
N(8)-C(47)-C(48)	121.7(4)		
N(8)-C(47)-C(46)	122.4(4)		

Table C-4-5. Anisotropic displacement parameters ( $\text{\AA}^2 \times 10^4$ ) for **1-Ir(dmap)<sub>2</sub>** (CCDC 769414). The anisotropic displacement factor exponent takes the form:  $-2p^2 [h^2 a^{*2} U^{11} + \dots + 2 h k a^* b^* U^{12}]$ .

	U <sup>11</sup>	U <sup>22</sup>	U <sup>33</sup>	U <sup>23</sup>	U <sup>13</sup>	U <sup>12</sup>
Ir(1)	137(1)	160(1)	235(1)	-51(1)	-33(1)	-58(1)
F(1)	187(14)	480(20)	352(15)	-146(14)	0(11)	-55(13)
F(2)	510(20)	480(20)	630(20)	-340(18)	-201(16)	256(16)
F(3)	1070(30)	161(19)	780(20)	-163(18)	-410(20)	-17(18)
F(4)	730(20)	380(20)	660(20)	-52(17)	-199(18)	-388(18)
F(5)	233(15)	355(19)	654(19)	-154(16)	-5(14)	-155(13)
F(6)	340(16)	394(19)	472(17)	-201(15)	70(13)	-214(14)
F(7)	540(20)	510(20)	480(18)	-161(17)	220(15)	-296(17)
F(8)	620(20)	630(30)	259(15)	-170(16)	68(14)	-185(18)
F(9)	412(17)	490(20)	367(15)	-224(15)	-104(13)	-90(15)
F(10)	255(14)	377(18)	301(14)	-109(13)	-39(11)	-148(12)
F(11)	162(13)	290(18)	521(17)	-96(14)	-9(12)	-64(12)
F(12)	308(16)	274(18)	574(18)	-165(15)	-55(14)	72(13)
F(13)	600(20)	145(16)	473(17)	-80(14)	-131(15)	-96(14)
F(14)	404(17)	286(18)	484(17)	-58(14)	-38(13)	-256(14)
F(15)	176(13)	246(17)	527(17)	-97(14)	-7(12)	-84(12)
N(1)	116(17)	150(20)	258(19)	-47(16)	-10(14)	-28(15)
N(2)	116(17)	210(20)	211(18)	-45(17)	-13(14)	-18(16)
N(3)	155(18)	160(20)	254(19)	-62(17)	-4(15)	-71(16)
N(4)	140(18)	190(20)	191(18)	-44(16)	-35(14)	-39(16)

N(5)	152(18)	170(20)	195(18)	-19(16)	-29(15)	-65(16)
N(6)	135(18)	140(20)	150(17)	-16(15)	-23(14)	-55(16)
N(7)	127(18)	220(20)	310(20)	-48(18)	-25(15)	-54(17)
N(8)	155(19)	280(30)	350(20)	-100(20)	15(16)	-100(20)
C(1)	110(20)	140(20)	280(20)	-30(20)	20(17)	-52(18)
C(2)	290(30)	160(30)	230(20)	-10(20)	-25(19)	-90(20)
C(3)	250(20)	250(30)	230(20)	-70(20)	-8(19)	-90(20)
C(4)	140(20)	230(30)	190(20)	-43(19)	-23(16)	-105(19)
C(5)	110(20)	210(30)	240(20)	-60(20)	-6(17)	-41(18)
C(6)	160(20)	240(30)	240(20)	-110(20)	12(18)	-51(19)
C(7)	150(20)	230(30)	280(20)	-110(20)	-15(18)	-36(19)
C(8)	90(20)	150(30)	380(30)	-90(20)	-28(18)	-24(18)
C(9)	110(20)	150(20)	280(20)	-60(20)	-3(17)	-36(18)
C(10)	140(20)	180(30)	260(20)	-50(20)	-14(17)	-63(18)
C(11)	220(20)	150(30)	270(20)	-10(20)	-31(18)	-61(19)
C(12)	180(20)	190(30)	210(20)	-20(20)	-32(18)	-10(20)
C(13)	150(20)	190(30)	230(20)	-60(20)	-32(17)	-61(18)
C(14)	160(20)	230(30)	220(20)	-60(20)	-31(17)	-70(19)
C(15)	110(20)	240(30)	220(20)	-80(20)	-2(16)	-89(19)
C(16)	170(20)	200(30)	220(20)	-100(20)	-38(18)	-28(19)
C(17)	180(20)	190(30)	280(20)	-110(20)	-15(18)	-71(19)
C(18)	130(20)	160(30)	320(20)	-80(20)	-38(18)	-67(18)
C(19)	96(19)	180(30)	270(20)	-50(20)	-15(17)	-55(18)
C(20)	210(20)	170(30)	240(20)	-70(20)	-34(18)	-51(19)
C(21)	250(20)	240(30)	280(20)	-100(20)	-60(20)	-10(20)
C(22)	390(30)	300(30)	330(30)	-160(30)	-140(20)	140(20)
C(23)	680(40)	160(30)	330(30)	-80(20)	-200(30)	-90(30)

C(24)	430(30)	250(30)	350(30)	-70(20)	-110(20)	-150(30)
C(25)	290(30)	170(30)	290(20)	-60(20)	-60(20)	-70(20)
C(26)	190(20)	180(30)	250(20)	-60(20)	-20(18)	-34(19)
C(27)	300(30)	240(30)	320(30)	-90(20)	0(20)	-90(20)
C(28)	380(30)	260(30)	330(30)	-50(20)	110(20)	-120(30)
C(29)	450(30)	330(30)	230(20)	-80(20)	20(20)	-60(30)
C(30)	310(30)	270(30)	300(30)	-100(20)	-60(20)	-60(20)
C(31)	270(20)	230(30)	260(20)	-40(20)	-47(19)	-80(20)
C(32)	230(20)	170(30)	190(20)	-29(19)	-62(18)	-68(19)
C(33)	180(20)	230(30)	230(20)	-60(20)	-24(18)	-75(19)
C(34)	290(30)	200(30)	310(20)	-100(20)	-70(20)	30(20)
C(35)	450(30)	120(30)	280(20)	-30(20)	-90(20)	-120(20)
C(36)	280(30)	180(30)	310(20)	-10(20)	-70(20)	-120(20)
C(37)	180(20)	170(30)	260(20)	-60(20)	-52(18)	-33(19)
C(38)	150(20)	150(30)	200(20)	-52(19)	-3(17)	-28(18)
C(39)	180(20)	150(30)	220(20)	-18(19)	-41(18)	-90(19)
C(40)	150(20)	180(30)	190(20)	-17(19)	-30(17)	-69(19)
C(41)	160(20)	200(30)	260(20)	-70(20)	-19(18)	-51(19)
C(42)	140(20)	180(30)	260(20)	-70(20)	-27(18)	-74(19)
C(43)	170(20)	270(30)	340(30)	-130(20)	2(19)	-100(20)
C(44)	110(20)	280(30)	490(30)	-130(30)	0(20)	-20(20)
C(45)	230(20)	130(30)	240(20)	-30(20)	-44(19)	-70(20)
C(46)	180(20)	140(30)	320(20)	-90(20)	-60(19)	-22(19)
C(47)	160(20)	260(30)	180(20)	-60(20)	-36(18)	-70(20)
C(48)	190(20)	170(30)	260(20)	0(20)	-42(18)	-80(20)
C(49)	220(20)	190(30)	220(20)	-50(20)	-9(18)	-80(20)
C(50)	190(30)	370(30)	440(30)	-170(30)	-30(20)	-50(20)

C(51)    200(20)    430(30)    290(20)    -100(20)    30(20)    -170(20)

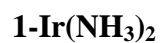


CALIFORNIA INSTITUTE OF TECHNOLOGY  
BECKMAN INSTITUTE  
X-RAY CRYSTALLOGRAPHY LABORATORY



Date 12 March 2010

**Crystal Structure Analysis of:**



(shown below)

**For** Investigator: Theis Brock-Nannestad ext. 6332  
Advisor: H. B. Gray ext. 6500  
Account Number: HBG.BP-1-BP.AMOCO  
**By** Michael W. Day 116 Beckman ext. 2734  
e-mail: mikeday@caltech.edu

Contents

Table 1. Crystal data

Figures Minimum overlap, unit cell contents

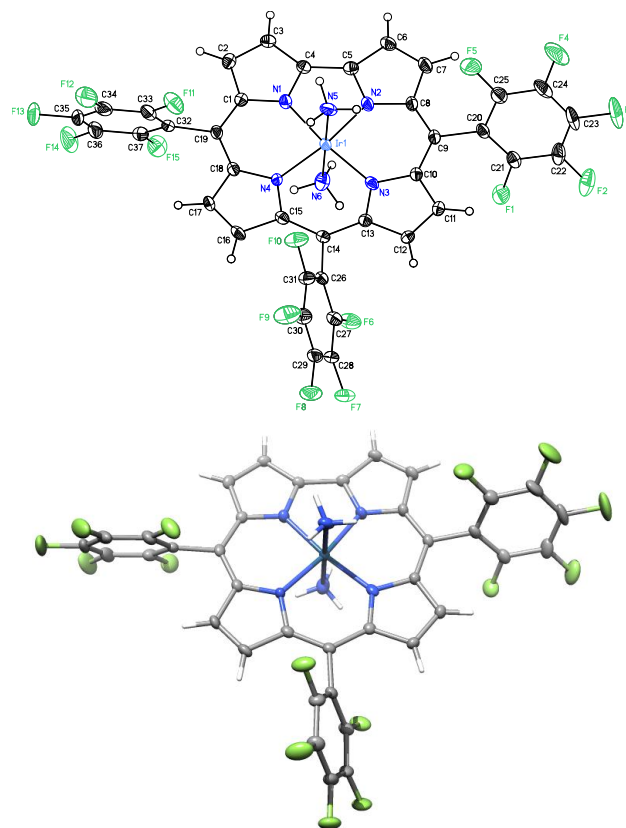
Table 2. Atomic coordinates

Table 3. Selected bond distances and angles

Table 4. Full bond distances and angles

Table 5. Anisotropic displacement parameters

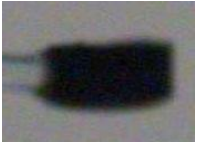
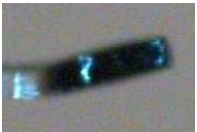
Table 6. Observed and calculated structure factors (available upon request)



**1-Ir(NH<sub>3</sub>)<sub>2</sub>**

**Note:** The crystallographic data have been deposited in the Cambridge Database (CCDC) and have been placed on hold pending further instructions from me. The deposition number is 769388. Ideally the CCDC would like the publication to contain a footnote of the type: "Crystallographic data have been deposited at the CCDC, 12 Union Road, Cambridge CB2 1EZ, UK, and copies can be obtained on request, free of charge, by quoting the publication citation and the deposition number 769388".

Table C-5-1. Crystal data and structure refinement for **1-Ir(NH<sub>3</sub>)<sub>2</sub>** (CCDC 769388)

Empirical formula	C <sub>37</sub> H <sub>14</sub> F <sub>15</sub> N <sub>6</sub> Ir	
Formula weight	1019.74	
Crystallization solvent	Dichloromethane/hexanes	
Crystal habit	Fragment	
Crystal size	0.30 x 0.12 x 0.07 mm <sup>3</sup>	
Crystal color	Black	

**Data Collection**

Type of diffractometer	Bruker KAPPA APEX II	
Wavelength	0.71073 Å MoKα	
Data collection temperature	100(2) K	
q range for 9859 reflections used in lattice determination	3.01 to 32.11°	
Unit cell dimensions	a = 17.9079(6) Å	
	b = 7.0034(3) Å	b = 102.528(2)°
	c = 27.0846(10) Å	
Volume	3316.0(2) Å <sup>3</sup>	
Z	4	
Crystal system	Monoclinic	
Space group	P 2 <sub>1</sub> /c	
Density (calculated)	2.043 Mg/m <sup>3</sup>	
F(000)	1960	
Data collection program	Bruker APEX2 v2009.7-0	
q range for data collection	1.16 to 32.14°	

Completeness to $q = 32.14^\circ$	99.6 %
Index ranges	$-26 \leq h \leq 26$ , $-10 \leq k \leq 10$ , $-40 \leq l \leq 40$
Data collection scan type	$\omega$ scans; 11 settings
Data reduction program	Bruker SAINT-Plus v7.66A
Reflections collected	67007
Independent reflections	11625 [ $R_{\text{int}} = 0.0633$ ]
Absorption coefficient	$4.153 \text{ mm}^{-1}$
Absorption correction	Gaussian
Max. and min. transmission	0.7532 and 0.5082

### Structure Solution and Refinement

Structure solution program	SHELXS-97 (Sheldrick, 2008)
Primary solution method	Patterson method
Secondary solution method	Difference Fourier map
Hydrogen placement	Geometric positions
Structure refinement program	SHELXL-97 (Sheldrick, 2008)
Refinement method	Full matrix least-squares on $F^2$
Data / restraints / parameters	11625 / 0 / 534
Treatment of hydrogen atoms	Riding
Goodness-of-fit on $F^2$	1.953
Final R indices [ $I > 2s(I)$ , 9482 reflections]	$R1 = 0.0374$ , $wR2 = 0.0556$
R indices (all data)	$R1 = 0.0524$ , $wR2 = 0.0571$
Type of weighting scheme used	Sigma
Weighting scheme used	$w = 1/\sigma^2(F_o^2)$

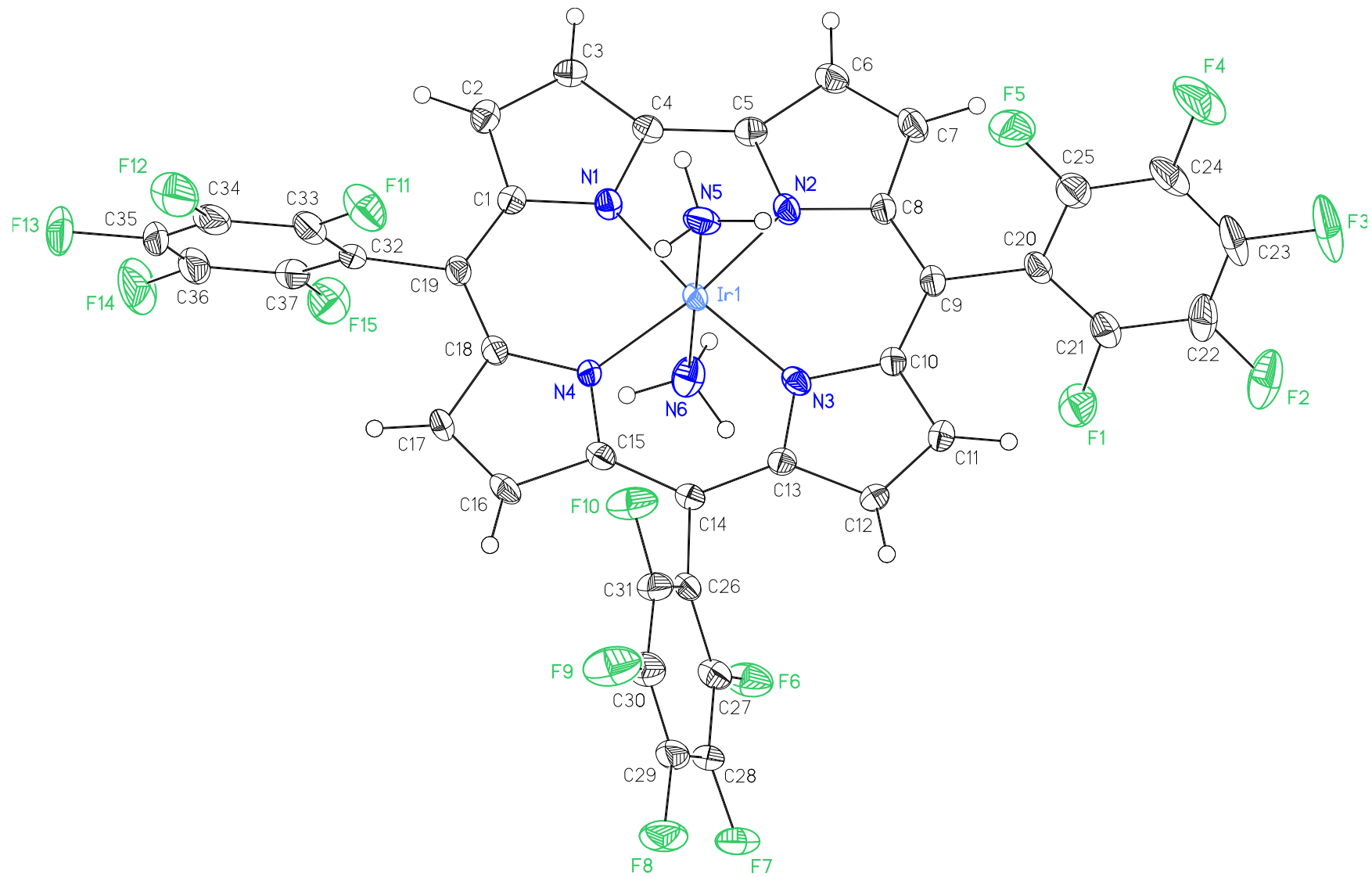
Max shift/error	0.003
Average shift/error	0.000
Largest diff. peak and hole	3.497 and -3.184 e.Å <sup>-3</sup>

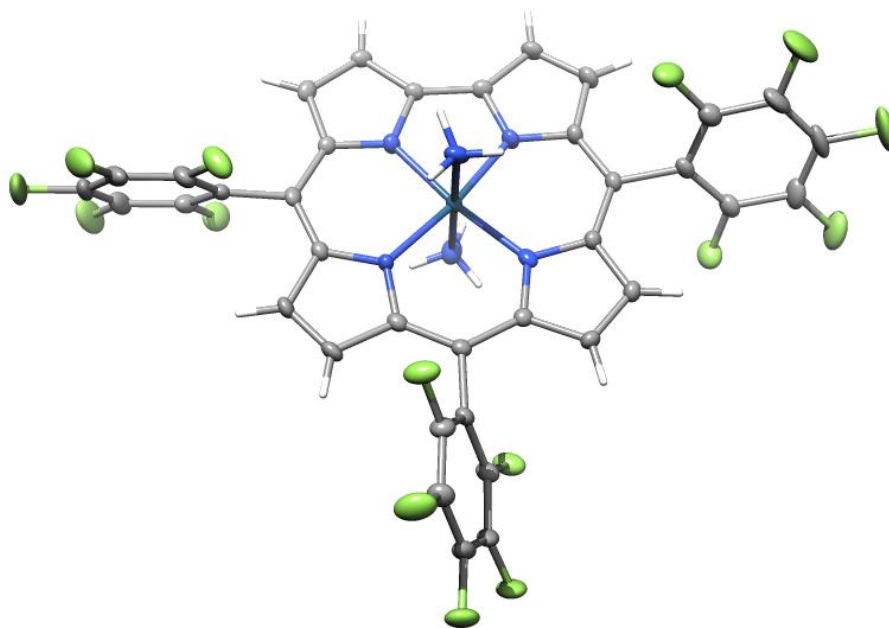
### Special Refinement Details

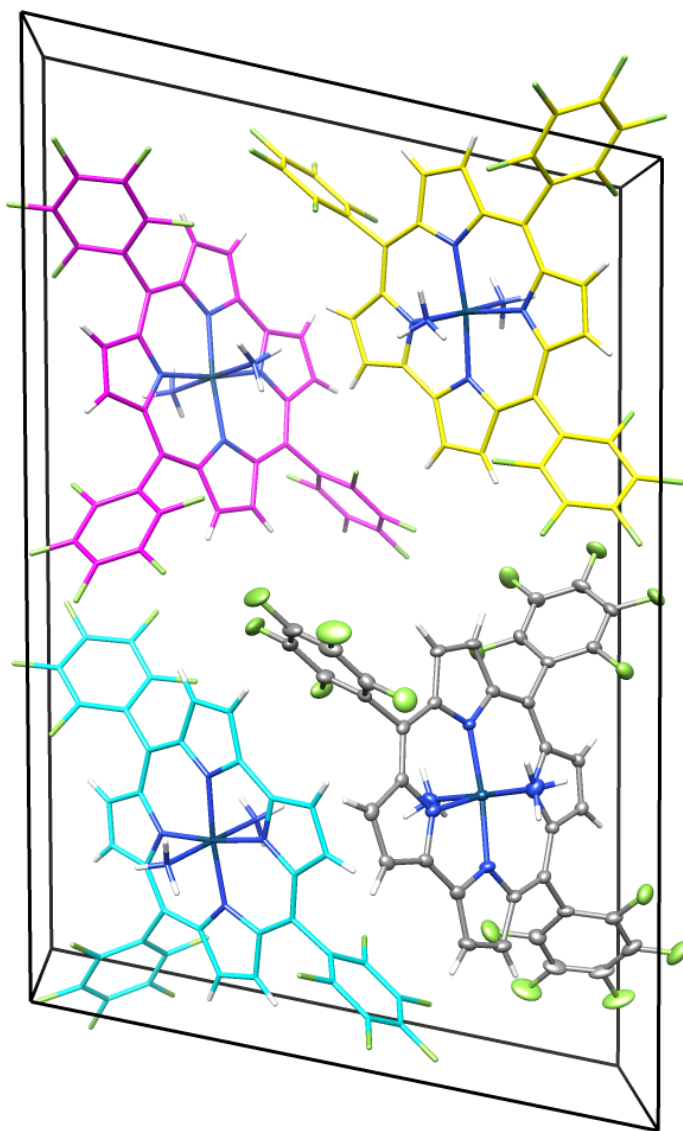
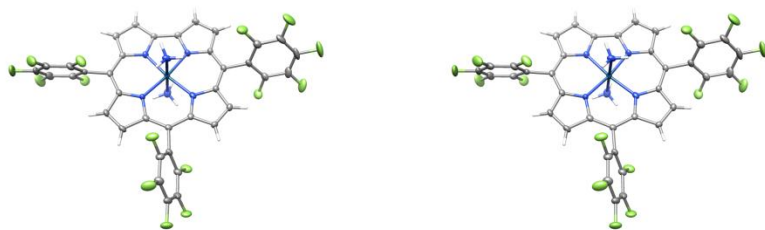
Crystals were mounted on a glass fiber using Paratone oil then placed on the diffractometer under a nitrogen stream at 100K.

Refinement of  $F^2$  against ALL reflections. The weighted R-factor ( $wR$ ) and goodness of fit ( $S$ ) are based on  $F^2$ , conventional R-factors ( $R$ ) are based on  $F$ , with  $F$  set to zero for negative  $F^2$ . The threshold expression of  $F^2 > 2\sigma(F^2)$  is used only for calculating R-factors(gt), etc., and is not relevant to the choice of reflections for refinement. R-factors based on  $F^2$  are statistically about twice as large as those based on  $F$ , and R-factors based on ALL data will be even larger.

All esds (except the esd in the dihedral angle between two l.s. planes) are estimated using the full covariance matrix. The cell esds are taken into account individually in the estimation of esds in distances, angles, and torsion angles; correlations between esds in cell parameters are only used when they are defined by crystal symmetry. An approximate (isotropic) treatment of cell esds is used for estimating esds involving l.s. planes.









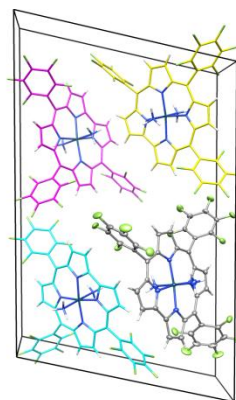
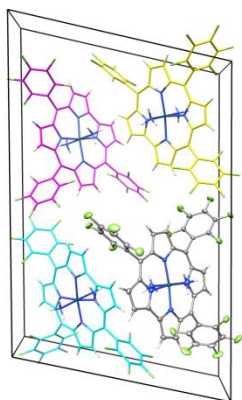


Table C-5-2. Atomic coordinates ( $\times 10^4$ ) and equivalent isotropic displacement parameters ( $\text{\AA}^2 \times 10^3$ ) for **1-Ir(NH<sub>3</sub>)<sub>2</sub>** (CCDC 769388).  $U(\text{eq})$  is defined as the trace of the orthogonalized  $U^{ij}$  tensor.

	x	y	z	$U_{\text{eq}}$
Ir(1)	7129(1)	-800(1)	3129(1)	15(1)
F(1)	9824(1)	721(3)	2408(1)	34(1)
F(2)	10506(1)	2679(3)	1778(1)	46(1)
F(3)	9673(1)	4887(3)	1037(1)	55(1)
F(4)	8125(1)	5065(3)	923(1)	57(1)
F(5)	7441(1)	3191(3)	1565(1)	41(1)
F(6)	9513(1)	1159(3)	4684(1)	34(1)
F(7)	10160(1)	3191(3)	5512(1)	34(1)
F(8)	9346(1)	5923(3)	5869(1)	37(1)
F(9)	7906(1)	6778(3)	5356(1)	44(1)
F(10)	7280(1)	4880(3)	4502(1)	34(1)
F(11)	4617(1)	-467(3)	3853(1)	39(1)
F(12)	3571(1)	-1587(4)	4366(1)	59(1)
F(13)	3592(1)	-5235(4)	4719(1)	63(1)
F(14)	4696(1)	-7682(3)	4579(1)	57(1)
F(15)	5756(1)	-6561(3)	4065(1)	37(1)
N(1)	6295(1)	-2626(4)	2928(1)	17(1)
N(2)	7195(1)	-1293(3)	2429(1)	18(1)
N(3)	8000(1)	987(3)	3244(1)	17(1)
N(4)	6939(1)	-526(3)	3817(1)	15(1)
N(5)	6407(1)	1517(4)	2898(1)	24(1)

N(6)	7862(1)	-3038(4)	3382(1)	27(1)
C(1)	5798(2)	-3341(4)	3193(1)	15(1)
C(2)	5303(2)	-4625(4)	2860(1)	20(1)
C(3)	5534(2)	-4614(4)	2395(1)	18(1)
C(4)	6162(2)	-3341(4)	2442(1)	16(1)
C(5)	6678(2)	-2552(4)	2154(1)	18(1)
C(6)	6831(2)	-2561(5)	1659(1)	23(1)
C(7)	7425(2)	-1322(4)	1654(1)	24(1)
C(8)	7652(2)	-489(4)	2149(1)	18(1)
C(9)	8200(2)	895(4)	2363(1)	17(1)
C(10)	8370(2)	1583(4)	2873(1)	17(1)
C(11)	8926(2)	2956(4)	3098(1)	18(1)
C(12)	8880(2)	3177(4)	3594(1)	18(1)
C(13)	8281(2)	1948(4)	3683(1)	16(1)
C(14)	7983(2)	1740(4)	4126(1)	16(1)
C(15)	7364(2)	591(4)	4188(1)	17(1)
C(16)	7035(2)	352(4)	4631(1)	21(1)
C(17)	6436(2)	-864(4)	4506(1)	20(1)
C(18)	6366(2)	-1445(4)	3986(1)	16(1)
C(19)	5836(2)	-2731(4)	3701(1)	17(1)
C(20)	8608(2)	1881(4)	2008(1)	20(1)
C(21)	9390(2)	1793(4)	2048(1)	23(1)
C(22)	9754(2)	2800(5)	1725(1)	30(1)
C(23)	9324(2)	3903(5)	1350(1)	34(1)
C(24)	8548(2)	3994(5)	1292(1)	33(1)
C(25)	8201(2)	3007(5)	1619(1)	26(1)
C(26)	8365(2)	2897(4)	4576(1)	17(1)

C(27)	9102(2)	2537(5)	4841(1)	21(1)
C(28)	9437(2)	3563(5)	5271(1)	23(1)
C(29)	9030(2)	4955(5)	5443(1)	26(1)
C(30)	8301(2)	5399(5)	5188(1)	26(1)
C(31)	7984(2)	4378(5)	4755(1)	23(1)
C(32)	5228(2)	-3463(5)	3952(1)	18(1)
C(33)	4649(2)	-2275(5)	4030(1)	28(1)
C(34)	4104(2)	-2847(6)	4287(1)	36(1)
C(35)	4125(2)	-4654(6)	4465(1)	38(1)
C(36)	4676(2)	-5907(6)	4392(1)	35(1)
C(37)	5221(2)	-5311(5)	4132(1)	25(1)

---

Table C-5-3. Selected bond lengths [ $\text{\AA}$ ] and angles [ $^\circ$ ] for **1-Ir(NH<sub>3</sub>)<sub>2</sub>** (CCDC 769388)

Ir(1)-N(2)	1.957(2)	N(2)-Ir(1)-N(1)	79.51(9)
Ir(1)-N(1)	1.952(2)	N(2)-Ir(1)-N(4)	172.25(10)
Ir(1)-N(4)	1.975(2)	N(1)-Ir(1)-N(4)	92.77(9)
Ir(1)-N(3)	1.971(2)	N(2)-Ir(1)-N(3)	93.06(9)
Ir(1)-N(6)	2.064(3)	N(1)-Ir(1)-N(3)	172.55(9)
Ir(1)-N(5)	2.084(2)	N(4)-Ir(1)-N(3)	94.67(9)
		N(2)-Ir(1)-N(6)	91.16(10)
		N(1)-Ir(1)-N(6)	89.32(10)
		N(4)-Ir(1)-N(6)	89.29(10)
		N(3)-Ir(1)-N(6)	90.29(10)
		N(2)-Ir(1)-N(5)	90.56(10)
		N(1)-Ir(1)-N(5)	92.24(10)
		N(4)-Ir(1)-N(5)	89.18(9)
		N(3)-Ir(1)-N(5)	88.35(10)
		N(6)-Ir(1)-N(5)	177.86(10)

Table C-5-4. Bond lengths [Å] and angles [°] for **1-Ir(NH<sub>3</sub>)<sub>2</sub>** (CCDC 769388)

Ir(1)-N(2)	1.957(2)	N(3)-C(13)	1.363(3)
Ir(1)-N(1)	1.952(2)	N(3)-C(10)	1.384(3)
Ir(1)-N(4)	1.975(2)	N(4)-C(15)	1.368(3)
Ir(1)-N(3)	1.971(2)	N(4)-C(18)	1.371(3)
Ir(1)-N(6)	2.064(3)	C(1)-C(19)	1.429(4)
Ir(1)-N(5)	2.084(2)	C(1)-C(2)	1.435(4)
F(1)-C(21)	1.339(3)	C(2)-C(3)	1.408(4)
F(2)-C(22)	1.325(4)	C(3)-C(4)	1.419(4)
F(3)-C(23)	1.346(3)	C(4)-C(5)	1.444(4)
F(4)-C(24)	1.344(4)	C(5)-C(6)	1.426(4)
F(5)-C(25)	1.343(4)	C(6)-C(7)	1.375(4)
F(6)-C(27)	1.338(3)	C(7)-C(8)	1.437(4)
F(7)-C(28)	1.344(3)	C(8)-C(9)	1.411(4)
F(8)-C(29)	1.351(3)	C(9)-C(10)	1.430(4)
F(9)-C(30)	1.335(3)	C(9)-C(20)	1.498(4)
F(10)-C(31)	1.345(3)	C(10)-C(11)	1.423(4)
F(11)-C(33)	1.351(4)	C(11)-C(12)	1.370(4)
F(12)-C(34)	1.350(4)	C(12)-C(13)	1.437(4)
F(13)-C(35)	1.354(3)	C(13)-C(14)	1.423(4)
F(14)-C(36)	1.340(4)	C(14)-C(15)	1.409(4)
F(15)-C(37)	1.339(4)	C(14)-C(26)	1.498(4)
N(1)-C(1)	1.354(3)	C(15)-C(16)	1.456(4)
N(1)-C(4)	1.380(3)	C(16)-C(17)	1.355(4)
N(2)-C(8)	1.353(3)	C(17)-C(18)	1.446(4)
N(2)-C(5)	1.374(4)	C(18)-C(19)	1.410(4)

C(19)-C(32)	1.492(4)	N(1)-Ir(1)-N(6)	89.32(10)
C(20)-C(21)	1.382(4)	N(4)-Ir(1)-N(6)	89.29(10)
C(20)-C(25)	1.388(4)	N(3)-Ir(1)-N(6)	90.29(10)
C(21)-C(22)	1.390(4)	N(2)-Ir(1)-N(5)	90.56(10)
C(22)-C(23)	1.373(5)	N(1)-Ir(1)-N(5)	92.24(10)
C(23)-C(24)	1.365(5)	N(4)-Ir(1)-N(5)	89.18(9)
C(24)-C(25)	1.374(4)	N(3)-Ir(1)-N(5)	88.35(10)
C(26)-C(27)	1.383(4)	N(6)-Ir(1)-N(5)	177.86(10)
C(26)-C(31)	1.386(4)	C(1)-N(1)-C(4)	111.9(2)
C(27)-C(28)	1.388(4)	C(1)-N(1)-Ir(1)	130.24(18)
C(28)-C(29)	1.358(4)	C(4)-N(1)-Ir(1)	117.82(18)
C(29)-C(30)	1.375(4)	C(8)-N(2)-C(5)	112.4(2)
C(30)-C(31)	1.384(4)	C(8)-N(2)-Ir(1)	129.84(19)
C(32)-C(33)	1.381(4)	C(5)-N(2)-Ir(1)	117.58(18)
C(32)-C(37)	1.385(4)	C(13)-N(3)-C(10)	109.9(2)
C(33)-C(34)	1.376(4)	C(13)-N(3)-Ir(1)	125.55(18)
C(34)-C(35)	1.352(5)	C(10)-N(3)-Ir(1)	124.27(19)
C(35)-C(36)	1.366(5)	C(15)-N(4)-C(18)	111.2(2)
C(36)-C(37)	1.386(4)	C(15)-N(4)-Ir(1)	124.51(18)
		C(18)-N(4)-Ir(1)	124.32(18)
N(2)-Ir(1)-N(1)	79.51(9)	N(1)-C(1)-C(19)	120.0(2)
N(2)-Ir(1)-N(4)	172.25(10)	N(1)-C(1)-C(2)	106.6(2)
N(1)-Ir(1)-N(4)	92.77(9)	C(19)-C(1)-C(2)	133.4(3)
N(2)-Ir(1)-N(3)	93.06(9)	C(3)-C(2)-C(1)	107.3(3)
N(1)-Ir(1)-N(3)	172.55(9)	C(2)-C(3)-C(4)	107.7(3)
N(4)-Ir(1)-N(3)	94.67(9)	N(1)-C(4)-C(3)	106.4(2)
N(2)-Ir(1)-N(6)	91.16(10)	N(1)-C(4)-C(5)	112.3(2)

C(3)-C(4)-C(5)	141.3(3)	C(16)-C(17)-C(18)	108.5(2)
N(2)-C(5)-C(6)	105.6(3)	N(4)-C(18)-C(19)	125.5(2)
N(2)-C(5)-C(4)	112.8(2)	N(4)-C(18)-C(17)	106.3(2)
C(6)-C(5)-C(4)	141.6(3)	C(19)-C(18)-C(17)	128.2(3)
C(7)-C(6)-C(5)	108.2(3)	C(18)-C(19)-C(1)	127.1(2)
C(6)-C(7)-C(8)	108.1(2)	C(18)-C(19)-C(32)	116.2(2)
N(2)-C(8)-C(9)	120.4(2)	C(1)-C(19)-C(32)	116.6(2)
N(2)-C(8)-C(7)	105.7(2)	C(21)-C(20)-C(25)	116.2(3)
C(9)-C(8)-C(7)	133.9(3)	C(21)-C(20)-C(9)	123.8(3)
C(8)-C(9)-C(10)	127.7(2)	C(25)-C(20)-C(9)	120.0(3)
C(8)-C(9)-C(20)	116.4(2)	F(1)-C(21)-C(20)	120.0(3)
C(10)-C(9)-C(20)	115.7(2)	F(1)-C(21)-C(22)	117.7(3)
N(3)-C(10)-C(9)	124.4(3)	C(20)-C(21)-C(22)	122.3(3)
N(3)-C(10)-C(11)	106.9(2)	F(2)-C(22)-C(23)	120.6(3)
C(9)-C(10)-C(11)	128.7(2)	F(2)-C(22)-C(21)	120.3(3)
C(12)-C(11)-C(10)	108.2(2)	C(23)-C(22)-C(21)	119.1(3)
C(11)-C(12)-C(13)	107.5(3)	F(3)-C(23)-C(24)	120.3(3)
N(3)-C(13)-C(14)	123.3(3)	F(3)-C(23)-C(22)	119.4(3)
N(3)-C(13)-C(12)	107.3(2)	C(24)-C(23)-C(22)	120.3(3)
C(14)-C(13)-C(12)	129.3(3)	F(4)-C(24)-C(23)	120.5(3)
C(15)-C(14)-C(13)	127.4(3)	F(4)-C(24)-C(25)	119.9(3)
C(15)-C(14)-C(26)	116.4(2)	C(23)-C(24)-C(25)	119.6(3)
C(13)-C(14)-C(26)	116.2(2)	F(5)-C(25)-C(24)	118.1(3)
N(4)-C(15)-C(14)	124.5(2)	F(5)-C(25)-C(20)	119.3(3)
N(4)-C(15)-C(16)	106.3(2)	C(24)-C(25)-C(20)	122.6(3)
C(14)-C(15)-C(16)	129.3(3)	C(27)-C(26)-C(31)	116.1(3)
C(17)-C(16)-C(15)	107.8(3)	C(27)-C(26)-C(14)	122.7(3)



C(31)-C(26)-C(14)	121.1(3)	C(34)-C(35)-C(36)	121.0(3)
F(6)-C(27)-C(28)	118.2(3)	F(14)-C(36)-C(35)	120.1(3)
F(6)-C(27)-C(26)	119.6(3)	F(14)-C(36)-C(37)	120.5(4)
C(28)-C(27)-C(26)	122.1(3)	C(35)-C(36)-C(37)	119.4(3)
F(7)-C(28)-C(29)	120.3(3)	F(15)-C(37)-C(36)	118.4(3)
F(7)-C(28)-C(27)	120.2(3)	F(15)-C(37)-C(32)	120.1(3)
C(29)-C(28)-C(27)	119.6(3)	C(36)-C(37)-C(32)	121.5(3)
F(8)-C(29)-C(30)	119.5(3)		
F(8)-C(29)-C(28)	119.9(3)		
C(30)-C(29)-C(28)	120.7(3)		
F(9)-C(30)-C(29)	120.5(3)		
F(9)-C(30)-C(31)	120.8(3)		
C(29)-C(30)-C(31)	118.7(3)		
F(10)-C(31)-C(30)	117.6(3)		
F(10)-C(31)-C(26)	119.6(3)		
C(30)-C(31)-C(26)	122.7(3)		
C(33)-C(32)-C(37)	116.3(3)		
C(33)-C(32)-C(19)	120.6(3)		
C(37)-C(32)-C(19)	123.0(3)		
F(11)-C(33)-C(34)	118.2(3)		
F(11)-C(33)-C(32)	119.0(3)		
C(34)-C(33)-C(32)	122.8(3)		
F(12)-C(34)-C(35)	121.4(3)		
F(12)-C(34)-C(33)	119.6(4)		
C(35)-C(34)-C(33)	119.0(3)		
F(13)-C(35)-C(34)	119.7(4)		
F(13)-C(35)-C(36)	119.4(4)		

Table C-5-5. Anisotropic displacement parameters ( $\text{\AA}^2 \times 10^4$ ) for **1-Ir(NH<sub>3</sub>)<sub>2</sub>** (CCDC 769388). The anisotropic displacement factor exponent takes the form:  $-2p^2[ h^2 a^*{}^2 U^{11} + \dots + 2 h k a^* b^* U^{12} ]$ .

	U <sup>11</sup>	U <sup>22</sup>	U <sup>33</sup>	U <sup>23</sup>	U <sup>13</sup>	U <sup>12</sup>
Ir(1)	164(1)	178(1)	115(1)	-11(1)	46(1)	-16(1)
F(1)	265(10)	384(12)	379(10)	59(9)	119(9)	85(10)
F(2)	406(13)	455(14)	646(14)	-104(12)	360(11)	-85(12)
F(3)	920(19)	400(13)	470(13)	13(11)	487(13)	-197(14)
F(4)	861(18)	477(14)	312(11)	219(10)	18(12)	-52(14)
F(5)	352(12)	445(14)	367(11)	131(9)	-42(10)	15(11)
F(6)	312(11)	421(13)	252(9)	-36(8)	-4(9)	133(10)
F(7)	257(10)	482(13)	230(9)	-5(9)	-70(8)	-5(10)
F(8)	372(12)	436(13)	242(9)	-140(9)	-41(9)	-74(11)
F(9)	391(12)	429(14)	444(12)	-244(10)	-15(10)	54(11)
F(10)	252(10)	380(11)	331(10)	-129(9)	-42(9)	92(10)
F(11)	433(13)	476(14)	302(10)	98(9)	165(10)	227(11)
F(12)	311(12)	1190(20)	307(11)	-32(12)	157(10)	186(14)
F(13)	486(14)	1130(20)	336(12)	-57(13)	241(11)	-416(15)
F(14)	845(18)	471(15)	423(13)	62(11)	215(12)	-360(14)
F(15)	433(13)	252(11)	433(12)	84(9)	92(10)	4(10)
N(1)	191(13)	169(13)	166(11)	-7(10)	65(10)	-14(11)
N(2)	211(13)	220(14)	137(11)	-19(9)	72(10)	-22(11)
N(3)	174(12)	206(14)	136(10)	37(10)	39(9)	60(11)
N(4)	139(12)	185(14)	122(10)	-9(9)	44(9)	-23(10)

N(5)	267(15)	257(14)	155(12)	-6(10)	-17(11)	-20(13)
N(6)	245(15)	263(16)	323(15)	-20(11)	122(12)	-8(13)
C(1)	152(15)	133(14)	176(13)	7(11)	37(11)	17(12)
C(2)	184(15)	164(17)	247(15)	32(11)	57(13)	9(12)
C(3)	192(15)	145(16)	176(13)	-19(10)	6(12)	11(12)
C(4)	193(15)	149(15)	149(13)	-15(11)	29(12)	15(13)
C(5)	195(15)	168(15)	177(13)	-34(11)	28(12)	6(14)
C(6)	268(17)	263(17)	144(13)	-32(12)	30(12)	-26(15)
C(7)	291(18)	285(18)	154(14)	-6(12)	86(13)	-20(15)
C(8)	198(15)	213(18)	157(13)	0(11)	70(12)	-33(13)
C(9)	180(15)	183(15)	169(12)	21(12)	67(11)	0(14)
C(10)	174(15)	180(15)	159(13)	6(11)	46(12)	-22(13)
C(11)	166(15)	167(16)	202(14)	11(11)	60(12)	-14(12)
C(12)	159(15)	181(16)	176(14)	-15(11)	20(12)	-35(13)
C(13)	152(14)	153(15)	164(13)	12(10)	26(11)	18(12)
C(14)	171(15)	169(15)	134(13)	1(10)	17(11)	19(13)
C(15)	188(15)	192(16)	139(12)	12(11)	32(11)	38(13)
C(16)	259(17)	257(18)	110(12)	1(11)	55(12)	27(14)
C(17)	217(15)	246(16)	139(12)	34(12)	79(11)	-9(15)
C(18)	175(15)	177(15)	151(13)	23(11)	53(12)	18(13)
C(19)	158(14)	192(16)	171(13)	58(11)	50(11)	24(13)
C(20)	275(18)	197(17)	132(13)	-18(11)	69(12)	-43(14)
C(21)	296(18)	232(18)	181(14)	-6(12)	98(13)	-3(15)
C(22)	360(20)	271(19)	342(18)	-69(15)	234(16)	-57(17)
C(23)	600(30)	240(20)	249(16)	0(13)	258(18)	-108(18)
C(24)	520(20)	280(20)	184(15)	86(14)	50(16)	-12(19)
C(25)	304(19)	260(19)	225(15)	22(13)	47(14)	-11(16)

C(26)	199(16)	201(16)	120(13)	5(11)	38(12)	-18(13)
C(27)	230(16)	233(16)	157(13)	-3(12)	33(12)	38(15)
C(28)	190(16)	318(18)	150(14)	36(12)	-15(12)	-29(15)
C(29)	297(19)	288(17)	164(14)	-22(13)	6(13)	-114(16)
C(30)	294(19)	251(19)	223(15)	-69(12)	50(14)	5(15)
C(31)	187(16)	264(18)	207(14)	-7(13)	-4(12)	20(15)
C(32)	165(15)	263(16)	120(13)	3(11)	17(11)	-34(14)
C(33)	282(18)	400(20)	163(14)	49(14)	54(13)	18(17)
C(34)	209(18)	720(30)	154(15)	-28(17)	47(14)	50(20)
C(35)	300(20)	700(30)	162(15)	-29(16)	92(15)	-250(20)
C(36)	420(20)	410(20)	210(15)	36(16)	50(15)	-210(20)
C(37)	242(17)	290(20)	203(15)	22(12)	-1(13)	-51(15)

---

Thanks for reading!